frontiers | Research Topics

Molecular interactions between bacterial pathogens and plants: Selected contributions to the 14th International Conference on Plant Pathogenic Bacteria (14th ICPPB)

Edited by
Chiaraluce Moretti, Roberto Buonaurio, Guido Sessa, Vittoria Catara, Michelle Teresa Hulin and George W. Sundin

Published in
Frontiers in Plant Science

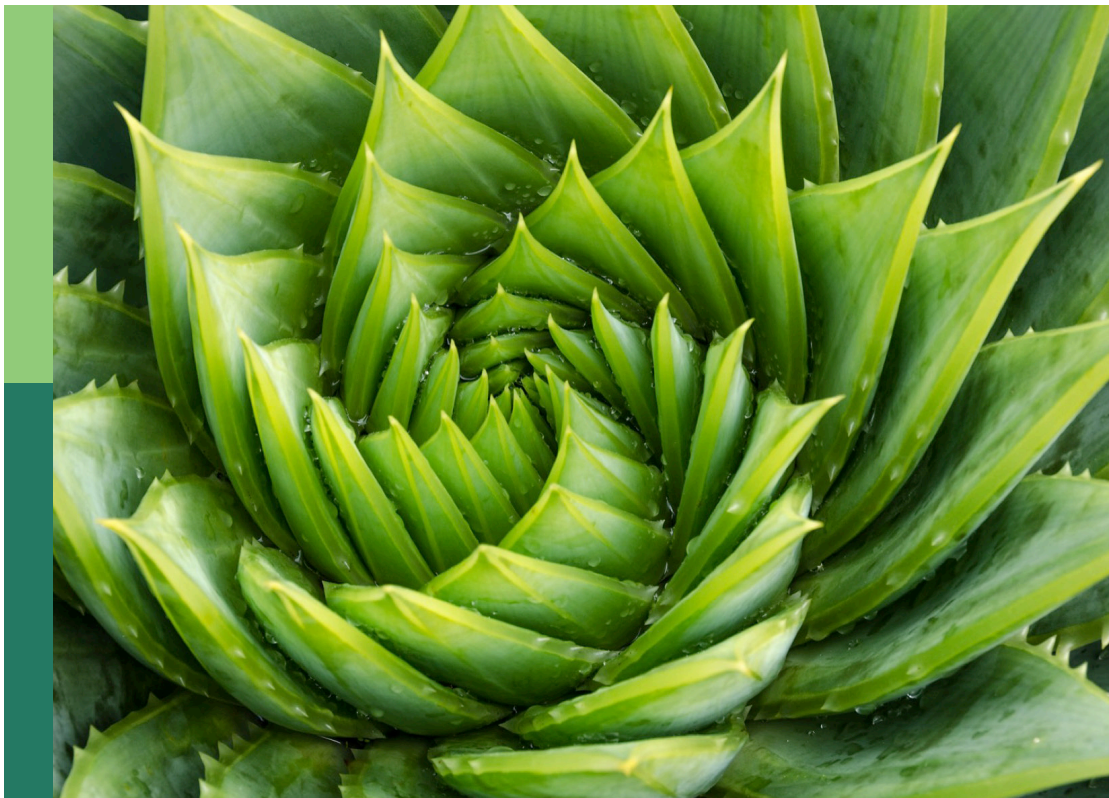

ISSN 1664-8714
ISBN 978-2-8325-4194-4
DOI 10.3389/978-2-8325-4194-4

About Frontiers

Frontiers is more than just an open access publisher of scholarly articles: it is a pioneering approach to the world of academia, radically improving the way scholarly research is managed. The grand vision of Frontiers is a world where all people have an equal opportunity to seek, share and generate knowledge. Frontiers provides immediate and permanent online open access to all its publications, but this alone is not enough to realize our grand goals.

Frontiers journal series

The Frontiers journal series is a multi-tier and interdisciplinary set of open-access, online journals, promising a paradigm shift from the current review, selection and dissemination processes in academic publishing. All Frontiers journals are driven by researchers for researchers; therefore, they constitute a service to the scholarly community. At the same time, the *Frontiers journal series* operates on a revolutionary invention, the tiered publishing system, initially addressing specific communities of scholars, and gradually climbing up to broader public understanding, thus serving the interests of the lay society, too.

Dedication to quality

Each Frontiers article is a landmark of the highest quality, thanks to genuinely collaborative interactions between authors and review editors, who include some of the world's best academicians. Research must be certified by peers before entering a stream of knowledge that may eventually reach the public - and shape society; therefore, Frontiers only applies the most rigorous and unbiased reviews. Frontiers revolutionizes research publishing by freely delivering the most outstanding research, evaluated with no bias from both the academic and social point of view. By applying the most advanced information technologies, Frontiers is catapulting scholarly publishing into a new generation.

What are Frontiers Research Topics?

Frontiers Research Topics are very popular trademarks of the *Frontiers journals series*: they are collections of at least ten articles, all centered on a particular subject. With their unique mix of varied contributions from Original Research to Review Articles, Frontiers Research Topics unify the most influential researchers, the latest key findings and historical advances in a hot research area.

Find out more on how to host your own Frontiers Research Topic or contribute to one as an author by contacting the Frontiers editorial office: frontiersin.org/about/contact

Molecular interactions between bacterial pathogens and plants: Selected contributions to the 14th International Conference on Plant Pathogenic Bacteria (14th ICPPB)

Topic editors

Chiaraluce Moretti — University of Perugia, Italy
Roberto Buonaurio — University of Perugia, Italy
Guido Sessa — Tel Aviv University, Israel
Vittoria Catara — University of Catania, Italy
Michelle Teresa Hulin — The Sainsbury Laboratory, United Kingdom
George W. Sundin — Michigan State University, United States

Citation

Moretti, C., Buonaurio, R., Sessa, G., Catara, V., Hulin, M. T., Sundin, G. W., eds. (2024). *Molecular interactions between bacterial pathogens and plants: Selected contributions to the 14th International Conference on Plant Pathogenic Bacteria (14th ICPPB)*. Lausanne: Frontiers Media SA. doi: 10.3389/978-2-8325-4194-4

Table of contents

frontiers | Frontiers in Plant Science

TYPE Editorial
PUBLISHED 11 December 2023
DOI 10.3389/fpls.2023.1345785

OPEN ACCESS

EDITED AND REVIEWED BY
Ann G. Matthysse,
University of North Carolina at Chapel Hill, United States

*CORRESPONDENCE
Chiaraluce Moretti
chiaraluce.moretti@unipg.it

RECEIVED 28 November 2023
ACCEPTED 30 November 2023
PUBLISHED 11 December 2023

CITATION
Buonaurio R, Moretti C, Catara V, Hulin MT, Sessa G and Sundin GW (2023) Editorial: Molecular interactions between bacterial pathogens and plants: selected contributions to the 14th International Conference on Plant Pathogenic Bacteria (14th ICPPB).
Front. Plant Sci. 14:1345785.
doi: 10.3389/fpls.2023.1345785

Editorial: Molecular interactions between bacterial pathogens and plants: selected contributions to the 14th International Conference on Plant Pathogenic Bacteria (14th ICPPB)

Roberto Buonaurio[1], Chiaraluce Moretti[1]*, Vittoria Catara[2], Michelle T. Hulin[3], Guido Sessa[4] and George W. Sundin[5]

[1]Dipartimento di Scienze Agrarie, Alimentari e Ambientali, Università degli Studi di Perugia, Perugia, Italy, [2]Department of Agriculture, Food and Environment, University of Catania, Catania, Italy, [3]The Sainsbury Laboratory, Norwich Research Park, Norwich, United Kingdom, [4]School of Plant Sciences and Food Security, Tel-Aviv University, Tel-Aviv, Israel, [5]Department of Plant Soil & Microbial Sci, Michigan State University, E Lansing, MI, United States

KEYWORDS

bacterial diagnosis, bacterial genomes, bacterial taxonomy, effectors, phytopathogenic bacteria

Editorial on the Research Topic

Molecular interactions between bacterial pathogens and plants: selected contributions to the 14th International Conference on Plant Pathogenic Bacteria (14th ICPPB)

'The Impact of Plant Pathogenic Bacteria on Global Plant Health' was the slogan accompanying the 14th International Conference on Plant Pathogenic Bacteria (ICPPB), held from 3rd to 8th July, 2022 at Assisi (Italy), which attracted 196 delegates from 37 countries across most continents. Among the 9 scientific sessions of the conference program, the session: Molecular interaction Between Bacterial Pathogens and Plants has been proposed as argument for the present Research Topic, a subject that attracted the attention of many plant pathologists. This Research Topic is dedicated to Nicola Sante Iacobellis co-Chair of the 14th ICPPB and Guido Sessa co-Editor of the present Research Topic who prematurely passed away (Figure 1).

What factors determine and modulate the pathogenicity and virulence of phytopathogenic bacteria in plants is a main question that phytobacteriologists have asked themselves whilst studying plant-bacterium interactions. The tremendous increase in the number of whole-genome sequences of bacterial strains and the powerful tools now available for interpreting sequencing data are providing essential information to answer to this question. The attention is mainly focused on type-3 effectors (T3Es) which in the form of a cocktail are injected into

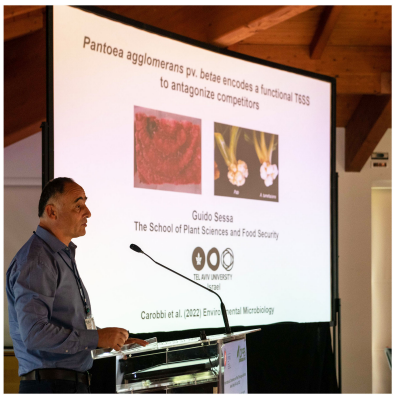

FIGURE 1
Nicola Sante Iacobellis (1949-2022) at the 13th ICPPB-Shanghai-China (2014). Guido Sessa (1964-2023) at the 14th ICPPB-Assisi-Italy (2022). Written informed consent was obtained from the individual(s) for the publication of any identifiable images or data included in this article.

plant cells by many phytopathogenic bacteria through a type-III secretion system and are able to manipulate host processes for the benefit of the bacteria and thus promote disease development.

Using Effectidor: an automated machine-learning-based web server for the prediction of T3Es (Wagner et al., 2022), Wagner et al. discover 6 new T3Es in the newly sequenced genome of *Xanthomonas hortorum* pv. pelargonii isolated in Israel and also in *Xanthomonas fragariae*. They also experimentally validated the translocation of these new T3Es, which are added to the list of many bacterial effectors known today.

Guido Sessa's group fully assembled the genomes of tumorigenic bacteria: *Pantoea agglomerans* pv. betae (Pab) which provokes disease on gypsophila and sugar beet and *P. agglomerans* pv. gypsophilae (Pag) on gypsophila (Manulis and Barash, 2003), and carried out a comparative sequence analysis of the Pab and Pag pathogenicity plasmids (Geraffi et al.). They found two novel type-3 chaperones of the ShcV and CesT families present in both pathovars with high similarity. Geraffi et al. also identified insertion sequences and transposons that may have contributed to the evolution of the two pathovars.

Orfei et al. sequenced the complete genome of *Pseudomonas syringae* pv. tomato strain DAPP-PG 215, race 0 (Buonaurio et al., 1996) and demonstrated that this strain has a race 1 genotype but displays a race 0 phenotype. The DAPP-PG 215 strain is phylogenetically closely related to a number of race 1 strains; its genome bearing *hopW1* and *avrA* genes, which are considered as diagnostic markers for race 1 (Jones et al., 2015), and not the *hopN1* gene, a marker for race 0 strains. However, the genome harbors a complete ortholog of *avrPto1*, which allows the strain to display a race 0 phenotype and is within a prophage: a mobile genetic element that can be responsible for horizontal gene transfer.

Studies aimed at the host plant in the plant-bacteria interactions are mainly focused on plant defense responses and try to answer how the bacterium evade the plant defenses to cause disease. These studies open up opportunities to identify new strategies to fight plant bacterial diseases.

Walls Are Thin1 (*WAT1*) is a susceptible plant gene encoding a tonoplast localized vacuolar auxin transporter first found in Arabidopsis that enables the infection process of vascular pathogens; the Arabidopsis *wat1-1* mutant was found to be resistant to a broad range of vascular pathogens, including *Ralstonia solanacearum* (Denancé et al., 2013).

Through RNAi and CRISPR/Cas9 strategy, Koseoglou et al. inactivated the orthologous gene *SlWAT1* in tomato and demonstrated that this inactivation both reduced free auxin contents and ethylene synthesis in tomato stems and suppressed the expression of specific bacterial virulence factors of the vascular bacterium *Clavibacter michiganensis*.

In nature and in general, *Xylella fastidiosa* attacks and provokes severe damage on woody hosts for example on olive trees. To facilitate the study of the interaction of this bacterium with the plants, several herbaceous models have been tried. Barò et. al. demonstrated that *Nicotiana benthamiana* is a suitable model as the bacterium reaches a high population level after the inoculation and induce a rapid symptom development with low variability in the response. The same Authors demonstrated that *N. benthamiana* treated with the antimicrobial peptide BP134 or plants in which this peptide gene was transiently expressed showed reduction in disease severity provoked by *X. fastidiosa*. Antimicrobial peptides against plant pathogenic bacteria, *X. fastidiosa* included, are therefore possible candidates to develop novel biopesticides (Badosa et al., 2022).

Efflux pumps form part of the resistance mechanism employed by bacteria to permit their survival in the hostile plant chemical environment (Pasqua et al., 2019). Pun et al. studied in *Pectobacterium brasiliense* the effect of some efflux pump inhibitors and plant-derived phytochemicals on bacterial activity and found that PabN and NMP were the best efflux pump inhibitors. They suggested that the efflux pump system AcrAB-TolC plays an important role in survival and fitness of *P. brasiliense* in the plant environment and that its inhibition is a viable strategy for controlling bacterial pathogenicity.

Effective management of plant bacterial diseases is very difficult (Sundin et al., 2016; Sharma et al., 2022). Determining the identity of bacterial plant pathogens is essential to disease management, and this process is linked to bacterial taxonomy (Bull and Koike, 2015).

Gašic´et al. proposed a novel species *Brenneria izbisi* as causal agent of deep bark canker of young walnut trees. Two other *Brenneria* spp. are described on walnut: *B. nigrifluens* and *B. rubrifaciens* as agents of shallow-bark canker and deep bark canker, respectively. They represent a serious threat to walnut production by the weakening of trees and consequent reduction in the number of nuts and in timber production. A rapid and specific conventional PCR protocol to identify the novel species was also proposed.

Kałuz˙na et al. developed molecular tools for identification of *Xanthomonas arboricola* pv. corylina that could be used with PCR, qPCR, and Loop-mediated isothermal amplification. The authors validated each of the tools using genomic DNA isolated from pure cultures of the bacterium and DNA isolated from artificially inoculated and field-infected plant material. These fast and accurate identification and detection methods will aid in the diagnosis and management of bacterial blight of hazelnut in nursery stock tissues, nurseries, and in both young and established orchards.

Finally, Hugouvieux-Cotte-Pattat et al. presented a taxonomical update of the *Dickeya* genus, whose species attack a wide range of crops and ornamentals causing soft rot symptoms. They resumed knowledge on the genus *Dickeya* and added new data from phenotypic, genomic and phylogenetic analyses.

Author contributions

RB: Writing – original draft, Writing – review & editing. CM: Writing – original draft, Writing – review & editing. VC: Writing – review & editing. MH: Writing – review & editing. GS: Writing – original draft. GS: Writing – review & editing.

Conflict of interest

The authors declare that the research was conducted in the absence of any commercial or financial relationships that could be construed as a potential conflict of interest.

Publisher's note

References

Badosa, E., Planas, M., Feliu, L., Montesinos, L., Bonaterra, A., and Montesinos, E. (2022). Synthetic peptides against plant pathogenic bacteria. *Microorganisms* 10.9, 1784. doi: 10.3390/microorganisms10091784

Bull, C. T., and Koike, S. T. (2015). Practical benefits of knowing the enemy: modern molecular tools for diagnosing the etiology of bacterial diseases and understanding the taxonomy and diversity of plant-pathogenic bacteria. *Annu. Rev. Phytopathol.* 53, 157–180. doi: 10.1146/annurev-phyto-080614-120122

Buonaurio, R., Stravato, V. M., and Capelli, C. (1996). Occurrence of *Pseudomonas syringae* pv. *tomato* race 1 in Italy on *Pto* gene-bearing tomato plants. *J. Phytopathol.* 144, 437–440. doi: 10.1111/j.1439-0434.1996.tb00320.x

Denancé, N., Ranocha, P., Oria, N., Barlet, X., Rivière, M. P., Yadeta, K. A., et al. (2013). Arabidopsis *wat1* (*walls are thin1*)-mediated resistance to the bacterial vascular pathogen, *Ralstonia solanacearum*, is accompanied by cross-regulation of salicylic acid and tryptophan metabolism. *Plant J.* 73, 225–239. doi: 10.1111/tpj.12027

Jones, L. A., Saha, S., Collmer, A., Smart, C. D., and Lindeberg, M. (2015). Genome-assisted development of a diagnostic protocol for distinguishing high virulence *Pseudomonas syringae* pv. *tomato* strains. *Plant Dis.* 99, 527–534. doi: 10.1094/PDIS-08-14-0833-RE

Manulis, S., and Barash, I. (2003). *Pantoea agglomerans* pvs. *gypsophilae* and *betae*, recently evolved pathogens? *Mol. Plant Pathol.* 4, 307–314. doi: 10.1046/j.1364-3703.2003.00178.x

Pasqua, M., Grossi, M., Zennaro, A., Fanelli, G., Micheli, G., Barras, F., et al. (2019). The varied role of efflux pumps of the MFS family in the interplay of bacteria with animal and plant cells. *Microorganisms* 7, 285. doi: 10.3390/microorganisms7090285

Sharma, A., Abrahamian, P., Carvalho, R., Choudhary, M., Paret, M. L., Vallad, G. E., et al. (2022). Future of bacterial disease management in crop production. *Annu. Rev. Phytopathol.* 60, 259–282. doi: 10.1146/annurev-phyto-021621-121806

Sundin, G. W., Castiblanco, L. F., Yuan, X. C., Zeng, Q., and Yang, C. H. (2016). Bacterial disease management: challenges, experience, innovation and future prospects. *Mol. Plant Pathol.* 17, 1506–1518. doi: 10.1111/mpp.12436

Wagner, N., Avram, O., Gold-Binshtok, D., Zerah, B., Teper, D., and Pupko, T. (2022). Effectidor: an automated machine-learning-based web server for the prediction of type-III secretion system effectors. *Bioinformatics* 38, 2341–2343. doi: 10.1093/bioinformatics/btac087

frontiers | Frontiers in Plant Science

TYPE Original Research
PUBLISHED 24 November 2022
DOI 10.3389/fpls.2022.1055186

OPEN ACCESS

EDITED BY
Chiaraluce Moretti,
University of Perugia, Italy

REVIEWED BY
Carrie Brady,
University of the West of England, United Kingdom
Teresa Ann Coutinho,
University of Pretoria, South Africa
David J. Studholme,
University of Exeter, United Kingdom

*CORRESPONDENCE
Katarina Gašić
gasickatarina@yahoo.com;
katarina.gasic@izbis.bg.ac.rs
Nemanja Kuzmanović
nemanja.kuzmanovic@julius-kuehn.de;
kuzmanovic1306@gmail.com

SPECIALTY SECTION
This article was submitted to Plant Pathogen Interactions, a section of the journal Frontiers in Plant Science

RECEIVED 27 September 2022
ACCEPTED 24 October 2022
PUBLISHED 24 November 2022

CITATION
Gašić K, Zlatković N and Kuzmanović N (2022) Polyphasic study of phytopathogenic bacterial strains associated with deep bark canker of walnut in Serbia revealed a new species, *Brenneria izbisi* sp. nov. *Front. Plant Sci.* 13:1055186. doi: 10.3389/fpls.2022.1055186

Polyphasic study of phytopathogenic bacterial strains associated with deep bark canker of walnut in Serbia revealed a new species, *Brenneria izbisi* sp. nov

Katarina Gašić[1]*, Nevena Zlatković[1] and Nemanja Kuzmanović[2]*

[1]Department of Plant Diseases, Institute for Plant Protection and Environment (IPPE), Belgrade, Serbia, [2]Julius Kühn Institute (JKI), Federal Research Centre for Cultivated Plants, Institute for Plant Protection in Horticulture and Urban Green, Braunschweig, Germany

Serious outbreaks of walnut deep bark canker were observed on young walnut trees (*Juglans regia* L.) in two localities in the northern part of Serbia during 2020. From the symptomatic walnut tissues, two types of bacterial colonies were isolated, predominantly, light cream, circular and smooth colonies, as well as small, yellowish, mucoid and convex ones. PCR analysis and phenotypic assays suggested that the former group belongs to *Brenneria* spp., while the latter isolates were identified as *Xanthomonas arboricola* pv. *juglandis*. Within the *Brenneria* group, two strains were identified as *Brenneria nigrifluens*, while other 15 strains did not belong to any *Brenneria* species described so far. Therefore, we selected four representative strains of the unknown *Brenneria* sp. and subjected them to polyphasic analysis. As expected, in a phylogenetic tree based on partial 16S rDNA sequences, four novel strains grouped with other *Brenneria* representatives, and showed close phylogenetic relationship to *Brenneria salicis*. Furthermore, multilocus sequence analysis (MLSA) based on the partial sequences of *atpD, gyrB*, *infB* and *rpoB* housekeeping genes and core-genome phylogeny indicated that the studied strains form a novel and a clearly separate *Brenneria* lineage. Overall genome relatedness indices showed that they represent a new *Brenneria* species. The new species can be differentiated from the other *Brenneria* spp. infecting walnut and closely related *B. salicis* strains based on phenotypic characteristics, as well. Moreover, the pathogenicity tests on two-year-old walnut plants proved the ability of strains to cause necrosis and longitudinal black lesions and cracks on the trunk and branches of walnut trees. Overall, polyphasic characterization showed that the studied strains isolated from walnut with symptoms of deep bark canker represent a novel species of the genus *Brenneria* for which the name *Brenneria izbisi* sp. nov. is proposed. The type strain of *B. izbisi* is KBI 423^T (= CFBP 9035^T = LMG 32479^T). To facilitate rapid identification of newly described species, a conventional PCR protocol and primers targeting the putative gene *hrpP*, were developed. Further study should

reveal the potential role of each pathogen isolated from symptomatic walnut in disease development as well as possible interaction between them.

KEYWORDS

Juglans regia, bacterial disease, MLSA, ANI, primer design, whole-genome sequencing, *Brenneria*, *Pectobacteriaceae*

Introduction

Global demand for tree nuts has increased considerably in recent years, leading to expansion of planted area of the almond, walnut, and hazels, as the three major nut crops. Walnut is considered as the most important nut crop worldwide, of which production is constantly increasing. According to FAOSTAT (2022)[1], the area of the walnut orchards reached 1.02 million ha, with total production 3.3 million tones in shell at global level in 2020. In Serbia, interest in English (Persian) walnut (*Juglans regia* L.) production has recently expanded due to the market and export potential. The total walnut planted area in 2017 was 3.307 ha, reaching 12.276 t of total yield, according to Statistical Office of the Republic of Serbia[2]. Commercial walnut plantations were mainly established with imported propagation material, mostly originating from Turkey, which is the fourth biggest producer after China, USA and Iran (FAOSTAT, 2022)[1].

Walnut production can be compromised by different biotic factors, including plant pathogenic bacteria. *Xanthomonas arboricola* pv. *juglandis* (*Xaj*) (Vauterin et al., 1995) is the causal agent of walnut bacterial blight (WBB), the most important bacterial disease of walnut worldwide, including Serbia (Du Plessis and van der Westhuizen, 1995; Scortichini et al., 2001; Kałuzna et al., 2014; Ivanović et al., 2015; Giovanardi et al., 2016; Fu et al., 2018). The symptoms of WBB can be observed on all aboveground organs, including leaves, twigs, catkins and fruits. *Xaj* has been also associated with symptoms of brown apical necrosis (BAN) at the stigmatic end of the fruit (Belisario et al., 2002; Moragrega and Özaktan, 2010; Moragrega et al., 2011), and vertical oozing canker (VOC) developed in woody tissue (Hajri et al., 2010). Symptoms of VOC are characterized by development of vertical cankers on affected trunks and branches, with oozing exudates occurring mainly during summer (Hajri et al., 2010). Other pathogens affecting walnut trunks and branches belong to the genus *Brenneria*. *Brenneria nigrifluens* (*Bn*) (Wilson et al., 1957; Hauben et al., 1998) is the causal agent of shallow bark canker, while *Brenneria rubrifaciens* (*Br*) causes deep bark canker on walnut (Wilson et al., 1967). Both diseases show similarities in external canker symptoms and production of black exudate (sap wood) and were first occurred in the USA (Wilson et al, 1957; Wilson et al, 1967). In Europe, *Bn* was first recorded in Spain (López et al., 1994), followed by its occurrence in Italy (Saccardi et al., 1998; Morone et al., 1998), Serbia (Popovic et al., 2013), France (Ménard et al., 2004), Hungary (Végh et al., 2014), and recently in Turkey (Soylu et al., 2021). On the other hand, *Br* was reported, for the first time in Europe, on walnut trees in Spain imported from California (González et al., 2002).

So far, among phytopathogenic bacteria causing disease on walnut in Serbia, *Xaj* was detected and characterized as a causal agent of WBB (Gavrilović and Arsenijević, 1998; Ivanović et al., 2015). In 2013, Popovic et al. (2013) reported the presence of *Bn* in a 30-year-old walnut orchard in the Fruška Gora region. However, recently, unusual symptoms of bark canker were observed on four-year-old walnut trees (*Juglans regia* L.) cv. Chandler in a 1-ha orchard in northern part of Serbia, province of Vojvodina (Vrbas) in September 2020. Disease symptoms included dark brown to black, roundish, sunken lesions on the bark of trunks and lower branches. Affected bark developed longitudinal cracks that oozed a dark liquid, leaving glossy dark traces just below the wounds. Removing the bark revealed extensive discoloration of the tissue in longitudinal blackish lesions that extended deeper into the xylem. On some trees, progressive infection resulted in cankers that spread along the trunk, subsequently killing the tree. The incidence of the disease was approx. 70%, and 1% of the trees died in the time of sampling. Subsequently, similar symptoms of disease were observed on four-year-old walnut trees in another walnut orchard (Sivac, 8 ha), in the same region. Propagation material, two-year old walnut trees, for both orchards was imported. The primary objective of the present study was to identify and characterize bacteria associated with the new walnut disease in Serbia.

Materials and methods

Plant sampling and bacterial isolation

The samples that contained parts of diseased walnut branches and trunks showing symptoms of deep bark canker and

1 https://www.fao.org/faostat/en/#data/QCL.

2 https://data.stat.gov.rs/Home/Result/13050301?languageCode=en-US.

longitudinal oozing cracks (Figures 1, 2) were collected in orchards in the north part of Serbia in the late summer (September, 2020). Bacterial isolation was carried out from several sections of the symptomatic walnut tissue. Briefly, fresh fragments from border area between apparently healthy and diseased tissue under the bark and deeper in the region of the xylem, were macerated in 1 ml of sterile distilled water (SDW). The macerate was incubated at room temperature for 10 min and streaked onto King's medium B (KB) (King et al., 1954), followed by incubation at 27°C. The sapwood samples found in small cracks were also used for isolation on KB medium. After 3 days, bacterial colonies were purified and maintained on KB medium for further testing. Long-term storage of bacterial isolates was achieved at -80°C in a mixture of nutrient broth medium and 30% glycerol (Schaad et al., 2001).

Sources of bacterial strains used within this study, including reference strains, are listed in Table 1 and Table S1.

Physiological and biochemical tests

In order to identify and characterize isolates, various physiological and biochemical tests were performed. They were tested for Gram reaction using 3% KOH, catalase activity, fluorescence on KB, oxidative–fermentative (O/F) test, oxidase activity, levan production, pectinolytic activity on potato slices and production of a hypersensitive reaction (HR) on tobacco (*Nicotiana tabacum* cv. 'Samsun') and geranium (*Pelargonium* x *hortorum*) leaves (Lelliott and Stead, 1987). The isolates were grown on different media such as KB, Yeast extract - Dextrose-Calcium carbonate agar (YDC), Yeast-Peptone-Glucose Agar (YPGA), Nutrient Agar supplemented with 5% sucrose w/v (NSA) (Schaad et al., 2001) Additional biochemical and physiological analyses of seven walnut isolates (KBI 423^T, KBI 424, KBI 429, KBI 430, KBI 447, KBI 446 and KBI 449), including two reference strains LMG 2709^T of *Brenneria salicis* (*Bs*) and LMG 2698^T of *Br*, were conducted using the API 20E, API 20NE, and API 50CH systems (bioMérieux). For API 20E and API 20NE, the pure bacterial cultures grown on KB medium for 24 h were suspended in 0.85% NaCl solution. Concentration of bacterial suspensions was adjusted to ~10^8 CFU/ml photometrically (OD_{600} = 0.3). Further, the test strips were handled by following manufacturer instructions. For API 50CH, the bacteria were suspended in API 50 CHB/E medium (bioMérieux) in the same concentration. API strips were incubated at 27°C for 48 h (Biosca and López, 2012). Obtained results were compared with data available in the literature (Brady et al., 2012; Brady et al., 2014). All API tests were conducted in three replicates.

Pathogenicity assay

Pathogenicity of the isolates was assessed by inoculating two-year-old walnut plants cv. Chandler grown in pots, by method of Moretti et al. (2007), with slight modifications. Six *Brenneria* isolates (KBI 423^T, KBI 424, KBI 429, KBI 446, KBI 447 and KBI 449) and one isolate of *Xaj* (KBI 435) were selected for testing. The plants were inoculated by infiltration of 20 µl of bacterial suspension (~10^8 CFU/ml, OD_{600} = 0.3) into 2-cm-long vertical stem wounds made aseptically by a scalpel. Two plants with three wounds (inoculation points), per each strain were inoculated. SDW was used as a negative control. Inoculated tissue was covered by wet cotton pad and wrapped with a Parafilm tape for four days to prevent drying out. One month post-inoculation, new, young saplings (shoots) were developed on the test plants. They were also inoculated by above described method with a slight

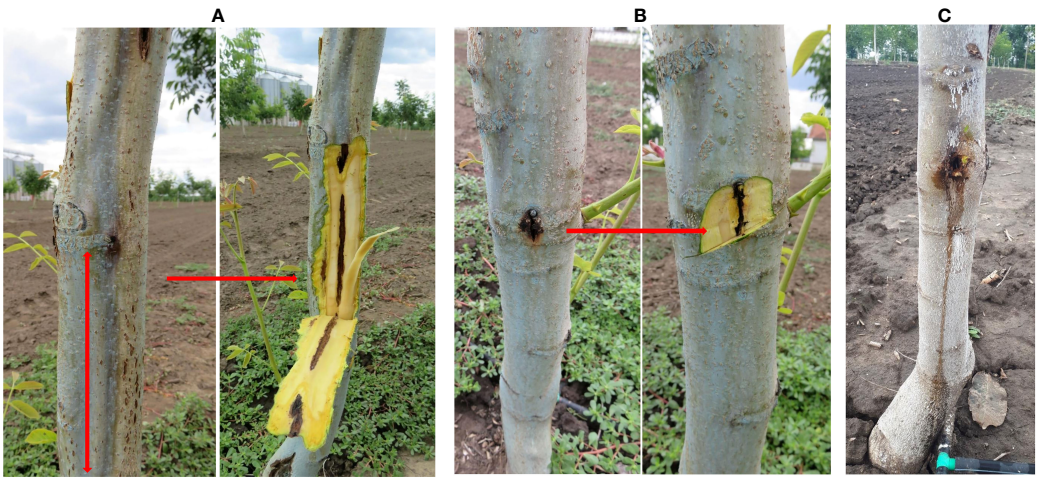

FIGURE 1
Symptoms of deep bark canker on walnut, before and after bark removal. **(A)** Dark brown to black, sunken longitudinal lesions under the bark of walnut; **(B)** Extensive discoloration of the tissue that extend deeper into the xylem; **(C)** Longitudinal oozing cracks. Natural infection.

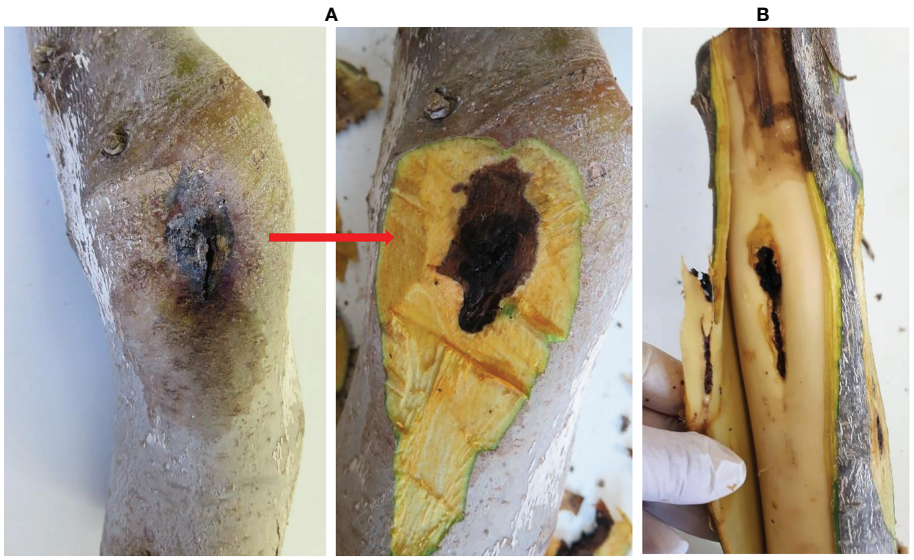

FIGURE 2
Isolation from the symptomatic walnut samples. **(A)** Dark, roundish, sunken lesions before and after removing the bark; **(B)** Necrotic lesions under the bark extended into the xylem tissue. Natural infection.

modification – 1 cm longitudinal wound was made by scalpel and there were two inoculation sites per plant. Test plants were maintained in the greenhouse for 2 months. Afterwards, the pots were moved outside and observed for the next 14 months. The appearance of external and internal symptoms was recorded two and 14 months post-inoculation. Re-isolation of bacteria from inoculated plants (two and 14 months post-inoculation) was performed on KB medium and their identity was confirmed by PCR assay.

Additionally, pathogenicity of the representative isolates (KBI 423^T, KBI 446 and KBI 435) was tested on immature walnut fruits prior to crust hardening. After surface sterilization with 70% alcohol, the fruits were injured on three sites by sterile tip and inoculated with 30 µl of tested bacterial suspension (~10^8 CFU/ml). The test was performed in three replications. The reference strain of *Bn* KBI 024 (Popovic et al., 2013), type strains LMG 2709^T of *Br* and LMG 2698^T of *Bs*, were used as controls. SDW was used as a negative control. The fruits were placed in a sterile, humid, plastic chamber and incubated at 27°C for 15 days in dark conditions. Bacteria were re-isolated on KB and their identity was confirmed by PCR assay.

DNA extraction

Total genomic DNA was extracted from pure bacterial cultures using the cetyl trimethyl ammonium bromide (CTAB) protocol, according to the instructions described by Angelini et al. (2001), with slight modifications. Bacterial suspensions (~10^9 CFU/ml) were prepared in 500 µl 10 mM phosphate saline buffer (Na_2HPO_4 × 12 H_2O 2.7 g/l, NaH_2PO_4 × 2 H_2O 0.4 g/l). Afterwards, 500 µl extraction buffer (3% CTAB, 1M Tris-HCL pH 8.0, 1.4 M NaCl, 20 mM EDTA, 3% PVP) was added in the equal volume of bacterial suspensions and incubated at 65°C for 20 min. The following steps were as described in original protocol.

For whole-genome sequencing, DNA of isolates KBI 423^T and KBI 447 was extracted using the DNeasy Plant Mini Kit (Qiagen, Hilden, Germany). The quality of extracted DNA was checked by gel electrophoresis on 0.8% agarose gel and then stored at −20°C for further analysis.

PCR analyses

Based on host plant, disease symptoms and colony morphology, we assumed that causal agents of infection might belong to genera *Brenneria* and/or *Xanthomonas*. Therefore, three PCR reactions were performed by using: *Bn*-specific primers F1/C3 (Loreti et al., 2008); primer pair BR1/BR3 specific for *Br* (McClean et al., 2008) and XajF/XajR primers specific for *Xaj* (Gironde et al., 2009). Additionaly, we applied a PCR with primers Es1A/Es4B, specific for *Bs* (Hauben et al., 1998). Amplified PCR products (5 µL) were separated by gel electrophoresis in 1.5% agarose gel in 0.5 × Tris-Borate-EDTA (TBE) buffer stained with 2% (v/v) Midori Green (MIDORI Green Advance, NIPPON Genetics EUROPE) and visualized by a digital imaging camera (Vilber Lourmat, France). All primers sequences used in this study are shown in Table S2.

10.3389/fpls.2022.1055186

TABLE 1 Bacterial strains used in this study and results of PCR analysis.

Strain	Species	Year of isolation	Origin	Host plant	Source[a]	PCR analysis				
						F1/C3	BR1/BR3	Es1A/Es4B	Bi-hrpP-F/Bi-hrpP-R	XajF/XajR
KBI 422	*Brenneria izbisi*	2020	Vrbas, Serbia	*Juglans regia*	This study	–	–	+	+	NT
KBI 423^T (=LMG 32479^T, =CFBP 9035^T)	*Brenneria izbisi*	2020	Vrbas, Serbia	*Juglans regia*	This study	–	–	+	+	NT
KBI 424	*Brenneria izbisi*	2020	Vrbas, Serbia	*Juglans regia*	This study	–	–	+	+	NT
KBI 425	*Brenneria izbisi*	2020	Vrbas, Serbia	*Juglans regia*	This study	–	–	+	+	NT
KBI 426	*Brenneria izbisi*	2020	Vrbas, Serbia	*Juglans regia*	This study	–	–	+	+	NT
KBI 427	*Brenneria izbisi*	2020	Vrbas, Serbia	*Juglans regia*	This study	–	–	+	+	NT
KBI 428	*Brenneria izbisi*	2020	Vrbas, Serbia	*Juglans regia*	This study	–	–	+	+	NT
KBI 429	*Brenneria izbisi*	2020	Vrbas, Serbia	*Juglans regia*	This study	–	–	+	+	NT
KBI 430	*Brenneria izbisi*	2020	Vrbas, Serbia	*Juglans regia*	This study	–	–	+	+	NT
KBI 431	*Brenneria izbisi*	2020	Vrbas, Serbia	*Juglans regia*	This study	–	–	+	+	NT
KBI 432	*Brenneria izbisi*	2020	Vrbas, Serbia	*Juglans regia*	This study	–	–	+	+	NT
KBI 433	*Brenneria izbisi*	2020	Vrbas, Serbia	*Juglans regia*	This study	–	–	+	+	NT
KBI 434	*Brenneria izbisi*	2020	Vrbas, Serbia	*Juglans regia*	This study	–	–	+	+	NT
KBI 447	*Brenneria izbisi*	2020	Sivac, Serbia	*Juglans regia*	This study	–	–	+	+	NT
KBI 448	*Brenneria izbisi*	2020	Sivac, Serbia	*Juglans regia*	This study	–	–	+	+	NT
KBI 446	*Brenneria nigrifluens*	2020	Sivac, Serbia	*Juglans regia*	This study	+	–	–	–	NT
KBI 449	*Brenneria nigrifluens*	2020	Sivac, Serbia	*Juglans regia*	This study	+	–	–	–	NT
KBI 435- KBI 439	*Xanthomonas arboricola* pv. *juglandis*	2020	Vrbas, Serbia	*Juglans regia*	This study	NT	NT	NT	NT	+
KBI 440- KBI 445	*Xanthomonas arboricola* pv. *juglandis*	2020	Sivac, Serbia	*Juglans regia*	This study	NT	NT	NT	NT	+
KBI 024	*Brenneria nigrifluens*	2011	Serbia	*Juglans regia*	KBI	+	–	–	–	NT
LMG 2709^T	*Brenneria rubrifaciens*	unknown	USA	*Juglans regia*	LMG	–	+	–	–	NT
LMG 2698^T	*Brenneria salicis*	1957	UK	*Salix alba*	LMG	–	–	+	–	NT

[a]KBI, Collection of Bacteria, Institute for Plant Protection and Environment, Belgrade, Serbia; LMG, Bacteria Collection, Ghent University, Belgium.
-, no amplification product observed on agarose gel; +, production of the specific amplification fragment from genomic DNA; NT- non tested.

Phylogenetic analysis of 16S rRNA and housekeeping genes

The 16S rRNA and housekeeping gene fragments were amplified and sequenced (Macrogene Europe, The Netherlands) for several representative strains. The partial sequence of 16S rDNA of strains KBI 423^T, KBI 424, KBI 428 and KBI 429 was amplified using universal pair of primers fD1 and rP2 (Weisburg et al., 1991). Four representative *Brenneria* strains (KBI 423^T, KBI 429, KBI 430 and KBI 447) belonging to the unknown species were selected for

multilocus sequence analysis (MLSA). PCR amplification and partial sequencing of four housekeeping genes, *atpD, gyrB, infB*, and *rpoB*, was conducted according to the protocol of Brady et al. (2008).

Chromatograms were visualized using FinchTV 1.4.0 software and sequences were processed using the MEGA 7 package (Kumar et al., 2016). In order to align the sequences, CLUSTAL W algorithm (Higgins et al., 1996) integrated into MEGA 7 software (Kumar et al., 2016) was used. For comparative analysis of the obtained sequences with the sequences deposited in the NIH GenBank, the BLASTn program was used (Altschul et al., 1997). The maximum likelihood (ML) phylogenies based on 16S rDNA and concatenated sequences of housekeeping genes were inferred using IQ-TREE 1.6.12 (Nguyen et al., 2015) software available through the IQ-TREE web server[3] (Trifinopoulos et al., 2016). A model selection was conducted using IQ-TREE ModelFinder (Kalyaanamoorthy et al., 2017). The best-fit DNA substitution models HKY+F+I+G4 (16S rDNA) and TIM2+F+I+G4 (housekeeping genes, concatenated dataset) were selected based on Bayesian Information Criterion (BIC). Branch support was assessed by ultrafast bootstrap analysis (UFBoot) using 1000 replicates (Hoang et al., 2018). The tree was visualized using FigTree, v1.4.4[4] (Rambaut, 2018).

Strains differentiation by rep-PCR

Genetic relatedness among the strains was evaluated by rep-PCR fingerprinting. Seventeen *Brenneria* spp. isolates recovered within this study were amplified in three PCR reactions by BOXA1R, REP1R-I/REP2-I and ERIC1R/ERIC2 primers (Versalovic et al., 1991; Versalovic et al., 1994). Amplified fragments were separated by gel electrophoresis in 1.5% agarose gel in 0.5 × TBE buffer and visualized as described above.

Whole-genome sequencing, assembly and annotation

Whole-genome sequencing was conducted for two *Brenneria* isolates, KBI 423^T and KBI 447. The library preparation, sequencing and initial processing of reads was performed by Novogene, Cambridge, United Kingdom. The genomic DNA was randomly sheared into short fragments (~350bp). DNA libraries were prepared with NEBNext Ultra II DNA Library Prep Kit for Illumina (New England Biolabs). Sequencing was performed on Illumina NovaSeq PE150 platform. A total of 2×8,784,885 and 2×8,152,797 paired-end reads were generated for strains KBI 423^T and KBI 447, respectively. Furthermore, adapter trimming and quality filtering of raw reads were conducted with Cutadapt ver. 3.7 (Martin, 2011). *De novo* sequence assembly was performed using SPAdes 3.15.3 (with options -k 21,33,55,77 and –isolate) (Prjibelski et al., 2020). Short (<200 bp) and low-coverage (<3-fold) contigs were discarded. Furthermore, the Illumina reads were mapped to the remaining contigs with BWA-MEM (Galaxy Version 0.7.17.2) (Li, 2013), to manually curate assemblies, involving correction of sequence errors and mis-assemblies. The genome sequences were annotated using Prokka (Galaxy Version 1.14.6+galaxy1) (Seemann, 2014) and NCBI Prokaryotic Genomes Annotation Pipeline (PGAP) (Tatusova et al., 2016).

Core-genome phylogenetic analysis

Core-genome phylogeny was inferred using the GET_HOMOLOGUES Version 11042019 (Contreras-Moreira and Vinuesa, 2013) and GET_PHYLOMARKERS Version 2.2.8_18Nov2018 (Vinuesa et al., 2018) software packages as described before (Kuzmanović et al., 2022). The dataset contained two strains studied (KBI 423^T and KBI 447), as well as reference strains of *Brenneria* (14 strains), *Dickeya* (3 strains), *Lonsdalea* (3 strains) and *Pectobacterium* (3 strains). As an outgroup, we used members of the family *Erwiniaceae*, including *Erwinia* spp. (4 strains) and *Pantoea* spp. (4 strains) (Table S3).

Overall genome relatedness indices

The species delineation was assessed by different overall genome relatedness indices (OGRIs), including the average nucleotide identity (ANI) (Goris et al., 2007) and digital DNA-DNA hybridization (dDDH) (Meier-Kolthoff et al., 2013). The ANI calculations were performed using PyANI program Version 0.2.11, with scripts employing BLAST+ (ANIb) and MUMmer (ANIm) algorithm to align the input sequences[5] (Pritchard et al., 2016), and OrthoANIu Version 1.2 (calculates orthologous ANI using USEARCH algorithm) (Yoon et al., 2017). The dDDH values were computed by the Genome-to-Genome Distance Calculator (GGDC 2.1)[6] using the recommended BLAST+ alignment and formula 2 (identities/HSP length) (Meier-Kolthoff et al., 2013).

Development of the specific PCR assay

For molecular detection, identification and differentiation of novel *Brenneria* strains characterized in this study, we developed

3 http://iqtree.cibiv.univie.ac.at.

4 http://tree.bio.ed.ac.uk/software/figtree/.

5 https://github.com/widdowquinn/pyani.

6 http://ggdc.dsmz.de/distcalc2.php.

a specific PCR assay. Specific primers were designed based on the sequence of the putative gene *hrpP* (locus_tag="NC856_01210" in assembly referring to strain KBI 423^T) coding for type III secretion system HrpP C-terminal domain-containing protein. Candidate primers were identified at nucleotide positions 90–114 and 407–429 and were designated Bi-hrpP-F (5′-TGATAGCTTTTGGGAAGAGTTCGCT-3′) and Bi-hrpP-R (5′-ACAGGATTCACGCCGATCTTTCA-3′), respectively. The PrimerQuest tool by Integrated DNA technologies (IDT) was used to design primers (Integrated DNA Technologies, Coralville, IA). The size of the amplification product is 340 bp. Specificity of the primer set was tested with 46 strains (Table S1) and additionally checked *in silico* by performing NCBI Primer-BLAST against the non-redundant (nr) and "Refseq representative genomes" databases[7].

The PCR amplifications were performed in a 15 µl mixture containing: 1 × Color OptiTaq PCR Master Mix (EURx, Gdańsk, Poland) (1.25 U OptiTaq DNA Polymerase; 1× Reaction Buffer with 1.5 mM $MgCl_2$; 0.2 mM of each dNTP), 0.5 µM of each primer and 1.5 µl template DNA. The thermal profile was as follows: initial denaturation at 95°C for 2 min, 35 cycles of denaturation at 95°C for 30 s, annealing at 60°C for 30 s, elongation at 72°C for 30 s, and final extension at 72°C for 5 min. Reaction were performed in a Thermal Cycler 2720 (Applied Biosystems, Foster City, CA, USA).

Accession numbers

The GenBank accession numbers for the partial 16S rRNA gene sequences of the Brenneria strains KBI 423T, KBI 424, KBI 428 and KBI 429 are MW485945 to MW485948, respectively. Generated (Table S3) partial sequences of housekeeping genes for Brenneria strains KBI 447, KBI 430, KBI 429, KBI 423T, were deposited in the NIH GenBank database under accession numbers ON228202 to ON228205 for atpD gene, ON638957 to ON638960 for infB, ON638961 to ON638964 for gyrB and ON638965 to ON638968 for rpoB, respectively (Table S3).

The Whole Genome Shotgun projects have been deposited at DDBJ/ENA/GenBankunder the accessions JAMPJT000000000 (KBI 447) and JAMPJU000000000 (KBI 423T); within the BioProject PRJNA832546. The versions described in this paper are the first versions, JAMPJT010000000 and JAMPJU010000000. The raw sequencing reads were deposited in the Sequence Read Archive (SRA) under the same BioProject PRJNA832546.

7 https://www.ncbi.nlm.nih.gov/pubmed/?term=22708584

Results

Sampling, isolation and phenotypic characterization of bacterial strains

Bacterial strains were isolated from the symptomatic walnut samples collected in two localities in the northern part of Serbia. After 2 to 3 days of incubation at 27°C on KB medium, two major types of colonies were observed. Light cream, circular and smooth colonies with entire margins were predominant on the KB plates. The second group consisted of small, yellowish, circular and convex colonies resembling *Xanthomonas* species. The former strains were Gram- and oxidase negative, facultatively anaerobic, levan positive, nonfluorescent, and did not produce bright-red pigment on YDC and YPGA medium. Seventeen tested isolates showed phenotypic characteristics as described for type *Brenneria* spp. (Table 1) (Brady et al., 2012). In particular, they showed no pectinolytic activity on potato slices. They did not induce hypersensitive reaction on tobacco leaves but induced HR reaction on geranium 24 h after inoculation. Strains KBI 446 and KBI 449 did not induce HR response in any test plant. No symptoms were observed on tissue inoculated with SDW.

Seven representative strains were selected for further analysis by API 20E, API 20NE, and API 50CH tests and compared with strain LMG 2698^T of *Bs*, LMG 2709^T of *Br*, as well as literature data for *B. goodwinii*, *B. alni*, *B. rosae* subsp. *rosae* and *Lonsdalea quercina* (Brady et al., 2012; Brady et al., 2014). Five representative strains (KBI 423^T, KBI 424, KBI 429, KBI 430 and KBI 447) showed phenotypic traits as follow: positive reactions for acid production from L-arabinose, D-galactose, inositol, melibiose, raffinose, potassium gluconate, glycerol, and negative reactions from gentiobiose, D-sorbitol, trehalose, turanose, amygdalin and D-xylose (Table 2). The obtained results were compared with features already determined for other *Brenneria* species (Brady et al., 2012), and we found that these strains showed unique characteristics as they did not fit into any already existing profile. Two remaining strains (KBI 446 and KBI 449) produced acid from L-arabinose, gentiobiose, inositol, melibiose, raffinose, D-sorbitol, trehalose, glycerol and D-xylose and showed negative reaction for amygdalin, indol, turanose, D-galactose, and potassium gluconate. These two strains had identical features as *Bn* previously described (Brady et al., 2012) (Table 2).

Eleven *Xanthomonas*-like isolates belonging to the second group were aerobic, Gram- and oxidase negative, catalase positive, forming yellow, round, mucoid and convex colonies on YPGA medium after 3 days of incubation at 27°C. These strains induced HR reaction on both, tobacco and geranium leaves.

Pathogenic properties of strains

In pathogenicity assay, extensive stem tissue necrosis developed around the point of inoculation of walnut plants

TABLE 2 Differential phenotypic characteristics for *B. izbisi* and other *Brenneria* and *Lonsdalea* species.

Characteristic	Species							
	***B. izbisi*sp. nov.** **KBI 423^T, 424, 429, 430, 447**	***B. salicis*** **LMG 2698^T**	***B. rubrifaciens*** **LMG 2709^T**	***B. roseae* ssp. *roseae*** **LMG 27714^T**	***B. nigrifluens*** **KBI 446, 449**	***B. goodwinii*** **FRB 141^T**	***B. alni*** **NCPPB 3934^T**	***L. quercina*** **ATCC 29281^T**
L-Arabinose	+	–	+	+	+	+	+	–
Amygdalin	–	–	–	–	–	+	+	–
D-Galactose	+	–	–	+	–	+	+	d
Gentiobiose	–	–	–	–	+	+	–	–
Inositol	+	+*	–	+	+	+	–	–
Melibiose	+	+*	–	–	+	+	–	–
Potassium gluconate	+	+	–	+	–	d	–	d
Raffinose	+	+	–	–	+	+	–	–
D-Sorbitol	–	–	–	+	+	+	–	–
Trehalose	–	–	–	–	+	+	+	d
Turanose	–	+*	–	–	–	+	+	+
D-Xylose	–	–	–	+	+	d	+	–
Glycerol	+	–	–	+	+	+	+	–

All data were obtained using API 50CH test kit (bioMérieux) under same conditions. Tested strains of *B. izbisi* sp. nov and *B. nigrifluens* were isolated in this sudy, while *B. rubrifaciens* and *B. salicis* reference strains were used as control strains. Data for reference strains *B. goodwinii* were taken from Denman et al., 2012, for *B. alni* and *Lonsdalea quercina* were taken from Brady et al., 2012, and for *B. rosae* subsp. *rosae* from Brady et al., 2014. +, positive; -, negative; d- 11-89% strains positive in 1-4 days; *- differ from literature data.

two months after inoculation with the novel *Brenneria* strains KBI 423^T, KBI 424, KBI 429 and KBI 447. Necrotic lesions were also observed in the inner bark tissue (Figure S1A). Lesions extended from the site of inoculation and small longitudinal cracks in the bark were formed. After bark removal, brown necrotic streaks extending deeper into the xylem were visible. After 14 months, the necrotic tissue under the bark of inoculated stems extended to 8 cm in length (Figure S1B). However, external cankers like those observed under natural conditions as well as oozing of a dark liquid from the wounds were not observed. Additionally, severe symptoms of deep tissue necrosis around the point of inoculation were observed on young branches three weeks after inoculation (Figure S1C). After removing the surface tissue, lesions appeared as longitudinal blackish streaks that extended deeper into inner tissue. Symptoms of internal necrosis were also observed in the plants inoculated with strains KBI 446 and KBI 449 of *Bn*. Strain KBI 435 of *Xaj* caused limited necrosis of stem and shoots tissue at point of inoculation. From all inoculated plants, bacteria were re-isolated on KB medium from the lesions on the stem and branches, respectively two and 14 months after inoculation. Identity of the strains was confirmed by specific PCR tests. Symptoms of necrosis did not develop on control plants, and we did not isolate any bacteria from the inner tissue.

In addition, characteristic symptoms of necrosis and sunken black lesions around the point of inoculation and deeper in the inner tissue were observed on young walnut fruits 14 days after inoculation with strains KBI 423^T, KBI 446 and KBI 435. Three weeks after inoculation, bacteria were re-isolated on KB and their identity was confirmed by specific PCR assays, described below. No symptoms developed on control fruits inoculated with *Bs* and SDW.

PCR identification

Different PCR assays were applied in order to identify isolates. Seventeen isolates of *Brenneria* sp. were PCR tested by using primers specific to *Bn*, *Br* and *Bs*. In PCR assay using primers Es1A/Es4B specific for *Bs*, a 553 bp DNA fragment was amplified in fifteen isolates (Table 1). PCR reaction with F1/C3 primers yielded specific 250 bp product in two remaining isolates (KBI 446 and KBI 449), indicating their affiliation to *Bn* species. Primers specific for *Br* did not amplify expected 409 bp fragment in any tested isolate. Identity of yellowish, small, circular colonies as *Xaj* was confirmed by using XajF/XajR primers amplifying specific 216 bp fragment (Table 1).

Strains differentiation by rep-PCR

The obtained genetic PCR profiles showed that the 15 novel *Brenneria* isolates represent a homogenous group, by using BOXA1R, ERIC1R/ERIC2 and REP1R-I/REP2-I primers. The isolates formed a unique fingerprint profile that differs from the profiles of *Bn, Br* and *Bs* used in the analysis (data not shown).

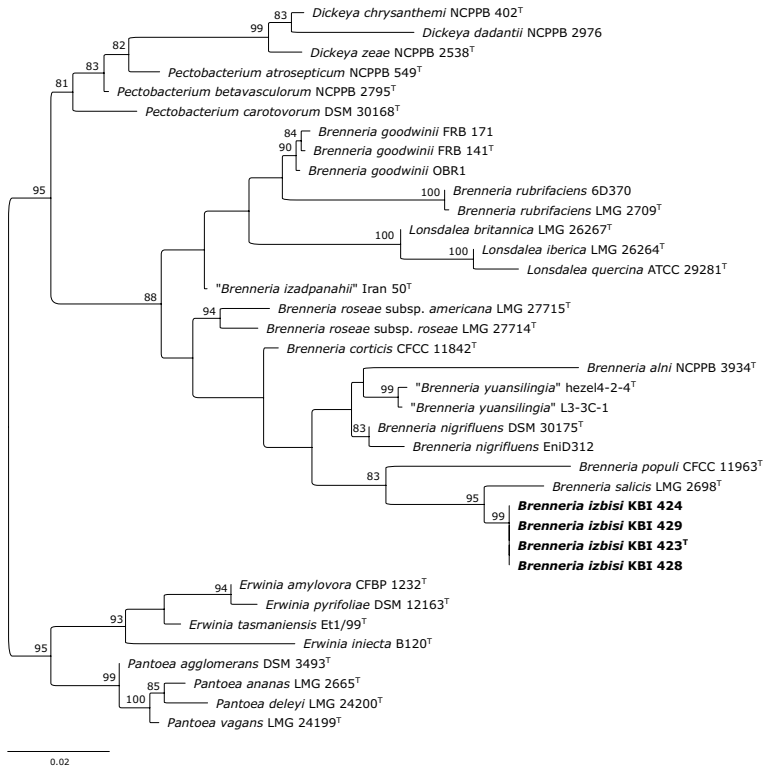

FIGURE 3
Maximum likelihood phylogenetic tree based on 16S rRNA gene sequence. Four representative *B. izbisi* strains isolated in this study are marked in bold. The best fitting model HKY+F+I+G4 was applied for tree construction. Ultrafast bootstrap support values (>70) are indicated at the nodes. Reference *Erwinia* spp. and *Pantoea* spp. were used as an outgroup to root the tree.

Moreover, two *Bn* isolates showed an identical profile to the *Bn* reference strain KBI 024.

Phylogenetic analysis of 16S rRNA and housekeeping genes

The partial 16S rRNA gene sequences of the novel *Brenneria* strains were identical, and showed highest nucleotide identity (98.42%) to the sequence of *Bs* type strain LMG 2698^T (Acc. No. AJ233419). Indeed, phylogenetic analysis based on 16S rDNA sequences also indicated that strains KBI 423^T, KBI 424, KBI 428 and KBI 429 were most closely related to *Bs* (Figure 3), although they formed a separate phylogenetic lineage within the genus *Brenneria*. Moreover, 16S rDNA phylogeny indicated that the genus *Brenneria* is polyphyletic, as it was intertwined with *Lonsdalea* spp. (Figure 3).

Partial sequences of *atpD, gyrB*, *infB* and *rpoB* genes were obtained for four novel *Brenneria* isolates (KBI 423^T, KBI 429, KBI 430 and KBI 447). Strains studied exhibited identical sequences for each of the four housekeeping genes. Phylogenetic trees were generated based on the sequence of each gene (data not shown), as well as on concatenated datasets of four housekeeping genes (Figure 4). In all phylogenetic trees, novel *Brenneria* strains formed a separate clade with 100% bootstrap support, with *Bs* located on an adjacent branch. In the phylogenetic tree generated from concatenated dataset, they clustered within the *Brenneria* clade B defined previously by Bakhshi Ganje et al. (2021) (Figure 4). Similarly as for 16S rRNA gene phylogeny, polyphyly of the genus *Brenneria* was evident in the MLSA tree. In particular, *Brenneria* clades A and B were separated by *Pectobacterium* strains included in the analysis (Figure 4).

Whole-genome sequences

Draft genome sequences of strains KBI 423^T and KBI 447 were obtained in this study (Table 3). The *de novo* assembly resulted in 66 (KBI 423^T) and 62 (KBI 447) contigs. The genome coverage was 638- (KBI 423^T) and 592-fold (KBI 447). The draft genome sequence of strain KBI 423^T consisted of 3,896,770 bp, with an average G+C content of 51.76%, while that of strain KBI 447 consisted of 3,897,516 bp, with an average G+C content of

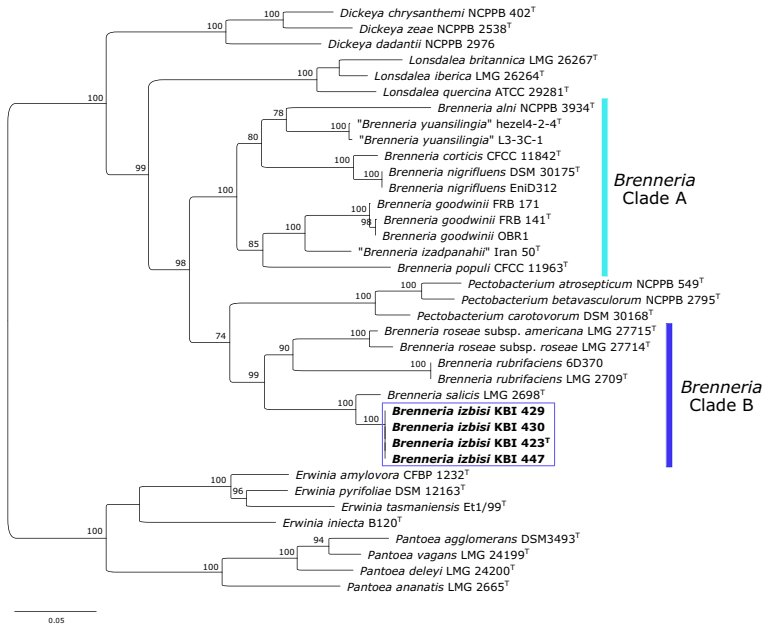

FIGURE 4
Maximum likelihood phylogenetic tree based on concatenated housekeeping genes *atpD, gyrB, infB* and *rpoB, (*2480 bp) sequences. The tree indicates the phylogenetic position of 4 representative *B. izbisi* strains (marked in bold and boxed). The best fitting model TIM2+F+I+G4 was applied for tree construction. Ultrafast bootstrap support values (>70) are indicated at the nodes. Reference *Erwinia* spp. and *Pantoea* spp. were used as an outgroup to root the tree.

51.76%. Other general features of draft genome sequences are sumarized in Table 3.

Core-genome phylogeny and overall genome relatedness indexes

A core-genome phylogenetic tree was reconstructed from the supermatrix obtained by concatenation of 663 top gene markers. Strains KBI 423^T and KBI 447 formed a separate cluster within the genus *Brenneria*, within the clade B defined previously by Bakhshi Ganje et al. (2021) (Figure 5). As indicated by 16S rRNA and housekeeping gene phylogenetic analyses, core-genome phylogeny confirmed that their closest relative was *Bs* strain LMG 2698^T (Figure 5). Core-genome phylogeny indicated monophyly of the genus *Brenneria*, with two well-separated clades A and B.

OGRIs computed (Table S4) revealed that KBI 423^T and KBI 447 represent a new *Brenneria* species, closely related to *Bs*. In particular, they shared 94.48% (ANIb), 94.68% (ANIm), 94.51% (orthoANIu) and 57.8% (dDDH) overall genome relatedness with the type strain of *Bs* (LMG 2698^T), which was below the proposed thresholds for species delineation (95–96% for ANI, and 70% for DDH) (Table S4). Obtained OGRIs were relatively

TABLE 3 General features of genome sequences obtained in this study.

	Strains	
	***Brenneria izbisi* KBI 423^T**	***Brenneria izbisi* KBI 447**
Contigs (N)	66	62
N50 (Kb)	279	279
Size (Mb)	3.9	3.9
GC Content (%)	51.8	51.76
Genes[a]	3,531	3,530
CDSs[a]	3,458	3,457
Accession number	JAMPJU000000000	JAMPJT000000000

[a]Numbers based on Prokka annotation.

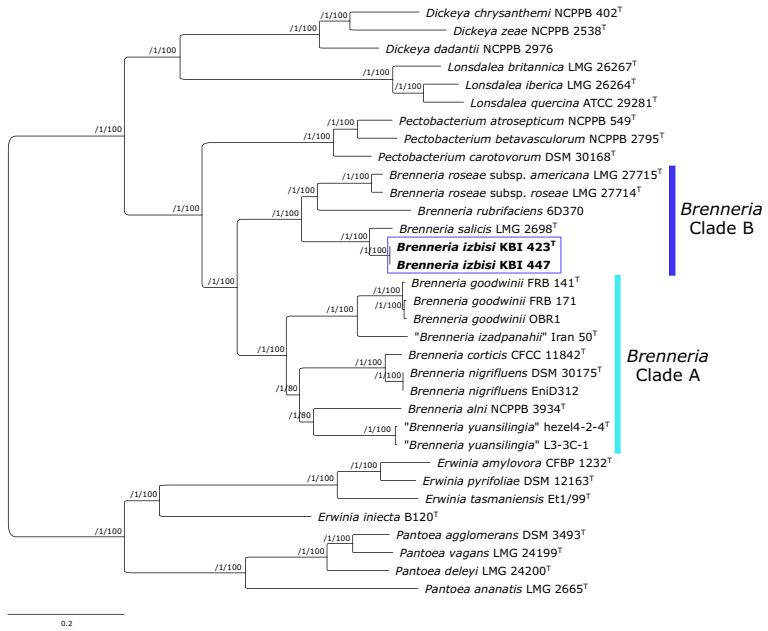

FIGURE 5
Maximum likelihood core-genome phylogenetic tree showing the evolutionary relationships between *Brenneria izbisi* (marked in bold and boxed) and related *Brenneria* spp. Reference *Dickeya*, *Lonsdalea* and *Pectobacterium* strains were also included in the analysis. Reference *Erwinia* spp. and *Pantoea* spp. were used as an outgroup to root the tree. The phylogeny was estimated under the GTR+F+ASC+R4 substitution model from the supermatrix obtained by concatenation of 663 top gene markers. The approximate Bayesian posterior probability values are shown at nodes. The scale bar represents the number of expected substitutions per site. DDBJ/ENA/GenBank whole-genome accession numbers are shown in Table S3. *Brenneria* clades A and B defined by Bakhshi Ganje et al. (2021) are indicated on the tree.

low when KBI 423^T and KBI 447 were compared with other *Brenneria* spp. (<87% for ANI, <31 for dDDH). A description of the novel *Brenneria* species, for which the name *Brenneria izbisi* sp. nov. is proposed, is given below.

Specific PCR assay for detection and identification of *Brenneria izbisi* sp. nov.

Genomic DNA of *B. izbisi* sp. nov. was amplified by using a conventional PCR assay with specific primers designed in this study. Using primers Bi-hrpP-F/Bi-hrpP-R, all tested strains of this species yielded the expected 340 bp amplicon. Contrarily, there was no amplification of DNA from the other 31 strains belonging to different species with this primer set (Table S1). Moreover, Primer-BLAST analysis against the nr database confirmed that the specificity of primers Bi-hrpP-F/Bi-hrpP-R is restricted to *B. izbisi*.

Discussion

During a 2020, serious outbreak of deep bark canker was observed on young walnut trees in several orchards in Serbia. The symptoms included the development of deep longitudinal cracks in trunks and lower branches that oozed a dark liquid, leaving glossy dark traces just below the wounds. High incidence of disease was recorded in the newly established orchards suggesting that the pathogen was most likely disseminated by planting material. From the symptomatic walnut trees, strains belonging to three phytopathogenic bacterial species were isolated: *Bn*, *Xaj* and *Brenneria* strains that we described as a novel bacterial species named *B. izbisi* (see the protologue below).

Characterization of a newly isolated *Brenneria* species (*B. izbisi*) was the primary objective of this study. Among 15 strains showing identical phenotypic characteristic and rep-PCR fingerprints, we selected four representatives for a more comprehensive characterization. Partial 16S rDNA sequences of these four strains were identical and showed the highest nucleotide identity (98.42%) to the type strain of *Bs* (LMG 2698^T). A nucleotide identity value for 16S rRNA gene sequences of 98.65% was proposed as the threshold for differentiating bacterial species (Kim et al., 2014). Distinctiveness of the four strains studied is also reflected in the 16S rRNA gene phylogenetic tree (Figure 3), where all four strains form a separate cluster with a strong bootstrap support, although a close phylogenetic relationship to *Bs* LMG 2698^T was evident.

An MLSA scheme based on partial gene sequencing of *atpD*, *gyrB*, *infB* and *rpoB* was proven to be useful for evaluation of the

phylogenetic position of species belonging to the genus *Brenneria* within the *Enterobacteriaceae* (Brady et al., 2012). The present study revealed that *B. izbisi* strains had identical sequences for all analyzed genes. Based on the concatenated sequences of the four housekeeping genes (Figure 4), all four strains form a cluster with 100% bootstrap support, clearly separated from the closest phylogenetic neighbor *Bs*.

Although 16S rRNA gene and MLSA phylogenies indicated that *B. izbisi* strains belong to the genus *Brenneria*, this genus was polyphyletic in these phylogenetic trees. Polyphyly of the genus *Brenneria* in 16S rRNA gene phylogenetic tree has been observed previously (Brady and Coutinho, 2021). Therefore, we performed phylogenomic analysis based on a large number of non-recombinant core marker genes derived from whole-genome sequence data, in order to generate a more robust phylogenetic tree. In a resulting core-genome phylogenetic tree based on 663 gene markers, the genus *Brenneria* was monophyletic, with two well-separated clades A and B defined previously by Bakhshi Ganje et al. (2021). The separate phylogenetic position of *B. izbisi* was further supported by core-genome phylogeny. Lastly, the novel species could be unequivocally delineated from closely related species using different OGRIs, including ANI and dDDH.

Biochemical and physiological tests revealed that all strains possess basic characteristics of *Brenneria* genus. However, there are differential features that can be used to distinguish *B. izbisi* from other *Brenneria* species as shown in Table 2.

The specific focus of this study was to resolve the etiology of deep bark canker of walnut in Serbia and to assess the involvement of *B. izbisi* in infection and disease development. Currently, there are eight *Brenneria* species with validly published names (*B. salicis, B. alni, B. goodwinii, B. roseae, B. corticis, B. populi, B. nigrifluens* and *B. rubrifaciens*)[8], including four subspecies (*Brenneria populi* subsp. *populi*, *Brenneria populi* subsp. *brevivirga*, *Brenneria roseae* subsp. *roseae* and *Brenneria roseae* subsp. *americana*) (Brady and Coutinho, 2021), as well as two species with not validly published names ("*Brenneria izadpanahii*" and "*Brenneria yuansilingia*") (Bakhshi Ganje et al., 2021; Sun et al., 2021). Upon submission of this manuscript, Kile et al. (2022) described a new *Brenneria* species, *Brenneria tiliae* isolated from symptomatic *Tilia* × *moltkei* and *Tilia* × *europaea* trees in the UK. However, this species was distantly related to *B. izbisi* (ANIb < 81%). Its closest relative was *B. corticis* and unlike *B. izbisi*, *B. tiliae* clustered with strains of *Brenneria* clade A (Bakhshi Ganje et al., 2021; Kile et al., 2022). Overall, all *Brenneria* species described so far are associated with symptoms of bark canker and stem bleeding of the woody plants such as trees of alder, willow, poplar or walnut (Brady and Coutinho, 2021). Two of these species, *Bn* and *Br*, cause shallow and deep bark canker, respectively. They represent a serious threat to walnut production by the weakening of trees and consequent reduction in the number of nuts and in timber production, as well as reduced yield. Recently, Allahveripour et al. reported that *B. roseae* subsp. *rosae* and *Gibbsiella quercinecans* were associated to the shallow bark canker of walnut tree in Iran (Allahverdipour et al., 2021).

Pathogenicity of the representatives of *B. izbisi* strains was assessed by inoculating young walnut trees and immature fruits. Stem and shoot inoculations of walnut growing in pots demonstrated that all tested isolates were pathogenic on walnut. Although artificial inoculation by *B. izbisi* strains did not result in formation of oozing cankers, the development of extensive tissue necrosis and degradation of host tissues, as well as pathogen presence and re-isolation from tissues distant from the sites of inoculation, indicated that this bacterium is able to colonize walnut tissue, cause lesions, and survive for a long period in walnut trees. Similar difficulties in reproducing symptoms of external cankers on woody plants after inoculation with different *Brenneria* species including *B. nigrifluens, B. rubrifaciens, B. quercina*, and *B. rosae* subsp. *rosae*, were reported by other authors (Wilson et al., 1957; González et al., 2002; Biosca et al., 2003; Allahverdipour et al., 2021). Possible explanation for this could be the differences between natural infection conditions and artificial inoculations, the inoculation period, or due to physiological state of the tissues at the inoculation time and the following weeks (Biosca et al., 2003).

Although *B. izbisi* was the predominant species isolated from the symptomatic walnut trees, we also isolated strains of *Bn* and *Xaj* from the same walnut samples. The presence of more than one pathogenic species in the same plant samples, such as *Bn* and *Xaj*, was previously reported (Hajri et al., 2010; Allahverdipour et al., 2021). Moreover, Mazzaglia et al., detected the presence of both fungi and bacteria in walnut bark lesions that were associated with bark canker on English walnut (Mazzaglia et al., 2005). As it has been reported in some other pathosystems, such as acute oak decline (Denman et al., 2018) and olive knot disease (Buonaurio et al., 2015), specific symptom development might be a result of multispecies interaction. A recent study of Doonan et al. (2019) supports this idea and indicates the role of microbial communities and polymicrobial interactions in AOD establishment. Although we clearly demonstrated in this study that *B. izbisi* strains alone were able to cause tissue necrosis and lesions on inoculated walnut plants, other pathogens might possibly contribute to more severe disease development and have a synergistic effect. In addition, different environmental factors might contribute to disease development, as well as inadequate nutrient supply that may cause low tree vitality or to increase susceptibility for diseases. It has been demonstrated the relation between nutrient availability and the occurrence of watermark disease caused by *Bs* on *Salix alba*, showing that excess nitrogen makes willow trees fast-growing and more susceptible for watermark

8 https://lpsn.dsmz.de/genus/brenneria.

disease (De Vos et al., 2007). However, further studies are necessary to elucidate the role of each species and/or other factors in the deep canker symptoms development on walnut trees.

In order to facilitate rapid identification of the new walnut pathogen, we developed a specific PCR assay targeting the putative gene *hrpP* coding for type III secretion system HrpP C-terminal domain-containing protein. This assay enables identification of *B. izbisi* strains and their differentiation from other *Brenneria* spp., including closely related *Bs*, but particularly *Bn* and *Br* as causal agents of similar walnut canker disease.

This paper reports the description of a new bacterial species named *B. izbisi* associated with deep bark canker of the walnut in Serbia. This is an emerging disease of young walnut in Serbia that might have a high economic impact in the future, considering the increase of walnut production and its growing significance. The fact that the disease occurred only in young walnut orchards, indicates that pathogen might be introduced with planting material. However, the presence of the other widely distributed pathogens of walnut in the diseased trees, require further studies to clarify the role of each pathogen in the walnut bark canker development, their relationships and possible interaction with plant and other microbial communities.

Description of *Brenneria izbisi* sp. nov.

Brenneria izbisi (iz.bi'si. N.L. gen. n. *izbisi*, of IZBIS [Institut za zaštitu bilja i životnu sredinu, eng. Institute for Plant Protection and Environment], where this taxonomic study was performed).

Bacterial cells are Gram-negative and oxidase-negative, facultatively anaerobic, levan positive, nonfluorescent, and do not produce bright-red pigment on YDC and YPGA medium. The strains showed no pectinolytic activity on potato slices. They do not induce hypersensitive reaction on tobacco leaves but induced response on geranium plants. Positive for fermentation of glycerol, L-arabinose, D-ribose, D-galactose, D-glucose, D-fructose, D-mannose, L-rhamnose, inositol, D-manitol, methyl-α-D-glucopyranoside, N-acetylglucosamine, arbutine, esculine, salicin, D-melibiose, D-saccharose, D-rafinose, potassium gluconate and negative for erythritol, D-arabinose, D-xylose, L-xylose, D-adonitol, methyl-β-D-xylopiranoside, L-sorbose, dulcitol, D-sorbitol, methyl-α-D-mannopyranoside, amygdalin, D-celobiose, D-maltose, D-lactose, D-trehalose, inulin, D-melezitose, starch, glycogen, xylitol, gentiobiose, D-turanose, D-lyxose, D-tagatose, D-fucose, L-fucose, D-arabitol, L-arabitol, potassium 2-ketogluconate and potassium 5-ketogluconate (API 50 CHB/E). Nitrate is not reduced to nitrite, nor reduced to N_2 gas. The strains do not produce indole, gelatinase, urease or acetoin but assimilate potassium gluconate and produce acid from glycerol.

The genomic G+C content of the type strain is 51.8 mol%. Its approximate genome size is 3.9 Mbp.

B. izbisi can be distinguished from other *Brenneria* spp. based on OGRIs (e.g. ANI and dDDH) and core-genome phylogeny, as well as by analysis of sequences of housekeeping genes. In addition, it showed unique phenotypic features, comparing with other *Brenneria* species.

The type strain, KBI 423^T (= CFBP 9035^T = LMG 32479^T) was isolated from walnut trees in Serbia in 2020. Whole-genome shotgun sequence of the strain KBI 423^T has been deposited at the NIH GenBank under the accession number JAMPJU000000000.

Data availability statement

The datasets presented in this study can be found in online repositories. The names of the repository/repositories and accession number(s) can be found in the article/Supplementary Material.

Author contributions

KG and NK conceived and designed the study. KG and NZ performed the experiments, KG, NZ, and NK analyzed data and wrote the manuscript. All authors read, discussed, edited and approved the submitted version of the manuscript.

Funding

The work of KG and NZ was supported by the Ministry of Education, Science and Technological Development, Republic of Serbia, Contract No. 451-03-68/2022-14/200010. The work of NK was funded by the Deutsche Forschungsgemeinschaft (DFG, German Research Foundation) – Project number 429677233.

Acknowledgments

The authors would like to thank Prof. Aharon Oren (The Hebrew University of Jerusalem, Israel) for helpful advice on nomenclatural aspects. This research was enabled, in part, through computational resources provided by the BMBF-funded de.NBI Cloud within the German Network for Bioinformatics Infrastructure (de.NBI) (031A532B, 031A533A, 031A533B, 031A534A, 031A535A, 031A537A, 031A537B, 031A537C, 031A537D, 031A538A). We thank to Prof. Aleksa Obradović (University of Belgrade, Faculty of Agriculture) for constructive advices during research. In addition, we thank

master student Marina Milošević for her contribution in rep-PCR and MLSA analysis.

Conflict of interest

The authors declare that the research was conducted in the absence of any commercial or financial relationships that could be construed as a potential conflict of interest.

Publisher's note

Supplementary material

The Supplementary Material for this article can be found online at: https://www.frontiersin.org/articles/10.3389/fpls.2022.1055186/full#supplementary-material

SUPPLEMENTARY FIGURE S1
Pathogenicity assay. Symptoms on walnut stem (A) two months after inoculation – no symptoms development on negative control (left), symptoms of tissue necrosis on the point of inoculation by the strain KBI 447. (B) 14 months after inoculation - no symptoms development on negative control (left), necrotic tissue under the bark extending deeper into the xylem (inoculation by the strain KBI 423) (middle and right). (C) Symptoms on young shoots three weeks after inoculation - no symptoms development on negative control (left), deep tissue necrosis around the point of inoculation (inoculation by the strain KBI 423).

References

Allahverdipour, T., Shahryari, F., and Falahi Charkhabi, N. (2021). *Gibbsiella quercinecans* and *Brenneria roseae* subsp. *roseae* associated to the canker disease of walnut trees in northwestern Iran. *Eur. J. Plant Pathol.* 161, 783–797. doi: 10.1007/s10658-021-02359-9

Altschul, S. F., Madden, T. L., Schäffer, A. A., Zhang, J., Zhang, Z., Miller, W., et al. (1997). Gapped BLAST and PSI-BLAST: A new generation of protein database search programs. *Nucleic Acids Res.* 25, 3389–3402. doi: 10.1093/nar/25.17.3389

Angelini, E., Clair, D., Borgo, M., Bertaccini, A., and Boudon-Padieu, E. (2001). "Flavescence dorée" in France and Italy – occurrence of closely related phytoplasma isolates and their near relationships to palatinate grapevine yellows and an alder yellows phytoplasma. *Vitis - J. Grapevine Res.* 40 (2), 79–86. doi: 10.5073/vitis.2001.40.79-86

Bakhshi Ganje, M., Mackay, J., Nicolaisen, M., and Shams-Bakhsh, M. (2021). Comparative genomics, pangenome, and phylogenomic analyses of *Brenneria* spp., and delineation of *Brenneria izadpanahii* sp. nov. *Phytopathology* 111, 78–95. doi: 10.1094/phyto-04-20-0129-fi

Belisario, A., Maccaroni, M., Corazza, L., Balmas, V., and Valier, A. (2002). Occurrence and etiology of brown apical necrosis on Persian (English) walnut fruit. *Plant Dis.* 86, 599–602. doi: 10.1094/pdis.2002.86.6.599

Biosca, E. G., González, R., López-López, M. J., Soria, S., Montón, C., Pérez-Laorga, E., et al. (2003). Isolation and characterization of *Brenneria quercina*, causal agent for bark canker and drippy nut of *Quercus* spp Spain. *Phytopathology* 93 (4), 485–492. doi: 10.1094/PHYTO.2003.93.4.485

Biosca, E. G., and López, M. M. (2012). Detection and identification methods and new tests as developed and used in the framework of COST 873 for bacteria pathogenic to stone fruits and nuts, *Brenneria nigrifluens* and *Brenneria rubrifaciens*. *J. Plant Pathol.* 94 (1, Supplement), S1.105–S1.113. doi: 10.4454/jpp.v94i1sup.017

Brady, C. L., Cleenwerck, I., Denman, S., Venter, S. N., Rodriguez-Palenzuela, P., Coutinho, T. A., et al. (2012). Proposal to reclassify *Brenneria quercina* (Hildebrand and schroth 1967) Hauben et al. 1999 into a new genus, *Lonsdalea* gen. nov., as *Lonsdalea quercina* comb. nov., descriptions of *Lonsdalea quercina* subsp. *quercina* comb. nov., *Lonsdalea quercina* subsp. *Iberica* subsp. nov. and *Lonsdalea quercina* subsp. *britannica* subsp. nov., emendation of the description of the genus *Brenneria*, reclassification of *Dickeya dieffenbachiae* as *Dickeya dadantii* subsp. *dieffenbachiae* comb. nov., and emendation of the description of *Dickeya dadantii*. *Int. J. Syst. Evol. Microbiol.* 62, 1592–1602. doi: 10.1099/ijs.0.035055-0

Brady, C., Cleenwerck, I., Venter, S., Vancanneyt, M., Swings, J., and Coutinho, T. (2008). Phylogeny and identification of *Pantoea* species associated with plants, humans and the natural environment based on multilocus sequence analysis (MLSA). *Syst. Appl. Microbiol.* 31 (6-8), 447–460. doi: 10.1016/j.syapm.2008.09.004

Brady, C., and Coutinho, T. (2021). "Brenneria," in *Bergey's manual of systematics of archaea and bacteria* (John Wiley and Sons., in association with Bergey's Manual Trust. ©2015, Bergey's Manual Trust.) doi: 10.1002/9781118960608.gbm01136.pub2

Brady, C. L., Hunter, G., Kirk, S., Arnold, D., and Denman, S. (2014). Description of *Brenneria roseae* sp. nov. and two subspecies, *Brenneria roseae* subspecies *roseae* ssp. nov and *Brenneria roseae* subspecies *americana* ssp. nov. isolated from symptomatic oak. *Syst. Appl. Microbiol.* 37, 391–401. doi: 10.1016/j.syapm.2014.04.005

Buonaurio, R., Moretti, C., da Silva, D. P., Cortese, C., Ramos, C., and Venturi, V. (2015). The olive knot disease as a model to study the role of interspecies bacterial communities in plant disease. *Front. Plant Sci.* 6. doi: 10.3389/fpls.2015.00434

Contreras-Moreira, B., and Vinuesa, P. (2013). GET_HOMOLOGUES, a versatile software package for scalable and robust microbial pangenome analysis. *Appl. Environ. Microbiol.* 79, 7696–7701. doi: 10.1128/AEM.02411-13

Denman, S., Brady, C., Kirk, S., Cleenwerck, I., Venter, S., Coutinho, T., et al. (2012). *Brenneria goodwinii* sp. nov., associated with acute oak decline in the UK. *Int. J. Syst. Evol. Microbiol.* 62, 2451–2456. doi: 10.1099/ijs.0.037879-0

Denman, S., Doonan, J., Ransom-Jones, E., Broberg, M., Plummer, S., Kirk, S., et al. (2018). Microbiome and infectivity studies reveal complex polyspecies tree disease in acute oak decline. *ISME J.* 12, 386–399. doi: 10.1038/ismej.2017.170

De Vos, B., Huvenne, H., Messens, E., and Maes, M. (2007). Nutritional imbalance caused by nitrogen excess is correlated with the occurrence of watermark disease in white willow. *Plant Soil* 301, 215–232. doi: 10.1007/s11104-007-9439-6

Doonan, J., Denman, S., Pachebat, J. A., and McDonald, J. (2019). Genomic analysis of bacteria in the acute oak decline pathobiome. *Microb. Genom.* 5 (1), e000240. doi: 10.1099/mgen.0.000240

Du Plessis, H. J., and van der Westhuizen, T. J. (1995). Identification of *Xanthomonas campestris* pv. *juglandis* from (Persian) English walnut nursery trees in South Africa. *J. Phytopathol.* 143, 449–454. doi: 10.1111/j.1439-0434.1995.tb04552.x

FAOSTAT. (2022). https://www.fao.org/faostat/en/#data/QCL/visualize. accessed September 2022.

Fu, B., Chen, Q., Wei, M., Zhu, J., Zou, L., Li, G., et al. (2018). Complete genome sequence of *Xanthomonas arboricola* pv. *juglandis* strain DW3F3, isolated from a *Juglans regia* L. bacterial blighted fruitlet. *Genome Announc.* 6, e00023–e00018. doi: 10.1128/genomeA.00023-18

Gavrilović, V., and Arsenijević, M. (1998). Etiological study of bacterial spots of walnut fruits. *Zaštita bilja/Plant Prot.* 49, 295–302.

Giovanardi, D., Bonneau, S., Gironde, S., Fischer-Le Saux, M., Manceau, C., and Stefani, E. (2016). Morphological and genotypic features of *Xanthomonas arboricola* pv. *juglandis* populations from walnut groves in Romagna region, Italy. *Eur. J. Plant Pathol.* 145, 1–16. doi: 10.1007/s10658-015-0809-2

Gironde, S., Guillaumes, J., and Manceau, C. (2009). "Specific detection of *Xanthomonas arboricola* pv. *juglandis* pathogen on walnut," in *EPPO conference on diagnostics*, vol. 1-1. (York, UK: Food and Environment Research Agency).

González, R., López-López, M. J., Biosca, E. G., López, F., Santiago, R., and López, M. M. (2002). First report of bacterial deep bark canker of walnut caused by *Brenneria (Erwinia) rubrifaciens* in Europe. *Plant Dis.* 86, 696. doi: 10.1094/pdis.2002.86.6.696b

Goris, J., Konstantinidis, K. T., Klappenbach, J. A., Coenye, T., Vandamme, P., and Tiedje, J. M. (2007). DNA-DNA Hybridization values and their relationship to whole-genome sequence similarities. *Int. J. Syst. Evol. Microbiol.* 57, 81–91. doi: 10.1099/ijs.0.64483-0

Hajri, A., Meyer, D., Delort, F., Guillaumes, J., Brin, C., and Manceau, C. (2010). Identification of a genetic lineage within *Xanthomonas arboricola* pv. *juglandis* as the causal agent of vertical oozing canker of Persian (English) walnut in France. *Plant Pathol.* 59, 1014–1022. doi: 10.1111/j.1365-3059.2010.02362.x

Hauben, L., Steenackers, M., and Swings, J. (1998). PCR-based detection of the causal agent of watermark disease in willows (*Salix* spp.). *Appl. Environ. Microbiol.* 64, 3966–3971. doi: 10.1128/AEM.64.10.3966-3971.1998

Higgins, D. G., Thompson, J. D., and Gibson, T. J. (1996). Using CLUSTAL for multiple sequence alignments. *Methods Enzymol.* 266, 383–402. doi: 10.1016/s0076-6879(96)66024-8

Hoang, D. T., Chernomor, O., Von Haeseler, A., Minh, B. Q., and Vinh, L. S. (2018). UFBoot2: Improving the ultrafast bootstrap approximation. *Mol. Biol. Evol.* 35, 518–522. doi: 10.1093/molbev/msx281

Ivanović, Ž., Popović, T., Janse, J., Kojić, M., Stanković, S., Gavrilović, V., et al. (2015). Molecular assessment of genetic diversity of *Xanthomonas arboricola* pv. *juglandis* strains from Serbia by various DNA fingerprinting techniques. *Eur. J. Plant Pathol.* 141, 133–145. doi: 10.1007/s10658-014-0531-5

Kałuzna, M., Pulawska, J., Waleron, M., and Sobiczewski, P. (2014). The genetic characterization of *Xanthomonas arboricola* pv. *juglandis*, the causal agent of walnut blight in Poland. *Plant Pathol.* 63, 1404–11416. doi: 10.1111/ppa.12211

Kalyaanamoorthy, S., Minh, B. Q., Wong, T. F. K., Von Haeseler, A., and Jermiin, L. S. (2017). Model finder: Fast model selection for accurate phylogenetic estimates. *Nat. Methods* 14, 587–589. doi: 10.1038/nmeth.4285

Kile, H., Arnold, D., Allainguilaume, J., Denman, S., and Brady, C. (2022). Brenneria tiliae sp. nov., isolated from symptomatic *Tilia* × *moltkei* and *Tilia* × *europaea* trees in the UK. *Int. J. Syst. Evol.* 72 (10). doi: 10.1099/ijsem.0.005515

Kim, M., Oh, H. S., Park, S. C., and Chun, J. (2014). Towards a taxonomic coherence between average nucleotide identity and 16S rRNA gene sequence similarity for species demarcation of prokaryotes. *Int. J. Syst. Evol.* 64 (Pt 2), 346–351. doi: 10.1099/ijs.0.059774-0

King, E. O., Ward, M., and Raney, D. E. (1954). Two simple media for the demonstration of pyocyanin and fluorescein. *J. Lab. Clin. Med.* 44, 301–307.

Kumar, S., Stecher, G., and Tamura, K. (2016). MEGA7: Molecular evolutionary genetics analysis version 7.0 for bigger datasets. *Mol. Biol. Evol.* 33, 1870–1874. doi: 10.1093/molbev/msw054

Kuzmanović, N., Biondi, E., Overmann, J., Puławska, J., Verbarg, S., Smalla, K., et al. (2022). Genomic analysis provides novel insights into diversification and taxonomy of *Allorhizobium vitis* (i.e. *Agrobacterium vitis*). *BMC Genomics* 23, 462. doi: 10.1186/s12864-022-08662-x

Lelliott, R. A., and Stead, D. E. (1987). "Methods for the diagnosis of bacterial diseases of plants," in *Methods in plant pathology*, vol. 2. (Oxford, UK: Blackwell Scientific Publications).

Li, H. (2013). Aligning sequence reads, clone sequences and assembly contigs with BWA-MEM. *arXiv: Genomics*. doi: 10.6084/m9.figshare.963153.v1

López, M. M., Marti, R., Morente, C., Orellana, N., Ninot, T., and Aleta, N. (1994). Phytopathogenic bacteria identified in walnut in Spain. *Investigacion Agraria Produccion Y Proteccion Vegetales* 2, 307–313.

Loreti, S., De Simone, D., and Gallelli, A. (2008). Detection and identification of *Brenneria nigrifluens*, the causal agent of the shallow bark canker of walnut by, PCR amplification. *J. Phytopathol.* 156 (7-8), 464–469. doi: 10.1111/j.1439-0434.2007.01393.x

Martin, M. (2011). Cutadapt removes adapter sequences from high-throughput sequencing reads. *EMBnet.journal* 17 (1), 10–12. doi: 10.14806/ej.17.1.200

Mazzaglia, A., Fabi, A., Belisario, A., Librandi, I., Cefalo, G., Varvaro, L., et al. (2005). Bark cankers on english walnut: an emerging disease. *Acta Hortic.* 705, 437–442. doi: 10.17660/ActaHortic.2005.705.63

McClean, A. E., Sudarshana, P., and Kluepfel, D. A. (2008). Enhanced detection and isolation of the walnut pathogen brenneria rubrifaciens, causal agent of deep bark canker. *Eur. J. Plant Pathol.* 122, 413–424. doi: 10.1007/s10658-008-9308-z

Meier-Kolthoff, J. P., Auch, A. F., Klenk, H.-P., and Göker, M. (2013). Genome sequence-based species delimitation with confidence intervals and improved distance functions. *BMC Bioinform.* 14, 1–14. doi: 10.1186/1471-2105-14-60

Ménard, M., Delort, F., Baudry, A., and Le Saux, M. (2004). First report of bacterial canker of walnut caused by *Brenneria nigrifluens* in France. *Plant Dis.* 88, 220. doi: 10.1094/pdis.2004.88.2.220b

Moragrega, C., Matias, J., Aletà, N., Montesinos, E., and Rovira, M. (2011). Apical necrosis and premature drop of Persian (English) walnut fruit caused by *Xanthomonas arboricola* pv. *juglandis*. *Plant Dis.* 95, 1565–1570. doi: 10.1094/PDIS-03-11-0259

Moragrega, C., and Özaktan, H. (2010). Apical necrosis of Persian (English) walnut (*Juglans regia*): an update. *J. Plant Pathol.* 92 (1), S67–S71. doi: 10.4454/jpp.v92i1sup.2507

Moretti, C., Silvestri, F. M., Rossini, E., Natalini, G., and Buonaurio, R. (2007). A protocol for rapid identification of *Brenneria nigrifluens* among bacteria isolated from bark cankers in Persian walnut plants. *J. Plant Pathol.* 89 (2), 211–218. doi: 10.4454/JPP.V89I2.745

Morone, C., Janse, J. D., and Scortichini, M. (1998). Bark canker of Persian walnut (Juglans regia) tree incited by *Erwinia nigrifluens* in Italy. *J. Phytopathol.* 146, 637–639. doi: 10.1111/j.1439-0434.1998.tb04766.x

Nguyen, L. T., Schmidt, H. A., Von Haeseler, A., and Minh, B. Q. (2015). IQ-TREE: A fast and effective stochastic algorithm for estimating maximum likelihood phylogenies. *Mol. Biol. Evol.* 32, 268–274. doi: 10.1093/molbev/msu300

Popovic, T., Ivanovic, Z., Zivkovic, S., Trkulja, N., and Ignjatov, M. (2013). First report of *Brenneria nigrifluens* as the causal agent of shallow-bark canker on walnut trees (*Juglans regia*) in Serbia. *Plant Dis.* 97 (11), 1504. doi: 10.1094/PDIS-03-13-0267-PDN

Pritchard, L., Glover, R. H., Humphris, S., Elphinstone, J. G., and Toth, I. K. (2016). Genomics and taxonomy in diagnostics for food security: soft-rotting enterobacterial plant pathogens. *Anal. Methods* 8, 12–24. doi: 10.1039/C5AY02550H

Prjibelski, A., Antipov, D., Meleshko, D., Lapidus, A., and Korobeynikov, A. (2020). Using SPAdes *De novo* assembler. *Curr. Protoc. Bioinf.* 70, e102. doi: 10.1002/cpbi.102

Rambaut, A. (2018) *Figtree v1.4.4*. Available at: http://tree.bio.ed.ac.uk/software/figtree/.

Saccardi, A., Bonetti, V., Melegatti, A., and Cristanini, M. (1998). Occurrence of *Erwinia nigrifluens* on English walnut (*Juglans regia*) tree in the veneto region (Northern Italy). *J. Plant Pathol.* 80, 63–65.

Schaad, N. W., Jones, J. B., and Chun, W. (2001). *Laboratory guide for identification of plant pathogenic bacteria (3rd edition)* (St. Paul, MN: APS Press).

Scortichini, M., Marchesi, U., and Di Prospero, P. (2001). Genetic diversity of *Xanthomonas arboricola* pv. *juglandis* (synonyms: *X. campestris* pv. *juglandis*; *X. juglandis* pv. *juglandis*) strains from different geographical areas shown by repetitive polymerase chain reaction genomic fingerprinting. *J. Phytopathol.* 149, 325–332. doi: 10.1046/j.1439-0434.2001.00628.x

Seemann, T. (2014). Prokka: rapid prokaryotic genome annotation. *Bioinformatics* 30, 2068–2069. doi: 10.1093/bioinformatics/btu153

Soylu, S., Kara, M., Bozkurt, İ.A., Soylu, E. M., Kurt, S., and Uysal, A. (2021). First report of bacterial shallow bark canker of walnut (*Juglans regia*) caused by *Brenneria nigrifluens* in Turkey. *J. Plant Pathol.* 103, 333. doi: 10.1007/s42161-020-00661-9

Sun, S., Liu, Y., Luan, F., and Li, Y. (2021)*Brenneria yuansilingia* sp. nov., isolated from symptomatic bark of willow canker. In: *Research square* (Accessed September 23, 2022).

Tatusova, T., DiCuccio, M., Badretdin, A., Chetvernin, V., Nawrocki, E. P., Zaslavsky, , et al. (2016). NCBI prokaryotic genome annotation pipeline. *Nucleic Acids Res.* 44, 6614–6624. doi: 10.1093/nar/gkw569

Trifinopoulos, J., Nguyen, L. T., Von Haeseler, A., and Minh, B. Q. (2016). W-IQ-TREE: A fast online phylogenetic tool for maximum likelihood analysis. *Nucleic Acids Res.* 44, W232–W235. doi: 10.1093/nar/gkw256

Vauterin, L., Hoste, B., Kersters, K., and Swings, J. (1995). Reclassification of *Xanthomonas*. *Int. J. Bacteriol.* 45, 472–489. doi: 10.1099/00207713-45-3-472

Végh, A., Tóth, A., Zámbó, Á., Borsos, G., and Palkovics, L. (2014). First report of bacterial bark canker of walnut caused by *Brenneria nigrifluens* in Hungary. *Plant Dis.* 98 (7), 988. doi: 10.1094/PDIS-09-13-0949-PDN

Versalovic, J., Koeuth, T., and Lupski, J. R. (1991). Distribution of repetitive DNA sequences in eubacteria and application to fingerprinting of bacterial genomes. *Nucleic Acids Res.* 19, 6823–6831. doi: 10.1093/nar/19.24.6823

Versalovic, J., Schneider, M., de Bruijn, F. J., and Lupski, J. R. (1994). Genomic fingerprinting of bacteria using repetitive sequence-based polymerase chain reaction. *Methods Mol. Biol.* 5, 25–40.

Vinuesa, P., Ochoa-Sánchez, L. E., and Contreras-Moreira, B. (2018). GET_PHYLOMARKERS, a software package to select optimal orthologous clusters for phylogenomics and inferring pan-genome phylogenies, used for a critical geno-taxonomic revision of the genus stenotrophomonas. *Front. Microbiol.* 9. doi: 10.3389/fmicb.2018.00771

Weisburg, W. G., Barns, S. M., Pelletier, D. A., and Lane, D. J. (1991). 16S ribosomal DNA amplification for phylogenetic study. *J. Bacteriol.* 173, 697–703. doi: 10.1128/jb.173.2.697-703.1991

Wilson, E. E., Starr, M. P., and Berger, J. A. (1957). Bark canker, a bacterial disease of the Persian walnut tree. *Phytopathology* 47, 669–673.

Wilson, E. E., Zeitoun, F. M., and Fredrickson, D. L. (1967). Bark phloem canker, a new disease of Persian walnut trees. *Phytopathology* 57, 618–621.

Yoon, S.-H., Ha, S.-M., Lim, J., Kwon, S., and Chun, J. (2017). A large-scale evaluation of algorithms to calculate average nucleotide identity. *Antonie Van Leeuwenhoek* 110, 1281–1286. doi: 10.1007/s10482-017-0844-4

frontiers | Frontiers in Plant Science

TYPE Original Research
PUBLISHED 01 December 2022
DOI 10.3389/fpls.2022.1061463

OPEN ACCESS

EDITED BY
Vittoria Catara,
University of Catania, Italy

REVIEWED BY
Giorgio Mariano Balestra,
University of Tuscia, Italy
Steven Earl Lindow,
University of California, Berkeley,
United States

*CORRESPONDENCE
Laura Montesinos
laura.montesinos@udg.edu

SPECIALTY SECTION
This article was submitted to Plant Pathogen Interactions, a section of the journal Frontiers in Plant Science

RECEIVED 04 October 2022
ACCEPTED 11 November 2022
PUBLISHED 01 December 2022

CITATION
Baró A, Saldarelli P, Saponari M, Montesinos E and Montesinos L (2022) *Nicotiana benthamiana* as a model plant host for *Xylella fastidiosa*: Control of infections by transient expression and endotherapy with a bifunctional peptide. *Front. Plant Sci.* 13:1061463. doi: 10.3389/fpls.2022.1061463

Nicotiana benthamiana as a model plant host for *Xylella fastidiosa*: Control of infections by transient expression and endotherapy with a bifunctional peptide

Aina Baró[1], Pasquale Saldarelli[2], Maria Saponari[2], Emilio Montesinos[1] and Laura Montesinos[1]*

[1]Institute of Food and Agricultural Technology-CIDSAV-XaRTA, University of Girona, Girona, Spain, [2]Institute for Sustainable Plant Protection, National Research Council (CNR), Bari, Italy

Transient expression of genes encoding peptides BP134 and BP178 by means of a *Potato virus X* (PVX) based-vector system, and treatment with synthetic peptides by endotherapy, were evaluated in the control of *Xylella fastidiosa* infections, in the model plant *Nicotiana benthamiana*. Transient production of BP178 significantly decreased disease severity compared to PVX and non-treated control (NTC) plants, without adverse effects. Plants treated with synthetic BP134 and BP178 showed consistently lower levels of disease than NTC plants. However, the coinfection with PVX-BP134 and *X. fastidiosa* caused detrimental effects resulting in plant death. The levels of *X. fastidiosa* in three zones sampled, upwards and downwards of the inoculation/treatment point, significantly decreased compared to the NTC plants, after the treatment with BP178, but not when BP178 was produced transiently. The effect of treatment and transient production of BP178 in the induction of defense-related genes was also studied. Synthetic BP178 applied by endotherapy induced the expression of *ERF1*, *PR1a*, *PAL*, *PALII* and *WRKY25*, while the transient expression of BP178 overexpressed the *Cath, Cyc, PR4a, 9-LOX* and *Endochitinase B* genes. Both treatments upregulated the expression of *PR1*, *PR3*, *PR4* and *CycT9299* genes compared to the NTC or PVX plants. It was concluded that the effect of BP178, either by endotherapy or by transient expression, on the control of the *X. fastidiosa* infections in *N. benthamiana*, was due in part to the induction of the plant defense system in addition to its bactericidal activity reported in previous studies. However, the protection observed when BP178 was transiently produced seems mainly mediated by the induction of plant defense, because the levels of *X. fastidiosa* were not significantly affected.

KEYWORDS

bifunctional peptide, bactericidal, plant defense elicitor, plant infections, nicotiana benthamiana, *Xylella fastidiosa*

1 Introduction

Xylella fastidiosa is a Gram-negative bacterium that inhabits the xylem vessels of near 600 plants from 85 taxonomic families (EFSA, 2020). Apart from Pierce's Disease of grapevines, which is one of the oldest known diseases caused by *X. fastidiosa* worldwide, the pathogen causes losses of economic importance in other crops, such as almond (*Prunus dulcis*), citrus (*Citrus* spp.) and olive (*Olea europaea*) (Baldi and La Porta, 2017; EPPO, 2019).

Up to now, there is no efficient cure for infected hosts (Kyrkou et al., 2018). Thus, *X. fastidiosa*-related diseases are still important threats to agriculture all over the world, mainly due to its high genetic plasticity, its xylem-limited nature, and the fact that host plants do not show symptoms during the first stages of the disease. Over the past decades, among several chemical compounds and plant extracts, antimicrobial peptides (AMPs) have been proposed as potential pesticides for disease control (Montesinos E, 2007; Jung and Kang, 2014; Breen et al., 2015). Advantages of their use include the existence of lytic peptides with potent antimicrobial and/or antibiofilm activities, defense elicitor peptides or even multifunctional peptides with reduced cytotoxicity and good biodegradability profiles (Badosa et al., 2022).

In addition, many of these AMPs have been used to create transgenic plants, some of them showing enhanced resistance to bacterial and fungal pathogens (López-García et al., 2012; Breen et al., 2015; Montesinos L. et al., 2017). The application of this technology is especially useful in controlling xylem and phloem-limited bacteria, as the expression of AMPs can be targeted into the vessel's lumen, which is difficult to access using conventional pesticides. One example is the production of grapevine lines expressing a neutrophil elastase and cecropin B, which conferred increased tolerance and trans-graft protection to Pierce's Disease (Dandekar et al., 2019).

Even though, as far as we know, there are no pesticides or transgenic plants based on AMPs commercialized up to date. The careful design, selection and evaluation of suitable peptides is essential for their improved development as novel and sustainable alternatives to synthetic chemical pesticides (Montesinos E. et al., 2012; Van Esse et al., 2020). BP178, a derivative peptide from the leader peptide BP100 (syn. BP134) that was designed for being expressed in plants (Badosa et al., 2013), has been successfully produced in rice seed endosperm, and conferred resistance to bacterial and fungal infections (Montesinos L. et al., 2017). Moreover, synthetic BP178 has been described as highly active against *X. fastidiosa in vitro* (Baró et al., 2020), and recently we confirmed its efficacy in controlling *X. fastidiosa* infections in almond plants (Moll et al., 2022). Synthetic BP178 was also capable of eliciting the innate immune system of tomato and almond plants (Montesinos L. et al., 2021; Moll et al., 2022). However, it is not known if the production of BP178 by transgenic host plants could protect them from *X. fastidiosa* infections.

A transient-expression system based on *Potato virus X* (PVX) has extensively been used in *N. benthamiana* plants to produce a wide range of proteins (Saitoh et al., 2001; Dickmeis et al., 2015; Röder et al., 2018), and specifically for screening AMPs against plant pathogens (Visser et al., 2012). This system has the advantage that *N. benthamiana* is a susceptible host for *X. fastidiosa* (Randall et al., 2009; EFSA, 2022), being a reliable pathosystem for testing the antimicrobial efficacy of BP178 when transiently expressed by this viral vector.

The specific aims of the present work were (i) to validate the *N. benthamiana* system as a model plant host for *X. fastidiosa*, (ii) to develop PVX plasmid constructs to produce the peptide BP178 and its parent peptide BP134 in *N. benthamiana* plants inoculated with *X. fastidiosa* IVIA 5387.2, and (iii) to study the effect of the application of the peptides by endotherapy or transient production in the population dynamics of the pathogen and in controlling infections, as well as in eliciting defense-response in the plants.

2 Materials and methods

2.1 Growth of plants and greenhouse conditions

4-week-old *N. benthamiana* plants were used for the experiments. All plants were maintained in 0.8 l pots in an environmentally controlled greenhouse at 25 ± 2 °C (day) and 18 ± 2 °C (night), with a minimum relative humidity of 60%, and with a photoperiod of 16 h light and 8 h dark. Prior to and during the experiments, plants were watered to saturation every three days, and fertilized with a 200 ppm solution of NPK (20:10:20) once a week. Also, all along the experiments, standard treatments with insecticide and acaricide were performed to avoid presence of vector insects or pests.

2.2 Synthesis of peptides

Peptides BP134 (KKLFKKILKYL-OH) and BP178 (KKLFKKILKYL-AGPA-GIGKFLHSAK-KDEL-OH) were synthesized (LIPPSO laboratory, Girona, Spain) using the solid phase procedure previously described (Badosa et al., 2013; Caravaca-Fuentes et al., 2021). Briefly, a Fmoc-Rink-MBHA resin (0.55 mmol/g) was used for the synthesis of BP134, and a PAC-ChemMatrix resin (0.66 mmol/g) for the synthesis of BP178. Peptides were synthesized with purity above 95% and characterized by ESI-MS (Badosa et al., 2013; Montesinos L. et al., 2021). Lyophilized peptides (acetate salts) were solubilized in sterile Milli-Q water to a stock concentration of 20 mM and filter sterilized through a 0.22 µm pore Whatman filter. Dilutions of peptides were prepared in sterile Milli-Q water to obtain the final desired concentrations.

2.3 PVX plasmid construction and evaluation of transient expression in plants

2.3.1. pCXI BP134 and pCXI BP178 plasmid construction and *N. benthamiana* inoculation

The pCXI scaffold (Cruz et al., 1996; Lee et al., 2014; Shukla et al., 2014), containing the PVX genome sequence under the Ca35S promoter was engineered to fuse the BP134 and BP178 peptide sequences to the viral coat protein (CP) *via* the foot and mouth disease virus (FMDV) 2A sequence. Primers CX1 BP134 2A and CX1 BP178 2A (Table 1) were coupled with the downstream primer CX1uni to amplify the entire PVX CP from pCXI. Amplifications were carried by using 1 unit of Phusion High Fidelity DNA polymerase (ThermoFisher Scientific) in a 50 µl reaction mix containing 0.5 µM reverse and forward primers, 200 µM dNTPs, 50 ng pCXI in 1x Phusion HF buffer. Cycling conditions were: 98°C for 30" followed by 25 cycles at 98°C 30", 54°C 30", 72°C 45" and a final elongation step of 72°C for 10'. The obtained amplicons were digested with EagI/SpeI and ligated to a similarly restricted pCXI to obtain the plasmids pCXI BP134 and pCXI BP178 by transformation in *Escherichia coli* strain DH5α. *N. benthamiana* plants at the 6-8 leaf stage were inoculated with pCXI BP134, pCXI BP178 (two different plasmids) and pCXI by Celite abrasion of three leaves with 5 µg of purified plasmid DNA, and plants were maintained in controlled greenhouse conditions.

Only in the case of PVX – BP134 plants, virus particles were partially purified from 100 g of *N. benthamiana* leaf tissues (Lee et al., 2014). Briefly, tissues were homogenized in 200 ml cold phosphate buffer and the slurry filtered with gauze and centrifuged at 7,800 g for 20 min at 4°C. The supernatant was added to 1% (v/v) Triton X-100, stirred for 1 h at 4°C and again clarified by centrifugation at 5,500 g for 10 min at 4°C. Virus particles, precipitated from the supernatant by NaCl/PEG stirring and centrifugation at 7,800 g for 10 min at 4°C, were resuspended in 10 ml 0.5 M phosphate buffer pH 7.2 and finally concentrated by high speed centrifugation in a swinging bucket rotor at 104,000 g for 75 min at 4°C. Pellet was resuspended in 0.2 ml of the same buffer.

2.3.2. Western blot analysis of pCXI BP134 and pCXI BP178 inoculated plants

Two weeks after the inoculation, 500 mg *N. benthamiana* leaf tissues were ground in 0.5 ml of extraction buffer [EB: 50 mM Tris, 10 mM potassium acetate, 1 mM sodium EDTA, 10 mM dithiothreitol, 0.5 mM phenylmethylsulfonyl fluoride (PMSF), 10% sucrose, pH 7.4] and successively centrifuged at 4,000 rpm to separate the supernatant. Proteins were fractionated in 12% SDS-polyacrylamide gels (Laemmli, 1970) and transferred to PVDF membrane (Millipore, Bedford) (Towbin et al., 1979). Membranes were preincubated in blocking buffer [1× TBS (0.01 M Tris-HCl pH 8.0, 0.15 M NaCl), 0.05% Tween 20,5% non-fat dried milk] and probed with the antibodies raised against the PVX and the peptides (GenScript Crop, Piscataway, USA), each at the 1:1,000 dilution in the same buffer. After overnight incubation at 5°C, the membranes were washed with 1× TBS-0.05% Tween and exposed to an anti-rabbit IgG alkaline phosphatase conjugate diluted at 1:2,000. Reactions were revealed by incubation with bromo-4-chloro 3-indolyl phosphate and nitroblue tetrazolium.

2.4 *X. fastidiosa*

X. fastidiosa subsp. *fastidiosa* strain IVIA 5387.2 (ST 1) first isolated from an almond tree in Mallorca (Spain) (Moralejo et al., 2019) and reisolated in our facilities from a *N. benthamiana* infected plant, was used within the different experiments. The strain was maintained at - 80°C in Pierce's Disease 2 (PD2) broth supplemented with 30% glycerol. When required, cryoconserved stock cultures were plated on buffered charcoal yeast extract (BCYE) solid medium and grown at 28°C for two passages of 5 days each.

2.5 Inoculation of *X. fastidiosa*

The inoculation of *X. fastidiosa* was performed by microinjection applied to the main stem as described previously (Baró et al., 2021; Moll et al., 2022). Briefly, a

TABLE 1 Primer sequences used to engineer the PVX viral vector for the expression of the *BP134* and *BP178* gene peptides.

Primer code	Sequence (5'-3')	Reference
CX1 BP134 2A	AAACGGCCGATGAGT*AAGAAACTGTTCAAGAAGATCCTTAAGTACCTC***TCCGGA**TCTAGAAATTTTG	This study
CX1 BP178 2A	AAACGGCCGATGAGT*AAGAAGCTGTTCAAGAAGATCCTCAAGTACCTCGCTGGACCAGCTGGCATCGGCAAGTTCCTCCACTCCGCCAAG* TCCGGATCTAGAAATTTTG.	
CX1uni	GTTGTAAAACGACGGCCAGT	Lee et al., 2014

The EagI restriction site used for cloning is underlined, while the BP134 and BP178 gene peptide sequences are in italic.

pathogen suspension, at 10^8 CFU/ml ($OD_{600} \cong 0.3$) confirmed by plate counting, was prepared in phosphate buffered saline (PBS), pelleted (10 min at 13,000 rpm) and resuspended in PD2 broth 1x, to avoid cell aggregation inside the syringe during injection and to ensure cell viability. Inoculations were performed using a high precision microinjector (NanoJet, Chemyx, Stafford, TX, USA) provided with a Hamilton 250 µl syringe including a thin needle with bevel tip (Bondaluz, Switzerland). The needle end was introduced into approximately one half the plant stem diameter to directly access the vascular system, as described previously. Three inoculations of *X. fastidiosa* suspension of 10 µl each (30 µl of total inoculum/plant, $3x10^6$ CFU/plant) were applied at the same side of the stem in a section of 3 cm at around 10 cm above the soil level (Figure 1).

Inoculated plants were cultivated in a Biosafety level II+ quarantine greenhouse authorized by the Plant Health Services, according to EPPO recommended containment conditions (EPPO, 2006), taking into consideration the quarantine status of *X. fastidiosa* in the EU (EFSA PLH Panel et al., 2018).

2.6 Endotherapy treatments

Endotherapy treatments with synthetic BP134 or BP178 were performed following the same procedure as described for pathogen inoculation. Briefly, three applications of 10 µl each of the stock solution at 20 mM (30 µl of peptide/plant, corresponding to 1.94 mg of BP178 or 0.84 mg of BP134 per plant) were performed at the same side of the stem in a section of 15 cm at around 5 cm above the substrate level (Figure 1).

2.7 Effect of treatments on plant infection

The effect of transient expression of *BP134* and *BP178* using the PVX system was compared with that of preventive treatments with synthetic BP134 and BP178 applied by endotherapy. In a first experiment, the effect was evaluated on the disease severity. Nine plants were used for each treatment: (i) non-treated control (NTC), (ii) synthetic BP134, (iii) synthetic BP178, (iv) PVX, (v) PVX expressing *BP134*, and (vi) PVX expressing *BP178*. Treatments, either with synthetic peptides, PVX systems or inoculations with *X. fastidiosa* suspension, were performed as described above. Preventive treatments of synthetic BP178 and BP134 were performed 24 h prior to *X. fastidiosa* inoculation, while the inoculation with PVX systems to the two selected basal leaves (Figure 1) was carried out one week before the inoculation of *X. fastidiosa*. Disease severity was assessed at 30 days post-inoculation of the pathogen (dpi) using the severity scale adapted from the one already described for grapevines (Clifford et al., 2013). The scale was the following 0 = no symptoms, 1 = from one to five leaves just beginning to show decay, 2 = from five to ten leaves showing significant decay, 3 = one-half or more of the leaves showing decay and few showing necrosis, 4 = all the leaves showing decay and one-half or more showing necrosis, 5 = dead plant.

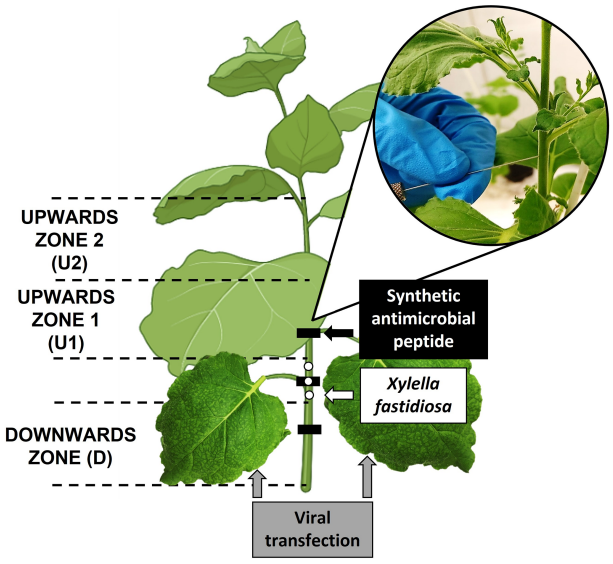

FIGURE 1
Scheme of pathogen inoculation, peptide application points, and the leaves transfected with PVX constructs, and details of inoculation/delivery process in the stem of the plant. The location of each sampling zone is also indicated: Upwards zones (U1 and U2) and downwards zone (D).

In a second experiment, the effect of BP178 on the disease severity and population levels of *X. fastidiosa* was evaluated using four sets of 15 plants each: (1) NTC, (2) synthetic BP178, (3) PVX and (4) PVX expressing *BP178*. The procedure for treatments and inoculation of *X. fastidiosa* were the same as in the previous experiment, and the severity score was evaluated using the already mentioned severity scale. Three plants were assessed for disease severity and sampled for population levels at 7, 14, 21, 30 and 40 dpi. The movement and the population levels of *X. fastidiosa* in xylem tissue were determined by qPCR as described in Baró et al., 2021. Briefly, the bark was removed from the stem samples and the xylem tissue was placed in extraction bags (Bioreba AG, Switzerland) with sterile PBS (ratio 1 ml PBS/0.2 g plant tissue). Homogenization was performed using a hammer followed by the Homex 6 semi-automated homogenizer (Bioreba AG, Switzerland). Bags were incubated at 4°C for 20 min prior to obtain the pelleted cells by centrifugation of 180 µl of homogenate. GeneJET Genomic DNA Purification Kit (Thermo Fisher Scientific, USA) was used for DNA extraction. Three plants for each dpi were analyzed and upward 1 (U1, 8 cm above the inoculation point), upward 2 (U2, 8 cm above U1) and downward (D, 8 cm below the inoculation point) zones were sampled individually for each plant (Figure 1). The number of cells present in the stem was expressed as $\log_{10}$ CFU/g by interpolating the C_T values of each sample in the standard curve (y=-3.42+44.77, R^2 0.9997).

2.8 Effect of treatments on the induction of defense-related genes in plants

The expression levels of defense-related genes in *N. benthamiana* leaves in response to the treatments with synthetic BP178 and of PVX expressing *BP178* were examined. Nine plants were used for each treatment. In addition, a NTC set in which distilled water was applied by endotherapy, and a set of plants expressing empty *PVX* construct alone, were also included. Treatments with either synthetic BP178 or PVX systems were performed as described above, 24 h and 1 week before sampling, respectively. The experiment was performed twice.

Leaf samples were collected and processed to extract RNA for reverse transcription quantitative real-time PCR (RT-qPCR) assays as described in Oliveras et al., 2018. Plant material was ground to a fine powder, and total RNA was extracted from leaves using PureLink Plant RNA Reagent (Invitrogen, Life Technologies). The RNA was solubilized in RNAse free water and was routinely subjected to DNAse treatment (Ambion® Turbo DNA-free™, Life Technologies). First-strand of complementary DNA (cDNA) was generated from total RNA using reverse transcriptase (High-Capacity cDNA Reverse Transcription Kit, Applied Biosystems).

To analyze gene expression in treated *N. benthamiana* plants, a quantitative real-time PCR (qPCR) was carried out in a fluorometric thermal cycler (qPCR Quant Studio 5, Applied Biosystems) by using SYBR®Green PCR Master Mix (Applied Biosystems) as described in Badosa et al., 2017.

Specific oligonucleotides used for the quantification of the target genes involved in plant defense mechanisms are described in Supplementary Table 1. For each gene system, the concentration of the primer pair was optimized to prevent non-specific reactions or artefacts that could hide the result, and the linearity within a range of number of copies of each gene was evaluated as well as the efficiency for each curve was calculated (efficiencies ranging from 80 to 98.8%, $R^2 \geq 0.98$). Melting curve analysis was performed after each amplification to verify amplification specificity. A constitutive gene (actin gene) was used as reference control.

The total reaction volume was 20 µl and the reaction mixture contained 1x SYBR®Green PCR Master Mix (2x), the optimized concentration of primers (either 100, 200 or 300 nM), and 2 µl of cDNA (RT reaction). The qPCR conditions were previously described by Badosa et al., 2017.

Relative quantification of gene expression was done using the $\Delta\Delta C_T$ method (Livak and Schmittgen, 2001), and the relative expression values were normalized against the actin gene as an internal control.

2.9 Data analysis

To test the effect of endotherapy and transient expression of *BP134* and *BP178* on the population levels of *X. fastidiosa* and disease severity in *N. benthamiana* plants, a one-way analysis of variance (ANOVA) was performed. Means were separated according to the Tukey's test at a P value of ≤ 0.05. The statistical significance of the gene expression data was determined using the REST2009 Software (Pfaffl et al., 2002). Expression levels higher than 2-fold change were considered differentially expressed.

3 Results

3.1 Transient expression of peptides BP134 and BP178 with the PVX system

The PVX viral vector system (Lee et al., 2014) was used to transiently express the *BP134* and *BP178* peptides in *N. benthamiana*. Engineered peptide gene sequences were fused to the viral coat protein (CP) *via* the foot and mouth disease virus (FMDV) 2A sequence, which allows the expression of free and CP-fused peptides by a ribosomal skip leading mechanism (Donnelly et al., 2001). About two weeks after the inoculation, upper leaves of plants infected with pCXI BP134 and pCXI

BP178 showed mild chlorosis and deformation (not shown). Western immunoblot analysis demonstrated that both chimeric viruses correctly replicate in *N. benthamiana* (Figure 2), since a band recognized by the anti PVX antibody was present in transfected plants. A protein band of the same size was recognized by a mixture of anti BP134 and BP178 antibodies in the same protein extracts. In addition, anti PVX and anti BP antibodies recognized the PVX CP-BP134 fusion proteins in purified viral particles from infected plants (Figure 2A). Even though it is described that the FMDV 2A sequence also allows the expression of free peptides, they were not detected in any of the protein extracts.

Two different pCXI BP178 plasmids were tested, which are indicated as extract 1 and 2 in Figure 2B. Since the PVX CP-BP178 protein was barely visible in one of them, it was decided to further continue the experiments using the plasmid expressing the highest amount of fusion protein (Figure 2B). No reactions were visible in protein extracts from wild-type plants (WT).

3.2 Symptoms development

The effect of preventive treatments with the synthetic peptides, as well as their transient expression using the PVX system was assessed on the disease severity caused by *X. fastidiosa* IVIA 5387.2 in *N. benthamiana* plants at 30 dpi. Both synthetic peptides, BP134 and BP178, as well as the transient expression of *BP178* significantly decreased disease severity compared to the NTC and PVX control plants, with an efficacy of 69.7%, 76.4% and 73.8%, respectively (Figure 3). NTC and PVX plants showed high levels of disease, and no significant differences in disease severity were observed between them. However, the highest disease severity was observed in plants transiently expressing the peptide *BP134*. In a second transfection experiment, the preventive treatment with BP178 and the production of PVX CP-BP178 in *N. benthamiana* plants confirmed the previously observed efficacy in controlling *X. fastidiosa* infections.

3.3 Dynamics of *X. fastidiosa*

The population of *X. fastidiosa* IVIA 5387.2 in *N. benthamiana* plants preventively treated or transiently expressing *BP178* is presented in Figure 4.

The preventive treatment with the synthetic peptide was the most effective in reducing *X. fastidiosa* cell number, with a maximum decrease of 2.4 to 3 log in all zones analyzed, compared to the NTC. Specifically, a reduction was observed in the U1 zone from 7 to 40 dpi, compared to NTC plants, and being maximum at 21 dpi. In the U2 zone, *X. fastidiosa* cells were not detected until 30 dpi (detection limit 10^3 CFU/g). After this time point an increase in the *X. fastidiosa* population levels was observed in the U2 zone, but they were significantly lower in *BP178* plants than those in the control plants. In the D zone,

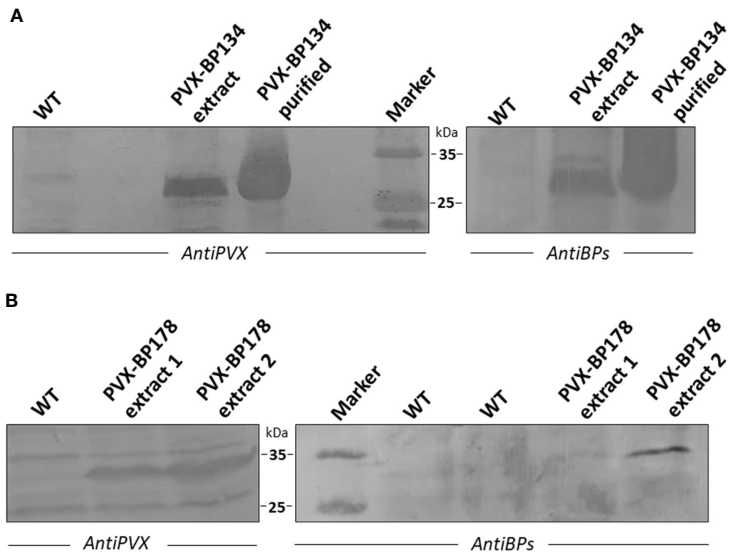

FIGURE 2
Western immunoblot analysis of PVX CP-BP134 and PVX CP-BP178 fusion proteins in total protein extracts from *Nicotiana bentamiana* leaf tissues. WT indicates protein extracts from leaves of non-transfected plants. **(A)** Extracts from PVX-BP134 and WT lines. Purified viral particles of PVX CP-BP134 were also analyzed. **(B)** Extracts from PVX-BP178 lines 1-2 and WT line. Immunodetection was performed using specific polyclonal anti-BP178/antiBP134 or antiPVX antibodies and NBT/BCIP colorimetric detection by alkaline phosphatase-conjugated antibodies.

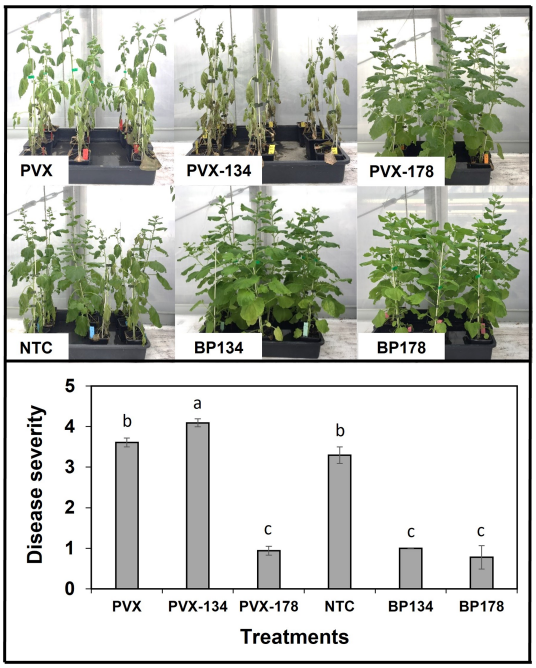

FIGURE 3
Effect of endotherapy with BP178 or BP134, and by heterologous production of the peptides on *Xylella fastidiosa* infections in *Nicotiana benthamiana* plants. The treatments were: PVX, empty vector; PVX-134, vector with BP134 gene; PVX-178, vector with BP178 gene; BP134, synthetic peptide; BP178, synthetic peptide; and NTC, non-treated control. Values are the means of nine plants (three replicates of three plants per each treatment), and error bars represent the standard deviation of the mean. Different letters between treatments correspond to statistically significant differences between treatments (Tukey's test, $p \leq 0.05$).

even though a slight reduction was observed compared to the other treatments, the difference was not as significant as in upward zones, except at 30 dpi, where a clear decrease in population levels is observed, with a reduction of 3 logs.

There was no significant difference in the dynamics of the *X. fastidiosa* population between NTC, PVX and PVX- *BP178* plants, which increased from 7 to 30 dpi and remained stable until 40 dpi in all plant parts analyzed.

3.4 Induction of plant-defense related genes

The ability of BP178 to induce the expression of defense-related genes was assessed in *N. benthamiana* plants using both strategies, endotherapy and transient expression. The expression of 24 genes is presented in Figure 5 by comparison of the levels of expression when applied by endotherapy (BP178 synthetic) or transiently expressed (PVX-BP178). Both treatments significantly upregulated the expression of *PR1*, *PR3*, *PR4* and *CycT9299* genes. When transiently expressed, *Cath, Cyc, PR4a, 9-LOX* and *Endochitinase B*, genes were also upregulated. Synthetic BP178 also induced the expression of *ERF1*, *PR1a*, *PAL* and *PALII* and *WRKY25*.

The effect of PVX and PVX-BP178 compared to the NTC plants is shown in Supplementary Figure 1. In both, PVX and PVX-BP178 treatments, *PR2, PR3, PR5, plastocyanin, PR1a* and *PR1* genes were upregulated, while genes *Cyt C, PR4a, Endochitinase B* and *PR4* were only upregulated when *BP178* was transiently expressed.

4 Discussion

BP134 and BP178 peptides have potent antibacterial activity against several bacterial plant pathogens, including *X. fastidiosa* (Badosa et al., 2013; Baró et al., 2020), and are very effective in protecting plants of agronomic interests from infections caused

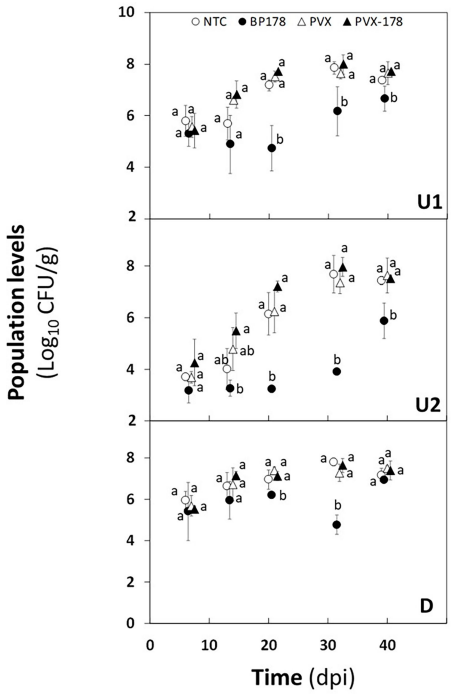

FIGURE 4
Effect of peptide treatment on *Xylella fastidiosa* subsp. *fastidiosa* population levels of *Nicotiana benthamiana* plants over a period of 40 days after pathogen inoculation. From top to bottom graph, *X. fastidiosa* population levels were estimated in the upward zones 1 (U1) and 2 (U2) and in the downward zone (D). Treatments correspond to non-treated control plants (white circle); endotherapy with BP178 (black circle); PVX transfection (white triangle); PVX-BP178 transfection (black triangle). Error bars represent the standard deviation of the mean. Different letters between treatments at specific sampling zones denote statistically significant differences between *X. fastidiosa* population levels (Tukey's test, $p \leq 0.05$).

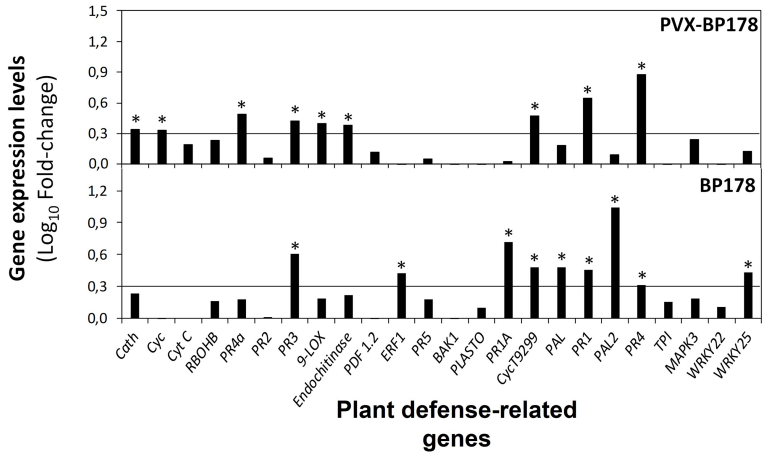

FIGURE 5
Expression levels of defense genes in *Nicotiana benthamiana* plants in response to endotherapy with synthetic BP178 or transient expression with PVX-BP178, using RT-qPCR analysis. Black line, cut-off values for genes with > 2-fold change value (log_{10}, 0.3) (Relative quantification method using $\Delta\Delta C_T$ method). Each BP178 treatment was compared to its appropriate control (i.e., PVX-BP178 compared to PVX control; BP178 applied by endotherapy compared to non-treated control plants, where plants were treated with water by endotherapy). Asterisks indicate significant values of fold-change.

by bacterial and fungal plant pathogens (Badosa et al., 2017; Montesinos L. et al., 2021). Recently we confirmed that BP178 applied by endotherapy and spray to almond plants was able to control infections caused by *X. fastidosa* (Moll et al., 2022). In the present work, we validated *N. benthamiana* as a model plant host for the study of *X. fastidiosa* and evaluated the effect of the transient expression of *BP134* and *BP178* in controlling infections in this model plant compared to the preventive application of the synthetic AMPs by endotherapy.

We demonstrated that *N. benthamiana* plants produce BP134 and BP178 when transiently expressed using a PVX-derived vector system. This agrees with the reports of stable genetic transformation and expression of *BP178* in rice using endosperm specific promoters (Montesinos L. et al., 2017). On the contrary, constitutive expression of *BP134* in rice plants had strong negative impact on rice fitness (Nadal et al., 2012). No yield quantification was performed in our study because when peptides are expressed using a virus-based vector system, transient production levels of heterologous peptides differ between plants, as it depends on physical factors influencing the viral vector infection, environmental conditions, and the physiological state of each plant (Sindarovska and Kuchuk, 2021). In the present study, absence of self-cleavage of the FMDV 2A sequence to obtain the free AMPs was also observed (Kovalskaya et al., 2011), which can be due to the amino acid sequence, as the ratio of fused CP and non-fused viral CP depends on it (Dickmeis et al., 2015). Even so, BP178 fused to the viral CP seems to maintain its activity when transiently produced in *N. benthamiana*, as it reduced *X. fastidiosa* disease severity with an efficacy of 74%. This observed activity agrees with the fact that BP178 has already been produced in the endosperm of rice seeds, showing a protective effect against the bacteria *Dickeya* sp. and the fungus *Fusarium verticillioides* (Montesinos L. et al., 2017).

Contrarily, PVX-BP134 transfected plants and inoculated with *X. fastidiosa* showed the highest severity index among all treatments, although the heterologous production of BP134 in non-pathogen inoculated *N. benthamiana* plants had no detrimental effect. We expected that the large fusion protein (CP-BP134) should not present toxicity because of the large size of the coat protein compared to BP134 (11 amino acids), as it was reported when the *BP134* gene alone was constitutively expressed in rice (Nadal et al., 2012). A possible explanation could be related to the effect of the coinfection itself. PVX infection leads to the synthesis of VSR HcPro in *Nicotiana tabacum*, a viral protein that suppress the plant PAMP Triggered Immunity (PTI), facilitating the multiplication of the pathogen (Navarro et al., 2008; Zvereva et al., 2016). Also, coinfection of rice with Rice yellow mottle virus and *Xanthomonas arboricola* pv. *oryzicola*, was reported to increase bacterial specific symptoms and bacterial load, compared to the bacterial infection alone (Tollenaere et al., 2017). Then, suppression of PTI by PVX together with the detrimental effects of coinfection could explain our results of an increase of symptoms during coinfection of the PVX and *X. fastidiosa*, compared to the *X. fastidiosa* infection alone. In addition, the coinfection of the PVX-BP134 and *X. fastidiosa* increased even more the disease symptoms observed with PVX and *X. fastidosa* coinfection. This should be considered together with the fact that, contrary to BP178, peptide BP134 did not have a significant induction of the

plant immune system (Oliveras et al., 2018). In addition, we cannot discard that the synthesis of CP-BP134 fusion may induce tylose overproduction or other gene products that promoted and exacerbated the symptoms of the disease, but we have not analyzed tylose formation and transcriptomic profiling of PVX-BP134 plants.

Endotherapy with BP134 or BP178 reduced *X. fastidiosa* infections in *N. benthamiana* with efficacies of at least 70%, the same order as compounds used in the field to control diseases caused by this pathogen. For example, *N*-acetyl cysteine (NAC) applications reduced *X. fastidiosa* symptoms between 75 and 80% in infected sweet orange plants under greenhouse conditions (Muranaka et al., 2013), and in olive orchards with initial *X. fastidiosa* incidence, but without showing a decrease in the pathogen population levels by qPCR (Dongiovanni et al., 2017). Endotherapy treatments using oxytetracycline in infected almond trees also showed a significant reduction of disease symptoms, around 73%, related with a low infectivity percentage in leaves detected by DAS-ELISA (Amanifar et al., 2016). In terms of reduction of the levels of *X. fastidiosa*, the microinjection of BP178 was effective compared to NTC plants. This agrees with the *in vitro* bactericidal activity already reported for this functional peptide (Baró et al., 2020). Nevertheless, one single preventive application of the BP178 was not enough to prevent disease in *N. benthamiana* plants, as remaining live cells were still able to grow after 20 dpi. This agrees with the results obtained in almond plants, where increasing the number of AMP applications resulted in a higher reduction of the bacterial population and, consequently of disease severity (Moll et al., 2022).

In contrast, when BP178 was transiently produced, the population levels of *X. fastidiosa* did not decrease compared to the NTC plants, despite the observed reduction of disease severity. This was associated with a higher tolerance of these plants to the pathogen due to an elicitation of the plant immune system triggered by the production of BP178 peptide, with no direct action against the pathogen, due to the upregulation of *PR1*, *PR3*, *PR4*, *PR4a*, *CycT9299*, *Cath*, *Cyc*, *9-LOX* and *Endochitinase*.

It has been reported that tolerance to plant pathogens does not necessarily affect its growth and virulence on the host (Pagan and Garcia-Arenal, 2020). For example, salicylic acid (SA) and ethylene mediate symptom development in *Arabidopsis* plants infected with *Xanthomonas* and *Pseudomonas*, without affecting the growth of both bacterial plant pathogens (Bent et al., 1992; O'Donnell et al., 2001).

We reported that genes coding endochitinase B, PR4 and PR1 proteins were induced in *N. benthamiana* PVX-BP178 plants. However, the endochitinase B and PR4 gene products do not act directly on bacteria because they are antifungal, as confirmed in many plant species including *N. tabacum*, and have been involved in abiotic stresses such as cold, salinity or wound stress (Ali et al., 2018). In addition, PR1 has been involved in plant growth and development (Breen et al., 2017). Then, none of these gene products are expected to influence the growth of *X. fastidiosa*. Among the upregulated genes in *N. benthamiana*, we observed two cyclophilin genes, known for their role in growth and development of plants, hormone signaling (i.e., auxin signaling) and drought tolerance, but not directly related to pathogen multiplication (Singh et al., 2020). Also, cathepsin B was induced, and in the case of *N. benthamiana* it was reported to be required for disease resistance to bacterial pathogens, and for induction of SA-related genes (van der Linde, 2012a, b). In fact, the induction of *cathepsin* gene is required for the induction of *9-LOX* gene to promote cell death (Christensen et al., 2015), which also is being overexpressed in our PVX-BP178 plants. It should be considered that here we have paid attention to only 24 genes in *N. benthamiana*, but many other genes may be implicated in the plant response. Upon treatment with BP178 in tomato (microarray) or almond (RNA seq) we have identified around 100 upregulated/downregulated genes (Montesinos et al., 2021; Moll et al., 2022). Unfortunately, these extensive transcriptomic studies have not been done with PVX-BP178 *N. benthamiana* plants.

Considering our results and the possible role of tyloses in limiting pathogen progression, the overproduction of tyloses is not compatible with the spread of *X. fastidosa* we have observed within the PVX-BP178 plants. Interestingly, Ingel et al., (2020) reported that tylose formation in xylem of grapevine affected by Pierce's Disease is related to upregulation of genes associated to ethylene-signaling, cell wall biogenesis and drought stress, whereas several genes related to photosynthesis and carbon fixation were downregulated. In our case, ERF1 (ethylene transcription factor) and Cyt C (when compared to PVX) that are involved in the ethylene pathway, were not overexpressed in PVX-BP178. Unfortunately, we have not analyzed the tylose formation, and we cannot discard an effect of the peptide treatment on its formation.

Regarding the effect of BP178 in other plants like almond or tomato, *MYB transcription factor*s, osmotin, zinc fingers, terpens or PAL genes were upregulated, whereas in Pierce's diseased grapevine plants, these genes were downregulated (Ingel et al., 2020).

Globally, we consider that transient expression of BP178 could have specific effects in the transcriptome of *N. benthamiana* that somehow compensates the negative effect of *X. fastidiosa* in host plants, but without affecting its population levels.

Since PVX is a plant pathogen, mainly affecting *Solanaceae* (Lico et al., 2015), inoculation with PVX alone induced the expression of several plant defense genes (*PR1*, *PR1a*, *PR2*, *PR3*, *PR5* and *plastocyanin*), compared to NTC plants. However, this effect was unable to prevent infections caused by *X. fastidiosa*. On the contrary, practically no symptoms were observed in PVX-BP178-infected plants in which, in addition to the induction of the genes induced by PVX alone, more genes like *Endochitinase B, Cyt C*, and two *PR4* genes, were overexpressed when comparing to NTC plants. The mechanism by which PVX promote this effect is still not well known. Virus presence in the xylem is poorly investigated although PVX was detected in the vessels of infected *N. benthamiana* (Betti et al., 2012). However, the low number of viable cells in the xylem which is mainly limited to parenchyma

associated cells, makes PVX replication and AMP release in the xylem not quantitative, which could explain the lack of decrease of *X. fastidiosa* levels in PVX-*BP178*-infected plants.

Activation of the plant immune system is a strategy that has reported promising results in the control of *X. fastidiosa*. For example, the application of menadione, a plant defense activator, reduced Pierce´s Disease symptoms between 40 and 50%, (Zhang et al., 2019). Also, the foliar and drench application of abscisic acid to potted vines significantly reduced Pierce´s Disease severity compared to control plants, but only when applied in the fall (Meyer and Kirkpatrick, 2011). So, the capacity of AMPs to activate the plant immune system in addition to their antimicrobial activity, and their possibility to be successfully expressed into the lumen of xylem vessels (Agüero et al., 2005; Dandekar et al., 2012; Dandekar et al., 2019), make them of high interest for the control of systemic plant diseases.

Several plant models have been used to study *X. fastidiosa*. After the first report of *X. fastidiosa* in *Catharanthus roseus* (Ueno et al., 1998), its potential as a plant model was studied (Monteiro et al., 2001). The first symptoms appeared on some of the plants two months after inoculation with *X. fastidosa* subsp. *pauca* 9a5c, and in all the plants after four months. Similar times to symptom development were observed when *Medicago sativa* was inoculated with *X. fastidosa* subsp. *pauca* DeDonno (Kubaa et al., 2019), but in this case limited systemic colonization was observed and a low number of non-inoculated shoots showed presence of the pathogen. Similarly, some ecotypes *of A. thaliana* have been used as a plant model, with colonization of distal tissues such as floral shoots and roots and population levels around 10^6 CFU/g already at 7 days post-inoculation (Pereira et al., 2019). However, no typical symptoms of necrosis or leaf scorch have been observed using this model plant (Rogers, 2012). *Nicotiana tabacum* was also described as a potential model (Lopes et al., 2000) and showed the first symptoms of leaf scorch between 6-8 weeks after inoculation and population levels of *X. fastidiosa* from 10^4 to 10^8 CFU/g tissue, but this system appears to be difficult to reproduce (Lopes et al., 2000; Alves et al., 2008; Francis et al., 2008; De La Fuente et al., 2013).

In our study with *N. benthamiana*, the strain IVIA 5387.2 causing ALS in Mallorca, showed high population levels of 10^8 CFU/g tissue at 3-4 weeks post-inoculation in the three plant zones analyzed and, in all plants, with a rapid development of symptoms and a low variability. Thus, *N. benthamiana* is proposed as a suitable model for the study of efficacy of compounds against *X. fastidiosa* and for other studies, with advantages over the previously used plant models.

The present study gives new insights into the potential of AMPs to control diseases caused by *X. fastidiosa*, more specifically using the expression of *BP178* in plant hosts. It also emphasizes the importance of the plant model *N. benthamiana* to perform *in planta* screening of functional peptides (and eventually other compounds) against *X. fastidiosa.*

Data availability statement

The original contributions presented in the study are included in the article/Supplementary Material, further inquiries can be directed to the corresponding author.

Author contributions

EM, PS and MS obtained the financial support. AB, PS, LM, MS, and EM designed the research, analyzed the data, and wrote the paper. AB, PS and LM conducted and performed the experiments. All authors contributed to the article and approved the submitted version.

Funding

This work was supported by grants from the European Union XF-ACTORS (Ref. 727987) and BeXyL (Ref. 101060593) projects. AB was recipient of a research grant from the Secretaria d'Universitats i Recerca, Departament d'Economia i Coneixement, Generalitat de Catalunya (Ref. 2018 FI B00334).

Acknowledgments

We thank Héctor Saravia and Gemma Roselló for participating in various tasks related to preparation and maintenance of the plant material. We also thank Professor Ulrich Commandeur and Dr Juliane Röder from RWTH Aachen University for their precious advices about the PVX skipping mechanism.

Conflict of interest

The authors declare that the research was conducted in the absence of any commercial or financial relationships that could be construed as a potential conflict of interest.

Publisher's note

Supplementary material

The Supplementary Material for this article can be found online at: https://www.frontiersin.org/articles/10.3389/fpls.2022.1061463/full#supplementary-material

References

Agüero, C. B., Uratsu, S. L., Greve, C., Powell, A. L., Labavitch, J. M., and Meredith, C. P. (2005). Evaluation of tolerance to pierce's disease and botrytis in transgenic plants of *Vitis vinifera* l. expressing the pear *PGIP* gene. *Mol. Plant Pathol.* 6, 43–51. doi: 10.1111/j.1364-3703.2004.00262.x

Ali, S., Ganai, B. A., Kamili, A. N., Bhat, A. A., Mir, Z. A., Bhat,, et al. (2018). Pathogenesis-related proteins and peptides as promising tools for engineering plants with multiple stress tolerance. *Microbiol. Res.* 212-213, 29-37. doi: 10.1016/j.micres.2018.04.008

Alves, E., Kitajima, E. W., and Leite, B. (2008). Interaction of *Xylella fastidiosa* with different cultivars of *Nicotiana tabacum*: a comparison of colonization patterns. *J. Phytopathol.* 151, 500–506. doi: 10.1046/j.1439-0434.2003.00759.x

Amanifar, N., Taghavi, M., and Salehi, M. (2016). *Xylella fastidiosa* from almond in Iran: overwinter recovery and effects of antibiotics. *Phytopathol. Mediterr.* 55, 337–345. doi: 10.14601/Phytopathol_Mediterr-17682

Badosa, E., Moiset, G., Montesinos, L., Talleda, M., Bardají, E., Feliu, L., et al. (2013). Derivatives of the antimicrobial peptide BP100 for expression in plant systems. *PloS One* 8, e85515. doi: 10.1371/journal.pone.0085515

Badosa, E., Montesinos, L., Camó, C., Ruz, L., Cabrefiga, J., Francés, J., et al. (2017). Control of fire blight infections with synthetic peptides that elicit plant defense responses. *J. Plant Pathol.* 99, 65–73. doi: 10.4454/jpp.v99i0.3915.

Badosa, E., Planas, M., Feliu, L., Montesinos, L., Bonaterra, A., and Montesinos, E. (2022). Synthetic peptides against plant pathogenic bacteria. *Microorganisms* 10, 1784. doi: 10.3390/microorganisms10091784

Baldi, P., and La Porta, N. (2017). *Xylella fastidiosa*: host range and advance in molecular identification techniques. *Front. Plant Sci.* 8. doi: 10.3389/fpls.2017.00944

Baró, A., Montesinos, L., Badosa, E., and Montesinos, E. (2021). Aggressiveness of Spanish isolates of *Xylella fastidiosa* to almond plants of different cultivars under greenhouse conditions. *Phytopathology* 111, 1994–2001. doi: 10.1094/PHYTO-02-21-0049-R

Baró, A., Mora, I., Montesinos, L., and Montesinos, E. (2020). Differential susceptibility of *Xylella fastidiosa* strains to synthetic bactericidal peptides. *Phytopathology* 110, 1018–1026. doi: 10.1094/PHYTO-12-19-0477-R

Bent, A. F., Innes, R. W., Ecker, J. R., and Staskawicz, B. J. (1992). Disease development in ethylene-insensitive *Arabidopsis thaliana* infected with virulent and avirulent *Pseudomonas* and *Xanthomonas* pathogens. *Mol. Plant Microbe Interact.* 5, 372–378. doi: 10.1094/mpmi-5-372

Betti, C., Lico, C., Maffi, D., D'Angeli, S., Altamura, M. M., Benvenuto, E., et al. (2012). *Potato virus x* movement in *Nicotiana benthamiana*: New details revealed by chimeric coat protein variants. *Mol. Plant Pathol.* 13, 198–203. doi: 10.1111/j.1364-3703.2011.00739.x

Breen, S., Solomon, P. S., Bedon, F., and Vincent, D. (2015). Surveying the potential of secreted antimicrobial peptides to enhance plant disease resistance. *Front. Plant Sci.* 6. doi: 10.3389/fpls.2015.00900

Breen, S., Williams, S. J., Outram, M., Kobe, B., and Solomon, P. S. (2017). Emerging insights into the functions of pathogenesis-related protein 1. *Trends Plant Sci.* 22, 871–879. doi: 10.1016/j.tplants.2017.06.013

Caravaca-Fuentes, P., Camó, C., Oliveras, À., Baró, A., Francés, J., Badosa, E., et al. (2021). A bifunctional peptide conjugate that controls infections of *Erwinia amylovora* in pear plants. *Molecules* 26, 3426. doi: 10.3390/molecules26113426

Christensen, S. A., Huffaker, A., Kaplan, F., Sims, J., Ziemann, S., Doehlemann, G., et al. (2015). Maize death acids, 9-lipoxygenase-derived cyclopente(a)nones, display activity as cytotoxic phytoalexins and transcriptional mediators. *Proc. Natl. Acad. Sci. U.S.A.* 112, 11407–11412. doi: 10.1073/pnas.1511131112

Clifford, J. C., Rapicavoli, J. N., and Roper, M. C. (2013). A rhamnose-rich O-antigen mediates adhesion, virulence, and host colonization for the xylem-limited phytopathogen *Xylella fastidiosa*. *Mol. Plant Microbe Interact.* 26, 676–685. doi: 10.1094/MPMI-12-12-0283-R

Cruz, S. S., Chapman, A. G., Roberts, I. M., Roberts, D. A., and Oparka, K. J. (1996). Assembly and movement of a plant virus carrying a green fluorescent protein overcoat. *Proc. Natl. Acad. Sci. U. S. A* 93, 6286–6290. doi: 10.1073/pnas.93.13.6286

Dandekar, A. M., Gouran, H., Ibáñez, A. M., Uratsu, S. L., Agüero, C. B., McFarland, S., et al. (2012). An engineered innate immune defense protects grapevines from pierce disease. *Proc. Natl. Acad. Sci. U. S. A* 109, 3721–3725. doi: 10.1073/pnas.1116027109

Dandekar, A. M., Jacobson, A., Ibáñez, A. M., Gouran, H., Dolan, D. L., Agüero, C. B., et al. (2019). Trans-graft protection against pierce's disease mediated by transgenic grapevine rootstocks. *Front. Plant Sci.* 10. doi: 10.3389/fpls.2019.00084

De La Fuente, L., Parker, J. K., Oliver, J. E., Granger, S., Brannen, P. M., van Santen, E., et al. (2013). The bacterial pathogen *Xylella fastidiosa* affects the leaf ionome of plant hosts during infection. *PloS One* 8, e62945. doi: 10.1371/journal.pone.0062945

Dickmeis, C., Honickel, M. M. A., Fischer, R., and Commandeur, U. (2015). Production of hybrid chimeric PVX particles using a combination of TMV and PVX-based expression vectors. *Front. Bioeng. Biotechnol.* 3. doi: 10.3389/fbioe.2015.00189

Dongiovanni, C., Di Carolo, M., Fumarola, G., Ciniero, A., Tauro, D., Palmisano, F., et al. (2017). Recenti sperimentazioni per il controllo di xylella. *Olivo e Olio* 4, 25–29. doi: 10.5281/zenodo.833397

Donnelly, M. L., Hughes, L. E., Luke, G., Mendoza, H., Dam, E. T., Gani, D., et al. (2001). The 'cleavage' activities of foot-and-mouth disease virus 2A site-directed mutants and naturally occurring '2A-like' sequences. *J. Gen. Virol.* 82, 1027. doi: 10.1099/0022-1317-82-5-1027

EFSA (2020). Update of the *Xylella* spp. host plant database - systematic literature search up to 30 June 2019. *EFSA J.* 18, 6114. doi: 10.2903/j.efsa.2020.6114

EFSA PLH Panel, Jeger, M., Caffier, D., Candresse, T., Chatzivassiliou, E., Dehnen-Schmutz, K., et al. (2018). Scientific opinion on the updated pest categorization of *Xylella fastidiosa*. *EFSA J.* 16, 5357. doi: 10.2903/j.efsa.2018.5357

EFSA (2022). Update of the *Xylella* spp. host plant database - systematic literature search up to 31 December 2021. *EFSA J.* 20, 7356. doi: 10.2903/j.efsa.2022.7356

EPPO (2006). PM 3/64 (1) intentional import of organisms that are plant pests or potential plant pests. *EPPO Bull.* 36, 191–194. doi: 10.1111/j.1365-2338.2006.00908.x

EPPO (2019). PM 7/24 (4) *Xylella fastidiosa*. *EPPO Bull.* 49, 175–227. doi: 10.1111/epp.12575

Francis, M., Civerolo, E. L., and Bruening, G. (2008). Improved bioassay of *Xylella fastidiosa* using *Nicotiana tabacum* cultivar SR1. *Plant Dis.* 92, 14–20. doi: 10.1094/PDIS-92-1-0014

Ingel, B., Reyes, C., Massonnet, M., Boudreau, B., Sun, Y., Sun, Q., et al. (2020). *Xylella fastidiosa* causes transcriptional shifts that precede tylose formation and starch depletion in xylem. *Mol. Plant Pathol.* 22, 175–188. doi: 10.1111/mpp.13016

Jung, Y.-Y., and Kang, K.-K. (2014). Application of antimicrobial peptides for disease control in plants. *Plant Breed. Biotech.* 2, 1–13. doi: 10.9787/PBB.2014.2.1.001

Kovalskaya, N., Zhao, Y., and Hammond, R. H. (2011). Antibacterial and antifungal activity of a snakin-defensin hybrid protein expressed in tobacco and potato plants. *Open Plant Sci. J.* 5, 29–42. doi: 10.2174/1874294701105010029

Kubaa, R. A., Giampetruzzi, A., Altamura, G., Saponari, M., and Saldarelli, P. (2019). Infections of the *Xylella fastidiosa* subsp. *pauca* strain "De donno" in alfalfa (*Medicago sativa*) elicits an overactive immune iesponse. *Plants (Basel)* 8, 335. doi: 10.3390/plants8090335

Kyrkou, I., Pusa, T., Ellegaard-Jensen, L., Sagot, M.-F., and Hansen, L. H. (2018). Pierce's disease of grapevines: a review of control strategies and an outline of an epidemiological model. *Front. Microbiol.* 9. doi: 10.3389/fmicb.2018.02141

Laemmli, U. K. (1970). Cleavage of structural proteins during the assembly of the head of bacteriophage T4. *Nature* 227, 680–685. doi: 10.1038/227680a0

Lee, K. L., Uhde-Holzem, K., Fischer, R., Commandeur, U., and Steinmetz, N. F. (2014). Genetic engineering and chemical conjugation of potato virus X. *Methods Mol. Biol.* 1108, 3–21. doi: 10.1007/978-1-62703-751-8_1

Lico, C., Benvenuto, E., and Baschieri, S. (2015). The two-faced potato virus X: from plant pathogen to smart nanoparticle. *Front. Plant Sci.* 6. doi: 10.3389/fpls.2015.01009

Livak, K. J., and Schmittgen, T. D. (2001). Analysis of relative gene expression data using real-time quantitative PCR and the 2-$\Delta\Delta C_T$ method. *Methods* 25, 402–408. doi: 10.1006/meth.2001.1262

Lopes, S. A., Ribeiro, D. M., Roberto, P. G., França, S. C., and Santos, J. M. (2000). *Nicotiana tabacum* as an experimental host for the study of plant-*Xylella fastidiosa* interactions. *Plant Dis.* 84, 827–830. doi: 10.1094/PDIS.2000.84.8.827

López-García, B., San Segundo, B., and Coca, M. (2012). "Antimicrobial peptides as a promising alternative for plant disease protection," in *Small wonders: peptides for disease control*. Eds. K. Rajasekaran, J. W. Cary, J. M. Jaynes and E. Montesinos (Washington DC: American Chemical Society), 263–294.

Meyer, M. M., and Kirkpatrick, B. C. (2011). Exogenous applications of abscisic acid increase curing of pierce's disease-affected grapevines growing in pots. *Plant Dis.* 95, 173–177. doi: 10.1094/PDIS-06-10-0446

Moll, L., Baró, A., Montesinos, L., Badosa, E., Bonaterra, A., and Montesinos, E. (2022). Induction of defense responses and protection of almond plants against

Xylella fastidiosa by endotherapy with a bifunctional peptide. *Phytopathology* 112, 1907-1916. doi: 10.1094/PHYTO-12-21-0525-R

Monteiro, P. B., Renaudin, J., Jagoueix-Eveillard, S., Ayres, A. J., Garnier, M., and Bové, J. M. (2001). *Catharanthus roseus*, an experimental host plant for the *Citrus* strain of *Xylella fastidiosa*. *Plant Dis.* 85, 246–251. doi: 10.1094/PDIS.2001.85.3.246

Montesinos, E. (2007). Antimicrobial peptides and plant disease control. *FEMS Microbiol. Lett.* 270, 1–11. doi: 10.1111/j.1574-6968.2007.00683.x

Montesinos, E., Badosa, E., Cabrefiga, J., Planas, M., Feliu, L., and Bardají, E. (2012). "Antimicrobial peptides for plant disease control," in *Small wonders: peptides for disease control*. Eds. K. Rajasekaran, J. W. Cary, J. M. Jaynes and E. Montesinos (Washington DC: American Chemical Society), 235–261.

Montesinos, L., Bundó, M., Badosa, E., San Segundo, B., Coca, M., and Montesinos, E. (2017). Production of BP178, a derivative of the synthetic antibacterial peptide BP100, in the rice seed endosperm. *BMC Plant Biol.* 17, 63. doi: 10.1186/s12870-017-1011-9

Montesinos, L., Gascón, B., Ruz, L., Badosa, E., Planas, M., Feliu, L., et al. (2021). A bifunctional synthetic peptide with antimicrobial and plant elicitation properties that protect tomato plants from bacterial and fungal infections. *Front. Plant Sci.* 12. doi: 10.3389/fpls.2021.756357

Moralejo, E., Borràs, D., Gomila, M., Montesinos, M., Adrover, F., Juan, A., et al. (2019). Insights into the epidemiology of pierce's disease in vineyards of mallorca, Spain. *Plant Pathol.* 68, 1458–1471. doi: 10.1111/ppa.13076

Muranaka, L. S., Giorgiano, T. E., Takita, M. A., Forim, M. R., Silva, L. F., Coletta-Filho, H. D., et al. (2013). N-acetylcysteine in agriculture, a novel use for an old molecule: focus on controlling the plant-pathogen *Xylella fastidiosa*. *PloS One* 8, 8e72937. doi: 10.1371/journal.pone.0072937

Nadal, A., Montero, M., Company, N., Badosa, E., Messeguer, J., Montesinos, L., et al. (2012). Constitutive expression of transgenes encoding derivatives of the synthetic antimicrobial peptide BP100: impact on rice host plant fitness. *BMC Plant Biol.* 12, 159. doi: 10.1186/1471-2229-12-159

Navarro, L., Jay, F., Nomura, K., He, S. Y., and Voinnet, O. (2008). Suppression of the microRNA pathway by bacterial effector proteins. *Science* 321, 964–967. doi: 10.1126/science.1159505

O'Donnell, P. J., Jones, J. B., Antoine, F. R., Ciardi, J., and Klee, H. J. (2001). Ethylene-dependent salicylic acid regulates an expanded cell death response to a plant pathogen. *Plant J.* 25, 315–323. doi: 10.1046/j.1365-313x.2001.00968.x

Oliveras, A., Baró, A., Montesinos, L., Badosa, E., Montesinos, E., Feliu, L., et al. (2018). Antimicrobial activity of linear lipopeptides derived from BP100 towards plant pathogens. *PloS One* 13, e0201571. doi: 10.1371/journal.pone.0201571

Pagán, I., and García-Arenal, F. (2020). Tolerance of plants to pathogens: a unifying view. *Annu. Rev. Phytopathol.* 58, 77–96. doi: 10.1146/annurev-phyto-010820-012749

Pereira, W. E. L., Ferreira, C. B., Caserta, R., Melotto, M., and de Souza, A. A. (2019). Xylella fastidiosa subsp. pauca and fastidiosa colonize arabidopsis systemically and induce anthocyanin accumulation in infected leaves. *Phytopathology* 109 (2), 225–232. doi: 10.1094/PHYTO-05-18-0155-FI

Pfaffl, M. W., Horgan, G. W., and Dempfle, L. (2002). Relative expression software tool (REST) for group-wise comparison and statistical analysis of relative expression results in real-time PCR. *Nucleic Acids Res.* 30, e36. doi: 10.1093/nar/30.9.e36

Randall, J. J., Goldberg, N. P., Kemp, J. D., Radionenko, M., French, J. M., Olsen, M. W., et al. (2009). Genetic analysis of a novel *Xylella fastidiosa* subspecies found in the southwestern united states. *Appl. Environ. Microbiol.* 75, 5631–5638. doi: 10.1128/AEM.00609-09

Röder, J., Dickmeis, C., Fischer, R., and Commandeur, U. (2018). Systemic infection of *Nicotiana benthamiana* with *Potato virus x* nanoparticles presenting a fluorescent iLOV polypeptide fused directly to the coat protein. *Biomed. Res. Int.* 2018, 9328671. doi: 10.1155/2018/9328671

Rogers, E. E. (2012). Evaluation of *Arabidopsis thaliana* as a model host for *Xylella fastidiosa*. *Mol. Plant Microbe Interact.* 25, 747–754. doi: 10.1094/MPMI-11-10-0270

Saitoh, H., Kiba, A., Nishihara, M., Yamamura, S., Suzuki, K., and Terauchi, R. (2001). Production of antimicrobial defensin in *Nicotiana benthamiana* with a potato virus X vector. *Mol. Plant Microbe Interact.* 14, 111–115. doi: 10.1094/MPMI.2001.14.2.111

Shukla, S., Dickmeis, C., Nagarajan, A. S., Fischer, R., Commandeur, U., and Steinmetz, N. F. (2014). Molecular farming of fluorescent virus-based nanoparticles for optical imaging in plants, human cells and mouse models. *Biopamater. Sci.* 2, 784. doi: 10.1039/C3BM60277J

Sindarovska, Y., and Kuchuk, M. (2021). Long-term *Potato virus x* (PVX)-based transient expression of recombinant GFP protein in *Nicotiana benthamiana* culture *in vitro*. *Plants* 10, 2187. doi: 10.3390/plants10102187

Singh, H., Kaur, K., Singh, M., Kaur, G., and Singh, P. (2020). Plant cyclophilins: multifaceted proteins with versatile roles. *Front. Plant Sci.* 11. doi: 10.3389/fpls.2020.585212

Tollenaere, C., Lacombe, S., Wonni, I., Barro, M., Ndougonna, C., Gnacko, F., et al. (2017). Virus-bacteria rice co-infection in Africa: Field estimation, reciprocal effects, molecular mechanisms, and evolutionary implications. *Front. Plant Sci.* 8. doi: 10.3389/fpls.2017.00645

Towbin, H., Staehelin, T., and Gordon, J. (1979). Electrophoretic transfer of proteins from poly- acrylamide gels to nitrocellulose sheets: Procedure and some applications. *Proc. Natl. Acad. Sci. U. S. A* 76, 4350–4354. doi: 10.1073/pnas.76.9.4350

Ueno, B., Funada, C. K., Yorinori, M. A., and Leite, R. P.Jr. (1998). First report of *Xylella fastidiosa* on *Catharanthus roseus* in Brazil. *Plant Dis.* 82, 712. doi: 10.1094/PDIS.1998.82.6.712A

van der Linde, K., Hemetsberger, C., Kastner, C., Kaschani, F., van der Hoorn, R. A., Kumlehn, J., et al. (2012a). A maize cystatin suppresses host immunity by inhibiting apoplastic cysteine proteases. *Plant Cell* 24, 285–1300. doi: 10.1105/tpc.111.093732

van der Linde, K., Mueller, A., Hemetsberger, C., Kaschani, F., van der Hoorn, R. A., and Doehlemann, G. (2012b). The maize cystatin CC9 interacts with apoplastic cysteine proteases. *Plant Signal. Behav.* 7, 1397–1401. doi: 10.4161/psb.21902

Van Esse, H. P., Reuber, T. L., and van der Does, D. (2020). Genetic modification to improve disease resistance in crops. *New Phytol.* 225, 70–86. doi: 10.1111/nph.15967

Visser, M., Stephan, D., Jaynes, J. M., and Burger, J. T. (2012). A transient expression assay for the *in planta* efficacy screening of an antimicrobial peptide against grapevine bacterial pathogens. *Lett. Appl. Microbiol.* 54, 543–551. doi: 10.1111/j.1472-765X.2012.03244.x

Zhang, S., Jain, M., Fleites, L. A., Rayside, P. A., and Gabriel, D. W. (2019). Identification and characterization of menadione and benzethonium chloride as potential treatments of pierce's disease of grapevines. *Phytopathology* 109, 233–239. doi: 10.1094/PHYTO-07-18-0244-FI

Zvereva, A. S., Golyaev, V., Turco, S., Gubaeva, E. G., Rajeswaran, R., Schepetilnikov, M. V., et al. (2016). Viral protein suppresses oxidative burst and salicylic acid-dependent autophagy and facilitates bacterial growth on virus-infected plants. *New Phytol.* 211, 1020–1034. doi: 10.1111/nph.13967

frontiers | Frontiers in Plant Science

TYPE Original Research
PUBLISHED 09 May 2023
DOI 10.3389/fpls.2023.1161702

OPEN ACCESS

EDITED BY
Roberto Buonaurio,
University of Perugia, Italy

REVIEWED BY
Padmani Sandhu,
Institute of Microbial Technology (CSIR), India
Lucy N. Moleleki,
University of Pretoria, South Africa

*CORRESPONDENCE
Iris Yedidia
irisy@volcani.agri.gov.il

RECEIVED 08 February 2023
ACCEPTED 19 April 2023
PUBLISHED 09 May 2023

CITATION
Pun M, Khazanov N, Galsurker O, Kerem Z, Senderowitz H and Yedidia I (2023) Inhibition of AcrAB-TolC enhances antimicrobial activity of phytochemicals in *Pectobacterium brasiliense*. *Front. Plant Sci.* 14:1161702. doi: 10.3389/fpls.2023.1161702

Inhibition of AcrAB-TolC enhances antimicrobial activity of phytochemicals in *Pectobacterium brasiliense*

Manoj Pun[1,2], Netaly Khazanov[3], Ortal Galsurker[1], Zohar Kerem[2], Hanoch Senderowitz[3] and Iris Yedidia[1]*

[1]The Institute of Plant Sciences, Volcani Center, Agricultural Research Organization (ARO), Rishon Lezion, Israel, [2]The Robert H. Smith Faculty of Agriculture, Food and Environment, The Hebrew University of Jerusalem, Rehovot, Israel, [3]Department of Chemistry, Bar-Ilan University, Ramat Gan, Israel

Introduction: The eons-long co-evolvement of plants and bacteria led to a plethora of interactions between the two kingdoms, in which bacterial pathogenicity is counteracted by plant-derived antimicrobial defense molecules. In return, efflux pumps (EP) form part of the resistance mechanism employed by bacteria to permit their survival in this hostile chemical environment. In this work we study the effect of combinations of efflux pump inhibitors (EPIs) and plant-derived phytochemicals on bacterial activity using *Pectobacteriun brasiliense* 1692 (Pb1692) as a model system.

Methods: We measured the minimal inhibitory concentration (MIC) of two phytochemicals, phloretin (Pht) and naringenin (Nar), and of one common antibiotic ciprofloxacin (Cip), either alone or in combinations with two known inhibitors of the AcrB EP of *Escherichia coli*, a close homolog of the AcrAB-TolC EP of Pb1692. In addition, we also measured the expression of genes encoding for the EP, under similar conditions.

Results: Using the FICI equation, we observed synergism between the EPIs and the phytochemicals, but not between the EPIs and the antibiotic, suggesting that EP inhibition potentiated the antimicrobial activity of the plant derived compounds, but not of Cip. Docking simulations were successfully used to rationalize these experimental results.

Discussion: Our findings suggest that AcrAB-TolC plays an important role in survival and fitness of Pb1692 in the plant environment and that its inhibition is a viable strategy for controlling bacterial pathogenicity.

KEYWORDS

AcrAB-TolC, efflux pumps, inhibitors, naringenin, *Pectobacterium brasiliense*, phloretin, virulence, PAβN

1 Introduction

Plants and bacteria have coevolved for over 480 million years producing a plethora of interactions between the kingdoms. To protect against pathogenic bacteria, plants produce a large array of secondary metabolites, of which phenolic compounds have been widely reported as antimicrobial agents (Pasqua et al., 2019). In response, phytopathogenic bacteria have evolved systems to deal with this rich chemical environment, including plasma membrane efflux pumps (EP) that remove toxic compounds from the cell, minimizing the pressure and facilitating survival and colonization of the host (Du et al., 2018; Pasqua et al., 2019). Large numbers of diverse and structurally unrelated compounds are excreted by EP, including disinfectants, dyes, organic solvents, detergents, bile acids, hormones, heavy metals, and a variety of defense active phytochemicals (Piddock, 2006; Alibert et al., 2017).

EP are commonly classified into five families based on their number of transmembrane spanning regions, energy sources and substrates. Of these five families, the resistance-nodulation-division (RND) superfamily is found only in Gram-negative bacteria. RND transporters are composed of a tripartite complex: an inner membrane protein, periplasmic membrane fusion protein (MFP) and an outer membrane protein (OMF). This arrangement facilitates efflux across both the inner and outer membrane, thereby conferring broad spectrum resistance to the cell (Wiggins, 2004; Zhao et al., 2021). These transporters are usually chromosomally encoded and are expressed constitutively in wild-type cells (Lomovskaya and Watkins, 2001; Wiggins, 2004; Elnasser et al., 2021).

Of the multiple RND transporters, the tripartite drug efflux complexes AcrAB-TolC and MexAB-OprM from *Escherichia coli* and *Pseudomonas aeruginosa* respectively, have been extensively studied (Li et al., 2015; Venter et al., 2015; Blanco et al., 2016; Cacciotto et al., 2018; Zhao et al., 2021). AcrAB-TolC is composed of three essential components: Homotrimeric protein AcrB which is embedded in the inner membrane and pumps out diverse substances using a proton gradient as an energy source, TolC a homotrimeric membrane protein with long cylindrical-like structure that provides conduit across the outer membrane, and AcrA which is a periplasmic adaptor protein that connects AcrB and TolC (Vargiu et al., 2014; Kim et al., 2015; Wang et al., 2017).

Similar to *E. coli*, plant pathogens in the order Enterobacterales use EP to protect the cell against the chemical environment. Such an example is *Pectobacterium brasiliense*, a Gram-negative plant-pathogen of the Pectobacteriaceae, a family of multiple genera that cause bacterial soft rot and blackleg diseases, leading to plant tissue maceration and finally wilting and collapse of the entire infected plant tissue (Lu et al., 2021; Oulghazi et al., 2021). *Pectobacteriun* along with *Dickeya* are distributed worldwide and ranked among the top 10 list of significant bacterial pathogens in agricultural ecosystems, based on their economic importance (Czajkowski et al., 2011; Mansfield et al., 2012; van der Wolf, 2021). Barabote et al. (2003) reported a role for *tolC* of *Erwinia chrysanthemi* (now *Dickeya chrysanthemi*) in survival and colonization of the pathogen in plant tissues, by protecting the bacterium from antimicrobial compounds produced by plants (Barabote et al., 2003). Similarly, AcrAB was shown as an essential component in conferring tolerance to apple phytoalexins in the fire blight pathogen *Erwinina amylovora*. Indeed, mutation in *acrB* significantly increased the pathogen's sensitivity and attenuated its virulence (Burse et al., 2004). Comprehensive analysis of different RND efflux pumps in *E. chrysanthemi* revealed two Acr-like systems and two Emr-like systems (Maggiorani Valecillos et al., 2006). RND superfamily proteins have also been reported in other Gram-negative plant associated bacteria such as *Agrobacterium tumefaciens*, the nitrogen-fixing symbiont *Rhizobium etli*, *Bradyrhizobium japonicum and Burkholderia glumae* (Burse et al., 2004; Al-karablieh et al., 2009; Vargas et al., 2011). Complete genome sequence of *P. brasiliense* (Pb1692) has been published, with two annotated genes for *acrB* (GT391_RS01465 and GT391_RS15000) (Liu and Filiatrault, 2020).

Taking the on-going interactions between plants and pathogens to the next level, plants have developed a host of efflux pump inhibitors (EPIs). These were demonstrated to enhance the antibacterial potency of selected plant-derived and other compounds, to expand their spectrum of activity, to reduce the rates of resistance development and to reverse resistance (Lomovskaya and Watkins, 2001; Lomovskaya and Bostian, 2006; Opperman and Nguyen, 2015; Venter et al., 2015; Lamut et al., 2019). Following these previous reports, in this work we aimed to increase the activity of existing antibacterial compounds, including known plant defense molecules, by targeting AcrB of Pb 1692. To this end, we assessed the antibacterial activity of selected phytochemicals [phloretin (Pht), naringenin (Nar), carvacrol, salicyclic and *p*-coumaric acids] in the absence and presence of several known EPIs, namely, Phe-Arg β-naphthylamide (PAβN), 1-(1-naphthylmethyl) piperazine (NMP), berberine, and quinoline and found a synergistic activity between the EPI PAβN and the phytochemicals Pht and Nar. The experimental results were supported and explained by molecular docking simulations.

2 Results

In this work, we set out to determine the effect of EPIs on the antibacterial activity of plant-derived phytochemicals under the assumption that the simultaneous application of both types of compounds will synergistically enhance antibacterial activity. To test this hypothesis, we determined minimum inhibitory concentrations (MIC) of several plant-derived phytochemicals in the absence and presence of several known EPIs.

2.1 Efflux inhibition increased ethidium bromide (EtBr) accumulation

We started by testing the activity of the EPIs on Pb1692 efflux inhibition. For this purpose, a common assay measuring the accumulation of the EP substrate EtBr inside the bacterial cells was used (Coldham et al., 2010). As shown previously by Coldham et al., 2010, the concentration of EtBr is expected to increase within the cells in correlation with EP inhibition. The positive control in these assays are dead cells, where the efflux is abolished by the lack of an active electrochemical gradient, in which EtBr accumulates

undisturbed inside the cells (Reens et al., 2018). The control for the inhibitory effect is live Pb1692 cells, without exposure to EPIs, and thus, fully functional EPs. Therefore, we expect to have the highest fluorescent (i.e. EtBr accumulation) in the heat-killed bacteria and the lowest fluorescent in live cells where the EP is fully functional.

EtBr accumulation (higher florescent level), revealed that PAβN was more effective in the inhibition of the efflux activity in Pb1692 than NMP or quinoline (Figure 1). Even at 25 μM of PAβN and 0.1 mM of NMP the efflux activity was inhibited (Figure 1A). In the case of quinoline, no accumulation of EtBr was observed leading to a similar pattern as the control treatment, for the tested concentrations 15 and 20 μM (Figure 1B). The different concentrations were selected based on the MIC results, where the highest concentration that did not show an effect on the growth of Pb1692 was selected for further investigation.

2.2 EPI effect on Minimum Inhibitory Concentration (MIC) of the plant derived small molecules

To determine MIC of EPIs and of selected compounds, a 2-fold serial dilutions using the broth-dilution method (Clinical and Laboratory Standards Institute, 2017) was used. The results are presented in Figure 2, and demonstrate that from among the EPIs tested here, quinoline displayed a relatively strong inhibitory effect on Pb1692 growth, resulting in a low MIC value of 120 μM. The other EPIs studied here, PAβN, NMP and berberine, showed MIC values of 800 μM, 2 mM and 3 mM, respectively. Time dependent growth curves relative to the control treatments DMSO (1%) and dH_2O are provided in Supplementary Figure 1.

Looking at the phenolic compounds (Nar, Pht, salicyclic and *p*-coumaric acids), a similar assay revealed only weak antimicrobial activity for Pht and carvacrol with the lowest MIC value of 1mM (see Figure 3 and Table 1). The antibiotic Cip, which impairs cell division in Gram-negative bacteria was used as a positive control and presented 4 orders of magnitude higher antimicrobial activity with a MIC value of 30.2 nM (10 ng/μl). Time dependent growth curves relative to control treatments with DMSO (1%) and dH_2O are presented in Supplementary Figure 2.

Next, MIC values for each of the phenolic compounds were determined in combination with each EPI (Table 1). The combinations that provided the most significant reduction in MIC value were those of PAβN at 50 μM with either Pht or Nar, leading to 5 and 12 fold reduction, respectively. A combination of carvacrol with PAβN resulted in reduced MIC value by 2 fold, revealing a stronger effect of the above compounds with the EPI.

2.3 Synergism between EPIs and the selected phytochemicals

The Checkerboard assay was used to determine whether certain combinations of EPIs with phenolic compounds exerted a

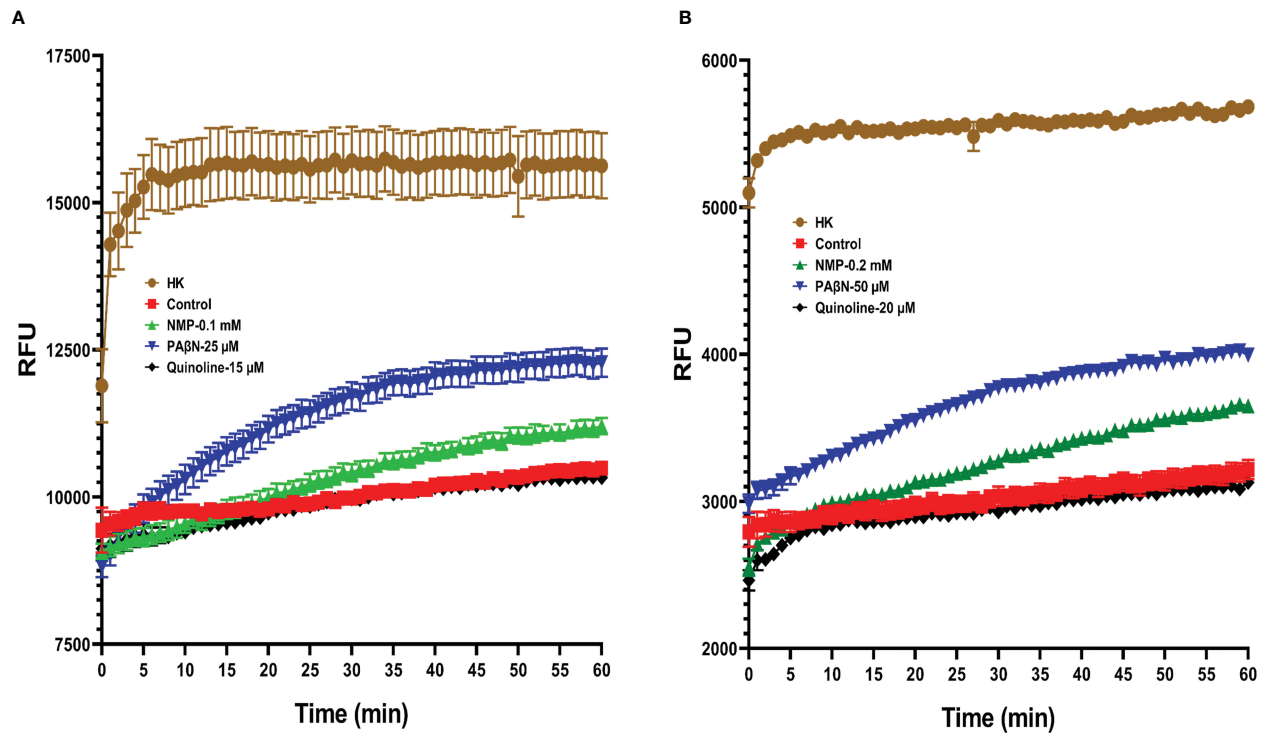

FIGURE 1
EtBr accumulation in the presence of different EPIs in *Pectobacterium brasiliense* (Pb1692), as observed by Relative Fluorescence Units (RFU). NMP, PAβN and quinoline were tested at concentrations of: **(A)** 0.1mM, 25μM and 15μM and **(B)** 0.2mM, 50μM and 20μM, respectively. All assays were performed in triplicate, and the representative results of one experiment are shown. (HK= heat killed bacteria, 1-(1-naphthylmethyl) piperazine (NMP), Phenylalanine-arginine-β-naphthylamide (PAβN) and quinoline).

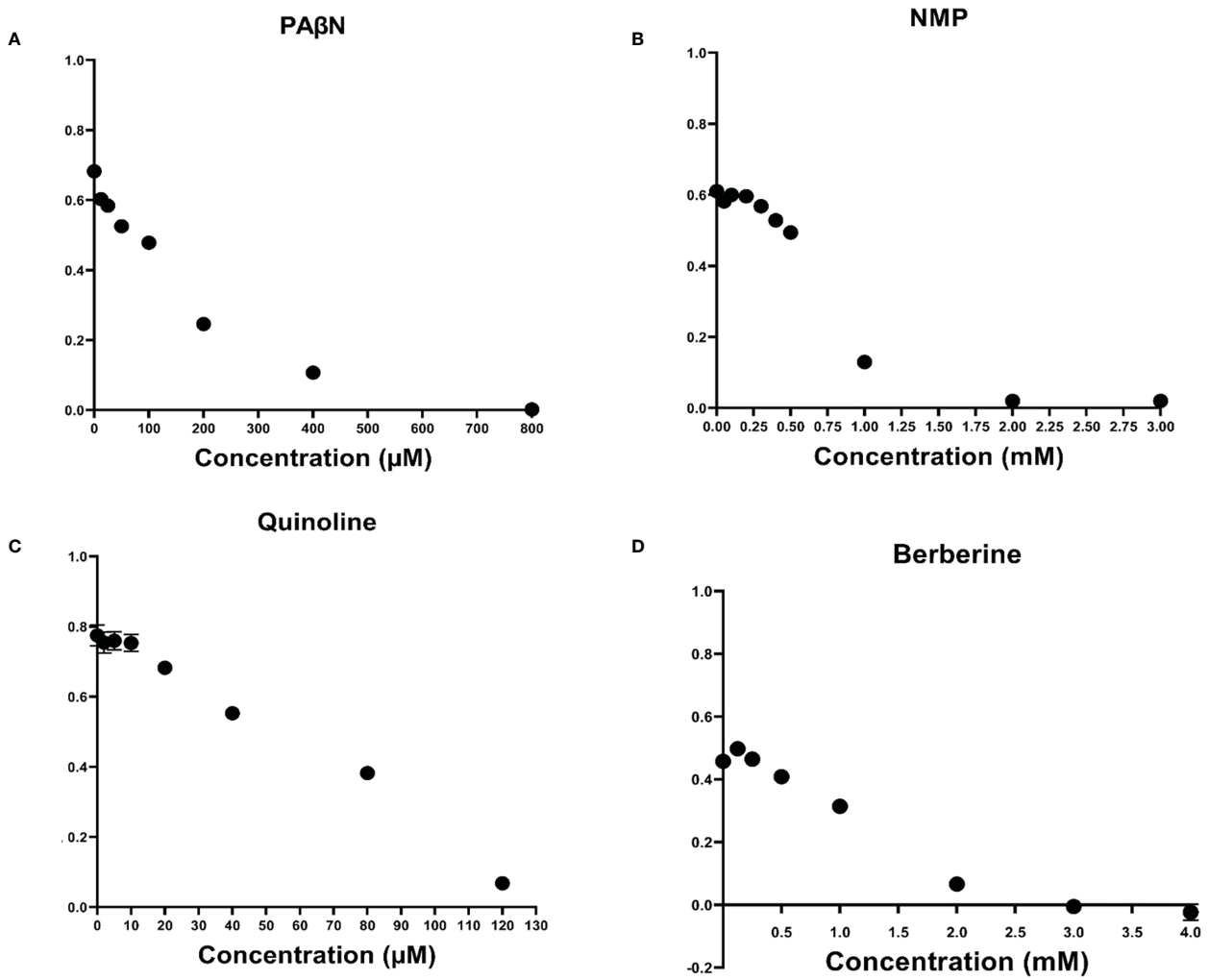

FIGURE 2
Effect of efflux pump inhibitors on the growth of *Pectobacterium brasiliense* (Pb1692). Growth (OD 600 nm) of Pb1692 at 18 h in the presence of two-fold increasing concentrations of **(A)** 1-(1-naphthylmethyl) piperazine (NMP), **(B)** Phenylalanine-arginine-β-naphthylamide (PAβN), **(C)** Quinoline, and **(D)** Berberine. Bacteria were grown in LB at 28°C, for 24 h and and growth was recorded every hour (bar = SE; n = 8). Each experiment was repeated twice. Analysis was made by GraphPad Prism 8.0.

synergistic effect on bacterial growth (expressed as MIC). The Fractional Inhibitory Concentration Index (FICI) was calculated from the growth inhibition results after 24 h of growth. FICI results for each combination are interpreted as follows: FICI ≤ 0.5, synergism; 0.5< FICI< 1, additive; 1 ≤ FICI< 2, indifferent; and FICI ≥ 2, antagonism. The results are presented in Table 2 and demonstrate that combining PAβN with either Pht or Nar led to a synergistic effect, with 5 and 12 fold reduction in their MIC value respectively. The other combinations tested with PAβN led to an additive effect only. NMP also led to a synergistic effect with Nar, whereas berberine and quinoline, presented an additive effect with some of the compounds. No synergistic effect was observed neither with PAβN, nor with NMP in combination with Cip, although it is a known substrate of the EP in *E. coli*. This was reflected in a calculated FICI value of 0.75 or 0.93 respectively, supporting an additive effect.

2.4 Differential expression of *acrAB-tolC* gene components in the presence of EPIs

To explore the effect of the compounds at sub-MIC concentrations on gene expression patterns of the components of *acrAB-tolC* genes, a qPCR analysis was performed. Primers for *acrA*, *acrB* and *tolC* in Pb1692 were designed (Supplementary Table 1). The expression of the tripartite genes was evaluated at two time points (15 min, and 2 h). These were selected based on our preliminary results as well as previous findings in *E. coli* (Kobayashi et al., 2006). Based on the FICI results, two substrates of AcrAB-TolC, Pht and Nar and one antibiotic Cip, were evaluated in this assay with and without the presence of the EPIs, PAβN and NMP.

The results are presented in Figure 4 and demonstrate that the expression of the efflux pump genes *acrA* and *TolC*, increased significantly at an early phase, following the application of either

10.3389/fpls.2023.1161702

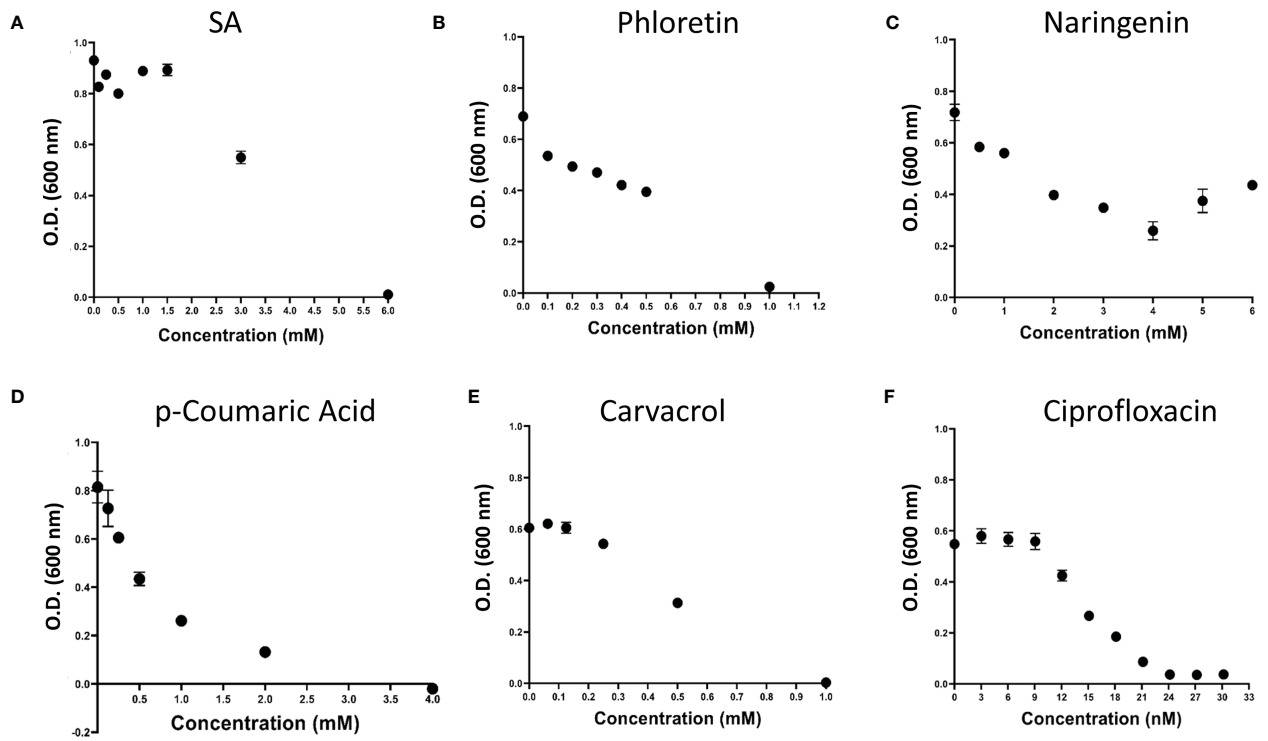

FIGURE 3
Effect of plant phenolic compounds and the antibiotic ciprofloxacin (Cip) on growth of *P. brasiliense* (Pb1692). Growth (OD 600 nm) of Pb1692 at 18 h in the presence of two-fold increasing concentration of **(A)** Salicylic acid, **(B)** Phloretin, **(C)** Naringenin, **(D)** *p*-Coumaric acid, **(E)** Carvacrol, **(F)** Ciprofloxacin. Bacteria were grown in LB at 28°C, for 24 h and growth was recorded every hour (bar = SE; n = 8). Analysis was made by GraphPad Prism 8.0.

Pht or Nar (at 15 min and 2 h) alone, or in combination with the EPIs (NMP and PAβN) (Figures 4A, E, alone; B, F combined). Relative to the control treatment, PAβN treatment induced higher transcripts levels of *acrA* and *TolC* genes after 2 h (Figures 4B, F), and had no effect on *acrB* expression level (Figures 4C, D). The expression of *acrB* was increased after 2 h following the application of the antibiotic Cip and the EPI NMP (2.5 fold) relative to the application of dH_2O. Unlike PAβN, the application of NMP at all time points, did not induce upregulation of *acrA* and *TolC* (Figures 4A, B, E, F). The *acrB* gene was upregulated when Cip was applied together with NMP or PAβN peaking at 2 h (Figures 4C, D). The combinations of the EPIs with Pht or Nar provided inconsistent results, with upregulation of the expression at 2 h only for the combination of NMP and Pht (Figure 4D).

2.5 Plant phenolic compounds in combination with EPIs, effectively reduce Pb1692 infection

The effect of the natural compounds and their combination with the selected EPIs (PAβN and NMP) was tested in potato tubers and in leaf discs of calla lily as hosts. Infection experiments were performed with Pb1692 according to previously described protocols

TABLE 1 MIC values of tested compounds and combinations.

	Compound	MIC				
		Alone	+ PAβN 50 µM	+ NMP 0.2 mM	+ Berberine 0.5 mM	+ Quinoline 20 µM
1	Phloretin	1 mM	0.2 mM	1 mM	1 mM	1 mM
2	Naringenin	>6 mM	0.5 mM	0.5 mM	2 mM	2 mM
3	Salicylic acid	6 mM	4 mM	4 mM	4 mM	4 mM
4	*p*-Coumaric acid	4 mM	2 mM	2 mM	ND	4 mM
6	Carvacrol	1 mM	500 µM	1 mM	1 mM	1 mM
7	Ciprofloxacin	30.2 nM	30.2 nM	30.2 nM	30.2 nM	30.2 nM

10.3389/fpls.2023.1161702

TABLE 2 FICI values of the studied EPIs-phenolic compounds combinations.

No	Compound	FICI value			
		PAβN	NMP	Berberine	Quinoline
1	Phloretin	0.33-0.26	0.75	1.1	>0.67
2	Naringenin	≤0.16	0.436	0.626	>0.67
3	Carvacrol	0.52	≥0.6	0.54	1.16
4	Salicyclic Acid	0.682	0.72	0.87	0.83
5	*p*-Coumaric Acid	0.52	0.55	ND	0.67
6	Ciprofloxacin	0.75	0.93	1.16	1.05

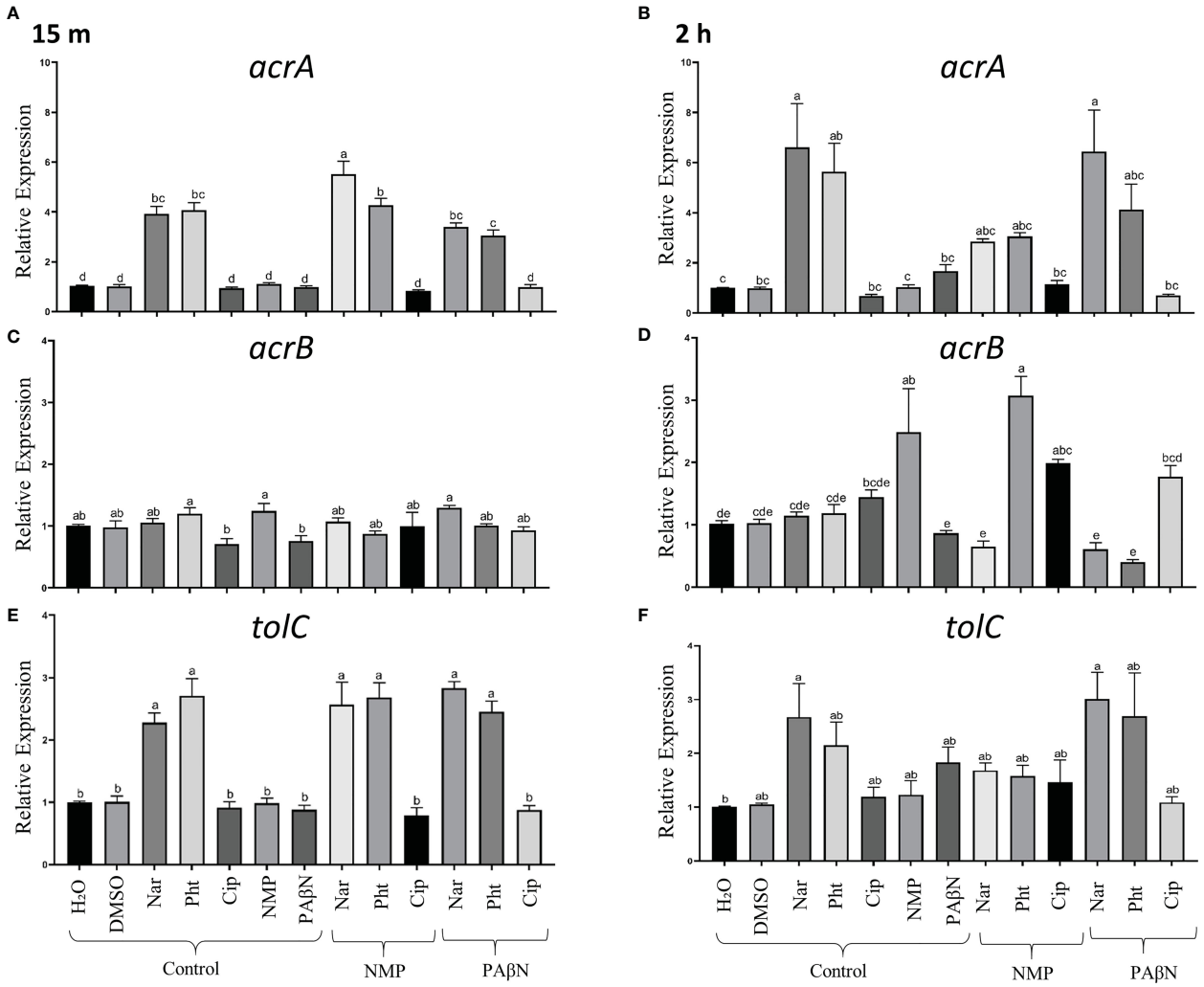

FIGURE 4
Effects of phloretin (Pht), naringenin (Nar), ciprofloxacin (Cip), NMP and PAβN alone and in combinations, on transcript levels of the tripartite genes associated with the efflux pump AcrAB-TolC in *Pectobacterium brasiliense* (Pb1692). The expression levels of *acrA*, *acrB*, and *tolC* were determined by qPCR of bacterial cultures grown in LB, 28°C at 15 min (first measurement) and 2 h, in the presence of the tested compounds or their combinations. **(A, B)** Relative expression of *acrA* at 15 min and 2 h post exposure to the compounds, respectively. **(C, D)** Relative expression of *acrB* as above, and **(E, F)** Relative expression of *tolC*, as above. Control samples were treated with dH_20 or 0.3% DMSO. Bars represent means + standard errors (SE) of the relative gene expression observed in three experiments, each with nine replicates per treatment. The experiments were repeated three times. One-way ANOVA with *post hoc* Tukey-Kramer HSD tests was used to analyze differences. Bars that are not labelled with the same letter are significantly different from each other ($P< 0.05$; bar = mean + SE; $n = 9$).

(Luzzatto et al., 2007; Joshi et al., 2015). All compounds were tested alone at non-growth-inhibiting concentrations, or in combinations of each phytochemical with the tested EPI. The results revealed significant effects on disease severity. The combination of NMP at 0.2 mM and PAβN at 50 µM with either Pht or Nar led to decreased disease symptoms in both calla lily leaves and potato tubers. Cip, which is also a known substrate of AcrB, did not exert the same inhibitory effect on disease development (Figure 5).

2.6 Computational studies

2.6.1 Homology modeling

In order to obtain atomic-scale information on how the different EPIs occupy the binding site of AcrB as well as to rationalize the experimental findings, we resorted to molecular docking. Since the crystal structure of the efflux transporter AcrB of Pb1692 has not been solved to date, a suitable homology model was first constructed and validated based on the crystal structure of *E. coli* AcrB (PDB code: 3AOD; see Figure 6 and the Methods section). Similar to AcrB of *E. coli*, AcrB of *P. brasiliense* is a homotrimer, with each of three monomers representing a different intermediate state along the transport process, namely, `access` (chain C) -`binding` (chain A) - `extraction` (chain B). Thus, the conformation of each of the monomers is different. The access and binding states are characterized by distinct binding sites termed the proximal and distal sites, respectively.

The resulting model was prepared for docking using Schordinger's protein preparation wizard (see Methods section for more details) and the four EPIs considered in this work were docked into the two sites. The results are presented in Table 3. In agreement with the experimental data, PAβN is predicted to be the best binder into both sites with Glide scores of -5.6 (distal site) and -7.7 (proximal site) kcal/mol.

The experimental results presented in this work suggest that PAβN inhibits the efflux of the two AcrB substrates, Pht and Nar, but not of the antibiotic Cip. To rationalize these observations, we docked Pht, Nar, and Cip into the proximal and distal binding sites either alone or in combination with PAβN. The results are presented in Table 4 and Figure 7, and suggest stronger binding of both Nar and Pht than of Cip to the proximal site of the pump either in the absence or in the presence of PAβN. Thus, the Nar +PAβN/Pht+PAβN combinations effectively block the entrance of compounds to the access site of the flux pump, more than the Cip +PAβN combination does. The summary of these observations is provided in a simplified model (Figure 8), that demonstrates how in contrast to the antibiotic Cip, the plant derived compounds Nar and Pht accumulate in the bacterial cell in response to EP inhibition.

3 Discussion

Plant pathogenic bacteria inhabit a complex chemical environment, in which they are exposed to diverse antimicrobial

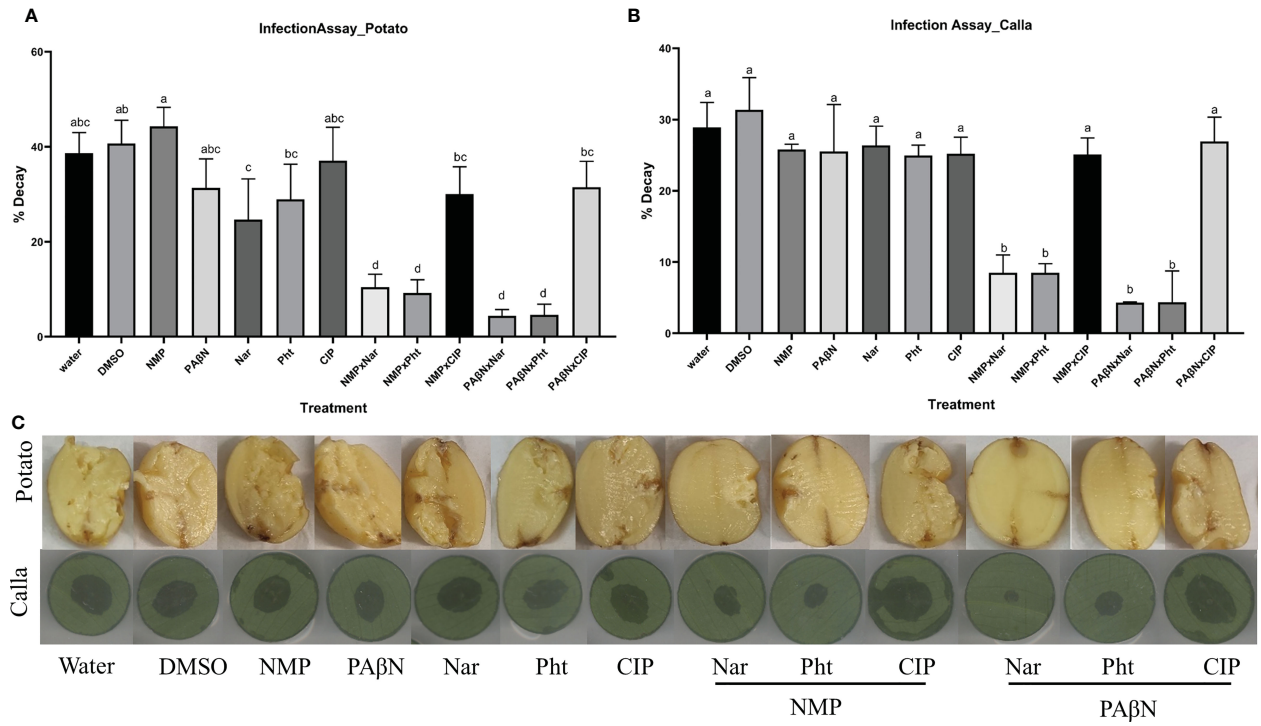

FIGURE 5
Effects of efflux pump inhibitors alone and in combinations with the plant derived compounds phloretin and naringenin (Pht and Nar, respectively) and the antibiotic Ciprofloxacin (Cip), on *Pectobacterium brasiliense* (Pb1692). Graphs represent infection of **(A)** potato tubers, and **(B)** calla lily leaf discs. **(C)** Photos of disease symptoms development in potato tubers (top) and calla lily leaf discs (bottom). Control treatment were dH_20 or 0.3% DMSO. One-way ANOVA with *post hoc* Tukey-Kramer HSD tests was used to analyze differences. Bars that are not labelled with the same letter are significantly different from each other ($P< 0.05$; bar = mean + SE; n = 40 for calla, 12 for potato).

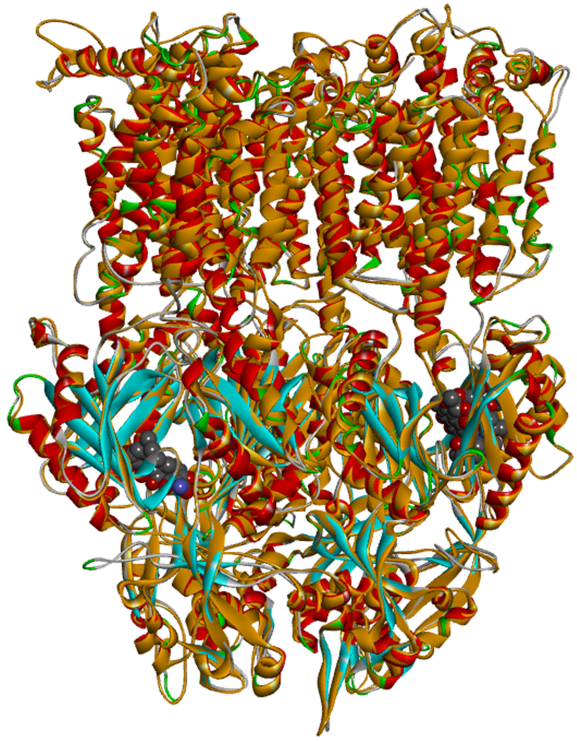

FIGURE 6
Superposition between *Escherichia coli* AcrB (PDB code: 3AOD; ribbon diagram color coded according to the secondary structure with alpha helices in red and beta sheets in blue) and the homology model of AcrB of *Pectobacterium brasiliense* Pb1692 (ribbon diagram colored in orange). The ligands (rifampicin and minocycline) are presented in CPK representation.

compounds produced by both plants and competing microorganisms. In order to colonize plants and initiate disease, plant pathogens must elude these toxic effects. Efflux pumps are one of the tools shaped by evolution to counteract the hostile environment (Burse et al., 2004; Al-karablieh et al., 2009; Martinez et al., 2009; Vargas et al., 2011; Alvarez-Ortega et al., 2013). The AcrAB-TolC complex has a significant role in detoxicification of intracellular toxic metabolites, yet, other transporters also take part in protecting bacterial cells from antimicrobial compounds (Cudkowicz and Schuldiner, 2019).

In the search for novel antibacterial mechanisms, the inhibition of AcrAB-TolC and the resulting accumulation of antimicrobial phytochemicals in the pathogen's cell is suggested and evaluated here in a plant pathogen model. To this end, the efficacy of four known EPIs, i.e. berberine, NMP, PAβN and quinoline, was evaluated in Pb1692 cells by monitoring the decrease of MIC values of several concomitantly applied antimicrobial phytochemicals. This led to the identification of PAβN and NMP as the best EPIs. Interestingly, these same compounds also exhibited a synergistic effect upon their application together with two plant derived phytochemicals, Pht and Nar (Table 2). The latter are well recognized substrates of the AcrAB-TolC machinery, and their increased efficacy may have resulted from the increase of their intracellular concentrations.

TABLE 3 Glide scores (kcal/mole) for the four EPIs considered in this work in the proximal (chain C) and distal (chain A) sites of the AcrB model.

Compound	Proximal Site	Distal Site
8-hydroxyquinoline	-5.6	-5.3
Berberine Chloride	-6.7	-4.8
1-(1-naphthylmethyl)- piperazine (NMP)	-5.3	-5.4
Phe-arg-β-naphtylamide (PAβN)	-7.7	-5.6

In *E. coli*, NMP was directly related to inhibition of AcrAB as demonstrated by reversed resistance to fluoroquinolones in an AcrAB overexpressor strain, and not in an AcrAB deficient mutant (Bohnert and Kern, 2005). The mode of action of NMP suggests that during pumping, NMP moves from the proximal to the distal pocket of AcrAB-TolC and straddles the G-loop instead of moving out. This interferes with normal substrate movement that may result in reversal of drug resistance (Li et al., 2015; Anes et al., 2019).

In contrast with Pht and Nar, the MIC value of the antibiotic Cip was not modified by the application of either PAβN or NMP in Pb 1692 (Table 1), suggesting that the inhibitors did not impair Cip efflux from the cell. This may suggest that the inhibitors block the passage of Nar or Pht through the efflux pathway to a higher degree than the passage of the antibiotic. In drug resistant *E. coli*, the pump preferentially removes PAβN, while the antibiotic accumulates in the cell until the concentration is sufficient to impair the target's activity. This mode of action allows in most cases to sensitize the bacteria, or completely reverse resistance to a given compound (Bolla et al., 2011).

TABLE 4 Glide scores (kcal/mole) for naringenin, phloretin, and ciprofloxacin in the proximal (chain C) and distal (chain A) binding sites of the AcrB model in the presence and absence of the EPI PAβN.

Compound	Proximal Site		Distal Site	
	- PAβN	+ PAβN	- PAβN	+ PAβN
Naringenin	-6.2	-6.9	-6.3	-6.2
Phloretin	-6.7	-6.8	-5.3	-4.7
Ciprofloxacin	-5.0	-5.8	-6.0	-4.9

In order to elucidate a possible mechanism for the higher antimicrobial activity of some combinations rather than others (i.e. PAβN with Pht or Nar, and NMP with Nar), the potential existence of a feedback gene expression machinery in response to the application of both EPIs and of their combinations with the phytochemicals was studied. A 2.5 -fold increase of *acrB* expression was observed in Pb1692 following 2 h of exposure to 0.2 mM NMP (Figures 4D), while both *acrA* and *tolC* were not upregulated (Figures 4A, B, E, F). Application of PAβN did not upregulate the overexpression of *acrB* (Figures 4C, D), but upregulated *acrA* and *tolC* genes, by 3- and 2-fold respectively (Figures 4B, F). These results are in agreement with previous studies that have demonstrated in other bacteria different expression patterns of the three components of the EP in response to different EPIs (Grimsey et al., 2020; Kaur et al., 2021). Studying the feedback induced by non-growth-inhibiting concentrations of Pht and Nar

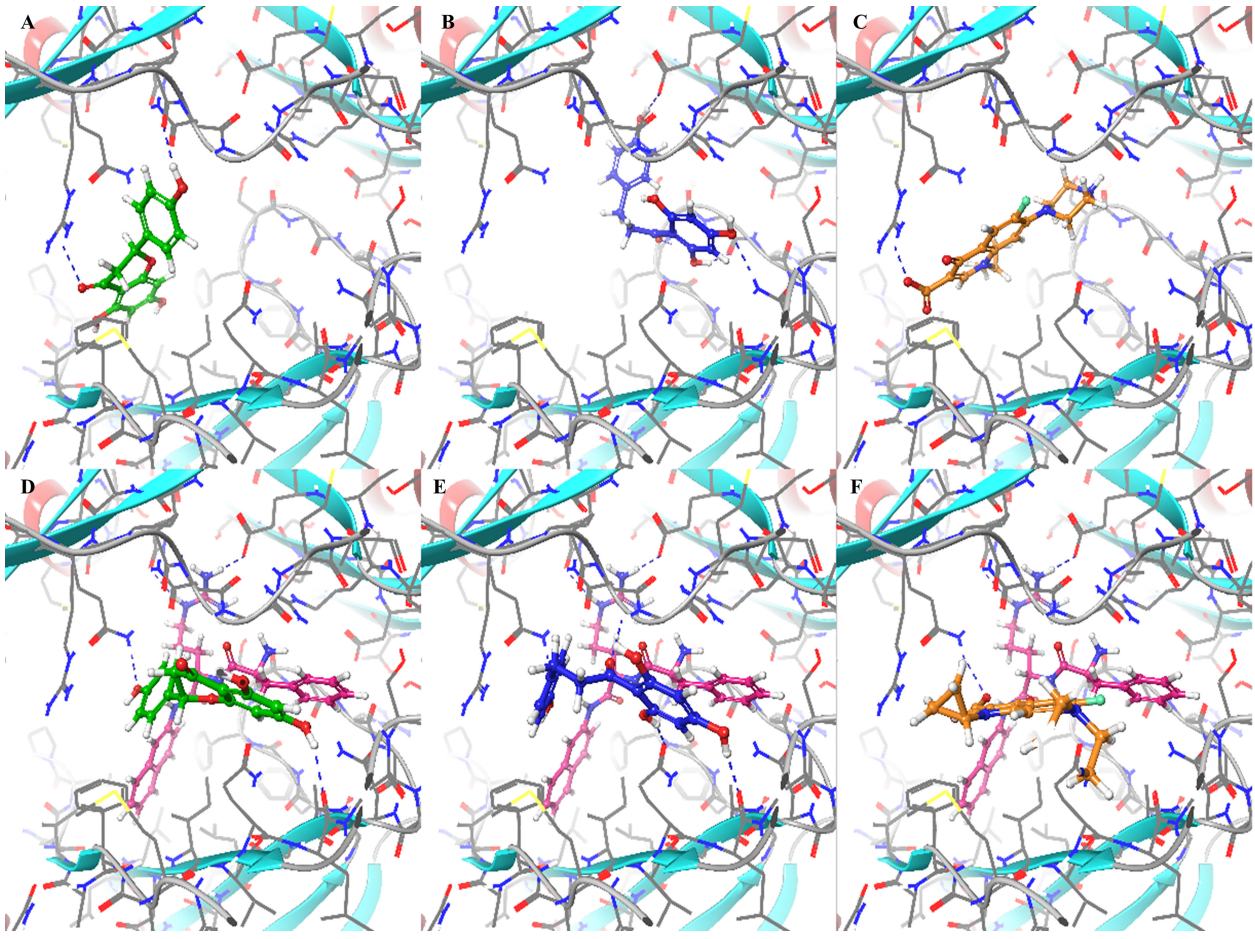

FIGURE 7
Binding modes of naringenin (Nar), phloretin (Pht), and ciprofloxacin (Cip) to the proximal binding site of the AcrB model either in the absence or the presence of PAβN: **(A)** Nar without PAβN, forms two hydrogen bonds with Arg716 and the backbone of Pro717. **(B)** Pht without PAβN, forms four hydrogen bonds with Asn622 and Glu816, and the backbone of Ser617 and Gly618. **(C)** Cip without PAβN, forms one hydrogen bond with Arg716. **(D)** Nar with PAβN, forms two hydrogen bonds with Gln827 and the backbone of Leu577. **(E)** Pht with PAβN, forms four hydrogen bonds with Gln576, Gln827, and the backbone of Leu577 and Gly719. **(F)** Cip with PAβN, forms one hydrogen bond with Gln827. The protein is presented as a ribbon diagram color coded according to the secondary structure with alpha helices in red and beta sheets in blue and the ligands are presented in a ball and stick representation. Hydrogen bonds are presented as blue dashed lines.

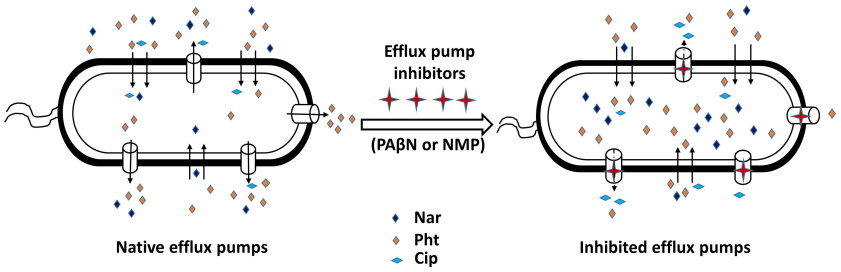

FIGURE 8
A simplified model illustrating the accumulation of phenolics from plants in Pectobaterium, following the application of synthetic efflux pump inhibitors (EPIs). The plant phenolics naringenin (Nar) and phloretin (Pht) are accumulating in the bacterium cells, while the antibiotic ciprofloxacin (Cip) is actively removed when either phenyl-arginine-β-naphthylamide (PAβN) (C) or 1-(1- naphthylmethyl)-piperazine (NMP) were applied.

revealed an early upregulation of the three components by both compounds at 15 min (first measurement point) post exposure. This up-regulation will contribute to the rapid excretion of these compounds from the cell and to increased bacterial resistance. The expression levels of *acrB* did not change when treated with Nar and Pht alone but the combination of NMP with Pht or Cip, and PAβN with Cip increased the expression of *acrB* (Figure 4D).

Surprisingly, the application of PAβN induced downregulation in the expression of the *acrB* gene (Figures 4C, D), relative to each compound alone, suggesting a mechanism for their accumulation in the bacterial cells and the observed lower MIC values in the presence of the EPI. The direct effect of Pht and Nar on EP gene expression and its down-regulation with the inhibitors, support the interference of the EPIs with AcrAB-TolC competence to protect the cells against the phytochemicals. In contrast, Cip, alone or in combination with NMP and PAβN had no effect on the expression levels of *acrA* and *TolC* at 15 min and at 2 h (Figures 4A, B, E, F), whereas *acrB* was upregulated after 2 h (Figure 4D). This result together with the observed unchanging MIC values may suggest that the EP was still effective in eliminating the antibiotic from the cell. Recent studies reported on the plasticity and redundancy of efflux transporters in *E. coli* (Cudkowicz and Schuldiner, 2019), suggesting that other transporters may be involved, mainly in plant pathogenic bacteria (Zeng and Charkowski, 2021). Upregulation of *acrB* in response to Cip treatment was also reported in *Salmonella enterica* (Ferrari et al., 2013), and upon resistance to antibiotics in *Enterobacter cloacae* upon exposure to cefepime (Liu et al., 2018).

The synergistic compounds combinations with FICI values of less than 0.5, i.e. Nar with either NMP or PAβN, and Pht with PAβN, induced a downregulation of *acrB* expression after 2 h (Figure 4D). Downregulation of *acrAB-tolC* is commonly observed with increased susceptibility to antibiotics (Li et al., 2011; Zhou et al., 2013; Dhara and Tripathi, 2020). Here, when the bacteria are more tolerant to the antimicrobial compounds, *acrB* is upregulated as with NMP, with Cip and Pht, and PAβN with Cip, which also displays higher FICI index (FICI > 0.5) (Table 2).

Infection assays were conducted using potato tubers and calla lily leaves as hosts of Pb1692, and disease symptoms were recorded to verify that plants may indeed be better protected by the application of EPIs and selected phytochemicals. The results have demonstrated the efficacy of the EPIs together with recognized antimicrobial phytochemicals in attenuating disease development. Both NMP and PAβN potentiated Pht or Nar activities on two hosts (Figure 5A, B, C), at concentrations that did not inhibit cell growth. The potentiation by the EPIs was differential, depending on the substrate, maybe suggesting why plants produce so many antimicrobial compounds in response to pathogen attacks. Here again, Cip did not provide protection and was probably efficiently eliminated from the bacterial cells. The infection results were consistent with previous studies showing that inactivation of AcrAB-TolC or its homologues resulted in reduced disease severity in plants (Barabote et al., 2003; Burse et al., 2004; Maggiorani Valecillos et al., 2006; Brown et al., 2007; Al-karablieh et al., 2009; Vargas et al., 2011). Nonetheless, we may not rule out the involvement of additional mechanisms in response to the low phytochemicals concentrations, including the inhibition of additional EP, effects on membrane permeability, and QS interference.

Finally, computational studies served to better infer how the application of EPIs may increase the efficacy of the selected phytochemicals and not of Cip. Similar studies have been recently employed by Kinana et al., 2016, to explain the behavior of PAβN and some of its analogs as substrates of the AcrB efflux pump in *E. coli* and as modulators of AcrB-induced nitrocefin efflux (Kinana et al., 2016). Yet, these studies primarily focused on the distal site whereas this work puts more emphasis on the proximal (access) site. In the absence of a crystal structure for Pb1692 AcrB, a homology model of the pump was first constructed based on the *E. coli* AcrB crystal structure. The remarkable similarity between the two structures supports the importance of these EP for bacterial fitness even under different lifestyles and environments. Next, docking of the four EPIs (berberine, NMP, PAβN and quinoline) to the homology model, suggested PAβN to be the best binder to both chains: A (proximal site) and C (distal site) of AcrB (Table 3). These results are in agreement with the quantitative EtBr accumulation assay (Figure 1). Finally, molecular docking suggested stronger binding of both Nar and Pht than of ciprofloxacin to the proximal site of the pump either in the absence or in the presence of PAβN (Table 4). Furthermore, the presence of PAβN slightly increases the predicted binding affinity of the two plant-derived compounds (as well as of Cip) to this site. This may suggest that the two phenolic compounds more effectively

block the efflux pathway than the antibiotics in accord with their increased accumulation in the cell when applied in combination with the EPI PAβN. Interestingly, the presence of PAβN seems to reduce the affinity of the antibiotic to the distal site facilitating its removal from the cell.

Looking at Table 4, we do not see the same trend in the predicted binding affinities for the proximal and distal sites. While the two phytochemicals are predicted to be better binders than the antibiotic to the proximal site either in the absence or presence of PAβN, only Nar is predicted to be a better binder than Cip to the distal site. However, since the transport process requires sequential binding to the proximal, distal and extrusion site, we suggest that the trend observed for the proximal site is sufficient to explain the experimental results.

The weaker interaction between AcrB and Cip in *E. coli* (Vargiu and Nikaido, 2012) and with tetracycline in *Klebsiella pneumonia* (Jamshidi et al., 2018) compared with PAβN has been reported, resulting in efflux of antibiotics through the transporter. Binding of PAβN to the hydrophobic pocket in AcrB causes an interference with the binding of other drug substrates similar to our findings (Vargiu and Nikaido, 2012; Jamshidi et al., 2018).

In summary, inhibition of the AcrAB-TolC pump in Pb1692 by EPIs to prevent it from excreting phytochemicals from the cytoplasm to the periplasm and the external environment, may serve as a mean by which plants control bacterial pathogenicity. Thus, efflux pumps in Pb1692 and by extension, in other plant pathogenic bacteria, may serve as plausible targets for novel and sustainable anti-bacterial targets.

4 Materials and methods

4.1 Minimum inhibitory concentration

The microplate dilution assay was employed to assess the minimum inhibitory concentration (MIC) of the various compounds as described by the Clinical and Laboratory Standards Institute guidelines (Clinical and Laboratory Standards Institute). In Each well, a total of 190 µL of LB broth containing 2-fold serial dilutions of each of the tested compounds was inoculated with 10 µL of bacterial suspension taken from 1×10^8 CFU of Pb1692 solution so that the final concentration in each well was 1×10^6 CFU. The wells (in 96-well microtiter plates) were incubated for 24 h at 28°C, with continuous shaking at 150 rpm. The MIC was recorded as the lowest concentration of compound that was able to inhibit the visible growth of bacteria (at OD 600 nm).

4.2 Time-kill test/checkerboard assay

Two-fold serially diluted concentrations of one of the combination's components were dispensed in the rows of a 96-well plate whereas two-fold serially diluted concentrations of the other component were dispensed in its columns. Each compound was diluted to different concentrations with growth effect close to control of the previously determined MIC. Briefly, each concentration of the tested EPI compound was mixed with different concentrations of the phytochemical compounds to a final volume of 190 µl in each well. The growth of Pb1692 was assessed by adding 10 µL of bacterial suspension ($1x10^8$ CFU/mL) into a well containing the combination of each EPI and tested compound. Following 24 h of incubation at 28°C, the plates were recorded. Each value was a mean of four replications out of three independent experiments.

The effects of the antimicrobial combinations were defined according to the fractional inhibitory concentration index (FICI) using the following equation:

$$FICI = \frac{MIC\ of\ compound\ A\ in\ combination}{MIC\ of\ compound\ A\ alone} + \frac{MIC\ of\ compound\ B\ in\ combination}{MIC\ of\ compound\ B\ alone}$$

4.3 Ethidium bromide accumulation assays

Accumulation of EtBr inside the bacterial cell, was measured according to Coldham et. al., 2010, with minor modifications. Briefly, a single colony of Pb1692 was cultured overnight at 28°C, and 10µL were transferred to fresh LB and incubated for 5 h at 28°C, under continuous shaking. Bacterial cells were collected by centrifugation at 4000 g and re-suspended in 1 mL PBS. The optical density of all suspensions was adjusted to 0.4 OD 600, and aliquots (0.18 mL) were transferred to a 96-well plate (flat-bottomed, black, Greiner Bio-one, Stonehouse, UK). The efflux inhibitors were added as follows: column 1: PBS blank; column 2: heat-inactivated Pb1692 (10 min at 90°C); column 3: control strain (No efflux inhibitor); columns 4 –12: efflux pump inhibitors at different concentrations. Eight replicates of each inhibitor were analyzed in each column. The plate was transferred to a Spark multimode microplate reader (Tecan Trading AG, Männedorf, Zurich, Switzerland), incubated at 28°C and EtBr (25 µg/ml) was added (20 µL) to each well to a final concentration of 2.5 µg/ml. Fluorescence was recorded using excitation and emission filters of 360 and 590 nm, respectively, with 5 flashes/well; readings were taken for 60 cycles with a 75 s delay between cycles, and a gain multiplier of 1460. Raw fluorescence values were analyzed using Excel (Microsoft) and included mean values for each column following subtraction of appropriate control blanks. Each experiment was repeated twice.

4.4 Gene expression

4.4.1 RNA extraction and cDNA preparation

Pb1692 cells were grown from a single colony for 16 h, at 28°C in LB under continuous shaking. Then fresh LB, with or without EPI (NMP and PAβN), antimicrobial compounds (Nar, Pht and CIP) and their combinations, was inoculated with $5x10^8$ CFU of bacterial suspension, in 15 mL LB, and incubated for 15 min and 2 h at 28°C, under continuous shaking. After15 min and 2 h, 2mL

samples were taken to an Eppendorf tube for RNA extraction. To extract RNA, GENEzol^{TM} Reagent kit (Geneaid Biotech Ltd, New Taipei City, Taiwan) was used, according to the manufacturer's instructions. The extracted RNA was used to prepare cDNA using a High Capacity cDNA Reverse Transcription kit (Applied Biosystems, Thermo Fisher Scientific Inc, Carlsbad, CA, USA). The cDNA reverse-transcription reaction was performed using a programmable thermal controller (MJ Research, St. Bruno, PQ, Canada) programmed to one cycle as step1: 25°C for 10 min, step 2: 37°C for 120 min, step 3: 85°C for 5 min and step 4: 10°C after which the cDNA was stored at -20°C for future use.

4.4.2 Quantification of *acrAB-tolC* gene expression by qRT-PCR

Real-time PCR was conducted to quantify the mRNA, as described by (Joshi et al., 2016). Briefly, all of the primers used in this study were designed using the National Center for Biotechnology Information (NCBI) primer BLAST software (http://www.ncbi.nlm.nih.gov/tools/primer-blast/). The generated primers were 100 to 120 bp in size and the melting temperatures of the primers were designed for 60°C, with a difference of less than 5°C for each primer pair (Table S1). To exclude the possibility of non-specific binding, primer sequences were analyzed by BLAST analysis (using NCBI BLAST software) against the database for the genus *Pectobacterium.* All PCR products were sequenced and found to represent the correct gene. The primer mixture for qRT-PCR contained 5 µL of Fast SYBR Green Master Mix (Applied Biosystems) and 0.8 µL (5 µM) of each forward and reverse primer. A total of 3.4 µL (17 ng) of cDNA was added to each well, so that the total reaction mixture would be 10 µL for each well. Reactions were performed using a Step One Plus Real-Time PCR system (Applied Biosystems) with the following cycling parameters: holding stage, 95°C for 20 s; cycling stage, 40 cycles of 95°C for 3 s and 60°C for 30 s; and melting curve stage, 95°C for 15 s, 60°C for 1 min and 95°C for 15 s. The data were analyzed by the comparative CT (ΔΔCT) method, with expression normalized to the expression of the reference gene *ffh*, as described by Takle et al. (2007).

5 Homology modeling

The model of each monomer (chain A, B, C) of *P. brasiliense* (Accession number at BLAST: WP_039274619) was constructed based on the AcrB of *E. coli* structure (PDB code: 3AOD (Nakashima et al., 2011), 80% sequence identity to *P. brasiliense*), using MODELLER (Marti-Renom et al., 2000; Webb and Sali, 2016). Sequence alignment between the target and the template was performed using the align2d python script in MODELLER v.9.20 and is presented in Supplementary Figure 4. After visual inspection of the alignment, models were generated using the default parameters in MODELLER (Figure 5). PROCHECK (Laskowski et al., 1993), was used to check the validity of the resulting models, and showed good stereochemical quality (89.0%, 86.4%, and 90.7% of residues to be in the most favorable regions of Ramachandran plots of AcrB chains A, B, and C models, respectively) and an overall G-factors of -0.14, -0.15, and -0.08 for AcrB chain A, B, and C models, respectively. The G-factor is a measure of how "normal" the protein structure is and of its stereochemical properties. A low G-factor (or very negative) indicates that the stereochemical properties correspond to a low-probability conformation of the protein. The more positive the G-factor values, the more stereochemically plausible the protein structure is. Prosa (Wiederstein and Sippl, 2007) profiles were generate and were found to be similar to those of the templates with z-score of -11.8, -11.4, and -12.09 for chain A, B, and C model, respectively. The RMSD between the models constructed in this work and the AcrB structure of *E. coli* (PDB code: 3AOD) is less than 3.0 Å.

5.1 Docking

Prior to docking, the protein model was process using the protein preparation wizard (Sastry et al., 2013) as implemented in Schrodinger's Maestro to: (A) Add missing atoms/sidechains, (B) Optimize the orientation of side chains of Gln, Asn, and His, (C) Set the correct protonation states of titratable residues based on predicted pKa values. Ligands were prepared for docking using Schordinger's LigPrep program to set correct protonation states. Docking was performed with the Glide program using the SP setting and default parameters. To validate the docking procedure, we first attempted to reproduce the crystallographic binding modes of minocycline and of rifampicin within the crystal structure of *E. coli* AcrB (PDB code 3AOD). These were satisfactorily reproduced to within 0.7 Å and 2.4 Å, respectively (based on lowest energy poses). For docking of EPIs, plant-derived compounds and plant-derived compounds in the presence of PAβN, the docking box was defined based on residues that are in radius of 4 Å from the docked minocycline in the distal pocket (chain A), and docked rifampicin in the proximal pocket (chain C) of the AcrB model.

In the docking studies we considered binding sites found in both the "access" and the "binding" states. These sites represent different intermediate states along the transport pathway for which we have crystal structure with inhibitors. Inhibition of one of these states is likely to affect the function of the efflux pump. We didn't consider the binding site in the "extrusion" state, since the crystal structure corresponding to the state was solved in the absence of a ligand.

6 Infection assays

To assess the effects of each compound and EPIs on Pb1692 virulence, and to depict a potential synergistic effect of the different combinations on infection capability of Pb1692, the severity of disease symptoms development was assessed in two host plants, *Zantedeschia aethiopica* (calla lily) and *Solanum tuberosum* (potato). The infection procedure was previously described (Luzzatto et al., 2007; Yishay et al., 2008; Joshi et al., 2016). For the assays, fully expanded young leaves of calla lily, or small (25–50

g) potato tubers, were surface-sterilized by soaking in 0.5% sodium hypochlorite solution for 20 min. Then, the samples were washed twice with sterile, double-distilled H_2O and air-dried under a laminar flow hood. Calla lily leaf discs 20 mm in diameter were excised and transferred to a Petri dish containing MS medium. Whole baby potato tubers cultivar 'Nicola' were used for the infection assay. Both the leaf discs and the potato tubers were pierced at the center with a sterile tip. Bacteria grown for 16 h, 28°C in liquid LB were diluted to 10^8 CFU/mL in sterile, double-distilled H_2O with or without the tested compound and incubated for 2 h at 28°C on a 150-rpm incubator shaker. After 2 h, leaf discs and potato tubers were inoculated with 10 µL of bacterial suspension (10^6 CFU) in the presence or absence of the tested compounds. The inoculated plant material was incubated at 28°C for 15 h and 48 h for calla lily and potato tubers respectively. Disease severity was expressed as the percentage of decayed tissues relative to the total leaf disc area or for the potato tubers, and quantified as the percentage of rotten tissue based on weight. The experiments were repeated three times with 10 replicates for calla lily and 4 replicates for potato tubers.

Data availability statement

The original contributions presented in the study are included in the article/Supplementary Material. Further inquiries can be directed to the corresponding author.

Author contributions

MP, NK, and OG, conducted the experiments, analyzed the data and prepared the manuscript. NK and HS analyzed computational docking data, IY, and ZK, planed and coordinated laboratory experiments, IY, ZK and HS, wrote and critically revised the manuscript. All authors contributed to the article and approved the submitted version.

Funding

The research was funded by BARD Research Grant IS-5502-22C.

Conflict of interest

The authors declare that the research was conducted in the absence of any commercial or financial relationships that could be construed as a potential conflict of interest.

Publisher's note

All claims expressed in this article are solely those of the authors and do not necessarily represent those of their affiliated organizations, or those of the publisher, the editors and the reviewers. Any product that may be evaluated in this article, or claim that may be made by its manufacturer, is not guaranteed or endorsed by the publisher.

Supplementary material

The Supplementary Material for this article can be found online at: https://www.frontiersin.org/articles/10.3389/fpls.2023.1161702/full#supplementary-material

References

Alibert, S., N'gompaza Diarra, J., Hernandez, J., Stutzmann, A., Fouad, M., Boyer, G., et al. (2017). Multidrug efflux pumps and their role in antibiotic and antiseptic resistance: a pharmacodynamic perspective. *Expert Opin. Drug Metab. Toxicol.* 13, 301–309. doi: 10.1080/17425255.2017.1251581

Al-karablieh, N., Weingart, H., and Ullrich, M. S. (2009). The outer membrane protein TolC is required for phytoalexin resistance and virulence of the fire blight pathogen *Erwinia amylovora*. *Microb. Biotechnol.* 2, 465–475. doi: 10.1111/j.1751-7915.2009.00095.x

Alvarez-Ortega, C., Olivares, J., and Martinez, J. L. (2013). RND multidrug efflux pumps: what are they good for? *Front. Microbiol.* 4, 7. doi: 10.3389/fmicb.2013.00007

Anes, J., Sivasankaran, S. K., Muthappa, D. M., Fanning, S., and Srikumar, S. (2019). Exposure to Sub-inhibitory concentrations of the chemosensitizer 1-(1-Naphthylmethyl)-Piperazine creates membrane destabilization in multi-drug resistant klebsiella pneumoniae. *Front. Microbiol.* 10, 92. doi: 10.3389/fmicb.2019.00092

Barabote, R. D., Johnson, O. L., Zetina, E., San Francisco, S. K., Fralick, J. A., and San Francisco, M. J. D. (2003). *Erwinia chrysanthemi* tolC is involved in resistance to antimicrobial plant chemicals and is essential for phytopathogenesis. *J. Bacteriol.* 185, 5772–5778. doi: 10.1128/JB.185.19.5772-5778.2003

Blanco, P., Hernando-Amado, S., Reales-Calderon, J. A., Corona, F., Lira, F., Alcalde-Rico, M., et al. (2016). Bacterial multidrug efflux pumps: much more than antibiotic resistance determinants. *Microorganisms.* 4, 14. doi: 10.3390/microorganisms4010014

Bohnert, J. A., and Kern, W. V. (2005). Selected arylpiperazines are capable of reversing multidrug resistance in *Escherichia coli* overexpressing RND efflux pumps. *Antimicrob. Agents Chemother.* 49, 849–852. doi: 10.1128/AAC.49.2.849-852.2005

Bolla, J. M., Alibert-Franco, S., Handzlik, J., Chevalier, J., Mahamoud, A., Boyer, G., et al. (2011). Strategies for bypassing the membrane barrier in multidrug resistant gram-negative bacteria. *FEBS Lett.* 585, 1682–1690. doi: 10.1016/j.febslet.2011.04.054

Brown, D. G., Swanson, J. K., and Allen, C. (2007). Two host-induced *Ralstonia solanacearum* genes, acrA and dinF, encode multidrug efflux pumps and contribute to bacterial wilt virulence. *Appl. Environ. Microbiol.* 73, 2777–2786. doi: 10.1128/AEM.00984-06

Burse, A., Weingart, H., and Ullrich, M. S. (2004). The phytoalexin-inducible multidrug efflux pump AcrAB contributes to virulence in the fire blight pathogen, *Erwinia amylovora*. *Mol. Plant Microbe Interact.* 17, 43–54. doi: 10.1094/MPMI.2004.17.1.43

Cacciotto, P., Ramaswamy, V. K., Malloci, G., Ruggerone, P., and Vargiu, A. V. (2018). Molecular modeling of multidrug properties of resistance nodulation division (RND) transporters. *Methods Mol. Biol.* 1700, 179–219. doi: 10.1007/978-1-4939-7454-2_11

Coldham, N. G., Webber, M., Woodward, M. J., and Piddock, L. J. V. (2010). A 96-well plate fluorescence assay for assessment of cellular permeability and active efflux in *Salmonella enterica* serovar *Typhimurium* and *Escherichia coli*. *J. Antimicrob. Chemother.* 65, 1655–1663. doi: 10.1093/jac/dkq169

Cudkowicz, N. A., and Schuldiner, S. (2019). Deletion of the major *Escherichia coli* multidrug transporter AcrB reveals transporter plasticity and redundancy in bacterial cells. *PloS One* 14, e0218828. doi: 10.1371/journal.pone.0218828

Czajkowski, R., Perombelon, M. C. M., Van Veen, J. A., and van der Wolf, J. M. (2011). Control of blackleg and tuber soft rot of potato caused by *Pectobacterium* and *Dickeya* species: a review. *Plant Pathol.* 60, 999–1013. doi: 10.1111/j.1365-3059.2011.02470.x

Dhara, L., and Tripathi, A. (2020). Cinnamaldehyde: a compound with antimicrobial and synergistic activity against ESBL-producing quinolone-resistant pathogenic enterobacteriaceae. *Eur. J. Clin. Microbiol. Infect. Dis.* 39, 65–73. doi: 10.1007/s10096-019-03692-y

Du, D., Wang-Kan, X., Neuberger, A., Van Veen, H. W., Pos, K. M., Piddock, L. J. V., et al. (2018). Multidrug efflux pumps: structure, function and regulation. *Nat. Rev. Microbiol.* 16, 523–539. doi: 10.1038/s41579-018-0048-6

Elnasser, Z., Elsamarneh, R., Obeidat, H., Amarin, Z., Jaradat, S., and Kaplan, N. (2021). *In-vitro* activity of tigecycline against multidrug-resistant gram negative bacteria: the experience of a university hospital. *J. Infect. Public Health* 14, 478–483. doi: 10.1016/j.jiph.2020.12.013

Ferrari, R. G., Galiana, A., Cremades, R., Rodriguez, J. C., Magnani, M., Tognim, M. C., et al. (2013). Expression of the *marA*, *soxS*, *acrB* and *ramA* genes related to the AcrAB/TolC efflux pump in *Salmonella enterica* strains with and without quinolone resistance-determining regions *gyrA* gene mutations. *Braz. J. Infect. Dis.* 17, 125–130. doi: 10.1016/j.bjid.2012.09.011

Grimsey, E. M., Fais, C., Marshall, R. L., Ricci, V., Ciusa, M. L., Stone, J. W., et al. (2020). Chlorpromazine and amitriptyline are substrates and inhibitors of the AcrB multidrug efflux pump. *mBio.* 11, e00465–e00420. doi: 10.1128/mBio.00465-20

Jamshidi, S., Sutton, J. M., and Rahman, K. M. (2018). Mapping the dynamic functions and structural features of AcrB efflux pump transporter using accelerated molecular dynamics simulations. *Sci. Rep.* 8, 10470. doi: 10.1038/s41598-018-28531-6

Joshi, J. R., Burdman, S., Lipsky, A., Yariv, S., and Yedidia, I. (2016). Plant phenolic acids affect the virulence of *Pectobacterium aroidearum* and p. carotovorum ssp. *brasiliense via* quorum sensing regulation. *Mol. Plant Pathol.* 17 (4), 487–500. doi: 10.1111/mpp.12295

Joshi, J. R., Burdman, S., Lipsky, A., and Yedidia, I. (2015). Effects of plant antimicrobial phenolic compounds on virulence of the genus *Pectobacterium*. *Res. Microbiol.* 166, 535–545. doi: 10.1016/j.resmic.2015.04.004

Kaur, U. J., Chopra, A., Preet, S., Raj, K., Kondepudi, K. K., Gupta, V., et al. (2021). Potential of 1-(1-napthylmethyl)-piperazine, an efflux pump inhibitor against cadmium-induced multidrug resistance in *Salmonella enterica* serovar *Typhi* as an adjunct to antibiotics. *Braz. J. Microbiol.* 52, 1303–1313. doi: 10.1007/s42770-021-00492-5

Kim, J. S., Jeong, H., Song, S., Kim, H. Y., Lee, K., Hyun, J., et al. (2015). Structure of the tripartite multidrug efflux pump AcrAB-TolC suggests an alternative assembly mode. *Mol. Cells* 38, 180–186. doi: 10.14348/molcells.2015.2277

Kinana, A. D., Vargiu, A. V., May, T., and Nikaido, H. (2016). Aminoacyl beta-naphthylamides as substrates and modulators of AcrB multidrug efflux pump. *Proc. Natl. Acad. Sci. U.S.A.* 113, 1405–1410. doi: 10.1073/pnas.1525143113

Kobayashi, A., Hirakawa, H., Hirata, T., Nishino, K., and Yamaguchi, A. (2006). Growth phase-dependent expression of drug exporters in *Escherichia coli* and its contribution to drug tolerance. *J. Bacteriol.* 188, 5693–5703. doi: 10.1128/JB.00217-06

Lamut, A., Masic, L. P., Kikelj, D., and Tomasic, T. (2019). Efflux pump inhibitors of clinically relevant multidrug resistant bacteria. *Medic. Res. Rev.* 39, 2460–2504. doi: 10.1002/med.21591

Laskowski, R. A., Macarthur, M. W., Moss, D. S., and Thornton, J. M. (1993). Procheck - a program to check the stereochemical quality of protein structures. *J. Appl. Crystallog.* 26, 283–291. doi: 10.1107/S0021889892009944

Li, X. Z., Plesiat, P., and Nikaido, H. (2015). The challenge of efflux-mediated antibiotic resistance in gram-negative bacteria. *Clin. Microbiol. Rev.* 28, 337–418. doi: 10.1128/CMR.00117-14

Li, B., Yao, Q., Pan, X. C., Wang, N., Zhang, R., Li, J., et al. (2011). Artesunate enhances the antibacterial effect of beta-lactam antibiotics against *Escherichia coli* by increasing antibiotic accumulation *via* inhibition of the multidrug efflux pump system AcrAB-TolC. *J. Antimicrob. Chemother.* 66, 769–777. doi: 10.1093/jac/dkr017

Liu, Y., and Filiatrault, M. J. (2020). Complete genome sequence of the necrotrophic plant-pathogenic bacterium. *Pectobacterium brasiliense Microbiol. Resour. Announc.* 1692 9, e00037–e00020. doi: 10.1128/MRA.00037-20

Liu, L., Yu, J., Tang, M., and Liu, J. (2018). Mechanisms of resistance in clinical isolates of *Enterobacter cloacae* that are less susceptible to cefepime than to ceftazidime. *Ann. Clin. Lab. Sci.* 48, 355–362.

Lomovskaya, O., and Bostian, K. A. (2006). Practical applications and feasibility of efflux pump inhibitors in the clinic–a vision for applied use. *Biochem. Pharmacol.* 71, 910–918. doi: 10.1016/j.bcp.2005.12.008

Lomovskaya, O., and Watkins, W. (2001). Inhibition of efflux pumps as a novel approach to combat drug resistance in bacteria. *J. Mol. Microbiol. Biotechnol.* 3, 225–236.

Lu, Q., Yan, F., Liu, Y., Li, Q., Yang, M., and Liu, P. (2021). Comparative genomic analyses reveal functional insights into key determinants of the pathogenesis of *Pectobacterium actinidiae* in kiwifruit. *Phytopathology.* 111, 789–798. doi: 10.1094/PHYTO-07-20-0287-R

Luzzatto, T., Golan, A., Yishay, M., Bilkis, I., Ben-Ari, J., and Yedidia, I. (2007). Priming of antimicrobial phenolics during induced resistance response towards *Pectobacterium carotovorum* in the ornamental monocot calla lily. *J. Agric. Food. Chem.* 55, 10315–10322. doi: 10.1021/jf072037

Maggiorani Valecillos, A., Rodriguez Palenzuela, P., and Lopez-Solanilla, E. (2006). The role of several multidrug resistance systems in *Erwinia chrysanthemi* pathogenesis. *Mol. Plant Microbe Interact.* 19, 607–613. doi: 10.1094/MPMI-19-0607

Mansfield, J., Genin, S., Magori, S., Citovsky, V., Sriariyanum, M., Ronald, P., et al. (2012). Top 10 plant pathogenic bacteria in molecular plant pathology. *Mol. Plant Pathol.* 13, 614–629. doi: 10.1111/j.1364-3703.2012.00804.x

Martinez, J. L., Sanchez, M. B., Martinez-Solano, L., Hernandez, A., Garmendia, L., Fajardo, A., et al. (2009). Functional role of bacterial multidrug efflux pumps in microbial natural ecosystems. *FEMS Microbiol. Rev.* 33, 430–449. doi: 10.1111/j.1574-6976.2008.00157.x

Marti-Renom, M. A., Stuart, A. C., Fiser, A., Sanchez, R., Melo, F., and Sali, A. (2000). Comparative protein structure modeling of genes and genomes. *Annu. Rev. Biophys. Biomol. Struct.* 29, 291–325. doi: 10.1146/annurev.biophys.29.1.291

Nakashima, R., Sakurai, K., Yamasaki, S., Nishino, K., and Yamaguchi, A. (2011). Structures of the multidrug exporter AcrB reveal a proximal multisite drug-binding pocket. *Nature.* 480, 565–U199. doi: 10.1038/nature10641

Opperman, T. J., and Nguyen, S. T. (2015). Recent advances toward a molecular mechanism of efflux pump inhibition. *Front. Microbiol.* 6, 421. doi: 10.3389/fmicb.2015.00421

Oulghazi, S., Sarfraz, S., Zaczek-Moczydlowska, M. A., Khayi, S., Ed-Dra, A., Lekbach, Y., et al. (2021). *Pectobacterium brasiliense*: genomics, host range and disease management. *Microorganisms.* 9, 106. doi: 10.3390/microorganisms9010106

Pasqua, M., Grossi, M., Zennaro, A., Fanelli, G., Micheli, G., Barras, F., et al. (2019). The varied role of efflux pumps of the MFS family in the interplay of bacteria with animal and plant cells. *Microorganisms.* 7, 285. doi: 10.3390/microorganisms7090285

Piddock, L. J. (2006). Multidrug-resistance efflux pumps - not just for resistance. *Nat. Rev. Microbiol.* 4, 629–636. doi: 10.1038/nrmicro1464

Reens, A. L., Crooks, A. L., Su, C. C., Nagy, T. A., Reens, D. L., Podoll, J. D., et al. (2018). A cell-based infection assay identifies efflux pump modulators that reduce bacterial intracellular load. *PloS Pathog.* 14, e1007115. doi: 10.1371/journal.ppat.1007115

Sastry, G. M., Adzhigirey, M., Day, T., Annabhimoju, R., and Sherman, W. (2013). Protein and ligand preparation: parameters, protocols, and influence on virtual screening enrichments. *J. Comput. Aided. Mol. Des.* 27, 221–234. doi: 10.1007/s10822-013-9644-8

Takle, G. W., Toth, I. K., and Brurberg, M. B. (2007). Evaluation of reference genes for real-time RT-PCR expression studies in the plant pathogen *Pectobacterium atrosepticum*. *BMC Plant Biol.* 7, 50. doi: 10.1186/1471-2229-7-50

van der Wolf, J. M., Acuña, I., De Boer, S. H., Brurberg, M. B., Cahill, G., Charkowski, A. O., et al (2021). *Diseases caused by Pectobacterium and Dickeya species around the world*. In F. Van Gijsegem, J. M. van der Wolf and I. K. Toth eds. *Plant diseases caused by Dickeya and Pectobacterium species*. Cham: Springer, 215–261. doi: 10.1007/978-3-030-61459-1_7

Vargas, P., Felipe, A., Michan, C., and Gallegos, M. T. (2011). Induction of *Pseudomonas syringae* pv. tomato DC3000 MexAB-OprM multidrug efflux pump by flavonoids is mediated by the repressor PmeR. *Mol. Plant Microbe Interact.* 24, 1207–1219. doi: 10.1094/MPMI-03-11-0077

Vargiu, A. V., and Nikaido, H. (2012). Multidrug binding properties of the AcrB efflux pump characterized by molecular dynamics simulations. *Proc. Natl. Acad. Sci. U S A.* 109, 20637–20642. doi: 10.1073/pnas.1218348109

Vargiu, A. V., Ruggerone, P., Opperman, T. J., Nguyen, S. T., and Nikaido, H. (2014). Molecular mechanism of MBX2319 inhibition of *Escherichia coli* AcrB multidrug efflux pump and comparison with other inhibitors. *Antimicrob. Agents Chemother.* 58, 6224–6234. doi: 10.1128/AAC.03283-14

Venter, H., Mowla, R., Ohene-Agyei, T., and Ma, S. (2015). RND-type drug efflux pumps from gram-negative bacteria: molecular mechanism and inhibition. *Front. Microbiol.* 6, 377. doi: 10.3389/fmicb.2015.00377

Wang, Y., Mowla, R., Guo, L., Ogunniyi, A. D., Rahman, T., De Barros Lopes, M. A., et al. (2017). Evaluation of a series of 2-napthamide derivatives as inhibitors of the drug efflux pump AcrB for the reversal of antimicrobial resistance. *Bioorg. Med. Chem. Lett.* 27, 733–739. doi: 10.1016/j.bmcl.2017.01.042

Webb, B., and Sali, A. (2016). Comparative protein structure modeling using MODELLER. *Curr. Protoc. Bioinf.* 54, 5.6.1–5.6.37. doi: 10.1002/cpbi.3

Wiederstein, M., and Sippl, M. J. (2007). ProSA-web: interactive web service for the recognition of errors in three-dimensional structures of proteins. *Nucl. Acids Res.* 35, 407–410. doi: 10.1093/nar/gkm290

Wiggins, P. (2004). Efflux pumps: an answer to gram-negative bacterial resistance? *Expert Opin. Investig. Drugs* 13, 899–902. doi: 10.1517/13543784.13.8.899

Yishay, M., Burdman, S., Valverde, A., Luzzatto, T., Ophir, R., and Yedidia, I. (2008). Differential pathogenicity and genetic diversity among pectobacterium carotovorum ssp. *carotovorum* isolates from monocot and dicot hosts support early genomic divergence within this taxon. *Environ. Microbiol.* 10 (10), 2746–2759. doi: 10.1111/j.1462-2920.2008.01694.x

Zeng, Y., and Charkowski, A. O. (2021). The role of ATP-binding cassette transporters in bacterial phytopathogenesis. *Phytopathology.* 111, 600–610. doi: 10.1094/PHYTO-06-20-0212-RVW

Zhao, Y., Liu, J., Jiang, T., Hou, R., Xu, G., Xu, H., et al. (2021). Resistance-nodulation-division efflux pump, LexABC, contributes to self-resistance of the phenazine di-N-Oxide natural product myxin in *Lysobacter* antibioticus. *Front. Microbiol.* 12, 618513 doi: 10.3389/fmicb.2021.618513

Zhou, X. Z., Jia, F., Liu, X. M., Yang, C., Zhao, L., and Wang, Y. J. (2013). Total alkaloids from *Sophora alopecuroides* l. increase susceptibility of extended-spectrum beta-lactamases producing *Escherichia coli* isolates to cefotaxime and ceftazidime. *Chin. J. Integr. Med.* 19, 945–952. doi: 10.1007/s11655-011-0899-4

frontiers | Frontiers in Plant Science

TYPE Original Research
PUBLISHED 31 May 2023
DOI 10.3389/fpls.2023.1082094

OPEN ACCESS

EDITED BY
Michelle Teresa Hulin,
The Sainsbury Laboratory, United Kingdom

REVIEWED BY
Per Hofvander,
Swedish University of Agricultural Sciences, Sweden
John Mansfield,
Imperial College London, United Kingdom

*CORRESPONDENCE
Yuling Bai
bai.yuling@wur.nl

RECEIVED 27 October 2022
ACCEPTED 05 May 2023
PUBLISHED 31 May 2023

CITATION
Koseoglou E, Hanika K, Mohd Nadzir MM, Kohlen W, van der Wolf JM, Visser RGF and Bai Y (2023) Inactivation of tomato *WAT1* leads to reduced susceptibility to *Clavibacter michiganensis* through downregulation of bacterial virulence factors.
Front. Plant Sci. 14:1082094.
doi: 10.3389/fpls.2023.1082094

Inactivation of tomato *WAT1* leads to reduced susceptibility to *Clavibacter michiganensis* through downregulation of bacterial virulence factors

Eleni Koseoglou[1,2], Katharina Hanika[1], Mas M. Mohd Nadzir[1], Wouter Kohlen[3], Jan M. van der Wolf[4], Richard G. F. Visser[1] and Yuling Bai[1]*

[1]Plant Breeding, Wageningen University & Research, Wageningen, Netherlands, [2]Graduate School Experimental Plant Sciences Wageningen University & Research, Wageningen, Netherlands, [3]Cluster of Plant Developmental Biology, Laboratory of Molecular Biology, Wageningen University & Research, Wageningen, Netherlands, [4]Biointeractions & Plant Health, Wageningen University & Research, Wageningen, Netherlands

Tomato bacterial canker caused by *Clavibacter michiganensis* (Cm) is considered to be one of the most destructive bacterial diseases of tomato. To date, no resistance to the pathogen has been identified. While several molecular studies have identified (*Cm*) bacterial factors involved in disease development, the plant genes and mechanisms associated with susceptibility of tomato to the bacterium remain largely unknown. Here, we show for the first time that tomato gene *SlWAT1* is a susceptibility gene to *Cm*. We inactivated the gene *SlWAT1* through RNAi and CRISPR/Cas9 to study changes in tomato susceptibility to *Cm*. Furthermore, we analysed the role of the gene in the molecular interaction with the pathogen. Our findings demonstrate that *SlWAT1* functions as an S gene to genetically diverse *Cm* strains. Inactivation of *SlWAT1* reduced free auxin contents and ethylene synthesis in tomato stems and suppressed the expression of specific bacterial virulence factors. However, CRISPR/Cas9 *slwat1* mutants exhibited severe growth defects. The observed reduced susceptibility is possibly a result of downregulation of bacterial virulence factors and reduced auxin contents in transgenic plants. This shows that inactivation of an S gene may affect the expression of bacterial virulence factors.

KEYWORDS

susceptibility genes, *Clavibacter michiganensis*, CRISPR/Cas9, auxin, ethylene, disease, Walls Are Thin1, bacterium

Introduction

Plant disease resistance is genetically controlled, mostly by dominantly inherited, race specific resistance (R) genes. In the presence of corresponding pathogen-derived effectors many R genes confer resistance through effector-triggered immunity (ETI) (Jones and Dangl, 2006). In plant-microbe interactions, resistance is a common outcome. In fact, a high degree of adaptation is required for microbes to become pathogenic (Hückelhoven et al., 2013). During their co-evolution pathogens have found ways to target and manipulate plant genes, referred to as susceptibility (S) genes, to promote disease development (Bai et al., 2008; Pavan et al., 2011; Appiano et al., 2015; Pessina et al., 2016; Acevedo-Garcia et al., 2017; Berg et al., 2017). S genes are important for biological functions of plants, which appears to be a significant factor in their retainment across species (Hückelhoven et al., 2013). This is exemplified by the *Mildew Locus O* (*MLO*) gene family that has been identified in plant species such as barley, tomato, Arabidopsis, grape, apple and cucumber (Cohn et al., 2014; Cox et al., 2017; Oliva et al., 2019). In contrast to dominant R genes, loss-of-function of S genes can potentially lead to recessively inherited, broad-spectrum, and durable resistance (van Damme et al., 2008; Pavan et al., 2010; Pavan et al., 2011; Huibers et al., 2013; Sun et al., 2016a; Berg et al., 2017; Santillán Martínez et al., 2020). For example, loss-of-function of genes in the glutamate decarboxylases (GADs) family provide enhanced resistance against the vascular bacterium *Ralstonia solanacearum* in Arabidopsis and tomato (*Solanum lycopersicum*) (Xian et al., 2020). In addition, mutation of *Sugars Will Eventually Be Exported Transporter* (*SWEET)* genes in multiple plant species has been demonstrated to be an effective strategy to obtain resistance to *Xanthomonas* spp (Cohn et al., 2014; Cox et al., 2017; Oliva et al., 2019).

Bacterial canker of tomato caused by the Gram-positive bacterium *Clavibacter michiganensis* (*Cm*), is considered to be one of the most important seed-borne diseases of tomato worldwide (Davis et al., 1984; Gartemann et al., 2008; Nouioui et al., 2018). The pathogen colonizes the vasculature of plants leading to systemic infections that result in wilting of leaves, vascular tissue necrosis and formation of cankers on the stems and petioles of plants, eventually leading to plant death (Eichenlaub and Gartemann, 2011; Sen et al., 2015; Chalupowicz et al., 2017).

On the molecular level of the tomato-*Cm* interaction, several bacterial factors involved in virulence are known. Full virulence of the *Cm* reference strain NCPBB382 requires the presence of two native plasmids, pCM1 and pCM2, where the major virulence factors *celA* and *pat-1* are located (Gartemann et al., 2008; Savidor et al., 2014). Loss of either of the plasmids leads to reduced virulence and loss of both results in an endophytic nonvirulent strain (Meletzus et al., 1993; Savidor et al., 2012). Several other proteins are encoded by genes located on the circular chromosome of *Cm* that are involved in the colonization of plants and induction of disease symptoms (Gartemann et al., 2008; Savidor et al., 2012; Savidor et al., 2014; Thapa et al., 2017). Such genes, include the transcriptional factors *vatr1* and *vatr2*, which act in the regulation of several other virulence genes. *vatr1* and *vatr2* are involved in the regulation of virulence factors, such as the endo- beta- 1,4- glucanase *celA*, subtilase proteinase *SbtC* and the serine proteases *pat-1* and *PhpA*, both on the chromosome and plasmids of *Cm* (Savidor et al., 2014).

While several molecular studies have identified bacterial factors involved in disease development, the mechanisms associated with susceptibility of tomato to the bacterium remain largely unknown. The only experimentally confirmed plant factor involved in disease development is the phytohormone ethylene (Balaji et al., 2008; Savidor et al., 2012; Savidor et al., 2014). During infection *Cm* promotes the production of host-derived ethylene by specifically upregulating the ethylene biosynthetic gene *ACO1*. Mutant *Never ripe* (*Nr*) tomato plants with impaired ethylene perception display significant *Cm* symptom development delay (Balaji et al., 2008). The observation that the nonvirulent *Cmm100* strain lacks the ability to induce the production of host derived ethylene further highlights the importance of ethylene in *Cm* symptom development (Savidor et al., 2012).

Despite extensive screenings of wild germplasm, resistance to the pathogen has not been identified yet (Sen et al., 2015). In our study, we hypothesized that impairment of S genes involved in the tomato-*Cm* interaction might result in loss-of-susceptibility. Therefore, we set out to identify tomato S genes potentially involved in the interaction.

Recently, the tomato ortholog of *Walls Are Thin1* (*SlWAT1*) was identified and inactivated through RNAi and CRISPR/Cas9 (Hanika et al., 2026). CRISPR/Cas9 mediated knock-out of the gene led to resistance to the vascular fungi *Verticillium dahliae*, *V. albo-altrum* and *Fusarium oxysporum f.* sp. *lycopersici* (Hanika et al., 2026). The Arabidopsis *WAT1* gene encodes for a tonoplast localized plant-specific protein. *WAT1* has been shown to be involved in vacuolar auxin transport and secondary cell wall biosynthesis (Ranocha et al., 2010; Ranocha et al., 2013). In *Arabidopsis* loss-of-function of the gene leads to enhanced resistance to a broad range of vascular pathogens, including the bacterium *Ralstonia solanacearum* (Denance et al., 2013). In cotton (*Gosypium hirsutum*) three *WAT* homologs have been identified. Simultaneous transient silencing of the cotton genes enhanced resistance to the vascular fungus *V. dahliae* (Tang et al., 2019). In both cotton and Arabidopsis resistance involves the repression of indole metabolism and altered contents of indole-3-acetic acid (IAA) and salicylic acid (SA) (Denance et al., 2013; Tang et al., 2019). In addition, local lignin deposition was associated with *V. dahliae* resistance in cotton (Tang et al., 2019). In this study, we show that impairment of *SlWAT1* through RNAi and CRISPR/Cas9 leads to broad-spectrum reduced susceptibility to genetically different *Cm* strains. Next to this, we show that downregulation of *SlWAT1* reduces auxin content in tomato stems and potentially affects the expression of bacterial virulence factors.

Results

Down-regulation of *SlWAT1* leads to broad-spectrum reduced susceptibility to *Cm*

To study the role of *SlWAT1* in susceptibility of tomato to *Cm*, homozygous T_3 progeny of two RNAi lines (RNAi::SlWAT1_1 (TV181036) and RNAi::SlWAT1_2 (TV181034)) derived from two independent transformants in cv. Moneymaker (cv. MM) background were used (Hanika et al., 2026). Expression analysis of the T_2 parental lines, revealed that the relative residual expression of lines RNAi::SlWAT1_1 and RNAi::SlWAT1_2 was on average 20% and 54%, respectively (Hanika et al., 2026). To evaluate the spectrum of resistance conferred by silencing of *SlWAT1*, lines RNAi::SlWAT1_1 and RNAi::SlWAT1_2 were challenged with four genetically diverse *Cm* strains (Jacques et al., 2012). Wilting symptoms on the infected plants were recorded from 7 to 20 days post inoculation (dpi). Severe wilting symptoms caused by all four genetically distinct *Cm* stains were observed on MM plants. Aggressiveness of the four strains differed, with NCPBB382 being the most aggressive and CFBP5843 being the least aggressive strain (Figure S1). Both T_3 lines used in the disease assays exhibited significant reduction of wilting symptoms to all tested strains (Figure 1). Mild wilting symptoms were observed on RNAi::SlWAT1_1 transgenic plants when inoculated with the most aggressive NCPBB382 strain. For RNAi::SlWAT1_2 mild symptoms were observed for strains NCPBB382 and IPO3356.

Bacterial growth is not limited in RNAi::SlWAT1_1 transgenic plants

To determine whether the reduction in observable wilting symptoms in the RNAi lines was correlated with changes in the bacterial growth *in planta*, the population dynamics of the four different strains were quantified at three time points (4 dpi, 7 dpi and 14 dpi). An estimated $5x10^5$ colony forming units (cfu)/mL was used for the inoculation of the plants. Over the course of infection, all *Cm* strains reached high population densities (~10^9 $\log_{10}$(cfu+1/g fresh stem tissue)). No significant statistical differences in population densities were observed between the susceptible cv. MM and transgenic plants for strains NCPBB382, IPO3356, CFBP5843 and CFBPB2493 (Figure 2).

CRISPR/Cas9- mediated knock-out of *SlWAT1* leads to loss-of-susceptibility to *Cm* without limiting bacterial growth

To exclude the possibility of interference of the residual expression of *SlWAT1* in the RNAi lines with the phenotype observed and to confirm our previous results, we decided to include a CRISPR/Cas9 mutant line in the experiments. Silencing of *SlWAT1* through RNAi did not lead to any observable adverse pleiotropic effects (Figure 3H). However, for the gene edited mutant line *slwat1*, severe growth retardation was observed, as previously described (Figure 3) (Hanika et al., 2026). Besides the severe growth retardation, lack of chlorophyll and strong accumulation of anthocyanins at the abaxial side of developing leaves at early developmental stages were also observed. The latter phenotypic abnormalities were alleviated as the plants grew older (Figures 3C, G).

Changes of tomato susceptibility in response to *Cm* due to different developmental stages have previously been reported. Generally, the severity of disease decreases and the incubation period becomes longer with inoculations at later developmental stages (Chang et al., 1992; Sharabani et al., 2013). Therefore, for the inoculation of the plants we decided to use control plants at the same developmental stage as the mutants (4^{th} leaf stage). To achieve synchroneity in the developmental stages of our two genotypes control plants were sown every week. When the control plants and the *slwat1* mutants were at the same developmental stage we challenged them with the hypervirulent strain NCPBB382. At 20 dpi, severe wilting symptoms were observed in the susceptible background cv. MM. No symptoms were observed in the *slwat1* mutants, confirming our previous results (Figures 4, S2A). When the *in planta* bacterial titers were quantified, no significant statistical changes were found between the susceptible cv. MM and *slwat1* mutants (Figure S2B).

Silencing of *SlWAT1* reduces auxin content and affects the expression of auxin related genes

Repression of indole metabolism and transcriptional changes of auxin related genes have been reported in Arabidopsis *wat1* mutants and cotton *WATs* silenced plants (Denance et al., 2013; Tang et al., 2019). In our experiments, we monitored the expression of genes involved in auxin transport and auxin responses at different infection time points (Figure 5). To evaluate the distribution of auxin in the stems of transgenic plants the expression of three auxin-related genes was studied at different timepoints. Genes *SlPIN1* and *LAX4* were selected on the basis of their function as an exporter and an importer of auxin, respectively (Pattison and Catalá, 2012). *IAA19* is a useful indicator, as it is primarily expressed in the absence of auxin (Tatematsu et al., 2004).

Firstly, we quantified the expression of *SlWAT1*. As expected, the gene was significantly downregulated in RNAi::SlWAT1_1 plants compared to the cv. MM background (Figures 5A, E). For the rest of the genes we studied no statistically significant differences were found between cv. MM and transgenic plants (Figure 5). At 1 dpi, genes *SlPIN1* and *IAA19* were upregulated in mock inoculated transgenic plants compared to cv.MM. Upon inoculation, their expression was downregulated in RNAi plants (Figures 5B, D). The same pattern of expression can be observed for gene *IAA19* also at 7 dpi (Figure 5H). At 1 dpi, the expression of the auxin importer *LAX4* was upregulated in RNAi plants inoculated with *Cm* (Figure 5C), while at 7 dpi the expression of the gene was

10.3389/fpls.2023.1082094

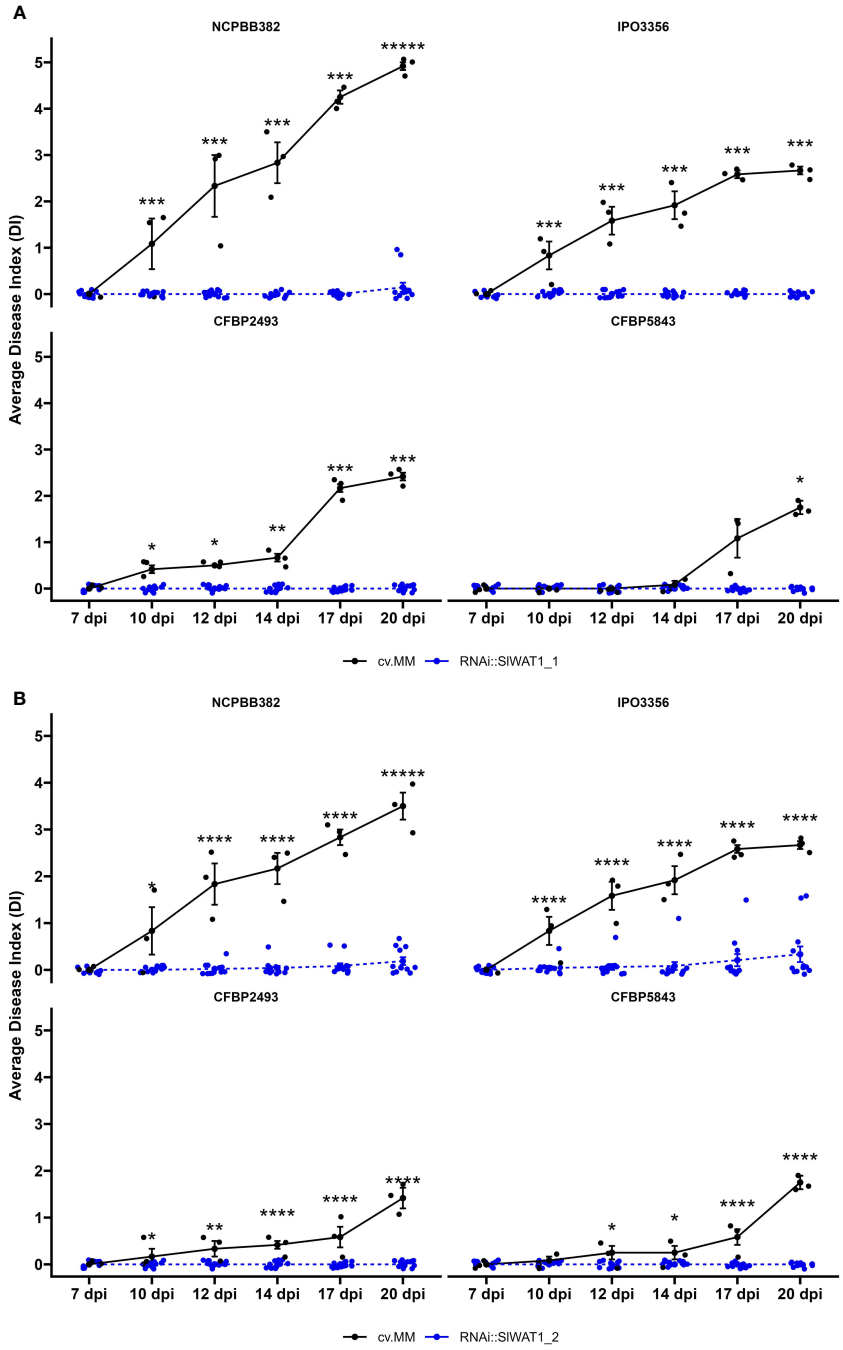

FIGURE 1
Disease index of *SlWAT1* RNAi silenced lines inoculated with genetically diverse *Cm* strains. Wilting symptom development of **(A)** RNAi::SlWAT1_1 and **(B)** RNAi::SlWAT1_2 lines compared to the background donor susceptible control cv. Moneymaker (cv.MM) from 7 days post inoculation (dpi) to 20 dpi. Means of both RNAi::SlWAT1 lines were significantly different from the cv.MM controls, for all strains used in the disease assay (n=12). Bars indicate the standard errors. Asterisks indicate significant differences (Student's t-test, *p ≤ 0.05; ***p ≤ 0.001,****p ≤ 0.0001).

comparable to that in cv. MM (Figure 5G). In contrast, the expression of auxin efflux transporter *SlPIN1* was upregulated at 7 dpi in infected RNAi plants compared to the cv.MM plants (Figure 5F).

Finally, we quantified the levels of auxin in different parts of tomato stems through LC-MS/MS. Free IAA content was quantified at the apical parts of the stem and hypocotyls of RNAi and cv. MM plants that were mock treated or inoculated (7 dpi). Our results confirm that silencing of *SlWAT1* significantly reduces free IAA levels in tomato stems. Consistent with the basipetal auxin transport from source to sink, we also observed a gradient in auxin concentration between the apical meristems and hypocotyls in both genotypes (Figure 6).

10.3389/fpls.2023.1082094

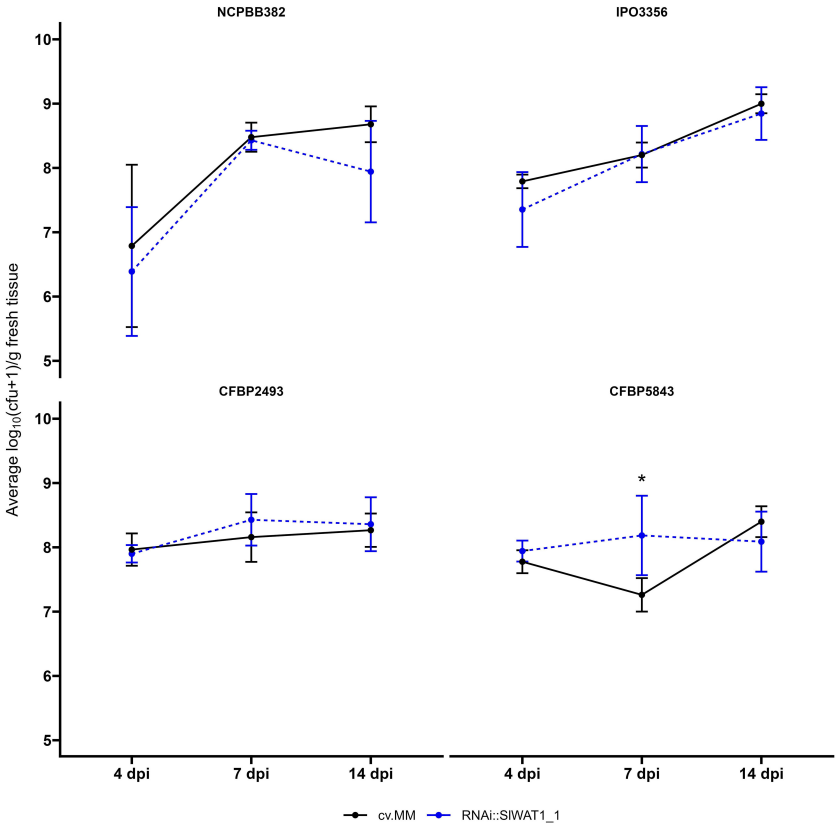

FIGURE 2
Clavibacter michiganensis population dynamics in cv. Moneymaker (cv.MM) and RNAi::SlWAT1_1 transgenic plants. Bacterial titers of the four bacterial strains used in the experiments were quantified at 4, 7 and 14 days post inoculation (dpi). Five biological replicates (n=5) were used per time point and bacterial strain. Lines represent the average $\log_{10}$(cfu+1/g fresh tissue) ± stdev. The experiments were repeated independently at least twice with similar results. Asterisks indicate statistical differences (Student's t-test, *p ≤ 0.05).

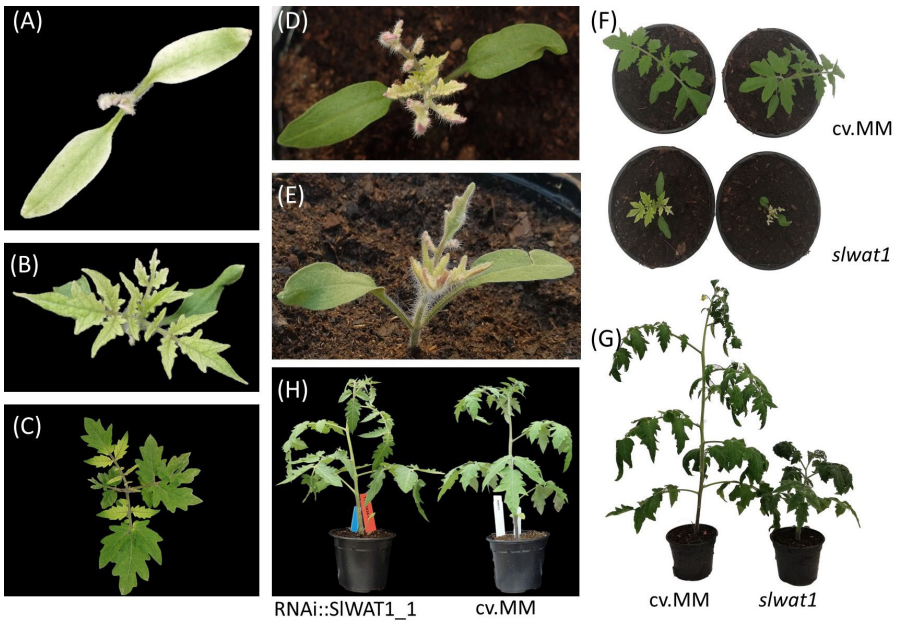

FIGURE 3
Pleiotropic phenotypes of *slwat1* knock-out mutant plants. **(A-C)** Lack of chlorophyll observed in developing *slwat1* mutants. **(D, E)** Anthocyanin accumulation in the abaxial side of leaves of developing mutants. Severe growth retardation in four weeks old **(F)** and ten weeks old **(G)** *slwat1* mutants compared to the cv. Moneymaker (cv.MM). **(H)** phenotype of 6 weeks old RNAi::SlWAT1_1 transgenic plants compared to cv.MM.

10.3389/fpls.2023.1082094

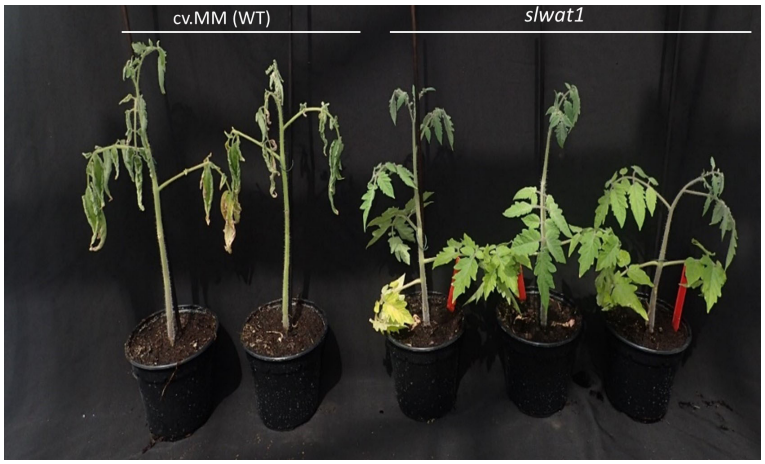

FIGURE 4
Symptom development of mutants *slwat1* in comparison to the susceptible background cv.MM inoculated with strain NCPBB382 at 20 days post inoculation.

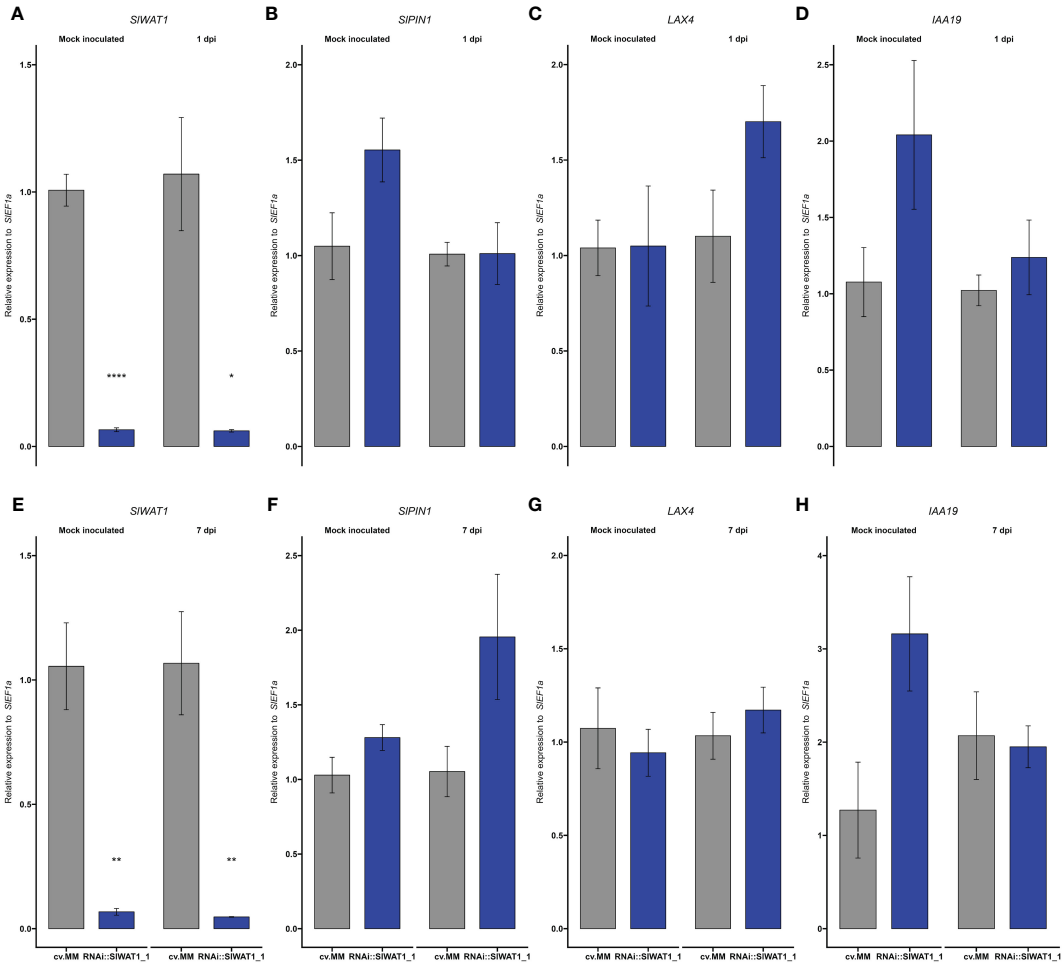

FIGURE 5
Expression of auxin transporter/signaling genes and auxin content is reprogrammed in RNAi::SlWAT1 plants. Relative expression of genes **(A, E)** *SlWAT1*, **(B, F)** *SlPIN1*, **(C, G)** *LAX4* and **(D, H)** *IAA19* in mock treated and *Cm* inoculated plants at 1 day post inoculation (dpi) and 7 dpi. Fold changes were normalized relative to expression of the *SlEf1α* in cv.MM plants. Bars represent the average fold change over three independent biological replicates (n=5). Error bars indicate standard errors of the mean.

10.3389/fpls.2023.1082094

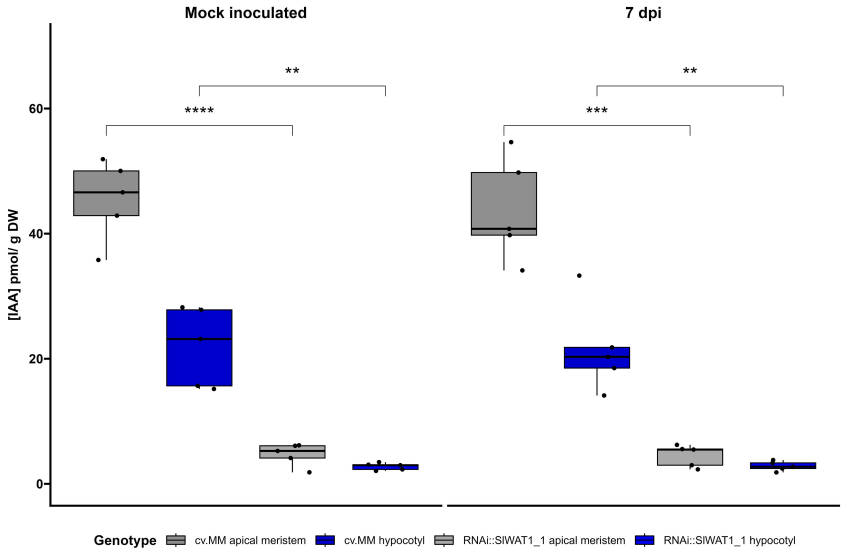

FIGURE 6
Free IAA content in different stem parts of cv. Moneymaker (cv. MM) and RNAi::SlWAT1_1 plants mock and inoculated at 7 days post inoculation (dpi). Boxplots of IAA concentration (pmol/g DW) in apical meristems and hypocotyls of the two genotypes. Lower and upper box boundaries represent the 25th and 75th percentiles, respectively. Lines in the boxes represent medians of five biological replicates (n=5). (Student's t-test, **p ≤ 0.01; ***p ≤ 0.001,****p ≤ 0.0001).

Ethylene biosynthesis is downregulated in *SlWAT1* silenced plants

Upregulation of ethylene biosynthesis through gene *ACO1* has been shown to contribute to the development of wilting symptoms in *Cm* infected plants (Balaji et al., 2008). Based on our previous observations that silencing of *SlWAT1* reduces symptom development on tomato plants, we hypothesized that silencing of the gene will have an effect on ethylene biosynthesis. Therefore, we examined the expression of gene *ACO1* in the RNAi::SlWAT1_1 plants. We found that the *ACO1* gene is constitutively downregulated in the RNAi plants compared to the cv. MM background, suggesting that ethylene biosynthesis is reduced in the *SlWAT1* silenced tomato plants (Figures 7, S3).

Inactivation of *SlWAT1* affects the expression of pathogen virulence factors

Recent studies in the interaction between *Pseudomonas syringae* DC3000 and *Arabidopsis* have revealed a role of IAA in the expression of bacterial virulence factors *in planta* and *in vitro* (Kunkel and Harper, 2018). Based on our data that free IAA content in the transgenic plants was significantly lower than in the susceptible cv. MM, we sought to investigate if silencing of *SlWAT1* has an effect on the regulation of *Cm* virulence factors. Plants of cv. MM and RNAi::SlWAT1_1 were inoculated with *Cm* strain NCPBB382 and stems parts were collected at 1 and 7 dpi. Total RNA from infected plants was isolated and was used to monitor the expression of bacterial virulence genes *celA*, *pat-1*, *vatr2* (*virulence associated transcriptional regulator2*) and *phpA*. At 1 dpi, no amplification of bacterial transcripts was possible due to the low proportion of bacterial mRNA in the total isolated RNA. At 7 dpi, no differences were found in the expression of genes *celA* and *pat-1* on cv. MM and RNAi plants (Figures 8A, B). Expression of transcription factor *vatr2* and its target *phpA*, however, was found to be downregulated in the RNAi plants at 7 dpi, with *phpA* being significantly downregulated (Figures 8C, D). Overall, our results indicate that silencing of *SlWAT1* affects the expression of virulence related genes in *Cm* during bacterial growth *in planta*, possibly through reduced IAA content.

Discussion

During their co-evolution with plants many pathogens have evolved the ability to manipulate host S genes to establish a compatible interaction (van Schie and Takken, 2014). Loss-of-function of host S genes can possibly alter a compatible interaction into a non-compatible one, leading to pathogen resistance (Pavan et al., 2010; Gawehns et al., 2013; van Schie and Takken, 2014). Here, we report that the loss-of-function of S gene *WAT1* in tomato leads to high tolerance to genetically distinct strains of the bacterial pathogen *Clavibacter michiganensis* (Figure 1).

WAT1 acts as an S gene that enables the infection process of vascular pathogens (Denance et al., 2013; Tang et al., 2019; Hanika et al., 2026). *WAT1* is a tonoplast localized vacuolar auxin transporter, that was first described as a S gene in *Arabidopsis thaliana* (Ranocha et al., 2010). The arabidopsis *wat1-1* mutant was found to be resistant to a broad range of vascular pathogens, including the bacterium *Ralstonia solanacearum* and the fungi *V. dahliae, V. album-altrum* and *F. oxysporum f.* sp. *lycopersici.* Its function as an S gene to fungal vascular wilts has also been reported in cotton and tomato (Tang et al., 2019; Hanika et al., 2026). In this

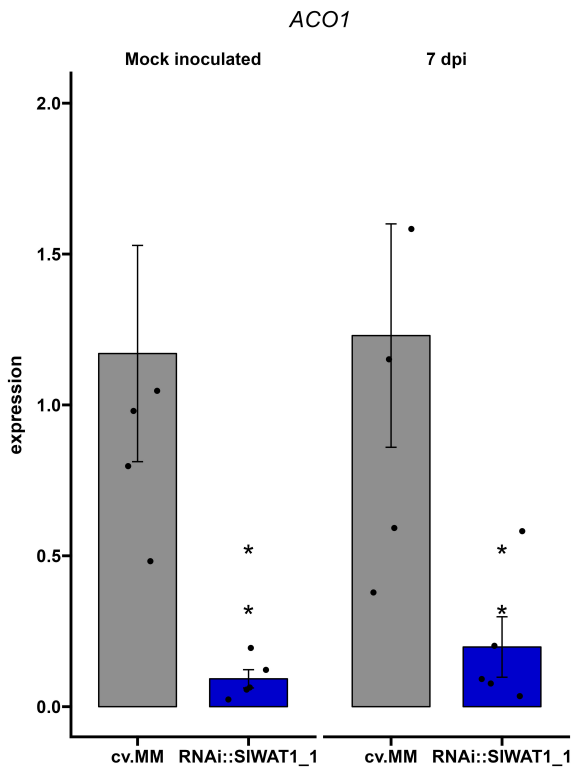

FIGURE 7
Expression of ethylene biosynthetic gene *ACO1* is constitutively downregulated in RNAi::SlWAT1_1 transgenic plants. Relative expression of gene *ACO1* in mock treated and *Cm* inoculated plants at 7 day post inoculation (dpi). Fold changes were normalized relative to expression of the gene in the control plants of cv. Moneymaker (cv.MM). Bars represent the average fold change over five independent biological replicates (n=5). Error bars indicate standard errors of the mean. Asterisks indicate significant differences to the expression prior to inoculation (Student's T test, *p≤ 0.05).

study, we show that inactivation of tomato homolog *SlWAT1* results in strong reduction of symptom development caused by genetically distinct *Cm* strains (Figure 1). These findings suggest the function of *WAT1* as an S gene is possibly conserved across plant species and that its loss-of-function can provide broad-spectrum resistance to vascular pathogens. This is an important trait that has been described for several other S genes (van Damme et al., 2008; Acevedo-Garcia et al., 2017; Oliva et al., 2019; Santillán Martínez et al., 2020; Thomazella et al., 2021).

Despite the strong reduction of wilting symptoms, growth of *Cm* was not suppressed by inactivation of *SlWAT1*, in contrast to what it has been reported for other pathogens (Tang et al., 2019; Hanika et al., 2026). According to our initial hypothesis, the residual expression of *SlWAT1* in the RNAi lines was possibly responsible for the mild symptoms observed and the sustained growth of the pathogen. To confirm the results we obtained from the disease assays and to study the effect of a full knock-out in the growth of the pathogen, we included a CRISPR/Cas9 mutant line in our experiments. In accordance with our previous results, we observed strong symptom reduction in *slwat1* mutant tomato plants. Further, we did not detect any significant differences in the *Cm* bacterial titers recovered from the *slwat1* mutants and the susceptible background. As previously observed virulence of Cm does not always correlate with population size. Strain Cmm100, which lacks the two plasmids involved in pathogenicity, cannot cause symptoms on tomato plants and acts as an endophyte. It can, however, grow to population densities that in some cases are higher than the virulent wild type strain. This has been attributed to plant cell death as symptom development advances (Chalupowicz et al., 2010). The high population densities of Cm in SlWAT1 inactivated plants might be an indication of less cell death, which may be a result of downregulation of bacterial virulence factors. As a result of less cell death the pathogen is able to grow to high population densities. This led us to hypothesize that *SlWAT1* is involved in symptom development, rather than sustainment of *Cm*. A major drawback in the use of mutant S genes to gain resistance to pathogens is the possibility of adverse pleiotropy (Sun et al., 2016b), as also observed in the case of tomato *SlWAT1*. Although a full knock-out of the gene led to severe growth defects (Figure 3), downregulation of the gene in the RNAi lines resulted in similar tolerance levels to the pathogen without a severe fitness cost on plant growth. In addition to RNAi, alterations in *cis*-regulatory regions of the gene to change its expression (Alonge et al., 2020), might provide a cost-free strategy to gain tolerance to *Cm*. Alternatively, the exploration of allelic variation in tomato germplasm may lead to the identification of natural variants that disrupt the compatible host-pathogen interaction without fitness costs, as it was done in the case of gene *ROD1* in rice (Gao et al., 2021).

Changes in hormonal homeostasis is a common strategy used by pathogens to promote disease. While upregulation of host derived ethylene has been found to promote wilting development by *Cm*, the role of other hormones in the infection process remains unclear (Balaji et al., 2008). Resistance conferred by inactivation of *WAT1* has been associated with altered crosstalk between auxin and SA in Arabidopsis and cotton (Denance et al., 2013; Tang et al., 2019). According to our findings ethylene biosynthesis and auxin content were reduced in *SlWAT1* inactivated plants. We found that the ethylene biosynthetic gene *ACO1*, that is specifically upregulated by *Cm* to promote wilting symptoms was constitutively downregulated in RNAi::SlWAT1_1 plants (Figures 6, S3). This is also in accordance with previous studies that found that symptom development, but not *Cm* bacterial growth was inhibited on *Nr* ethylene insensitive plants (Balaji et al., 2008).

We also found that the content of free IAA in stem tissues of the RNAi plants was significantly lower than in cv. MM (Figure 6). In addition, expression of auxin related genes was altered by *SlWAT1* impaired plants upon *Cm* inoculation (Figures 5A–H). At 1 dpi, we found that the expression of auxin influx gene *LAX4* was upregulated in *Cm* inoculated RNAi plants, while the expression of auxin efflux gene *SlPIN1* was upregulated in mock inoculated RNAI plants. Although rather speculative, these changes in the expression of auxin transporter genes might be induced by *Cm* in an attempt to increase auxin influx around the inoculation point. The lower expression of *IAA19* in infected plants (at 1 and 7 dpi) compared to mock inoculated RNAi plants could also suggest that the auxin contents around the inoculation site are indeed increased during infection, since *IAA19* is upregulated in the absence of auxin (Tatematsu et al., 2004). Finally, the upregulation of *SlPIN1* in *Cm* infected *SlWAT1* inactivated plants at 7 dpi, might act as a late compensatory mechanism for the absence of *SlWAT1*, which also facilitates auxin efflux.

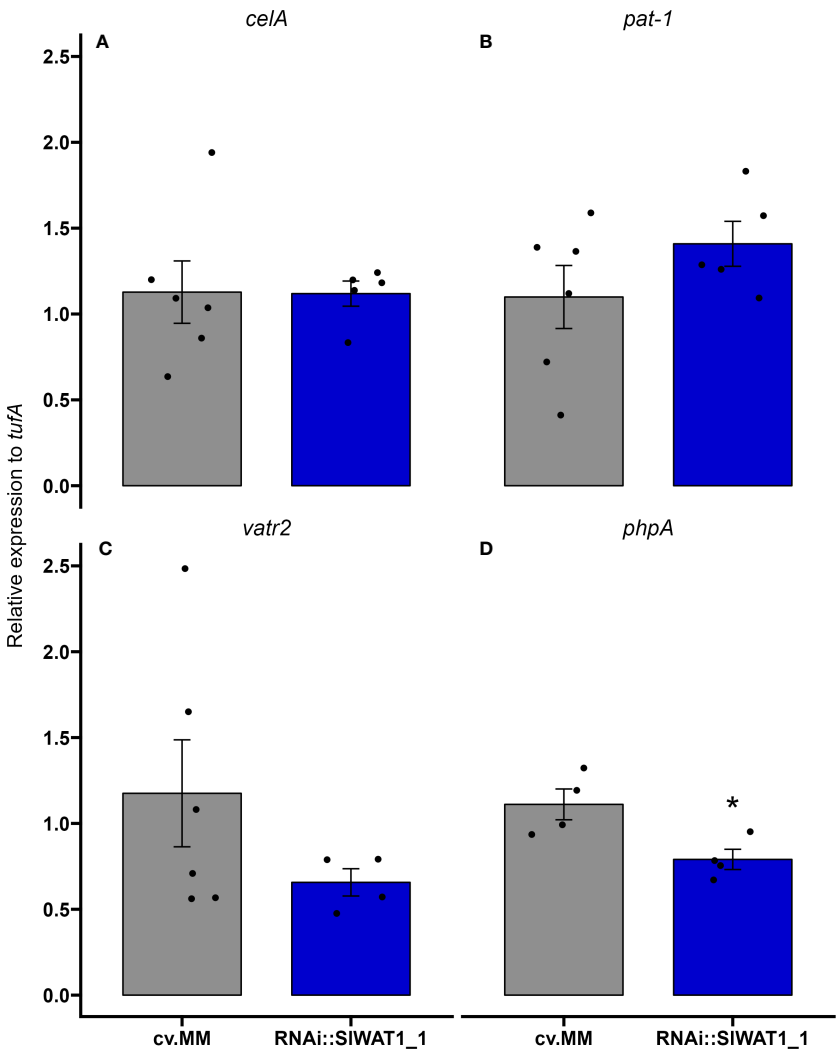

FIGURE 8
Inactivation of *SlWAT1* affects the expression of specific bacterial virulence genes *in planta*. Relative expression of genes **(A)** *celA*, **(B)** *pat-1*, **(C)** *vatr2* and **(D)** *phpA* on susceptible cv. Moneymaker (cv.MM) and RNAi::SlWAT1_1 plants inoculated with *Cm* strain NCPBB382 at 7 days post inoculation (dpi). Fold changes were normalized relative to expression of the genes in cv.MM plants. Bars represent the average fold change over five independent biological replicates (n=5). Error bars indicate standard errors of the mean. Asterisks indicate significant differences to the expression of the genes in the different genotypes (Student's T test, *p≤ 0.05).

Higher contents of SA have been reported for arabidopsis and cotton *WAT1* impaired plants (Denance et al., 2013; Tang et al., 2019). This could be a direct consequence of the reduction of free IAA content, as the SA and auxin hormonal pathways are mutually antagonistic (Wang et al., 2007). Although SA is a known regulator of defenses against pathogens, knowledge on its role in resistance against *Cm* is limited. Recently, it was shown that exogenous application of SA reduces the bacterial populations on tomato cotyledons (Yokotani et al., 2021). The infection of *NahG* transgenic tomato plants with impaired SA accumulation, however, did not result in higher susceptibility to the pathogen (Barda et al., 2015).

Growing evidence suggests that host derived auxin is an important signaling molecule involved in plant-bacteria interactions (Denance et al., 2013; McClerklin et al., 2018; Djami-Tchatchou et al., 2019; Mashiguchi et al., 2019). Recent studies have reported a direct effect of auxin in the regulation of *Pseudomonas syringae DC300* bacterial genes involved in virulence (Aragón et al., 2014; Djami-Tchatchou et al., 2019). Elevated IAA content in Arabidopsis quadruple mutant *tir1 afb1 afb4 afb5*, as well as the addition of IAA in *P. syringae DC300* cultures led to the repression of genes involved in the production of T3SS at early timepoints. The expression of genes involved in late infection stages, however, was significantly upregulated by elevated IAA contents (Djami-Tchatchou et al., 2019). Additionally, auxin produced by bacteria itself can act as a virulence factor (McClerklin et al., 2018). Based on our observations of the significant reduction of symptom development and the significantly lower free IAA content in RNAi::SlWAT1_1 plants, we hypothesized that auxin might play a role in the regulation of *Cm* virulence genes. Therefore, we monitored the transcript levels of virulence factors *celA*, *pat-1*, *vatr2* and *phpA in planta* (Figure 7). Interestingly, we observed that

transcription factor *vatr2* and its target *phpA* were downregulated at 7 dpi. This suggests that inactivation of *SlWAT1* leads to downregulation of *Cm* virulence genes, possibly through the reduced contents of free IAA in the stems of transgenic plants. Previous, transcriptomics analysis has shown that the virulence factors *celA* and *pat-1* reach the peak of their expression between 24 and 72 hours post inoculation and gene expression is reduced after that point (Chalupowicz et al., 2010). This might be the reason why we did not detect a difference in the expression of *celA* and *pat-1* isolated from cv.MM and RNAi::SlWAT1_1 plants at 7 dpi. To definitely conclude, however, that auxin directly affects the expression of bacterial genes after supplementation of cultures with IAA could be monitored. Moreover, meta-transcriptomics analysis through RNA-seq on infected *SlWAT1* inactivated plants and their susceptible background could be deployed in different experimental timepoints, in order to elucidate the complete pathways involved in the molecular interaction of the organisms (Guo et al., 2021). Future studies on how *Cm* responds to IAA, as well as the production of IAA non-responsive *Cm* mutants, could allow us to fully study and understand the role of auxin as a signaling molecule in the pathosystem. Finally, the possibility of changes in the metabolome of the plants due to perturbations in hormonal changes, might influence the expression of bacterial virulence factors, requires further examination.

Materials and methods

Plant materials

The present study included the susceptible *Solanum lycopersicum* cv. Moneymaker MM as a control, T_3 progeny of two independent stable transformants (RNAi::SlWAT1_1, RNAi::SlWAT1_2) in which the *SlWAT1* gene was silenced through RNAi in cv. MM background and T_2 progeny of a bi-allelic heterozygous CRISPR/Cas9 generated *slwat1* mutant line (Hanika et al., 2026). Prior to infection, transgenic plantlets were screened for the presence of the RNAi silencing construct based on the presence of the 35S and NPTII markers. *slwat1* mutants were screened for the presence of mutant alleles through PCR based genotyping and sequencing.

Plants were grown in a climate regulated greenhouse compartment at 24°C/18°C under a 12h/12h day/night regime. Relative humidity in the compartment was kept to ~60%.

DNA isolation and genotyping

For the genotyping of the RNAi transgenic and *slwat1* mutant plants genomic DNA was isolated using a modified protocol for cetyl trimethylammonium bromide (CTAB) extraction method (Doyle, 1991). PCR was performed with DreamTaq DNA polymerase (Thermo Scientific) and target specific primers (Table S1). The PCR products of the RNAi transgenic plants were visualized on 1% agarose gel for the screening of the presence of NPTII and 35S transgene markers. PCR products of mutant plants were sequenced through Illumina sequencing (Macrogen Europe, Amsterdam).

Bacterial strains and growth conditions

Four genetically diverse *Cm* strains were used in the experiments, i.e. *Cm* strains NCPBB382, IPO3356 (rifampicin resistant mutant), CFBP2493 and CFBP5843 were used in the experiments (Jacques et al., 2012). Prior to plant inoculation the strains were grown for two days at 25° C on TBY plates (10 gL^{-1} tryptone, 5 gL^{-1} yeast extract, 5 gL^{-1} sodium chloride, 15 gL^{-1} bacteriological agar). Plates were supplemented with appropriate antibiotics when needed (25 µl/mL rifampicin).

Disease assay

Tomato plants at the fourth true leaf stage were inoculated by a petiole clipping off method. The petioles of the first two fully expanded leaves were clipped off with razor blades immersed in the bacterial inoculum and 5 µl of the bacterial inoculum were directly pipetted on the lowest wound. Bacterial inocula of the four bacterial strains were prepared by re-suspending cells in Ringer's buffer to a final concentration of ~10^8 cfu/ml (OD_{600} = 0.1). Prior to re-suspension the *Cm* strains were streaked on TBY plates, supplemented with appropriate antibiotics when needed, and incubated at 25°C for two days. Symptom development (wilting) was monitored up to 20 days post inoculation (dpi). A disease index (DI) scale based on the development of wilting symptoms on the leaves was used (0; no symptoms- 5; all leaves wilting). Per strain, 12 transgenic T_3 plants and three susceptible cv. MM control plants were used. The same procedure was used for the disease assays of *slwat1* mutants. At least five biological replicates of *slwat1* mutants were used in the experiments. Four biological replicates of the susceptible cv. MM were used as controls.

Bacterial quantification

Bacterial quantification was done through serial dilution plating. Whole stems collected ~1 cm above the lowest inoculation point and up to the apical meristem were sampled at three time points; 4 dpi, 7 dpi and 14 dpi. Stems were pulverized and homogenized in Ringer's solution (Sigma Aldrich). 50 µl of serial dilutions of the homogenate (10^1 –10^6) were plated on SCM-F selective plates (Duchefa Biochemie). The medium was supplemented with 1.9 g L^{-1} yeast extract, 20 µL L^{-1} nalidixic acid (100 mg mL^{-1}), 8 mL L^{-1} trimetroprim in MetOH 100% (10 mg/mL), 1 ml L^{-1} cyclohexamide in MetOH 100% (100 mg $mL^{-1)}$, 1 mL potassium tellurite (1%), 50 ml L^{-1} nicotinic acid (2 mg/mL). Plates were supplemented with appropriate antibiotics when necessary (25 µl/mL rifampicin). Plates were incubated at 25°C for 7 days. Colonies on the plates were counted 7 days post plating and the $\log_{10}$(cfu+1/g fresh tissue) per plate was calculated. Five biological replicates of RNAi::SlWAT1_1 plants and the susceptible cv. MM were used per time point. Two technical replicates per sample were plated. The same procedure was used

for the quantification of *in planta* bacterial titers of strain NCPBB382 in *slwat1* mutants. Five biological replicates per time point were used.

RNA extraction/cDNA synthesis

Stem samples of ~2 cm in length were collected above the inoculation point. The stems were processed using a Precellys Evolution tissue homogenizer (Bertin Technologies) at 7000 RPM for two rounds of 15 sec, with the cryolysis option on. RNA extraction and on column DNase treatment were done using the RNeasy Mini Kit (Qiagen) and RNase-Free DNase Set (Qiagen) following the manufacturer's instructions. 500 ng of first strand cDNA was synthesized using the iScript cDNA synthesis kit (Bio-rad).

Gene expression analysis

Expression levels of tomato genes *SlWAT1*, *ACO1*, *IAA19*, *SlPIN1*, *LAX4* on mock treated and *Cm* infected control and RNAi::SlWAT1_1 transgenic plants were monitored through RT-qPCR at 1 and 7 dpi using specific gene primers (Table S1). The expression of bacterial virulence genes *celA*, *pat-1, vatr2* and *phpA* on infected cv. MM and RNAi::SlWAT1_1 was also assessed at 1 and 7 dpi using target specific primers (Table S1). 5 and 25 ng of cDNA were used as a template for the reactions for the quantification of plant and bacterial transcripts, respectively. Reactions were done in duplicates. At least four biological samples were used per treatment and time point. RT-qPCR was done on a CFX96 Touch Deep Well Real Time PCR Detection system (Bio-Rad).

Prior to cDNA synthesis for the expression analysis of the bacterial virulence genes, the total RNA isolated was run on 1% agarose gel to confirm the absence of gDNA from the samples. The Livak $2^{-\Delta\Delta Ct}$ method was used to normalize and calibrate transcript values relative to the endogenous *SlEf1α* for tomato and gene *tufA* for the bacterial genes.

Auxin quantification

Auxin was quantified through Liquid Chromatography- Mass Spectrometry (LC-MS/MS). Plant stem parts were collected and flash frozen in liquid nitrogen. The collected tissue was processed using a Precellys Evolution tissue homogenizer (Bertin Technologies) at 7000 RPM for two rounds of 15 sec, with the cryolysis option on. ~25 mg of tissue were used for the auxin extraction. Ground stem samples were extracted with 1 mL of cold methanol containing [phenyl $^{13}C_6$]-IAA (0.1 nmol/mL) as an internal standard in a 2-mL eppendorf tube and purified as previously described (Ruyter-Spira et al., 2011; Schiessl et al., 2019). Samples were filtered through a 0.45 µm Minisart SRP4 filter (Sartorius, Goettingen, Germany) and measured on the same day. Auxin was analyzed on a Waters Xevo TQs tandem quadruple mass spectrometer as previously described (Ruyter-Spira et al., 2011; Gühl et al., 2021).

Data availability statement

The data presented in the study are deposited in the National Center for Biotechnology Information (NCBI) repository, accession numbers OP832215 and OP832216.

Author contributions

YB, JW, RV, and EK designed the experiments. YB, JW, and RV supervised the work. EK executed the experiments and performed the data analysis. KH generated the transgenic lines and CRISPR/Cas9 mutants. MMN was involved in the initial characterization of the gene. WK performed the auxin quantification. EK drafted the manuscript. JW, RV, and YB critically reviewed and edited the manuscript. All authors contributed to the article and approved the submitted version.

Funding

This research was (partially) funded by NWO Science domain (NWO-ENW) project 8440590003, which is financed by the Dutch Research Council (NWO).

Acknowledgments

The authors would like to thank Patricia van der Zouwen for the maintenance of the bacterial strains used in this study and her advice about the bacterial quantification.

Conflict of interest

The authors declare that the research was conducted in the absence of any commercial or financial relationships that could be construed as a potential conflict of interest.

Publisher's note

Supplementary material

The Supplementary Material for this article can be found online at: https://www.frontiersin.org/articles/10.3389/fpls.2023.1082094/full#supplementary-material

References

Acevedo-Garcia, J., Gruner, K., Reinstädler, A., Kemen, A., Kemen, E., Cao, L., et al. (2017). The powdery mildew-resistant arabidopsis mlo2 mlo6 mlo12 triple mutant displays altered infection phenotypes with diverse types of phytopathogens. *Sci. Rep.* 7 (1). doi: 10.1038/s41598-017-07188-7

Alonge, M., Wang, X., Benoit, M., Soyk, S., Pereira, L., Zhang, L., et al. (2020). Major impacts of widespread structural variation on gene expression and crop improvement in tomato. *Cell* 182 (1), 145–61.e23. doi: 10.1016/j.cell.2020.05.021

Appiano, M., Pavan, S., Catalano, D., Zheng, Z., Bracuto, V., Lotti, C., et al. (2015). Identification of candidate MLO powdery mildew susceptibility genes in cultivated solanaceae and functional characterization of tobacco NtMLO1. *Transgenic Res.* 24 (5), 847–858. doi: 10.1007/s11248-015-9878-4

Aragón, I. M., Pérez-Martínez, I., Moreno-Pérez, A., Cerezo, M., and Ramos, C. (2014). New insights into the role of indole-3-acetic acid in the virulence ofPseudomonas savastanoipv.savastanoi. *FEMS Microbiol. Lett.* 356 (2), 184–192. doi: 10.1111/1574-6968.12413

Bai, Y., Pavan, S., Zheng, Z., Zappel, N. F., Reinstadler, A., Lotti, C., et al. (2008). Naturally occurring broad-spectrum powdery mildew resistance in a central American tomato accession is caused by loss of mlo function. *Mol. Plant Microbe Interact.* 21 (1), 30–39. doi: 10.1094/MPMI-21-1-0030

Balaji, V., Mayrose, M., Sherf, O., Jacob-Hirsch, J., Eichenlaub, R., Iraki, N., et al. (2008). Tomato transcriptional changes in response to clavibacter michiganensis subsp. michiganensis reveal a role for ethylene in disease development. *Plant Physiol.* 146 (4), 1797–1809. doi: 10.1104/pp.107.115188

Barda, O., Shalev, O., Alster, S., Buxdorf, K., Gafni, A., and Levy, M. (2015). Pseudozyma aphidis induces salicylic-Acid-Independent resistance to clavibacter michiganensis in tomato plants. *Plant Disease.* 99 (5), 621–626. doi: 10.1094/PDIS-04-14-0377-RE

Berg, J. A., Appiano, M., Bijsterbosch, G., Visser, R. G. F., Schouten, H. J., and Bai, Y. (2017). Functional characterization of cucumber (Cucumis sativus l.) clade V MLO genes. *BMC Plant Biol.* 17 (1). doi: 10.1186/s12870-017-1029-z

Chalupowicz, L., Barash, I., Reuven, M., Dror, O., Sharabani, G., Gartemann, K.-H., et al. (2017). Differential contribution of clavibacter michiganensis ssp. michiganensis virulence factors to systemic and local infection in tomato. *Mol. Plant Pathol.* 18 (3), 336–346. doi: 10.1111/mpp.12400

Chalupowicz, L., Cohen-Kandli, M., Dror, O., Eichenlaub, R., Gartemann, K. H., Sessa, G., et al. (2010). Sequential expression of bacterial virulence and plant defense genes during infection of tomato withClavibacter michiganensissubsp.michiganensis. *Phytopathology* 100 (3), 252–261. doi: 10.1094/PHYTO-100-3-0252

Chang, R. J., Ries, S. M., and Pataky, J. K. (1992). Effects of temperature, plant-age, inoculum concentration, and cultivar on the incubation period and severity of bacterial canker of tomato. *Plant Disease.* 76 (11), 1150–1155. doi: 10.1094/PD-76-1150

Cohn, M., Bart, R. S., Shybut, M., Dahlbeck, D., Gomez, M., Morbitzer, R., et al. (2014). Xanthomonas axonopodis virulence is promoted by a transcription activator-like effector–mediated induction of a SWEET sugar transporter in cassava. *Mol. Plant-Microbe Interactions* 27 (11), 1186–1198. doi: 10.1094/MPMI-06-14-0161-R

Cox, K. L., Meng, F., Wilkins, K. E., Li, F., Wang, P., Booher, N. J., et al. (2017). TAL effector driven induction of a SWEET gene confers susceptibility to bacterial blight of cotton. *Nat. Commun.* 8, 15588. doi: 10.1038/ncomms15588

Davis, M. J., Gillaspie, A. G., Vidaver, A. K., and Harris, R. W. (1984). Clavibacter: a new genus containing some phytopathogenic coryneform bacteria, including clavibacter xyli subsp. xyli sp. nov., subsp. nov. and clavibacter xyli subsp. cynodontis subsp. nov., pathogens that cause ratoon stunting disease of sugarcane and be. *Int. J. Systematic Bacteriol.* 34 (2), 107–117. doi: 10.1099/00207713-34-2-107

Denance, N., Ranocha, P., Oria, N., Barlet, X., Riviere, M. P., Yadeta, K. A., et al. (2013). Arabidopsis wat1 (walls are thin1)-mediated resistance to the bacterial vascular pathogen, ralstonia solanacearum, is accompanied by cross-regulation of salicylic acid and tryptophan metabolism. *Plant J.* 73 (2), 225–239. doi: 10.1111/tpj.12027

Djami-Tchatchou, A. T., Harrison, G. A., Harper, C. P., Wang, R., Prigge, M. J., Estelle, M., et al. (2019). Dual role of auxin in regulating plant defense and bacterial virulence gene expression during pseudomonas syringae PtoDC3000 pathogenesis. *Mol Plant Microbe Interact.* 33, 1059–1071. doi: 10.1101/2019.12.29.881581

Doyle, J. (1991). *DNA Protocols for plants* (Berlin Heidelberg: Springer), 283–293.

Eichenlaub, R., and Gartemann, K.-H. (2011). The clavibacter michiganensis subspecies: molecular investigation of gram-positive bacterial plant pathogens. *Ann. Rev. Phytopathol.* 49, 1, 445–464. doi: 10.1146/annurev-phyto-072910-095258

Gao, M., He, Y., Yin, X., Zhong, X., Yan, B., Wu, Y., et al. (2021). Ca2+ sensor-mediated ROS scavenging suppresses rice immunity and is exploited by a fungal effector. *Cell* 184 (21), 5391–404.e17. doi: 10.1016/j.cell.2021.09.009

Gartemann, K. H., Abt, B., Bekel, T., Burger, A., Engemann, J., Flugel, M., et al. (2008). The genome sequence of the tomato-pathogenic actinomycete clavibacter michiganensis subsp. michiganensis NCPPB382 reveals a Large island involved in pathogenicity. *J. Bacteriol.* 190 (6), 2138–2149. doi: 10.1128/jb.01595-07

Gawehns, F., Cornelissen, B. J. C., and Takken, F. L. W. (2013). The potential of effector-target genes in breeding for plant innate immunity. *Microbial. Biotechnol.* 6 (3), 223–229. doi: 10.1111/1751-7915.12023

Gühl, K., Holmer, R., Xiao, T. T., Shen, D., Wardhani, T. A. K., Geurts, R., et al. (2021). The effect of exogenous nitrate on LCO signalling, cytokinin accumulation, and nodule initiation in medicago truncatula. *Genes* 12 (7), 988. doi: 10.3390/genes12070988

Guo, L., Yu, H., Wang, B., Vescio, K., DeIulio, G. A., Yang, H., et al. (2021). Metatranscriptomic comparison of endophytic and pathogenic fusarium-arabidopsis interactions reveals plant transcriptional plasticity. *Mol. Plant Microbe Interact.* 34 (9), 1071–1083. doi: 10.1094/MPMI-03-21-0063-R

Hanika, K., Schipper, D., Chinnappa, S., Oortwijn, M., Schouten, H. J., Thomma, B. P. H. J., et al. (2021). Impairment of tomato WAT1 enhances resistance to vascular wilt fungi despite severe growth defects. *Front. Plant Sci.* 2021, 12. doi: 10.3389/fpls.2021.721674

Hückelhoven, R., Eichmann, R., Weis, C., Hoefle, C., and Proels, R. K. (2013). Genetic loss of susceptibility: a costly route to disease resistance? *Plant Pathol.* 62, 56–62. doi: 10.1111/ppa.12103

Huibers, R. P., Loonen, A. E., Gao, D., Van den Ackerveken, G., Visser, R. G., and Bai, Y. (2013). Powdery mildew resistance in tomato by impairment of SlPMR4 and SlDMR1. *PloS One* 8 (6), e67467. doi: 10.1371/journal.pone.0067467

Jacques, M. A., Durand, K., Orgeur, G., Balidas, S., Fricot, C., Bonneau, S., et al. (2012). Phylogenetic analysis and polyphasic characterization of clavibacter michiganensis strains isolated from tomato seeds reveal that nonpathogenic strains are distinct from c. *michiganensis subsp michiganensis* 78 (23), 8388–8402. doi: 10.1128/AEM.02158-12

Jones, J. D., and Dangl, J. L. (2006). The plant immune system. *Nature* 444 (7117), 323–329. doi: 10.1038/nature05286

Kunkel, B. N., and Harper, C. P. (2018). The roles of auxin during interactions between bacterial plant pathogens and their hosts. *J. Exp. Botany* 69 (2), 245–254. doi: 10.1093/jxb/erx447

Mashiguchi, K., Hisano, H., Takeda-Kamiya, N., Takebayashi, Y., Ariizumi, T., Gao, Y., et al. (2019). Agrobacterium tumefaciensEnhances biosynthesis of two distinct auxins in the formation of crown galls. *Plant Cell Physiol.* 60 (1), 29–37. doi: 10.1093/pcp/pcy182

McClerklin, S. A., Lee, S. G., Harper, C. P., Nwumeh, R., Jez, J. M., and Kunkel, B. N. (2018). Indole-3-acetaldehyde dehydrogenase-dependent auxin synthesis contributes to virulence of pseudomonas syringae strain DC3000. *PloS Pathog.* 14 (1), e1006811. doi: 10.1371/journal.ppat.1006811

Meletzus, D., Bermphol, A., Dreier, J., and Eichenlaub, R. (1993). Evidence for plasmid-encoded virulence factors in the phytopathogenic bacterium clavibacter michiganensis subsp. michiganensis NCPPB382. *J. Bacteriol.* 175 (7), 2131–2136. doi: 10.1128/jb.175.7.2131-2136.1993

Nouioui, I., Carro, L., García-López, M., Meier-Kolthoff, J. P., Woyke, T., Kyrpides, N. C., et al. (2018). Genome-based taxonomic classification of the phylum actinobacteria. *Front. Microbiol.* 9. doi: 10.3389/fmicb.2018.02007

Oliva, R., Ji, C., Atienza-Grande, G., Huguet-Tapia, J. C., Perez-Quintero, A., Li, T., et al. (2019). Broad-spectrum resistance to bacterial blight in rice using genome editing. *Nat. Biotechnol.* 37 (11), 1344–1350. doi: 10.1038/s41587-019-0267-z

Pattison, R. J., and Catalá, C. (2012). Evaluating auxin distribution in tomato (Solanum lycopersicum) through an analysis of the PIN and AUX/LAX gene families. *Plant J.* 70 (4), 585–598. doi: 10.1111/j.1365-313X.2011.04895.x

Pavan, S., Jacobsen, E., Visser, R. G., and Bai, Y. (2010). Loss of susceptibility as a novel breeding strategy for durable and broad-spectrum resistance. *Mol. Breed.* 25 (1), 1–12. doi: 10.1007/s11032-009-9323-6

Pavan, S., Schiavulli, A., Appiano, M., Marcotrigiano, A. R., Cillo, F., Visser, R. G., et al. (2011). Pea powdery mildew er1 resistance is associated to loss-of-function mutations at a MLO homologous locus. *Theor. Appl. Genet.* 123 (8), 1425–1431. doi: 10.1007/s00122-011-1677-6

Pessina, S., Lenzi, L., Perazzolli, M., Campa, M., Dalla Costa, L., Urso, S., et al. (2016). Knockdown of MLO genes reduces susceptibility to powdery mildew in grapevine. *Hortic. Res.* 3, 16016. doi: 10.1038/hortres.2016.16

Ranocha, P., Denance, N., Vanholme, R., Freydier, A., Martinez, Y., Hoffmann, L., et al. (2010). Walls are thin 1 (WAT1), an arabidopsis homolog of medicago truncatula NODULIN21, is a tonoplast-localized protein required for secondary wall formation in fibers. *Plant J.* 63 (3), 469–483. doi: 10.1111/j.1365-313X.2010.04256.x

Ranocha, P., Dima, O., Nagy, R., Felten, J., Corratge-Faillie, C., Novak, O., et al. (2013). Arabidopsis WAT1 is a vacuolar auxin transport facilitator required for auxin homoeostasis. *Nat. Commun.* 4, 2625. doi: 10.1038/ncomms3625

Ruyter-Spira, C., Kohlen, W., Charnikhova, T., Van Zeijl, A., Van Bezouwen, L., De Ruijter, N., et al. (2011). Physiological effects of the synthetic strigolactone analog GR24 on root system architecture in arabidopsis: another belowground role for strigolactones? *Plant Physiol.* 155 (2), 721–734. doi: 10.1104/pp.110.166645

Santillán Martínez, M. I., Bracuto, V., Koseoglou, E., Appiano, M., Jacobsen, E., Visser, R. G. F., et al. (2020). CRISPR/Cas9-targeted mutagenesis of the tomato susceptibility gene PMR4 for resistance against powdery mildew. *BMC Plant Biol.* 20 (1). doi: 10.1186/s12870-020-02497-y

Savidor, A., Chalupowicz, L., Teper, D., Gartemann, K. H., Eichenlaub, R., Manulis-Sasson, S., et al. (2014). Clavibacter michiganensis subsp. michiganensis Vatr1 and Vatr2 transcriptional regulators are required for virulence in tomato. *Mol. Plant Microbe Interact.* 27 (10), 1035–1047. doi: 10.1094/mpmi-02-14-0061-r

Savidor, A., Teper, D., Gartemann, K.-H., Eichenlaub, R., Chalupowicz, L., Manulis-Sasson, S., et al. (2012). The clavibacter michiganensis subsp. michiganensis –tomato interactome reveals the perception of pathogen by the host and suggests mechanisms of infection. *J. Proteome Res.* 11, 2, 736–750. doi: 10.1021/pr200646a

Schiessl, K., Lilley, J. L. S., Lee, T., Tamvakis, I., Kohlen, W., Bailey, P. C., et al. (2019). NODULE INCEPTION recruits the lateral root developmental program for symbiotic nodule organogenesis in medicago truncatula. *Curr. Biol.* 29 (21), 3657–68.e5. doi: 10.1016/j.cub.2019.09.005

Sen, Y., van der Wolf, J., Visser, R. G. F., and Van Heusden, S. (2015). Bacterial canker of tomato: current knowledge of detection, management, resistance, and interactions. *Plant Disease.* 99 (1), 4–13. doi: 10.1094/PDIS-05-14-0499-FE

Sharabani, G., Shtienberg, D., Borenstein, M., Shulhani, R., Lofthouse, M., Sofer, M., et al. (2013). Effects of plant age on disease development and virulence ofClavibacter michiganensissubsp.michiganensison tomato. *Plant Pathol.* 62 (5), 1114–1122. doi: 10.1111/ppa.12013

Sun, K., Wolters, A.-M. A., Loonen, A. E. H. M., Huibers, R. P., van der Vlugt, R., Goverse, A., et al. (2016a). Down-regulation of arabidopsis DND1 orthologs in potato and tomato leads to broad-spectrum resistance to late blight and powdery mildew. *Transgenic Res.* 25 (2), 123–138. doi: 10.1007/s11248-015-9921-5

Sun, K., Wolters, A.-M. A., Vossen, J. H., Rouwet, M. E., Loonen, A. E. H. M., Jacobsen, E., et al. (2016b). Silencing of six susceptibility genes results in potato late blight resistance. *Transgenic Res.* 25 (5), 731–742. doi: 10.1007/s11248-016-9964-2

Tang, Y., Zhang, Z., Lei, Y., Hu, G., Liu, J., Hao, M., et al. (2019). Cotton WATs modulate SA biosynthesis and local lignin deposition participating in plant resistance against verticillium dahliae. *Front. Plant Sci.* 10. doi: 10.3389/fpls.2019.00526

Tatematsu, K., Kumagai, S., Muto, H., Sato, A., Watahiki, M. K., Harper, R. M., et al. (2004). MASSUGU2 encodes Aux/IAA19, an auxin-regulated protein that functions together with the transcriptional activator NPH4/ARF7 to regulate differential growth responses of hypocotyl and formation of lateral roots in arabidopsis thaliana. *Plant Cell.* 16 (2), 379–393. doi: 10.1105/tpc.018630

Thapa, S. P., Pattathil, S., Hahn, M. G., Jacques, M.-A., Gilbertson, R. L., and Coaker, G. (2017). Genomic analysis of clavibacter michiganensis reveals insight into virulence strategies and genetic diversity of a gram-positive bacterial pathogen. *Mol. Plant-Microbe Interactions®* 30 (10), 786–802. doi: 10.1094/MPMI-06-17-0146-R

Thomazella, D. P. D. T., Seong, K., Mackelprang, R., Dahlbeck, D., Geng, Y., Gill, U. S., et al. (2021). Loss of function of a DMR6 ortholog in tomato confers broad-spectrum disease resistance. *Proc. Natl. Acad. Sci.* 118 (27), e2026152118. doi: 10.1073/pnas.2026152118

van Damme, M., Huibers, R. P., Elberse, J., and Van den Ackerveken, G. (2008). Arabidopsis DMR6 encodes a putative 2OG-Fe(II) oxygenase that is defense-associated but required for susceptibility to downy mildew. *Plant J.* 54 (5), 785–793. doi: 10.1111/j.1365-313X.2008.03427.x

van Schie, C. C., and Takken, F. L. (2014). Susceptibility genes 101: how to be a good host. *Annu. Rev. Phytopathol.* 52, 551–581. doi: 10.1146/annurev-phyto-102313-045854

Wang, D., Pajerowska-Mukhtar, K., Culler, A. H., and Dong, X. (2007). Salicylic acid inhibits pathogen growth in plants through repression of the auxin signaling pathway. *Curr. Biol.* 17 (20), 1784–1790. doi: 10.1016/j.cub.2007.09.025

Xian, L., Yu, G., Wei, Y., Rufian, J. S., Li, Y., Zhuang, H., et al. (2020). A bacterial effector protein hijacks plant metabolism to support pathogen nutrition. *Cell Host Microbe* 28 (4), 548–57.e7. doi: 10.1016/j.chom.2020.07.003

Yokotani, N., Hasegawa, Y., Sato, M., Hirakawa, H., Kouzai, Y., Nishizawa, Y., et al. (2021). Transcriptome analysis of clavibacter michiganensis subsp. michiganensis-infected tomatoes: a role of salicylic acid in the host response. *BMC Plant Biol.* 21 (1). doi: 10.1186/s12870-021-03251-8

frontiers | Frontiers in Plant Science

TYPE Original Research
PUBLISHED 02 June 2023
DOI 10.3389/fpls.2023.1155341

OPEN ACCESS

EDITED BY
Michelle Teresa Hulin,
The Sainsbury Laboratory, United Kingdom

REVIEWED BY
David J. Studholme,
University of Exeter, United Kingdom
Manoj Choudhary,
University of Florida, United States
Ziyue Zeng,
National Institute of Agricultural Botany (NIAB), United Kingdom

*CORRESPONDENCE
Tal Pupko
talp@tauex.tau.ac.il

RECEIVED 31 January 2023
ACCEPTED 10 May 2023
PUBLISHED 02 June 2023

CITATION
Wagner N, Ben-Meir D, Teper D and Pupko T (2023) Complete genome sequence of an Israeli isolate of *Xanthomonas hortorum* pv. pelargonii strain 305 and novel type III effectors identified in *Xanthomonas*. *Front. Plant Sci.* 14:1155341. doi: 10.3389/fpls.2023.1155341

Complete genome sequence of an Israeli isolate of *Xanthomonas hortorum* pv. pelargonii strain 305 and novel type III effectors identified in *Xanthomonas*

Naama Wagner[1], Daniella Ben-Meir[1], Doron Teper[2] and Tal Pupko[1]*

[1]The Shmunis School of Biomedicine and Cancer Research, George S. Wise Faculty of Life Sciences, Tel Aviv University, Tel Aviv, Israel, [2]Department of Plant Pathology and Weed Research, Institute of Plant Protection Agricultural Research Organization (ARO), Volcani Institute, Rishon LeZion, Israel

Xanthomonas hortorum pv. pelargonii is the causative agent of bacterial blight in geranium ornamental plants, the most threatening bacterial disease of this plant worldwide. *Xanthomonas fragariae* is the causative agent of angular leaf spot in strawberries, where it poses a significant threat to the strawberry industry. Both pathogens rely on the type III secretion system and the translocation of effector proteins into the plant cells for their pathogenicity. Effectidor is a freely available web server we have previously developed for the prediction of type III effectors in bacterial genomes. Following a complete genome sequencing and assembly of an Israeli isolate of *Xanthomonas hortorum* pv. pelargonii - strain 305, we used Effectidor to predict effector encoding genes both in this newly sequenced genome, and in *X. fragariae* strain Fap21, and validated its predictions experimentally. Four and two genes in *X. hortorum* and *X. fragariae*, respectively, contained an active translocation signal that allowed the translocation of the reporter AvrBs2 that induced the hypersensitive response in pepper leaves, and are thus considered validated novel effectors. These newly validated effectors are XopBB, XopBC, XopBD, XopBE, XopBF, and XopBG.

KEYWORDS

Xanthomonas, type-III secretion system, Effector proteins, type-III effectors, machine learning, Effectidor

1 Introduction

The *Xanthomonas* genus includes dozens of species divided to thousands of subspecies and strains with a wide range of lifestyles: from commensal, to opportunistic, to pathogenic. Among them are some of the major plant pathogens worldwide, affecting more than 400 plant species (Timilsina et al., 2020). These pathogens rely on the type III secretion system (T3SS) and type III effectors (T3Es) for their pathogenicity. The effectors

alter processes within the host cell for the benefit of the bacteria and thus promote disease in the plant (White et al., 2009; Ryan et al., 2011; An et al., 2019). Identification of the full effector repertoire encoded within the genome of a pathogenic bacterium is a prerequisite for detailed understanding of the molecular interactions between the pathogen and its host.

Discovering novel effectors is a challenging task, as effectors are highly diverse in their functionality, size, and structure. Moreover, the effector repertoire varies even among closely related strains (Jalan et al., 2013; Jiménez-Guerrero et al., 2020). The T3SS recognizes T3Es based on a secretion signal located in their N-terminus (Michiels and Cornelis, 1991; Sory and Cornelis, 1994). However, despite extensive efforts to characterize it, the secretion signal of T3Es is not characterized enough to allow accurate prediction of effectors as a sole feature (Wagner et al., 2022a). We have previously developed and applied machine-learning techniques to identify T3Es and type IVb effectors in various pathogenic bacteria (Burstein et al., 2009; Lifshitz et al., 2013; Lifshitz et al., 2014; Burstein et al., 2015; Burstein et al., 2016; Teper et al., 2016; Nissan et al., 2018; Jiménez-Guerrero et al., 2020; Ruano-Gallego et al., 2021). Following these efforts, we developed Effectidor: an automated machine-learning based web server for the prediction of T3Es (Wagner et al., 2022b). Effectidor combines dozens of different features to achieve accurate classification, e.g., sequence similarity to previously validated effectors, sequence similarity to host proteins, and atypical GC-content. Another feature is the sequence similarity to closely related bacteria without T3SS (putative effectors are expected not to have strong hits when searching against such genomes). Additional features that we consider are the amino acid composition, the genomic organization (effectors often reside close to each other in the genome), existence of known regulatory elements that are recognized by transcriptional regulators that regulate the T3SS and some of the T3Es, such as the plant-inducible promoter (PIP)-BOX (Cunnac et al., 2004; Koebnik et al., 2006), and a signal score reflecting the likelihood of the existence of a secretion signal in the 100 N-terminal amino-acids of the protein (Wagner et al., 2022a). Using these features, Effectidor trains a machine-learning classifier on the known effectors and non-effectors of the specific bacterial genome it analyzes, and outputs a prediction for all the other protein coding genes in the genome, reflecting their likelihood to encode an effector. Thus, we can pinpoint the T3Es candidates in the genome with no need for labor and cost intensive full-genomic screening. In this work we applied Effectidor to two *Xanthomonas* pathogens: *Xanthomonas fragariae*, the causative agent of angular leaf spot (ALS) in strawberries, and *X. hortorum* pv. pelargonii, the causative agent of bacterial blight in geranium.

The pathogen *X. fragariae* (Xfrg) was first reported in Minnesota, the United States in 1960 (Kennedy and King, 1962), and since then it has spread worldwide (Mazzucchi et al., 1973; McGechan and Fahy, 1976; Gubler et al., 2007; Matthews-Berry and Reed, 2009; Fernández-Pavía et al., 2014; Kamangar et al., 2017; Wu et al., 2020; Song et al., 2021). This bacterium is a quarantine pathogen in Europe and it is currently widely spread in North America, where it causes substantial loss in the strawberry nursery industry (Puławska et al., 2020). In severe cases of the disease the crop production is significantly reduced either due to death of the plant or due to changes in the appearance of the fruit, which make them unmarketable. Yet, the most severe economic threat is to nurseries, where the bacteria spread easily. Currently there are neither resistant strawberry plants, nor effective treatments against the pathogen (Wang et al., 2018).

The bacterium *X. hortorum* pv. pelargonii (Xhp) is the causal agent of bacterial blight in geranium ornamental plants (also known by the name "pelargonium"). This is the most threatening bacterial disease of these plants worldwide (Barel et al., 2015; Balaž et al., 2016). The disease is widespread in various states of the USA, Europe, Australia and Israel, and may cause heavy economic losses. Warm and wet conditions favor infection and disease development. Normally, Xhp penetrates the plant *via* natural openings or wounds, and spreads systemically through the vascular system. Symptoms are characterized by wilting of the plant, localized water-soaked lesions that often become necrotic and rotted cuttings. All commercial cultivars of geranium are susceptible to Xhp (Zhang et al., 2009).

In this work, we aimed to discover new T3Es in these two pathogens. We first sequenced the genome of an Israeli isolate of Xhp, combining short and long reads to obtain high quality genome sequence. Next, we applied Effectidor (Wagner et al., 2022a; Wagner et al., 2022b; Wagner et al., 2022c) to predict T3Es in these two genomes. Our results suggested the existence of unknown T3Es in both genomes, i.e., putative T3Es without significant sequence similarity to previously identified effectors. We next experimentally validated the translocation of some of these putative T3Es in a T3SS mediated manner. We validated two and four novel T3Es in Xfrg and Xhp, respectively.

2 Materials and methods

2.1 Bacterial strains and plant material

The bacterium *X. hortorum* pv. pelargonii (Xhp) strain 305 was isolated from geranium plants in Israel and was a gift from Dr. Shulamit Manulis-Sasson from the Agricultural Research Organization (ARO), Volcani Center Israel (Barel et al., 2015). Genomic DNA of *X. fragariae* (Xfrg) Fap21 (BioSamble SAMN05505397) (Henry and Leveau, 2016) was kindly provided by Dr. Joël Pothier (Zurich University of Applied Sciences). For the translocation assays, we used *X. euvesicatoria* (Xeu) *hrpG* ΔavrBs2* (Roden et al., 2004). For cloning, we used NEB 5-alpha *Escherichia coli* that were obtained from New England Bio-Labs inc.

Strains of *E. coli* and *Xanthomonas* were grown in Luria–Bertani (LB), broth or agar, at 37°C and 28°C, respectively. The antibiotics used were spectinomycin (Sp; 100 μg/ml), kanamycin (Kan; 50 μg/ml) and gentamicin (Gm; 10 μg/ml). All antibiotics were from Sigma-Aldrich.

Pepper plants (*Capsicum annuum*) ECW20R (Kearney and Staskawicz, 1990) were grown in the greenhouse at 25°C and kept in long-day conditions (16 h light, 8 h dark).

2.2 Genome sequencing of *X. hortorum* pv. pelargonii 305

Genomic DNA of Xhp305 was isolated from 3 ml of overnight culture using Wizard® Genomic DNA Purification Kit – Promega. Microbial *De novo* sequencing was performed at Novogene Co., Ltd. using both PacBio (PacBio Sequel II) and Illumina (NovaSeq 6000) platforms. The shotgun genomic library for short-read sequencing and the library for long-read sequencing were prepared by the service provider, who also performed quality control. The Illumina sequencing yielded 17,914,078 paired-end reads of length 150 bp. The PacBio sequencing yielded, after trimming, 245,660 subreads, with mean length of 11,006 bp, N50 of 13,343 bp, for a total of 2,704 Mbp.

2.2.1 Genome assembly and annotation

For *de novo* assembly, the whole set of PacBio subreads was used as input for Canu v2.2 (Koren et al., 2017) with the following parameters: -pacbio-raw genomeSize = 5.6m. The average coverage was assessed by mapping corrected and trimmed reads obtained by Canu v2.2 against the assembly using BWA v0.7.17 (Li and Durbin, 2009) with default parameter values, calculating the alignment depth using SAMtools v1.3.3 (Li et al., 2009) with default parameter values, and the average depth per molecule using awk. We then used the draft genome and the corrected PacBio reads as input for Circlator (Hunt et al., 2015), together with BWA v0.7.17 (Li and Durbin, 2009), prodigal v2.6.3 (Hyatt et al., 2010), SAMtools v1.3.3 (Li et al., 2009), MUMmer v3.23 (Kurtz et al., 2004), and Canu v2.2 (Koren et al., 2017) to circularize the chromosome and plasmids, with the following parameters: circlator all –assembler canu. Following this step, we used the Illumina reads to polish the assembly using Pilon v1.22 (Walker et al., 2014), BWA v0.7.17 (Li and Durbin, 2009) and SAMtools v1.3.3 (Li et al., 2009) with the default parameter values and including –changes to keep track of the corrections done in the assembly. We applied three rounds of polishing using Pilon, until no further corrections were introduced in the fourth round. The average coverage of the Illumina reads was assessed in the same manner as assessed for the PacBio reads. For genome annotation, we used Prokka v1.13.3 (Seemann, 2014) with default parameter values.

2.3 Effectors prediction

Effectidor v1.04 (Wagner et al., 2022b) was used for T3Es predictions in each of the two genomes. The pipeline within Effectidor is divided into the following steps: (1) Defining the positive T3Es in the input genome either based on the input supplied by the user or based on homology to previously validated T3Es from various strains (this dataset can be viewed and downloaded from https://effectidor.tau.ac.il/data.html. For the analysis done in this work, version 1.04 was used). The homology criteria are E-values smaller than 10^{-10} and at least 70% identical matches. If less than five effectors are identified based on this cutoff, the last criterion is reduced by 10 (i.e., 60% identical matches are required instead of 70%) until a minimum of 40% identical matches; (2) Defining the negative set (i.e., non T3Es encoded in the input genome) based on homology to proteins of *E. coli* K12 MG1655 (accession GCF_000005845.2); (3) Feature extraction. The features used in Effectidor vary based on the provided input. While the only mandatory input in Effectidor is a FASTA file containing all the ORFs records in the genome, additional inputs allow extraction of features outside the gene sequence alone. In our analysis we provided the following additional inputs, available in the advanced options of Effectidor: (3.1) GFF file, which holds information about the location of all the genes in the genome and allows Effectidor to extract genome organization features; (3.2) FASTA file of the full genome, which allows, together with the GFF file, to search for the PIP-box regulatory element in the promoters of the genes; (3.3) ZIP archive with FASTA files holding protein records of *Luteimonas* sp. MC1825 (accession GCF_014764385), *Lysobacter capsica* 55 [accession GCF_001442785 (de Bruijn et al., 2015)], *Pseudoxanthomonas suwonensis* J1 [accession GCF_000972865 (Hou et al., 2015)], *Stenotrophomonas maltophilia* K279a [accession GCF_000072485 (Crossman et al., 2008)], and *Xylella fastidiosa* 9a5c [accession GCF_000006725 (Simpson et al., 2000; Marques et al., 2001)] that were used as input for the proteomes of closely related bacteria without T3SS. This input allows to run homology searches against these proteomes, and the results of these searches often serve as informative features for the machine-learning classifier, as T3Es are not expected to be found in these genomes, whereas many of the non-T3Es – are. In addition to these inputs, we conducted all searches including the optional feature that predicts the presence of the type 3 secretion signal in the protein sequence (Wagner et al., 2022a); (4) Training a machine learning classifier. Following the feature extraction step, several classifiers (i.e., Linear Discriminant Analysis, Naïve Bayes, Support Vector Machine, Logistic Regression, K Nearest Neighbors, and Random Forest) are trained on the labeled data (i.e., T3Es and non-T3Es defined in the first step). The labeled data are split into train and test sets, the classifiers are first trained in cross-validation on the training set (including feature selection) and are finally evaluated on the test set. The evaluation method used in Effectidor is the Area Under the Precision-Recall Curve (AUPRC). The temporary best classifier is defined as the one with the highest AUPRC on the test set. All classifiers are then evaluated according to the following criteria: (4.1) AUPRC measured on the test set is smaller than that achieved by the temporary best classifier by no more than 30%; (4.2) The range of the prediction scores of the genes in the training set is at least 0.75, to ensure that not all samples are classified as negative/positive; (4.3) The AUPRC measured on the train set and on the test set are compared, and the difference must be smaller than 0.25, to reduce chances of overfitting. The classifiers that meet all these criteria, are then merged to form a final voting classifier; (5) Applying the final classifier to identify potential novel T3Es in the genome. The final voting classifier is then applied to produce a score between 0 and 1 for each ORF in the genome. This score reflects the likelihood for this ORF to encode a T3E. Of note, in case all classifiers were dropped for not meeting some of the criteria mentioned in (4.3), the final classifier used to produce these predictions is a vote over all classifiers. In this case a message is

sent to the user of Effectidor. Genomes with a small number of known effectors are more susceptible to it.

2.4 Translocation assay

2.4.1 Plasmid construction

The plasmid pAvrBs2-HR (KanR) containing the Hypersensitive Response (HR) domain of *avrBs2* (amino acids 62–574), fused to an haemagglutinin (HA) tag (Teper et al., 2016), was used as vector for cloning and expression of candidate effector genes. The vector was linearized with XhoI and XbaI restriction enzymes (Thermo Fisher Scientific). The putative T3E genes of Xhp and Xfrg, including 24 bp upstream of their ATG start codon, were PCR amplified (Phusion Hot Start II High-Fidelity DNA Polymerase, Thermo Scientific) from genomic DNA of Xhp305 and XfrgFap21 using gene specific primers (Supplementary Table S1). In most cases the whole candidate gene was amplified, but in two cases, (PML25_02815 and PML25_02835) where the suspected gene was extremely long (> 3,000 bp), only the first ~600 bp were amplified. PCR products were purified and assembled (Gibson Assembly® Cloning Kit, NEB) into the linearized pAvrBs2-HR vector, upstream to the HR domain, according to the manufacturer directions. Assembly products were initially transformed into NEB 5-alpha competent *E. coli* according to the kit's instructions and grown on LB-Kan plates. The plasmids were then mobilized into Xeu *hrpG*ΔavrBs2* that constitutively expresses the T3S apparatus and contains a mutation in the *avrBs2* gene, by using pRK2013 as a helper plasmid in triparental mating, as previously described (Figurski and Helinski, 1979). Conjugants were selected on LB-Kan-Gm plates. Presence of the recombinant plasmid was verified in each conjugated recipient by colony PCR using insert specific primers and by Sanger sequencing using the same primers.

2.4.2 Translocation

For translocation assays (Roden et al., 2004), overnight bacterial cultures were suspended in 10 mM $MgCl_2$ at an optical density of 0.1 (at 600 nm) and infiltrated into the leaves of 7-week-old ECW20R (carrying the Bs2 gene) pepper using a needleless syringe. Elicitation of HR was monitored at 36 h post-inoculation. For visualization of cell death, leaves were harvested and soaked for 24 h in a bleaching solution (40% ethanol, 40% chloroform, 10% acetic acid), and then transferred to a recovery solution (40% glycerol, 10% ethanol). For each translocation assay, three leaves of at least three pepper plants were infiltrated. Experiments were repeated three times with similar results.

3 Results

3.1 Genome assembly of *X. hortorum* pv. pelargonii strain 305

The genome assembly of Xhp305 was carried out using both long (PacBio Sequel II) and short (Illumina NovaSeq 6000) reads. Using the long reads of PacBio we could close the circular genome, and the short Illumina reads were used to polish the assembly. The assembly resulted with three circular molecules: a chromosome of 5,216,813 bp, and two plasmids of 188,317 bp, and 51,091 bp, with average coverage of 36X, 35X, and 54X, respectively. The assembly polishing using the Illumina reads resulted with a few corrections in the chromosome and in the smaller plasmid. The average coverage of the assembly measured by mapping the Illumina reads was 454X, 467X, and 1,674X for the chromosome and plasmids, respectively. The coverage of the plasmids relative to the chromosome, measured both using the PacBio and the Illumina reads, suggests that the larger plasmid has a copy number of one, while the copy number of the smaller plasmid is either two or three, depending on the coverage of the PacBio versus Illumina, respectively. The average GC content of the chromosome is 0.64, while the average GC contents of the larger and smaller plasmids are 0.59 and 0.62, respectively. The chromosome and plasmids hold 4,357, 191, and 62 coding sequences, respectively. Genome assembly features are available in Table 1. The sequencing data and assembled genome were deposited to NCBI and can be found in BioProject PRJNA926924. The annotation available in NCBI was done using the internal PGAP annotation pipeline of NCBI. It differs from the annotation we obtained using Prokka, mainly in the prediction of translation start sites. The genomic features estimated here are based on the Prokka annotation. Our downstream analysis was done using Prokka annotation, and this annotation is available in the supplementary data.

3.1.1 Detection of recent transposon duplication

Interestingly, an identical DNA segment of 11,818 bp, containing ten ORFs (see Supplementary Table S2), was found both on the chromosome and on the smaller plasmid. This segment is identical by DNA sequence based on the PacBio assembly, and no corrections were introduced within it using the Illumina reads mapping. Based on Prokka annotation, the first and last ORFs in this segment encode for two DNA transposases (IS3 family transposase ISMex7 and Tn3 family transposase ISPa43), which explains this duplication (termed transposon from now on). In

TABLE 1 Features of the assembled Xhp305 genome following sequencing with PacBio and Illumina, assembly with Canu, polish with Pilon, and annotation with Prokka.

Feature	Chromosome	plasmid1	plasmid2
Size (bp)	5,216,813	188,317	51,091
No. of circular contigs	1	1	1
No. of CDSs	4,357	191	62
G+C content (%)	63.8	58.8	62.1
Pac-bio average coverage	36X	35X	54X
Illumina average coverage	454X	467X	1,674X
No. of tRNA genes	54	1	0
No. of T3Es (+ No. of T3Es that were validated here)	35(+4)	0	1(+1)

FIGURE 1
Gene order on the transposon found both on the chromosome and plasmid of Xhp305. The locus tags above represent ORFs on the plasmid, and below represent ORFs on the chromosome. ELAGFFLI_02299/ELAGFFLI_04662 was validated here as a T3E, named XopBB.

order to verify the location of the two identical transposons (one chromosomal and one on the plasmid) we performed several PCR reactions on the total DNA prep we had previously sent for sequencing: Primers were designed to produce ~900 bp products covering the junction points between the chromosome/transposon or the plasmid/transposon (see primers table in the supplementary data), assuming that no product would be obtained in the plasmid/transposon combination if the transposon only existed on the chromosome and vice versa. Results of the PCR reaction (Figure S1) clearly show that the identical transposon can be found both on the chromosome and on the plasmid. The PCR products were Sanger-sequenced and found to be identical to the sequences of their respective source; chromosome or plasmid. The lack of point mutations between the two copies of the transposon indicates that the duplication event was very recent, on an evolutionary scale. A BLASTn search of the two transposases at the edges of this transposon, yielded identical hits to the chromosome of other Xhp strains. This suggests that the transposon was originally on the chromosome and was then duplicated to the plasmid of Xhp305. Among the ten ORFs found on the transposon we identified two T3Es, HopBB1 and XopBB. The latter was validated here (see below). Other than the T3Es and the transposases, according to Prokka annotation, it also holds a chromosome partition protein SMC (Strunnikov, 2006), a DNA replication and repair protein, and a HTH-type transcriptional regulator HmrR, which stands for heavy metal-responsive regulator. The order and location in the genome of the ORFs on this segment is illustrated in Figure 1.

3.1.2 T3SS and T3Es genes on the genome

The Xhp305 genome possesses a full hrp2 class T3SS on the chromosome, but some of these genes are with a low percentage of identical matches to the respective *X. campestris* pv. campestris (Xcc) hrp2 genes that were used as reference. Specifically, ELAGFFLI_00568 (PML25_02850) has only 35% identity with Xcc HrpE (AAM40519), and ELAGFFLI_00569 (PML25_02855) has only 45% identity with Xcc HrpD6 (AAM40520). The genes order is the same as in the reference T3SS cluster from Xcc. Figure 2 shows the cluster of T3SS genes, adjacent T3E genes and harpins (Choi et al., 2013). Other than the two T3Es on the transposon, all the other T3Es found in this genome are on the chromosome.

3.1.3 Xhp305 genome compared to other *Xanthomonas hortorum* genomes

To compare the genome of Xhp305 with other *Xanthomonas hortorum* (Xh) genomes, we downloaded all the fully sequenced genomes of Xh available in NCBI on January 10th 2023, and used them, together with our genome of Xhp305, as well as Xfrg genome, as input for M1CR0B1AL1Z3R (Avram et al., 2019). M1CR0B1AL1Z3R is a web server for the analysis of large-scale microbial genomics data. We used default parameter values with the following changes: Maximal e-value cutoff of 10^{-4}, Xfrg genome as an outgroup for the phylogeny reconstruction, and bootstrap over the species tree. The following genomes of Xh were analyzed: (1) Xh strain VT106 (accession GCF_008728175); (2) Xh pv. vitians LM16734 [accession GCF_014338485 (Morinière et al., 2021)]; (3) Xh pv. vitians strain CFBP498 (accession GCF_903978195 (Dia et al., 2020)); (4) Xh strain Oregano108 (accession GCF_026651895); (5) Xh strain jj2001 [accession GCF_024339125); (6) Xh pv. gardneri strain JS749-3 [accession

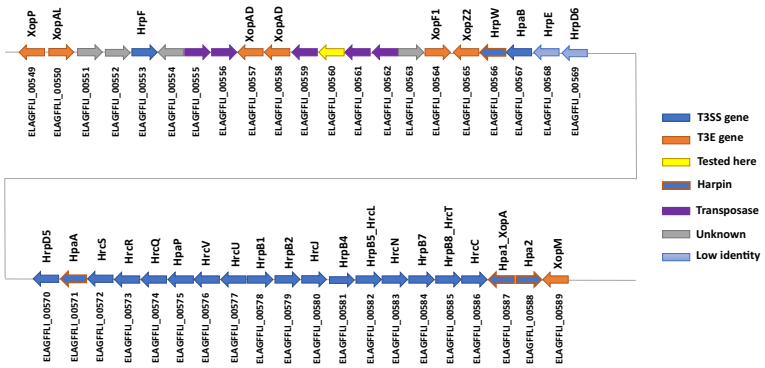

FIGURE 2
Illustration of the gene order of the hrp2 cluster and adjacent T3E genes on the chromosome of Xhp305. In blue are the hrp2 genes. In light blue are genes with low sequence similarity (less than 50% identity) to the respective hrp2 gene of Xcc. In orange are T3E genes, while genes with orange frame and blue filling are harpins. In yellow is a gene that was tested here for translocation and was not translocated.

GCF_001908755 (Richard et al., 2017)]; (7) Xh pv. gardneri strain ICMP7383 [accession GCF_001908775 (Richard et al., 2017)]; (8) Xh pv. gardneri strain CFBP8129 [accession GCF_903978225 (Dia et al., 2020)]; and (9) Xh strain B07-007 (accession GCF_002285515). The following Xhp, other than Xhp305, were also included in the analysis: (1) Xhp strain OSU778 (accession GCA_025452115); (2) Xhp strain OSU498 (accession GCA_024498995); and (3) Xhp strain OSU493 (accession GCF_024499015). Together with the strains studied here, Xhp305 and Xfrg, a total of 14 strains were used in this analysis.

Using a minimum identity score of 80%, M1CR0B1AL1Z3R found 5,983 orthologous groups among these 14 genomes. Figure S2 summarizes the frequencies of the orthologous groups' sizes. As can be seen in this figure, of these 5,983 groups, 2,350 groups included genes shared by all genomes, thus defining the core genome. Using this core genome, M1CR0B1AL1Z3R reconstructed the phylogenetic tree (Figure 3). Based on this tree, we infer that the Israeli isolate, Xhp305, is evolutionary close to Xhp strain OSU778, isolated from a geranium leaf sample in the USA in 2012.

In addition to the phylogeny, the average GC-content of the ORFs in the genomes was evaluated and compared between all the genomes. While the GC content measured for the ORFs of Xfrg was lower than that of *X. hortorum* genomes, with an average of 0.628, the GC content measured for Xhp genomes was the highest, ranging between 0.643 and 0.645, and the GC content measured for the ORFs of Xhp305 was slightly lower with an average of 0.641 (Figure 4).

A similar analysis using M1CR0B1AL1Z3R was conducted to compare the plasmids of Xhp305 with the plasmids of other *X. hortorum* genomes. Apart from Xhp305, out of the 12 *X. hortorum* genomes (including three Xhp genomes and 9 *X. hortorum* genomes of other pathovars, as listed above), 11 had plasmids and thus were included in this analysis. The *X. hortorum* strain jj2001 was the only genome without plasmids and was therefore excluded from this analysis. Each of the other genomes had between one and three plasmids. Interestingly, only 5% of the genes found on the larger plasmid of Xhp strain 305 had putative orthologous genes on other pelargonii strains. In fact, most of the genes on the larger plasmid had orthologs on plasmids of other *X. hortorum* variants (other than the pelargonii pathovar). Our observation suggests that this plasmid was acquired by Xhp305 from another pathovar. In contrast, only 50% of the genes on the smaller plasmid had orthologs on plasmids of other *X. hortorum* genomes.

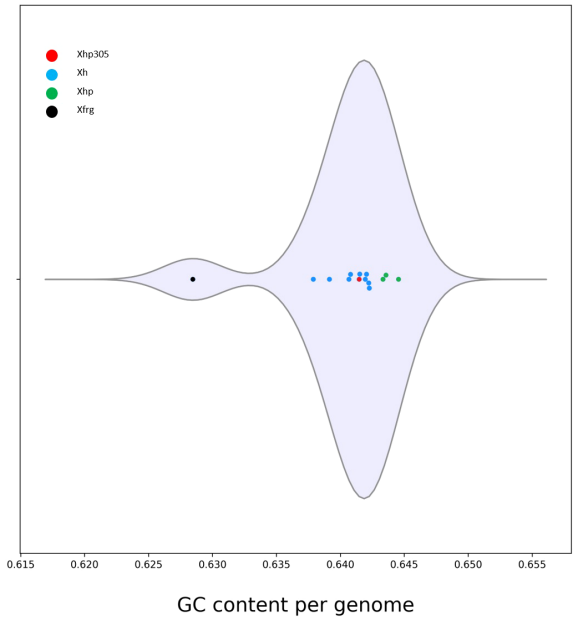

FIGURE 4
Distribution of the GC content per genome measured by M1CR0B1AL1Z3R, for Xanthomonas hortorum, Xhp305, and Xfrg. The distribution is presented in a violin plot.

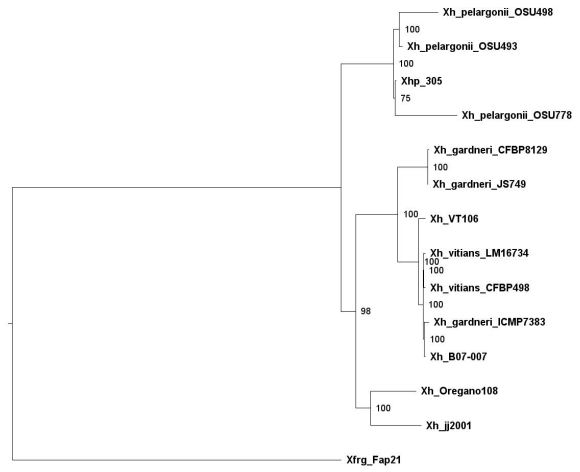

FIGURE 3
Phylogenetic tree of *Xanthomonas hortorum*, Xhp305, and Xfrg, reconstructed by M1CR0B1AL1Z3R based on the core genome of these strains.

3.2 Effectidor predictions

Before running a machine-learning model, Effectidor searches for ORFs with significant sequence similarity to a database of previously validated T3Es from a large set of organisms (see Methods section 2.3). Another option is to provide a list of positives (i.e., known T3Es) as input, in addition or instead of the internal homology search. This list of positives, if supplied, should be in a FASTA format. For the analysis of Xfrg we chose to supply a list of positives instead of the internal search, as the built-in homology search resulted with only half of the known T3Es in this strain, due to high percentage of identity cutoff (70%) that led to missing some of the more distant homologs. The list of positives to consider was supplied by Dr. Doron Teper, accounting for sequence similarity to previously validated effectors from *Xanthomonas*, *Pseudomonas syringae*, *Ralstonia solanacearum*, *Acidovorax*, and *Pantoea* sp., sharing identity lower than 70%, as T3Es. While Effectidor can still build a classifier based on a partial effector list,

providing the full list of T3Es is preferable for better representation of the T3Es genomic organization, providing larger training set, and thus for more accurate predictions. For Xfrg this list of positives included 47 T3Es (Table 2). For Xhp305, Effectidor was executed without providing a list of positives, and in its internal homology search, it yielded 36 T3Es, which we consider as positive samples for training the machine-learning algorithm (Table 2).

In the next step within Effectidor, a machine-learning classifier was trained on the known T3Es found in the first step. Based on the trained classifiers, other than homology to effectors, among the ten most important features we used in these analyses were amino acid similarity to effectors vs. to non-effectors (Figures 5A2, 5B2), and score of the secretion signal in the N-terminal region (Wagner et al., 2022a) with 24 and 41 T3Es out of 36 and 47 in Xhp305 and Xfrg, respectively, with a signal score higher than 0.5 (Figures 5A1, 5B1). Homology to proteins of closely related bacteria without the T3SS was also important with only one and two T3Es in Xfrg and Xhp, respectively, which show high similarity to some of their proteins (Figures 5A3, 5B3). Specifically, the protein encoded by BER92_03985 of Xfrg showed sequence similarity to OtsA of *Stenotrophomonas* and *Pseudoxanthomonas*, the protein encoded by ELAGFFLI_03189 (PML25_15775 + 141bp upstream) of Xhp showed sequence similarity to WQ53_RS02800, glycoside hydrolase family 30 protein of *Pseudoxanthomonas*, and the protein encoded by ELAGFFLI_01251 (PML25_06220) of Xhp showed sequence similarity to OtsA of *Stenotrophomonas* from *Luteimonas* and *Pseudoxanthomonas*. The genomic organization of T3Es and specifically the distance to the closest known T3E on the genome was the next contributing feature, with 28 and 23 T3Es in Xfrg and Xhp, respectively, which were less than 15 ORFs away from a known effector on the genome (Figures 5A4, 5B4). In Xfrg the PIP-box was also important for the prediction, with 14 of the T3Es with a complete PIP-box (Figure 5B5), while in Xhp the GC-content was more important than the PIP-box for the predictions (Figure 5A5). Figure 5 shows the distribution of these features' values among T3Es and non-T3Es in Xhp305 and Xfrg.

Following the training step, the trained classifier was applied to the remaining genes in the given genome, to yield prediction scores, reflecting the likelihood of each of the genes to encode a T3E. This step yielded several high-scoring predictions in each genome (Tables 3, 4). The features of these highly ranked genes reveal that most of them have a high secretion signal score predicted for the N-terminal region of the protein sequence. Many of them have a perfect or nearly perfect PIP-box in their promoter. In addition, some of them show sequence similarity to known T3Es, or reside in proximity to other T3Es on the genome (Tables 3, 4). Of note, the sequence similarity to known effector, when present, was not high enough for these putative T3Es to be considered positive in the previous step, i.e., the identity percentage was less than 70%.

Out of the above predictions, several candidates were chosen for experimental validation. Candidates were selected based on predictions rank, lack of significant sequence similarity to known effectors in *Xanthomonas*, and minimal length (peptides smaller than 75 amino acids were ignored). In addition, two proteins that were identified as T3Es based on homology to previously validated T3Es were used as positive controls. Of note, additional putative T3Es that we did not validate exist (see discussion).

3.3 Four Xhp and two Xfrg predicted T3E proteins are translocated into plant cells *via* the T3SS

To examine the translocation of predicted effectors, we utilized a reporter system based on the delivery of a truncated form of the Xeu T3E AvrBs2 (amino acids 62–574) into susceptible plant cells. $AvrBs2_{62-574}$ lacks a translocation signal, but is sufficient to elicit HR in plants expressing the *Bs2* resistance gene (Roden et al., 2004). The deleted translocation signal is supplied (or not) by the cloned candidate effector. The conjugant strains we obtained were tested for elicitation of HR in the pepper line ECW20R, which encodes a functional *Bs2*-resistance gene.

Our results show that the following candidates induced the HR 36 h post infection (Figure 6): Xhp conjugants: ELAGFFLI_04662 (conjugant of PML25_23150+PML25_23155)/ELAGFFLI_02299 (conjugant of PML25_11405+PML25_11410), identical genes on the chromosome and plasmid, respectively, named hereafter XopBB; ELAGFFLI_03194 (PML25_15800 + 60bp upstream), named hereafter XopBC; ELAGFFLI_00506 (PML25_02555 + 252bp upstream), named hereafter XopBD; and ELAGFFLI_01101 (PML25_05510 - 249bp upstream), named hereafter XopBE. Xfrg conjugants: BER92_21920, named XopBF; and BER92_22150, named XopBG.

Of note, the protein encoded by the gene PML25_02815 of Xhp contains 15 conserved SKW repeats, previously described in the effector XopAD of Xeu (Teper et al., 2016). It tested negative in the translocation assay, see discussion.

No HR was observed in leaf areas inoculated with *Xeu* strains expressing the other tested constructs (Tables 3, 4). Xeu expressing ELAGFFLI_00550 (XopAL) and ELAGFFLI_00565 (XopZ2), of the latter we cloned only the first 200 N-terminal amino acids, were tested as positive controls and also induced HR on pepper leaves (Figure 6). The parent strain Xeu *hrpG* ΔavrBs2* expressing the $AvrBs2_{62-574}$::HA fusion ("empty" vector) was tested on the same pepper leaves, as negative control. As expected, this strain did not cause HR. All in all, four out of six Xhp genes and two out of six Xfrg genes we tested encode proteins that elicited HR response in the pepper line ECW20R, which encodes a functional *Bs2* resistance gene (Figure 6). Thus, all six can be defined as novel T3Es.

3.4 Presence of the newly discovered T3E genes in other strains

We next conducted sequence similarity searches to identify the taxonomic distribution of the newly identified T3Es.

The 332 amino acids long XopBB protein from Xhp305 is encoded by two identical genes, on the chromosome and on the smaller plasmid. We searched for homology of XopBB to a list of previously validated T3Es from *Xanthomonas*, *Pseudomonas*

TABLE 2 Known effectors found in (A) Xfrg and (B) Xhp305.

A - Xfrg						B - Xhp			
Locus	Effector family	Score	Locus	Effector family	Score	Locus	NCBI locus	Effector family	Score
BER92_23180	XopP	0.99	BER92_05605	XopAV	0.93	**ELAGFFLI_00550**	**PML25_02765**	**XopAL**	**0.99**
BER92_17495	XopX	0.99	BER92_12855	BapC	0.90	ELAGFFLI_00564	PML25_02830	XopF1	0.99
BER92_23185	XopP	0.99	BER92_12860	Hpa1	0.85	ELAGFFLI_04661	PML25_23145^{-43}	HopBB1	0.99
BER92_17490	XopF	0.99	BER92_17220	HopBL	0.84	ELAGFFLI_02298	PML25_11400^{-82}	HopBB1	0.99
BER92_23190	XopP	0.99	BER92_23165	HopBL	0.83	ELAGFFLI_00094	PML25_00480	XopAI	0.99
BER92_21950	HopBL	0.99	BER92_02515	XopV	0.82	ELAGFFLI_00549	PML25_02760	XopP	0.99
BER92_06295	XopAD	0.99	BER92_12375	HopBL	0.81	**ELAGFFLI_00565**	**PML25_02835**	**XopZ2**	**0.99**
BER92_18835	XopP	0.99	BER92_12940	XopA	0.81	ELAGFFLI_00650	PML25_03270	XopX	0.99
BER92_04220	XopL	0.99	BER92_23140	HopBD	0.81	ELAGFFLI_00589	PML25_02955^{+84}	XopM	0.99
BER92_02460	XopAD	0.99	BER92_03985	RipTPS	0.80	ELAGFFLI_03853	PML25_19105^{+36}	XopE2	0.99
BER92_01070	HopAS1	0.99	BER92_07165	XopM	0.80	ELAGFFLI_03195	PML25_15805^{+16}	XopQ	0.99
BER92_00360	HopBL	0.99				ELAGFFLI_03642	PML25_18040^{ir}	HopAK1	0.98
BER92_03355	XopF	0.99				ELAGFFLI_00566	PML25_02840^{-32}	HrpW	0.98
BER92_23155	XopC	0.99				ELAGFFLI_01371	PML25_06830^{-41}	XopD	0.98
BER92_18830	XopP	0.99				ELAGFFLI_00093	PML25_00475	XopAA	0.98
BER92_12975	XopF	0.99				ELAGFFLI_04247	PML25_21105^{+221}	XopAD	0.98
BER92_23085	XopC	0.99				ELAGFFLI_00302	PML25_01490	XopN	0.98
BER92_15380	XopAE	0.99				ELAGFFLI_00558	PML25_02805^{ir}	XopAD	0.98
BER92_11120	XopAG	0.99				ELAGFFLI_00557	PML25_02805^{ir}	XopAD	0.98
BER92_17775	XopN	0.99				ELAGFFLI_03644	PML25_18045	HopAK1	0.98
BER92_12970	XopZ	0.99				ELAGFFLI_03193	PML25_15795	XopAY	0.98
BER92_05755	XopC	0.99				ELAGFFLI_03199	PML25_15820	XopG	0.97
BER92_16595	XopR	0.99				ELAGFFLI_01370	PML25_06820^{+64}	XopK	0.97
BER92_15420	XopK	0.99				ELAGFFLI_03178	PML25_15720^{+475}	XopAM	0.97
BER92_22830	XopAD	0.99				ELAGFFLI_00588	PML25_02950^{+38}	Hpa2	0.97
BER92_05600	XopQ	0.99				ELAGFFLI_00411	PML25_02035	XopB	0.97
BER92_22580	XopE	0.99				ELAGFFLI_00055	PML25_00280	AvrBs2	0.97
BER92_15425	XopAU	0.99				ELAGFFLI_03189	PML25_15775^{+47}	SrfJ	0.96
BER92_02195	XopAD	0.99				ELAGFFLI_00571	PML25_02865	HpaA	0.96
BER92_18860	XopB	0.98				ELAGFFLI_01251	PML25_06220	RipTPS	0.95
BER92_15435	XopAF	0.98				ELAGFFLI_01852	–	XopAQ	0.89
BER92_14315	XopAM	0.98				ELAGFFLI_00587	PML25_02945^{+42}	XopA	0.75
BER92_22445	HopBL	0.98				ELAGFFLI_00017	PML25_00090^{-23}	AvrRxv	0.71

(Continued)

TABLE 2 Continued

A - Xfrg						B - Xhp			
Locus	Effector family	Score	Locus	Effector family	Score	Locus	NCBI locus	Effector family	Score
BER92_01845	AvrBs2	0.97				ELAGFFLI_00798	PML25_04005^{+6}	PthG	0.70
BER92_21340	HopBL	0.97				ELAGFFLI_02490	PML25_12355	CigR	0.43
BER92_22450	HopBL	0.96				ELAGFFLI_03643	PML25_18040^{ir}	HopAK1	0.39

In bold are positive controls used for the translocation assay. "Score" is the prediction score given by Effectidor, reflecting the likelihood of this gene to encode a T3E. For Xhp305 genes, both Prokka and PGAP (NCBI) annotation locus tags are mentioned. The difference between the two annotations is in superscript, such that (-) and (+) mean the protein is shorter and longer than Prokka annotation, respectively. All these differences are in the N-terminus. Irregular differences ("ir" in superscript): ELAGFFLI_03642 respective PGAP annotation is with a start codon upstream to Prokka annotation and is a pseudogene with a frameshift; ELAGFFLI_00558 and ELAGFFLI_00557 are both part of the respective PGAP annotation; ELAGFFLI_01852 is not found in PGAP annotation; ELAGFFLI_03643 is part of its respective PGAP annotation.

syringae, *Ralstonia solanacearum*, *Acidovorax*, and *Pantoea* sp, supplied by Dr. Doron Teper (available in the supplementary data), using BLASTp. The best hit was to APS58_0178 of *Acidovorax citrulli* M6 that we have previously reported as a putative T3E based on sequence similarity to HopF2 (Jiménez-Guerrero et al., 2020). The alignment between XopBB and APS58_0178 shared 50% identical matches on 70% coverage. In a regular BLASTp search, closer putative homologs were found in *X. hortorum*, *X. campestris*, and *X. hydrangea* (Table 5). All these inferred homologs are annotated as hypothetical proteins.

The Xhp305 T3E XopBC shares some sequence similarity with XopAV (Teper et al., 2016) and XopAY (Yang et al., 2015); The validated XopAV from Xeu is a protein of 165 amino acids. In contrast, XopBC is 249 amino acids long. The pairwise alignment between these two proteins is only between the 49 most N-terminal amino acids of XopBC, and a region near the C-terminus of XopAV, where they share only 50% identity. In contrast, XopBC shares 52% identity over 92% coverage with XopAY, which is encoded by a gene adjacent to the gene encoding for XopBC. We therefore hypothesize that XopBC and XopAY are two paralogs. XopBC was annotated as XopAV in the PGAP annotation of NCBI. Nevertheless, since the sequence similarity observed between XopBC and the validated XopAV is between the N-terminal region of XopBC, which is expected to hold the translocation signal, and the C-terminal region of XopAV, which is expected to hold the active part of the effector, and since both of these effectors were found to encode an active translocation signal which enabled them to be translocated into pepper leaves in the translocation assay, we hypothesize that these are two different effectors, and that XopBC is a newly identified effector. A BLAST search using XopBC as query reveals the presence of putative homologs of this protein in *X. hortorum, X. campestris, X. arboricola*, *X. hydrangea*, and *X. codiaei* (Table 5). These proteins are annotated as XopAV, based on a sequence similarity similar to the one we found between XopBC and XopAV. These proteins share a higher sequence similarity with XopBC than with the validated XopAV from Xeu, and with the

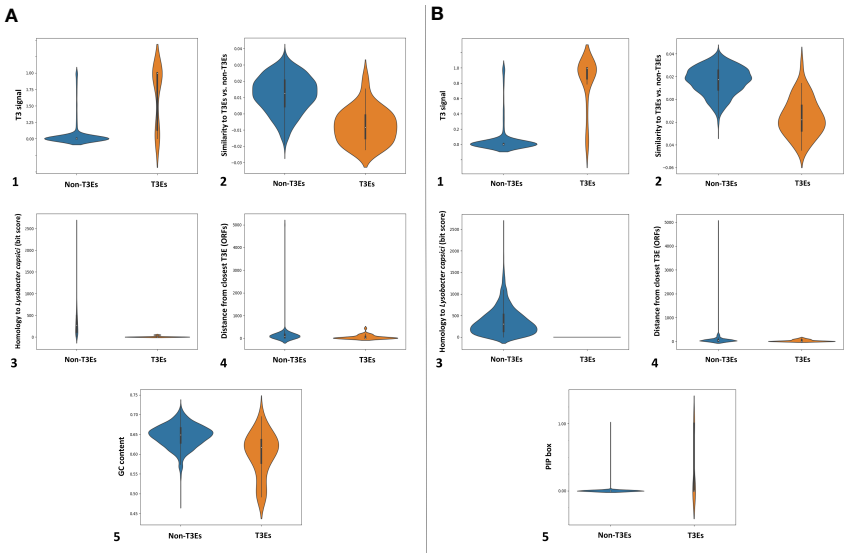

FIGURE 5
Distribution of informative feature values for T3Es and non-T3Es in Xhp305 **(A)** and Xfrg **(B)**, as analyzed by Effectidor. The distributions are presented in violin plots.

TABLE 3 Top T3Es predictions and translocation assay results in Xfrg, with informative features values.

Locus	Score	Protein length	PIP-box	Secretion signal	Distance to closest T3E	Bit score to T3Es (T3E name)	Translocated
BER92_11960	0.83	556	V	0.475	80	214 (NopAC)	not tested
BER92_12965	0.77	371	–	0.997	1	407 (HrpW)	not tested
BER92_02770	0.72	465	V	0.017	50	179 (NopAC)	not tested
BER92_22860	0.61	134	V	0.995	111	0	not tested
BER92_22075	0.58	282	V	0.996	272	0	no
BER92_21920 (XopBF)	**0.57**	**163**	**–**	**0.990**	**18**	**81 (XopAV)**	**yes**
BER92_12945	0.57	311	V	0.065	1	140 (HrpW)	not tested
BER92_12955	0.56	90	–	0.781	3	0	not tested
BER92_22365	0.56	101	–	0.997	48	0	no
BER92_19605	0.56	142	V	0.929	1	0	not tested
BER92_21675	0.55	96	–	0.998	6	0	not tested
BER92_17025	0.54	192	–	0.981	2	0	not tested
BER92_22150 (XopBG)	**0.52**	**158**	**V**	**0.858**	**7**	**0**	**yes**
BER92_18820	0.52	165	V	0.973	2	0	not tested
BER92_18825	0.52	188	–	0.042	1	0	not tested
BER92_02200	0.52	157	–	0.002	1	83 (XopAD)	no
:	:	:	:	:	:	:	:
BER92_19140	0.40	338	–	0.991	51	0	no

PIP-box: "V"-perfect PIP-box is found in the gene promoter; "-"-lack of PIP-box in the gene promoter. Score: a score given by the classifier, reflecting the likelihood of the gene to encode a T3E. Secretion signal: a score reflecting the likelihood of an existence of a type 3 secretion signal within the protein sequence. Distance to closest T3E: number of genes on the genome separating between the given gene and a known T3E. Bit score to T3Es: alignment score of the best sequence similarity found to a known T3E within Effectidor's T3Es database. In bold are the newly identified translocated T3Es.

above results we suggest that they should not be annotated as XopAV, but rather as XopBC.

XopBD of Xhp305 did not have hits to any of the validated T3Es from *Xanthomonas*, *Pseudomonas syringae*, *Ralstonia*, *Acidovorax*, and *Pantoea* sp. It has some sequence similarity (60% identity over 69% coverage) to a protein from *Xanthomonas campestris* pv. raphani 756C, a pathogen of the plant model organism *Arabidopsis thaliana*, which was previously suggested as a T3E candidate XopAT, based on the presence of a PIP box and a −10 box-like sequence upstream of the coding sequence, low GC content, and eukaryotic motifs (Bogdanove et al., 2011). It has not been validated yet, and its function is unknown. ORFs with higher sequence similarity to XopBD were found in *X. hortorum*, *X. arboricola*, *X. cucurbitae*, *X. codiaei*, and *X. campestris* (Table 5). All these putative homologs are annotated as hypothetical proteins.

XopBE of Xhp305 shows distant sequence similarity (47% identity) to XopC1 (Noël et al., 2003). Putative closer homologs were found in *X. hortorum* and Xfrg (Table 5). The proteins found in *X. hortorum* are annotated as hypothetical protein whereas in Xfrg they are annotated as hydrolase-like protein or hypothetical protein.

Multiple sequence alignments (MSAs), of the abovementioned T3Es and their homologs from *Xanthomonas*, produced by Clustal Omega (Sievers and Higgins, 2014; Madeira et al., 2022) using default parameter values, are available in the supplementary data. All the homologs listed in Table 5 and used to produce the MSAs share at least 70% identity and 70% coverage with the respective T3E.

Of the six effector candidates tested in Xfrg, two tested positive in the translocation assay: BER92_21920 (XopBF) and BER92_22150 (XopBG).

XopBF is a hypothetical protein with unknown function. It shares some sequence similarity (identity of ~40%) with the proteins homologous to our newly validated XopBC ("XopAV", see above) of several strains of *Xanthomonas*, among which are: *X. hortorum* (WP_159087131, WP_176339450, WP_180336534, WP_168958006, WP_152025508, WP_268212485), *X. campestris* (WP_228439322, WP_169705357, WP_273676157), *X. arboricola* (WP_212583737, WP_080591365, WP_104562523), *X. oryzae* (WP_019303846, WP_113343065, WP_075244353, WP_044757351, WP_027704160, WP_047339610, WP_041183112, WP_240113023, WP_029217345, WP_113221815, WP_113335989, WP_113000154, WP_069963882), *X. codiaei* (WP_104539725), and *X. prunicola* (WP_101363523). Proteins with higher sequence similarity are

TABLE 4 Top T3Es predictions and translocation assay results in Xhp.

Locus	Score	Protein length	PIP-box	Secretion signal	Distance to closest T3E	Bit score to T3Es (T3E name)	Translocated
ELAGFFLI_02299 ELAGFFLI_04662 (PML25_11405+ PML25_11410/ PML25_23150+ PML25_23155) (XopBB)	**0.98**	**332**	**V**	**0.999**	**1**	**238 (APS58_0178)**	**yes**
ELAGFFLI_00330 (PML25_01630)	0.96	372	V	1.000	28	259 (XopR)	not tested
ELAGFFLI_03194 (PML25_15800^{-20}) (XopBC)	**0.94**	**249**	**V**	**1.000**	**1**	**201 (XopAV)**	**yes**
ELAGFFLI_00560 (PML25_02815)	0.94	990	–	0.041	2	755 (XopAD)	no
ELAGFFLI_00506 (PML25_02555^{-84}) (XopBD)	**0.91**	**304**	**V**	**0.975**	**43**	**225 (XopAT)**	**yes**
ELAGFFLI_01763 (PML25_08750)	0.85	556	V	0.762	88	214 (NopAC)	no
ELAGFFLI_00820 (PML25_04110)	0.70	468	V	0.006	22	181 (NopAC)	not tested
ELAGFFLI_01101 (PML25_05510^{+83}) (XopBE)	**0.64**	**337**	**–**	**0.644**	**149**	**294 (XopC)**	**yes**
ELAGFFLI_04382 (PML25_21815^{-3})	0.57	525	mm	1.000	47	188 (AvrB4-1)	not tested
ELAGFFLI_01276 (PML25_06350)	0.54	251	mm	0.677	25	183 (XopH)	not tested
ELAGFFLI_00092 (PML25_00470^{+91})	0.52	156	–	0.155	1	164 (APS58_0178)	not tested

PIP-box: "V"-perfect PIP-box is found in the gene promoter; "-"-lack of PIP-box in the gene promoter; "mm"-PIP-box with one mismatch is found in the gene promoter. Score: a score given by the classifier, reflecting the likelihood of the gene to encode a T3E. Secretion signal: a score reflecting the likelihood of an existence of a type 3 secretion signal within the protein sequence. Distance to closest T3E: number of genes on the genome separating between the given gene and a known T3E. Bit score to T3Es: alignment score of the best sequence similarity found to a known T3E within Effectidor's T3Es database. In bold are the newly identified translocated T3Es. Both Prokka and PGAP (NCBI) annotation locus tags are mentioned. The difference between the two annotations is in superscript, such that (-) and (+) mean the protein is shorter and longer than Prokka annotation, respectively. All these differences are in the N-terminus. Irregular differences between the two annotations: XopBB, encoded by ELAGFFLI_02299 and ELAGFFLI_04662 on the chromosome and plasmid, respectively, was broken into two ORFs in PGAP annotation, PML25_11405+ PML25_11410/ PML25_23150+ PML25_23155, such that the first ORF in each pair is annotated as a pseudogene lacking a C-terminus. In bold are the newly identified translocated T3Es.

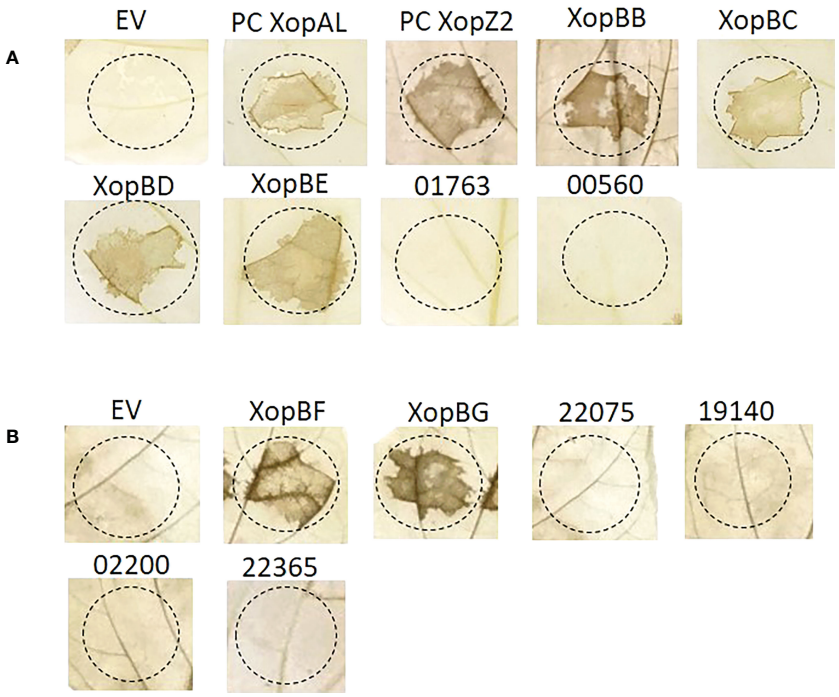

FIGURE 6
Translocation assay for predicted effectors in Xhp **(A)** and Xfrg **(B)**. Xeu hrpG*ΔavrBs2 bacteria were introduced with the indicated putative effectors of Xhp305 and Xfrg, fused to the HR domain of AvrBs2. Overnight cultures were infiltrated into leaves of pepper ECW20R var, which carries the Bs2 resistant gene. Leaves were harvested 48 h later, bleached in a bleaching solution and photographed. EV, empty vector; PC, positive control.

TABLE 5 Presence of the newly discovered T3Es in *Xanthomonas*.

T3E	*X. cucurbitae*	*X. hydrangeae*	*X. arboricola*	*X. campestris*	*X. codiaei*	*X. hortorum*	*X. fragariae*
XopBB	–	WP_232372966	–	WP 256267875 WP_227971037 WP_221284749 WP_228434360 WP_274340180 WP_274508026 WP_164493567 WP_116891014	–	WP 180313544 WP_268215251 WP_268215250 WP 168959150 WP_273664738	–
XopBC	–	WP 210762087 WP_275415019 WP_275415023	WP 080591365 WP 212583737 WP_104562523	WP 273676157 WP_228439322 WP_169705357	WP_104539725	WP_268212485 WP_176339450 WP_168958006 WP_159087131 WP_152025508	–
XopBD	WP_158251449 WP_274396588	–	WP_126750625 WP_153064930	WP_227971169 WP_228878756 WP_139328362 WP_146011555 WP_274340431	WP_146091904	WP_168959089 WP 233366577 WP_251762182	–
XopBE	–	–	–	–	–	WP 168960092 WP_211317318	WP_269122454 WP_208587355 WP_197493698
XopBF	–	–	–	–	–	–	WP_134656590 WP_269125207 WP_159088880
XopBG	–	–	–	–	–	–	WP_159087733 WP_159088353

annotated as hypothetical proteins and are restricted to Xfrg (Table 5).

Finally, the gene product of BER92_22150, XopBG, has various putative homologs, all restricted to sub-strains of Xfrg (Table 5). These are all hypothetical proteins with unknown function. Surprisingly, no homologs were detected in other *Xanthomonas* strains. The only other putative homology found, to some degree (coverage of 99% and identity of 45%), is a hypothetical protein from *Xylophilus ampelinus* (WP_146228602), a grapevines pathogen that encodes a T3SS. This pathogen was previously termed *Xanthomonas ampelina*. It should be noted that this newly identified effector emphasizes the power of Effectidor in discovering novel T3Es without any sequence similarity to known effectors.

4 Discussion

The goal of this work was to identify and validate novel T3Es using the Effectidor web server. We selected two pathogens, Xhp and Xfrg, for which we had DNA samples. These species are not extensively studied, and we thus hypothesized there may be unknown effectors within them. To this end, we first sequenced an Israeli isolate of Xhp – strain 305 and assembled its genome. Analysis of the obtained genome revealed a recently duplicated transposon between the chromosome and the smaller of the two plasmids. Moreover, one of the newly validated T3Es was found on this transposon, both on the chromosome and on the plasmid.

We next applied Effectidor on our newly assembled Xhp305 genome, as well as on Xfrg Fap21 genome, to find putative novel T3Es within them. We tested six candidates in each of these genomes. In Xfrg and Xhp we showed that two of the six and four of six candidates, respectively, were translocated and elicited HR on pepper leaves. Interestingly, one of the two T3Es we validated in Xfrg (XopBG encoded by BER92_22150) was found to be unique to Xfrg and showed no sequence similarity to any of the previously identified T3Es. As XopBG is restricted to Xfrg, it is possible that it plays a significant role in Xfrg pathogenicity and host specificity. It would be interesting to further study its structure and molecular function within its native host.

Effectidor combines dozens of features for the learning and prediction, none of which is capable to fully differentiate between effectors and non-effectors by itself. Among these features are sequence similarity to known T3Es, amino acid composition, proximity to effectors on the genome, existence of regulatory elements such as the PIP-box in the promoter, and prediction of the secretion signal in the N-terminal region. While effectors tend to cluster together on the genome in pathogenicity islands (Marcelletti and Scortichini, 2015), with ~60% of the T3Es residing in proximity of up to 15 ORFs from another T3E, there are also non-effectors in proximity to known T3Es. Thus, predictions based on proximity alone will miss some T3Es and will yield many false positives. Similarly, the PIP-box was found to be the regulatory motif to which HrpG/HrpX transcription regulators bind to regulate the expression of the T3SS and effector genes in *Xanthomonas* (Koebnik et al., 2006), yet we found a PIP-box in the promoters

of only 38% of the T3Es, while it was found also in 9% of the non-T3Es. The translocation signal prediction is an informative feature, with 78% of the T3Es with a score higher than 0.5, but some non-T3Es also have a score higher than 0.5. Thus, prediction based on this feature alone will lead to ~20% precision, which is far from optimal. By combining these and additional features in a machine-learning classification algorithm, Effectidor predicts effectors, in a way that could not be achieved by using any of the features separately.

We validated putative effectors using a truncated *avrBs2* reporter gene, which has a functional HR domain but lacks a translocation signal. Candidate genes were cloned upstream to the truncated *avrBs2* domain, assuming that genuine effectors would supply the translocation signal, and thus elicit HR on pepper leaves. Nevertheless, not all T3Es have a strong enough translocation signal and some require the assistance of chaperones for translocation. Furthermore, expressing the candidate on a plasmid, in a strain other than its original strain could mean that these were not the optimal conditions for the effector to be translocated. Thus, a negative result in this assay does not necessarily rule out the possibility that these candidates act as T3Es in the original pathogen they were isolated from. This may be the case with gene ELAGFFLI_00560 of Xhp, which tested negative in the translocation assay. This protein contains 15 conserved SKW repeats, previously described in the effector XopAD of Xeu (Teper et al., 2016). Its predicted secretion signal score based on the annotated ORF was only 0.041. Since the prediction of ORFs occasionally suffers from mis-annotation of the start codon, we cloned this gene from an alternative start codon, 48 bp upstream to the predicted start codon. The predicted secretion signal score of this alternative N-terminus was 0.83. Nevertheless, it was not translocated in our system. This again raises the possibility that ELAGFFLI_00560 requires assistance of a chaperone for translocation, which was absent in the Xeu system under the given conditions.

In this work we tested six candidates of each of the two pathogens, but according to the predictions of Effectidor, additional putative T3Es exist. Candidates for validation in this work were chosen based on prediction score and features such as lack of significant sequence similarity to previously validated T3Es, yet additional ORFs follow this rule. In Tables 3 and 4 are listed putative T3Es that were not tested. These candidates include BER92_11960, BER92_12965, BER92_02770, BER92_22860, BER92_12945, BER92_12955, BER92_19605, BER92_21675, BER92_17025, BER92_18820, and BER92_18825 in Xfrg Fap21, and ELAGFFLI_00330 (putative XopR), ELAGFFLI_00820, ELAGFFLI_04382 (putative XopAH/AvrB), ELAGFFLI_01276 (putative hopD2, based on Prokka annotation), and ELAGFFLI_00092 in Xhp305.

Identifying the T3E repertoire of a bacterial pathogen is a first step towards understanding the pathogen-host interaction at the molecular level. Open questions for further research include: (1) Validating the additional putative T3Es identified by Effectidor in both Xfrg21 and Xhp305; (2) Understanding how the T3Es are regulated within the bacteria; (3) Understanding their secretion signal; (4) Finding whether their translocation depends on specific chaperons; (5) Determining the order of their translocation into the host; (6) Finding their functions within the host cell, which include discovering their interaction with host molecules and among themselves. We hope that computational tools, including machine-learning, in the future, can help accelerate discoveries towards such a detailed understanding of the molecular pathways involved in the pathogenicity.

Data availability statement

The sequencing data and assembled genome were deposited to NCBI and can be found in BioProject PRJNA926924.

Author contributions

NW, DBM, DT and TP conceived the project. DBM prepared Xhp DNA for sequencing and performed all cloning and expression of effector candidates. DBM and DT executed translocation assays. NW assembled Xhp305 genome and performed all computational analysis. NW and DBM wrote the manuscript. All authors contributed to the article and approved the submitted version.

Funding

Israel Science Foundation (ISF) [2818/21 to TP]. NW was supported in part by a fellowship from the Edmond J. Safra Center for Bioinformatics at Tel Aviv University.

Acknowledgments

Israel Science Foundation (ISF) [2818/21 to T.P.]; NW was supported in part by a fellowship from the Edmond J. Safra Center for Bioinformatics at Tel Aviv University; TP's research is supported in part by the Edouard Seroussi Chair for Protein Nanobiotechnology, Tel Aviv University. We thank Dr. Shulamit Manulis and Dr. Joël Pothier who provided us with the Xhp305 bacteria and the Xfrg DNA, respectively. TP would like to thank Prof. Jeff Chang from Oregon State University for hosting him during a sabbatical and for numerous discussions on plant-pathogen interactions.

Conflict of interest

The authors declare that the research was conducted in the absence of any commercial or financial relationships that could be construed as a potential conflict of interest.

Publisher's note

Supplementary material

The Supplementary Material for this article can be found online at: https://www.frontiersin.org/articles/10.3389/fpls.2023.1155341/full#supplementary-material

SUPPLEMENTARY FIGURE 1

Transposon verification by PCR. PCR primers: (1) chromosome F/transposon R, (2) transposon F/chromosome R, (3) plasmid F/transposon R, (4) transposon F/plasmid R, (5) Control: primers from within the transposon, (6) Control – no template.

SUPPLEMENTARY FIGURE 2

Orthologous genes group size distribution, among the 13 *X. hortorum* genomes and the Xfrg genome, as found by M1CR0B1AL1Z3R. Group of size k means the ortholog was found in k of the 14 genomes. This figure is an output of M1CR0B1AL1Z3R.

References

An, S. Q., Potnis, N., Dow, M., Vorhölter, F. J., He, Y. Q., Becker, A., et al. (2019). Mechanistic insights into host adaptation, virulence and epidemiology of the phytopathogen *Xanthomonas*. *FEMS Microbiol. Rev.* 44, 1–32. doi: 10.1093/femsre/fuz024

Avram, O., Rapoport, D., Portugez, S., and Pupko, T. (2019). M1CR0B1AL1Z3R–a user-friendly web server for the analysis of large-scale microbial genomics data. *Nucleic Acids Res.* 47, W88–W92. doi: 10.1093/NAR/GKZ423

Balaž, J., Ivanović, Ž., Davidović, A., Iličić, R., Janse, J., and Popović, T. (2016). Characterization of *Xanthomonas hortorum* pv. pelargonii isolated from geranium in Serbia. *Plant Dis.* 100, 164–170. doi: 10.1094/PDIS-03-15-0295-RE

Barel, V., Chalupowicz, L., Barash, I., Sharabani, G., Reuven, M., Dror, O., et al. (2015). Virulence and in planta movement of *Xanthomonas hortorum* pv. pelargonii are affected by the diffusible signal factor (DSF)-dependent quorum sensing system. *Mol. Plant Pathol.* 16, 710–723. doi: 10.1111/MPP.12230/SUPPINFO

Bogdanove, A. J., Koebnik, R., Lu, H., Furutani, A., Angiuoli, S. V., Patil, P. B., et al. (2011). Two new complete genome sequences offer insight into host and tissue specificity of plant pathogenic xanthomonas spp. *J. Bacteriol.* 193, 5450–5464. doi: 10.1128/JB.05262-11

Burstein, D., Amaro, F., Zusman, T., Lifshitz, Z., Cohen, O., Gilbert, J. A., et al. (2016). Genomic analysis of 38 *Legionella* species identifies large and diverse effector repertoires. *Nat. Genet.* 48, 167–175. doi: 10.1038/ng.3481

Burstein, D., Satanower, S., Simovitch, M., Belnik, Y., Zehavi, M., Yerushalmi, G., et al. (2015). Novel type III effectors in *Pseudomonas aeruginosa*. *MBio* 6, e00161-15. doi: 10.1128/mBio.00161-15

Burstein, D., Zusman, T., Degtyar, E., Viner, R., Segal, G., and Pupko, T. (2009). Genome-scale identification of *Legionella pneumophila* effectors using a machine learning approach. *PloS Pathog.* 5, e10000508. doi: 10.1371/journal.ppat.1000508

Choi, M. S., Kim, W., Lee, C., and Oh, C. S. (2013). Harpins, multifunctional proteins secreted by gram-negative plant-pathogenic bacteria. *Mol. Plant Microbe Interact.* 26, 1115–1122. doi: 10.1094/MPMI-02-13-0050-CR

Crossman, L. C., Gould, V. C., Dow, J. M., Vernikos, G. S., Okazaki, A., Sebaihia, M., et al. (2008). The complete genome, comparative and functional analysis of *Stenotrophomonas maltophilia* reveals an organism heavily shielded by drug resistance determinants. *Genome Biol.* 9, R74.1–R74.13. doi: 10.1186/GB-2008-9-4-R74

Cunnac, S., Boucher, C., and Genin, S. (2004). Characterization of the cis-acting regulatory element controlling HrpB-mediated activation of the type III secretion system and effector genes in *Ralstonia solanacearum*. *J. Bacteriol.* 186, 2309–2318. doi: 10.1128/JB.186.8.2309-2318.2004

de Bruijn, I., Cheng, X., de Jager, V., Expósito, R. G., Watrous, J., Patel, N., et al. (2015). Comparative genomics and metabolic profiling of the genus *Lysobacter*. *BMC Genomics* 16, 991. doi: 10.1186/S12864-015-2191-Z

Dia, N. C., Rezzonico, F., Smits, T. H. M., and Pothier, J. F. (2020). Complete or high-quality draft genome sequences of six *Xanthomonas hortorum* strains sequenced with short- and long-read technologies. *Microbiol. Resour. Announc.* 9, e00828-20. doi: 10.1128/MRA.00828-20

Fernández-Pavía, S. P., Rodríguez-Alvarado, G., Garay-Serrano, E., and Cárdenas-Navarro, R. (2014). First report of *Xanthomonas fragariae* causing angular leaf spot on strawberry plants in méxico. *Plant Dis.* 98, 682. doi: 10.1094/PDIS-07-13-0691-PDN

Figurski, D. H., and Helinski, D. R. (1979). Replication of an origin-containing derivative of plasmid RK2 dependent on a plasmid function provided in trans. *Proc. Natl. Acad. Sci. U. S. A.* 76, 1648–1652. doi: 10.1073/PNAS.76.4.1648

Gubler, W. D., Feliciano, A. J., Bordas, A. C., Civerolo, E. C., Melvin, J. A., and Welch, N. C. (2007). First report of blossom blight of strawberry caused by *Xanthomonas fragariae* and *Cladosporium cladosporioides* in California. *Plant Dis.* 83, 400. doi: 10.1094/PDIS.1999.83.4.400A

Henry, P. M., and Leveau, J. H. J. (2016). Finished genome sequences of *Xanthomonas fragariae*, the cause of bacterial angular leaf spot of strawberry. *Genome Announc.* 4, e01271–e01216. doi: 10.1128/GENOMEA.01271-16

Hou, L., Jiang, J., Xu, Z., Zhou, Y., and Leung, F. C. C. (2015). Complete genome sequence of *Pseudoxanthomonas suwonensis* strain J1, a cellulose-degrading bacterium isolated from leaf- and wood-enriched soil. *Genome Announc.* 3, e00614-15. doi: 10.1128/GENOMEA.00614-15

Hunt, M., De Silva, N., Otto, T. D., Parkhill, J., Keane, J. A., and Harris, S. R. (2015). Circlator: automated circularization of genome assemblies using long sequencing reads. *Genome Biol.* 16, 1–10. doi: 10.1186/S13059-015-0849-0/FIGURES/3

Hyatt, D., Chen, G.-L., LoCascio, P. F., Land, M. L., Larimer, F. W., and Hauser, L. J. (2010). Prodigal: prokaryotic gene recognition and translation initiation site identification. *BMC Bioinf.* 11, 119. doi: 10.1186/1471-2105-11-119

Jalan, N., Kumar, D., Andrade, M. O., Yu, F., Jones, J. B., Graham, J. H., et al. (2013). Comparative genomic and transcriptome analyses of pathotypes of *Xanthomonas citri* subsp. citri provide insights into mechanisms of bacterial virulence and host range. *BMC Genomics* 14, 551. doi: 10.1186/1471-2164-14-551

Jiménez-Guerrero, I., Pérez-Montaño, F., Da Silva, G. M., Wagner, N., Shkedy, D., Zhao, M., et al. (2020). Show me your secret(ed) weapons: a multifaceted approach reveals a wide arsenal of type III-secreted effectors in the cucurbit pathogenic bacterium *Acidovorax citrulli* and novel effectors in the *Acidovorax* genus. *Mol. Plant Pathol.* 21, 17–37. doi: 10.1111/mpp.12877

Kamangar, S. B., Van Vaerenbergh, J., Kamangar, S., and Maes, M. (2017). First report of angular leaf spot on strawberry caused by *Xanthomonas fragariae* in Iran. *Plant Dis.* 101, 1031. doi: 10.1094/PDIS-11-16-1659-PDN

Kearney, B., and Staskawicz, B. J. (1990). Widespread distribution and fitness contribution of *Xanthomonas campestris* avirulence gene avrBs2. *Nature* 346, 385–386. doi: 10.1038/346385A0

Kennedy, B. W., and King, T. H. (1962). Angular leafspot of strawberry caused by xanthomonas fragariae sp. nov. *Phytopathology* 52, 873–875.

Koebnik, R., Krüger, A., Thieme, F., Urban, A., and Bonas, U. (2006). Specific binding of the *Xanthomonas campestris* pv. vesicatoria AraC-type transcriptional activator HrpX to plant-inducible promoter boxes. *J. Bacteriol.* 188, 7652–7660. doi: 10.1128/JB.00795-06

Koren, S., Walenz, B. P., Berlin, K., Miller, J. R., Bergman, N. H., and Phillippy, A. M. (2017). Canu: scalable and accurate long-read assembly *via* adaptive k-mer weighting and repeat separation. *Genome Res.* 27, 722–736. doi: 10.1101/GR.215087.116

Kurtz, S., Phillippy, A., Delcher, A. L., Smoot, M., Shumway, M., Antonescu, C., et al. (2004). Versatile and open software for comparing large genomes. *Genome Biol.* 5, 1–9. doi: 10.1186/GB-2004-5-2-R12/FIGURES/3

Li, H., and Durbin, R. (2009). Fast and accurate short read alignment with burrows–wheeler transform. *Bioinformatics* 25, 1754–1760. doi: 10.1093/bioinformatics/btp324

Li, H., Handsaker, B., Wysoker, A., Fennell, T., Ruan, J., Homer, N., et al. (2009). The sequence alignment/map format and SAMtools. *Bioinformatics* 25, 2078–2079. doi: 10.1093/BIOINFORMATICS/BTP352

Lifshitz, Z., Burstein, D., Peeri, M., Zusman, T., Schwartz, K., Shuman, H. A., et al. (2013). Computational modeling and experimental validation of the *Legionella* and *Coxiella* virulence-related type-IVB secretion signal. *Proc. Natl. Acad. Sci. U. S. A.* 110, E707–E715. doi: 10.1073/pnas.1215278110

Lifshitz, Z., Burstein, D., Schwartz, K., Shuman, H. A., Pupko, T., and Segal, G. (2014). Identification of novel *Coxiella burnetii* Icm/Dot effectors and genetic analysis of their involvement in modulating a mitogen-activated protein kinase pathway. *Infect. Immun.* 82, 3740–3752. doi: 10.1128/IAI.01729-14

Madeira, F., Pearce, M., Tivey, A. R. N., Basutkar, P., Lee, J., Edbali, O., et al. (2022). Search and sequence analysis tools services from EMBL-EBI in 2022. *Nucleic Acids Res.* 50, W276–W279. doi: 10.1093/NAR/GKAC240

Marcelletti, S., and Scortichini, M. (2015). Comparative genomic analyses of multiple *Pseudomonas* strains infecting *Corylus avellana* trees reveal the occurrence of two genetic clusters with both common and distinctive virulence and fitness traits. *PloS One* 10, e0131112. doi: 10.1371/journal.pone.0131112

Marques, M. V., Da Silva, A. M., and Gomes, S. L. (2001). Genetic organization of plasmid pXF51 from the plant pathogen *Xylella fastidiosa*. *Plasmid* 45, 184–199. doi: 10.1006/PLAS.2000.1514

Matthews-Berry, S. S., and Reed, P. J. (2009). Eradication of the first outbreak of *Xanthomonas fragariae* in the united kingdom. *EPPO Bull.* 39, 171–174. doi: 10.1111/J.1365-2338.2009.02284.X

Mazzucchi, U., Alberghina, A., and Dalli, A. (1973). Occurrence of *Xanthomonas fragariae* Kennedy et king in Italy. *Phytopathol. Z.* 76, 367–370. doi: 10.1111/j.1439-0434.1973.tb02680.x

McGechan, J. K., and Fahy, P. C. (1976). Angular leaf spot of strawberry, *Xanthomonas fragariae*: first record of its occurrence in Australia, and attempts to eradicate the disease. *Aust. Plant Pathol. Soc Newsl.* 5, 57–59. doi: 10.1071/APP9760057

Michiels, T., and Cornelis, G. R. (1991). Secretion of hybrid proteins by the *Yersinia* yop export system. *J. Bacteriol.* 173, 1677–1685. doi: 10.1128/jb.173.5.1677-1685.1991

Morinière, L., Lecomte, S., Gueguen, E., and Bertolla, F. (2021). *In vitro* exploration of the *Xanthomonas hortorum* pv. vitians genome using transposon insertion sequencing and comparative genomics to discriminate between core and contextual essential genes. *Microb. Genomics* 7, 546. doi: 10.1099/MGEN.0.000546

Nissan, G., Gershovits, M., Morozov, M., Chalupowicz, L., Sessa, G., Manulis-Sasson, S., et al. (2018). Revealing the inventory of type III effectors in *Pantoea agglomerans* gall-forming pathovars using draft genome sequences and a machine-learning approach. *Mol. Plant Pathol.* 19, 381–392. doi: 10.1111/mpp.12528

Noël, L., Thieme, F., Gaübler, J., Büttner, D., and Bonas, U. (2003). XopC and XopJ, two novel type III effector proteins from *Xanthomonas campestris* pv.vesicatoria. *J. Bacteriol.* 185, 7092–7102. doi: 10.1128/JB.185.24.7092-7102.2003

Puławska, J., Warabieda, W., Pothier, J. F., Gétaz, M., and van der Wolf, J. M. (2020). Transcriptome analysis of *Xanthomonas fragariae* in strawberry leaves. *Sci. Rep.* 10, 1–10. doi: 10.1038/S41598-020-77612-Y

Richard, D., Boyer, C., Lefeuvre, P., Canteros, B. I., Beni-Madhu, S., Portier, P., et al. (2017). Complete genome sequences of six copper-resistant *Xanthomonas* strains causing bacterial spot of solaneous plants, belonging to *X. gardneri*, *X. euvesicatoria*, and *X. vesicatoria*, using long-read technology. *Genome Announc.* 5, e01693-16. doi: 10.1128/GENOMEA.01693-16

Roden, J. A., Belt, B., Ross, J. B., Tachibana, T., Vargas, J., and Mudgett, M. B. (2004). A genetic screen to isolate type III effectors translocated into pepper cells during *Xanthomonas* infection. *Proc. Natl. Acad. Sci. U. S. A.* 101, 16624–16629. doi: 10.1073/pnas.0407383101

Ruano-Gallego, D., Sanchez-Garrido, J., Kozik, Z., Núñez-Berrueco, E., Cepeda-Molero, M., Mullineaux-Sanders, C., et al. (2021). Type III secretion system effectors form robust and flexible intracellular virulence networks. *Sci. (80-.).* 371, eabc9531. doi: 10.1126/science.abc9531

Ryan, R. P., Vorhölter, F. J., Potnis, N., Jones, J. B., Van Sluys, M. A., Bogdanove, A. J., et al. (2011). Pathogenomics of *Xanthomonas*: understanding bacterium-plant interactions. *Nat. Rev. Microbiol.* 9, 344–355. doi: 10.1038/NRMICRO2558

Seemann, T. (2014). Prokka: rapid prokaryotic genome annotation. *Bioinformatics* 30, 2068–2069. doi: 10.1093/bioinformatics/btu153

Sievers, F., and Higgins, D. G. (2014). Clustal omega. *Curr. Protoc. Bioinforma.* 48, 3.13.1–3.13.16. doi: 10.1002/0471250953.BI0313S48

Simpson, A. J. G., Reinach, F. C., Arruda, P., Abreu, F. A., Acencio, M., Alvarenga, R., et al. (2000). The genome sequence of the plant pathogen *Xylella fastidiosa*. the *Xylella fastidiosa* consortium of the organization for nucleotide sequencing and analysis. *Nature* 406, 151–157. doi: 10.1038/35018003

Song, Z., Yang, C., Zeng, R., Gao, S., Cheng, W., Gao, P., et al. (2021). First report of strawberry crown rot caused by *Xanthomonas fragariae* in China. *Plant Dis.* 105, 2711. doi: 10.1094/PDIS-03-21-0574-PDN

Sory, M.-P., and Cornelis, G. R. (1994). Translocation of a hybrid YopE-adenylate cyclase from *Yersinia enterocolitica* into HeLa cells. *Mol. Microbiol.* 14, 583–594. doi: 10.1111/j.1365-2958.1994.tb02191.x

Strunnikov, A. V. (2006). SMC complexes in bacterial chromosome condensation and segregation. *Plasmid* 55, 135–144. doi: 10.1016/J.PLASMID.2005.08.004

Teper, D., Burstein, D., Salomon, D., Gershovitz, M., Pupko, T., and Sessa, G. (2016). Identification of novel *Xanthomonas euvesicatoria* type III effector proteins by a machine-learning approach. *Mol. Plant Pathol.* 17, 398–411. doi: 10.1111/mpp.12288

Timilsina, S., Potnis, N., Newberry, E. A., Liyanapathiranage, P., Iruegas-Bocardo, F., White, F. F., et al. (2020). *Xanthomonas* diversity, virulence and plant–pathogen interactions. *Nat. Rev. Microbiol.* 18, 415–427. doi: 10.1038/s41579-020-0361-8

Wagner, N., Alburquerque, M., Ecker, N., Dotan, E., Zerah, B., Pena, M. M., et al. (2022a). Natural language processing approach to model the secretion signal of type III effectors. *Front. Plant Sci.* 13. doi: 10.3389/FPLS.2022.1024405

Wagner, N., Avram, O., Gold-Binshtok, D., Zerah, B., Teper, D., and Pupko, T. (2022b). Effectidor: an automated machine-learning-based web server for the prediction of type-III secretion system effectors. *Bioinformatics* 38, 2341–2343. doi: 10.1093/bioinformatics/btac087

Wagner, N., Teper, D., and Pupko, T. (2022c). "Predicting type III effector proteins using the effectidor web server," in *Bacterial virulence*. Ed. O. Gal-Mor (New York, New York, USA: Springer US), 25–36. doi: 10.1007/978-1-0716-1971-1_3

Walker, B. J., Abeel, T., Shea, T., Priest, M., Abouelliel, A., Sakthikumar, S., et al. (2014). Pilon: an integrated tool for comprehensive microbial variant detection and genome assembly improvement. *PloS One* 9, e112963. doi: 10.1371/JOURNAL.PONE.0112963

Wang, H., McTavish, C., and Turechek, W. W. (2018). Colonization and movement of *Xanthomonas fragariae* in strawberry tissues. *Phytopathology* 108, 681–690. doi: 10.1094/PHYTO-10-17-0356-R/ASSET/IMAGES/LARGE/PHYTO-10-17-0356-R_F4.JPEG

White, F. F., Potnis, N., Jones, J. B., and Koebnik, R. (2009). The type III effectors of *Xanthomonas*. *Mol. Plant Pathol.* 10, 749–766. doi: 10.1111/J.1364-3703.2009.00590.X

Wu, H. Y., Lai, Q. J., Wu, Y. M., Chung, C. L., Chung, P. C., and Lin, N. C. (2020). First report of *Xanthomonas fragariae* causing angular leaf spot on strawberry (fragaria x ananassa) in Taiwan. *Plant Dis.* 105, 1187. doi: 10.1094/PDIS-07-20-1631-PDN

Yang, L., Su, H., Yang, F., Jian, H., Zhou, M., Jiang, W., et al. (2015). Identification of a new type III effector XC3176 in Xanthomonas campestris pv. campestris. *Wei Sheng Wu Xue Bao* 55, 1264–1272. Available at: https://europepmc.org/article/med/26939454

Zhang, S., Sairam, R. V., Grefer, D., Feasel, J., Ferencak, M., and Goldman, S. L. (2009). Resistance to *Xanthomonas campestris* pv. pelargonii in geranium and diagnosis of the bacterial blight using polymerase chain reaction. *Taylor Fr.* 42, 1109–1117. doi: 10.1080/03235400701622378

frontiers | Frontiers in Plant Science

TYPE Original Research
PUBLISHED 20 June 2023
DOI 10.3389/fpls.2023.1168480

OPEN ACCESS

EDITED BY
Vittoria Catara,
University of Catania, Italy

REVIEWED BY
David J. Studholme,
University of Exeter, United Kingdom
Agata Motyka-Pomagruk,
Intercollegiate Faculty of Biotechnology of University of Gdańsk and Medical University of Gdańsk, Poland

*CORRESPONDENCE
Nicole Hugouvieux-Cotte-Pattat
nicole.cotte-pattat@insa-lyon.fr

RECEIVED 17 February 2023
ACCEPTED 22 May 2023
PUBLISHED 20 June 2023

CITATION
Hugouvieux-Cotte-Pattat N, Pédron J and Van Gijsegem F (2023) Insight into biodiversity of the recently rearranged genus *Dickeya*.
Front. Plant Sci. 14:1168480.
doi: 10.3389/fpls.2023.1168480

Insight into biodiversity of the recently rearranged genus *Dickeya*

Nicole Hugouvieux-Cotte-Pattat[1]*, Jacques Pédron[2] and Frédérique Van Gijsegem[2]

[1]Microbiologie Adaptation et Pathogénie, UMR 5240 CNRS, University Lyon, INSA Lyon, Villeurbanne, France, [2]Institute of Ecology and Environmental Sciences, Sorbonne University, CNRS, INRAE, Paris, France

The genus *Dickeya* includes plant pathogenic bacteria attacking a wide range of crops and ornamentals as well as a few environmental isolates from water. Defined on the basis of six species in 2005, this genus now includes 12 recognized species. Despite the description of several new species in recent years, the diversity of the genus *Dickeya* is not yet fully explored. Many strains have been analyzed for species causing diseases on economically important crops, such as for the potato pathogens *D. dianthicola* and *D. solani*. In contrast, only a few strains have been characterized for species of environmental origin or isolated from plants in understudied countries. To gain insights in the *Dickeya* diversity, recent extensive analyzes were performed on environmental isolates and poorly characterized strains from old collections. Phylogenetic and phenotypic analyzes led to the reclassification of *D. paradisiaca* (containing strains from tropical or subtropical regions) in the new genus, *Musicola*, the identification of three water species *D. aquatica*, *D. lacustris* and *D. undicola*, the description of a new species *D. poaceaphila* including Australian strains isolated from grasses, and the characterization of the new species *D. oryzae* and *D. parazeae*, resulting from the subdivision of the species *D. zeae*. Traits distinguishing each new species were identified from genomic and phenotypic comparisons. The high heterogeneity observed in some species, notably for *D. zeae*, indicates that additional species still need to be defined. The objective of this study was to clarify the present taxonomy of the genus *Dickeya* and to reassign the correct species to several *Dickeya* strains isolated before the current classification.

KEYWORDS

Pectobacteriaceae, soft-rot, *Musicola*, *Dickeya*, phytopathogens, pectinases

Abbreviations: NCPPB, National Collection of Plant Pathogenic Bacteria, UK; CFBP, Collection Française de Bacteíries Phytopathogènes, France; IPO, Institute for Plant Protection, Netherlands; PD, Plant Protection Service, Netherlands; IFB, Intercollegiate Faculty of Biotechnology, Poland; SUPP, Shizuoka University of Plant Pathology, Japan; MAFF, Ministry of Agriculture, Forestry and Fisheries, Japan; LMG, Laboratory of Microbiology of Ghent University, Belgium; DSM, DSMZ-German Collection of Microorganisms and Cell Cultures, Germany; ICMP, International Collection of Microorganisms from Plants, New Zealand; PCWDE, plant cell wall degrading enzyme; NRPS, non-ribosomal peptide synthetase; PKS, polyketide synthase.

Introduction

Members of the genus *Dickeya* belong to the family *Pectobacteriaceae* in the order *Enterobacterales* (Adeolu et al., 2016). Most of them are phytopathogenic bacteria and several species have a broad host range; they infect numerous vegetable crops and ornamental plants, including both monocot and dicot plants (Charkowski et al., 2012; Toth et al., 2021; van der Wolf et al., 2021). These pathogens cause either soft rots or vascular wilts in their plant hosts in temperate, tropical and subtropical climates (Charkowski et al., 2012). The soft rot symptoms are due to the action of bacterial pectinases associated with other plant cell wall-degrading enzymes (PCWDEs), which degrade the main structural components of the middle lamella and primary plant cell wall (Van Gijsegem et al., 2021). These devastating plant pathogens have a significant impact on agriculture, causing crop losses both in fields and during storage. *Dickeya* was classified among the top ten most important bacterial plant pathogens based on its economic and scientific impact (Mansfield et al., 2012). While most *Dickeya* strains have been isolated from diseased plants, some strains have also been found in surface water (Parkinson et al., 2014; Potrykus et al., 2016; Hugouvieux-Cotte-Pattat et al., 2019; Oulghazi et al., 2019; Pedron and Van Gijsegem, 2019; Ben Moussa et al., 2022).

The history of *Dickeya* classification began in 2005 with the proposal to place strains formerly designated *Pectobacterium chrysanthemi* (formerly *Erwinia chrysanthemi*) or *Brenneria paradisiaca* into the new genus *Dickeya* (Samson et al., 2005). At this time, the genus *Dickeya* comprised six recognized species, namely *Dickeya chrysanthemi, Dickeya dadantii*, *Dickeya dianthicola, Dickeya dieffenbachiae*, *Dickeya paradisiaca*, and *Dickeya zeae* (Samson et al., 2005). Thereafter, new changes were proposed in the genus *Dickeya*. Members of the species *D. dieffenbachiae* were reclassified as a subspecies of *D. dadantii* (i.e. *D. dadantii* subsp. *dieffenbachiae*) (Brady et al., 2012). Then, classification largely evolved with the identification of new *Dickeya* species and the contribution of genomics. *Dickeya solani* was identified as the causal agent of severe disease outbreaks of potatoes in Europe (van der Wolf et al., 2014). The novel species *Dickeya fangzhongdai* was isolated from pear trees in China (Tian et al., 2016) and from orchids in different countries (Alic et al., 2018). Recently, some members of the heterogeneous species *D. zeae* were reclassified into *Dickeya oryzae* including rice strains (Wang et al., 2020) and *Dickeya parazeae* (Hugouvieux-Cotte-Pattat and Van Gijsegem, 2021). Three new *Dickeya* species were also isolated from water sources. *Dickeya aquatica* was isolated from freshwaters in Scotland and Finland (Parkinson et al., 2014). *Dickeya lacustris* was found in lake water and in the rhizosphere of waterside plants in France (Hugouvieux-Cotte-Pattat et al., 2019). *Dickeya undicola* was found in water samples collected in Malaysia and France (Oulghazi et al., 2019). In addition, old strains from collection isolated in Australia from sugarcane or other *Poaceae* were classified as *D. poaceiphila* (Hugouvieux-Cotte-Pattat et al., 2020). More recently, the species *D. paradisiaca* has been reassigned to the new genus *Musicola*, including two species *Musicola paradisiaca* and *Musicola keenii* (Hugouvieux-Cotte-Pattat et al., 2021). Thus, the genus *Dickeya* currently comprises twelve validly accepted species: *D. aquatica, D. chrysanthemi, D. dadantii, D. dianthicola, D. fangzhongdai, D. lacustris*, *D. oryzae*, *D. paradisiaca, D. poaceiphila, D. solani, D. undicola*, and *D. zeae*.

Assigning the correct bacterial species to new and old *Dickeya* strains is necessary. The large host-range and non-specific symptoms of the soft-rot diseases increase the importance of taxonomy for accurate identification of the causal pathogens (Toth et al., 2021). Phenotypic analyses, mainly based on biochemical and nutritional traits, were previously used to differentiate species. This method remains interesting for a first classification of a large number of strains. However, the taxonomy has rapidly evolved with the use of genetic and genomic tools. Sequencing of the housekeeping genes *recA* or *gapA* is routinely used to refine interspecific phylogenetic positions of strains from the genus *Dickeya* (Parkinson et al., 2009; Suharjo et al., 2014; Cigna et al., 2017). Whole-genome sequence data are now widely used to understand the evolutionary and taxonomic relationships in bacteria. Thus, both phenotypic analysis and comparative genomics are key tools to improve the taxonomy of cultivable strains.

The virulence equipment of the phytopathogenic *Dickeya* species is based on the production and secretion of a battery of PCWDEs (Van Gijsegem et al., 2021). These bacteria have a high capacity of production and secretion of enzymes possessing pectinase, cellulase or protease activity. The maceration symptom is mainly due to the activity of pectate lyases of the PL1 family (Hugouvieux-Cotte-Pattat et al., 2014), acting together with several accessory pectinases, the cellulase CelZ and a few metalloproteases (Van Gijsegem et al., 2021). The multiplication of PCWDEs in *D. dadantii* 3937 is partly due to gene duplications leading to clusters of homologous genes, namely *pelADE*, *pelBC*, *pehXVW*, and *prtABC* (Hugouvieux-Cotte-Pattat et al, 1996; Hugouvieux-Cotte-Pattat et al, 2014). However, virulence is multifactorial and additional virulence determinants have been identified (Van Gijsegem et al., 2021). Different protein secretion systems (T1SS to T6SS) are present in *Dickeya*. The T2SS Out drives the secretion of extracellular pectinases and of the cellulase CelZ; it is essential for virulence and present in all *Dickeya* members. Most *Dickeya* members possess the T1SS Prt devoted to the secretion of the proteases and the T3SS Hrp secreting a few effectors. In contrast, the equipment in T4SS, T5SS or T6SS largely varies among *Dickeya* species (Van Gijsegem et al., 2021). *Dickeya* members produce an array of secondary metabolites involved in plant-bacteria interactions, competition to other microorganisms, or adaptation to diverse environments. In particular, they carry large gene clusters that encode complex non-ribosomal peptide synthetases (NRPS) and polyketide synthases (PKS) (Van Gijsegem et al., 2021).

Many *Dickeya* strains have been stored in international bacterial collections but this material deserves to be better valued (Broders et al., 2022). For example, the analysis of old *Dickeya* strains from the French Collection of Phytopathogenic Bacteria, CFBP (https://cirm-cfbp.fr/) contributed to clarify the taxonomy and

epidemiology of the *Pectobacterium* species (Portier et al., 2020) and allowed the description of the two species *D. poaceiphila* and *M. keenii* (Hugouvieux-Cotte-Pattat et al., 2020; Hugouvieux-Cotte-Pattat et al., 2021). Most *Dickeya* strains isolated and analyzed before 2010s came from diseased crop plants, and there was a need to expand exploration to other environments. *Dickeya* strains are more difficult to isolate from environmental samples which contain many other bacteria, whereas rotten tissues contain almost only the causal agent. This approach was however possible thanks to a powerful semi-selective medium (Hélias et al., 2012) which allowed the isolation of the new aquatic species *D. aquatica*, *D. lacustris*, and *D. undicola* (Parkinson et al., 2014; Hugouvieux-Cotte-Pattat et al., 2019; Oulghazi et al., 2019).

The objective of this study was to present an updated view of the taxonomy of the genus *Dickeya* and to reassign the correct species to *Dickeya* strains isolated before the current classification. We resumed knowledge on the genus *Dickeya* and added new data from phenotypic, genomic and phylogenetic analyses. We tried to favour inter-species comparison by applying the analyses uniformly to all the *Dickeya* species. As the taxonomy within the *Dickeya* genus has been subject to several changes over the past 10 years, this update on the genomic and phenotypic biodiversity within this taxon is supported by information on the strains belonging to each *Dickeya* species.

Materials and methods

Strains

Strains of each species are listed in Tables 1–7; S1, with the plant hosts, country of origin and isolation date when these data were available. *Musicola* strains are listed in Table 1, *D. aquatica*, *D. lacustris*, *D. poaceiphila* and *D. undicola* strains in Table 2, *D. dadantii* strains in Tables 3; S1, *D. dianthicola* and *D. solani* strains in Tables 4; S1, *D. fangzhongdai* strains in Tables 5; S1, *D. chrysanthemi* in Table 6, and *D. oryzae, D. parazeae* and *D. zeae strains* in Tables 7; S1.

Growth conditions and phenotypic analysis

To test their growth with different carbon sources, strains were inoculated onto M63 minimal medium plates supplemented with a sole carbon source (2 g l^{-1}). The enzyme secretion was assessed on plates containing an enzyme substrate (Hugouvieux-Cotte-Pattat et al., 2019). For the detection of pectinase activity, bacteria were grown on M63 agar plates supplemented with 2 g l^{-1} glycerol and 4 g l^{-1} polygalacturonic acid. After incubation for 24 h at 30°C, plates

TABLE 1 The characterized *Musicola* strains.

Strain designations	Origin: Country, year, plant	Identification criteria
Musicola paradisiaca		
Species authority: Hugouvieux-Cotte-Pattat et al., 2021		
CFBP4178^T (NCPPB2511^T)	Colombia 1970, *Musa paradisiaca*	genome, phenotype
Ech703	Australia, *Solanum tuberosum*	genome
CFBP3696 (NCPPB4430)	Cuba 1987, *Musa paradisiaca*	genome, phenotype
CFBP3699	Cuba 1987, *Zea mays*	genome, phenotype
CFBP1445	Colombia 1972, *Musa paradisiaca*	genes *gapA*, *recA*, *dnaX*, *leuS*
CFBP1446	Colombia 1972, *Musa paradisiaca*	genes *gapA*, *recA*, *dnaX*, *leuS*
CFBP1451	Colombia 1972, *Musa paradisiaca*	genes *gapA*, *recA*, *dnaX*, *leuS*
CFBP3477	Colombia 1968, *Musa paradisiaca*	genes *gapA*, *recA*, *dnaX*, *leuS*
CFBP2811 (NCPPB2512)	Colombia 1973, *Musa paradisiaca*	genes *recA*, *dnaX*, *leuS*
CFBP 4179 (NCPPB2513)	Colombia 1973, *Musa paradisiaca*	genes *recA*, *dnaX*, *leuS*
NCPPB2477	Jamaica 1972, *Musa paradisiaca*	phenotype
NCPPB2915	Panama (<1977), *Musa* sp.	phenotype
NCPPB2924	Panama (<1977), *Musa* sp.	phenotype
E353	PRC (China)	gene RNA 16S
572 (= Dickey 141)	*Musa paradisiaca*	gene RNA 16S
Musicola keenii		
Species authority: Hugouvieux-Cotte-Pattat et al., 2021		
A3967^T (CFBP722,		
CFBP8732^T, LMG31880^T)	France 1965, *Solanum lycopersicon*	genome, phenotype

TABLE 2 The characterized strains of D. aquatica, D. lacustris, D. poaceiphila and D. undicola.

Strain designations	Origin: Country, year, plant/habitat	Identification criteria
D. aquatica		
Species authority: Parkinson et al., 2014		
174/2^T (LMG 27354^T, NCPPB 4580^T)	UK 2012, river water	genome, phenotype
DW0440	Finland 2005, river water	genome
CSL RW240	UK, river water	genome
181/2	UK 2012, river water	genes *gyrB, infB, rpoB*
Dw054	Finland 2005, river water	16S rRNA gene
Dw0431	Finland, river water	16S rRNA gene
Dw0512	Finland 2005, river water	16S rRNA gene
JDA74 (CFBP8722)	France 2018, *Solanum dulcamara* rhizosphere	gene *gapA*, phenotype
Not clearly identified strains		
Ca3A, Ca3B	Ireland 2016, *Daucus carota*	gene *recA*
D. lacustris		
Species authority: Hugouvieux-Cotte-Pattat et al., 2019		
S29^T (CFBP8647^T, LMG308990^T)	France 2017, lake water	genome, phenotype
isb1	Pakistan 2021, *Homo sapiens* stool	genome
S12 (CFBP8648)	France 2017, lake water	gene *gapA*, phenotype
S39 (CFBP8649)	France 2017, *Solanum dulcamara* rhizosphere	gene *gapA*, phenotype
J114 (CFBP8721)	France 2018, lake water	gene *gapA*, phenotype
S15	France 2017, lake water	gene *gapA*, phenotype
S24	France 2017, lake water	gene *gapA*, phenotype
D. poaceiphila		
Species authority: Hugouvieux-Cotte-Pattat et al., 2020		
NCPPB569^T (CFBP8731^T)	Australia 1958, *Saccharum officinarum*	genome, phenotype
CFBP2040	Australia 1980, *Megathyrsus maximus*	genome, phenotype
CFBP1537 (SR149)	Australia 1958, *Saccharum officinarum*	gene *gapA*, phenotype
D. undicola		
Species authority: Oulghazi et al., 2019		
2B12^T (CFBP8650^T) LMG30903^T	Malaysia 2014, lake water	genome, phenotype
FVG1-MFV-O17	France, 2017, surface water	genome, phenotype
FVG10-MFV-A16	France, 2016, surface water	genome, phenotype
Ca8	RC (Taiwan), *Daucus carota*	genes *dnaA, dnaJ, dnaX, gyrB, recA*
CFBP7083 (CITA C-29)	Spain 2005, *Allium cepa*	gene *gapA*

were flooded with a saturated solution of copper acetate. Clear haloes appear around colonies secreting pectate-lyases. Cellulase activity was detected on M63 agar plates supplemented with 2 g l^{-1} glycerol and 10 g l^{-1} carboxymethylcellulose. After incubation for 24 h at 30°C, the plates were overflowed with 10 mg ml^{-1} Congo red solution for 10 min and washed for 5 min with 1 M NaCl. Clear haloes surround colonies secreting cellulases. Protease production was tested on LB plates supplemented with skim milk (12.5 g l^{-1}). After incubation at 30°C for 24 to 48 h, clear haloes are visible around colonies secreting proteases.

PCR, amplicon sequencing and recA phylogenetic analysis

The strains were subjected to PCR with primers specific for the gene *gapA* (gapAF and gapAR, 0.8 kb amplicon) (Cigna et al., 2017). The PCR products were sequenced in both directions with the same set of primers, using a commercial service (Microsynth France, Vaulx-en-Velin France). These *gapA* sequences were used for strain identification using BlastN comparison and construction of phylogenetic trees including the type strains. In addition, several *recA* and 16S rRNA sequences were retrieved from NCBI databases and used to define or verify the species affectation of the strain. Several strains firstly identified as *E. chrysanthemi* or *Dickeya* sp. were assigned to species that were not recognized at the time of their isolation.

The phylogenetic tree based on the *recA* gene was constructed using the pipeline Phylogeny.fr (http://www.phylogeny.fr/phylogeny.cgi); the nucleotide sequences are aligned with MUSCLE (Edgar, 2004), the phylogenetic tree is reconstructed using the maximum likelihood method implemented in the PhyML program (Guindon and Gascuel, 2003) and graphical representation is performed with TreeDyn (Dereeper et al., 2008). The *recA* sequences were retrieved from the NCBI database; accession numbers are given in the tree.

Comparative genomic analysis

The dDDH values were calculated using the webserver Genome-to-Genome Distance Calculator (GGDC) version 2.1 with the formula 2 (Meier-Kolthoff et al., 2013). The Average Nucleotide Identity (ANI) based on the Nucleotide MUMmer algorithm (Delcher et al., 2002) was calculated using the JSpecies Web Server with default parameters (Richter and Rosselló-Móra, 2009). The dDDH value of 70% and the cut-off ANI values of 95–96% between two strains were considered for species delineation (Goris et al., 2007).

To determine the phylogenetic position of *Dickeya* species, the phylogenomic tree was constructed from concatenated protein sequences of 963 unique homologous proteins (293566 sites). It was computed using the BioNJ distance method (Criscuolo and Gascuel, 2008). Two hundred bootstrap replicates were performed to assess the statistical support of each node.

Results and discussion

The new genus *Musicola*, analysis of old strains from collections

After analysis of a large panel of strains, Samson et al. (2005) proposed the species *D. paradisiaca* which comprised the former *Brenneria paradisiaca* type strain CFBP 4178^T and six *E. chrysanthemi* strains (CFBP 1445, CFBP 1446, CFBP 1451, CFBP 3477, CFBP 3696, CFBP 3699). This classification was mainly based on phylogenetic analyses of 16S rRNA gene sequences which suggested that these strains were phylogenetically distant to all *Brenneria* species. Recently, genomic analyses have suggested that the differences between *D. paradisiaca* and other *Dickeya* species justify the creation of a separate genus (Pritchard et al, 2016; Pedron and Van Gijsegem, 2019). The genus *Musicola* was recognized in 2021, on the basis of phenotypic, phylogenetic and genomic arguments (Hugouvieux-Cotte-Pattat et al., 2021). Most *D. paradisiaca* strains were isolated from banana trees (*Musa paradisiaca*) in tropical or subtropical countries (Dickey and Victoria, 1980) (Table 1).

The species previously named *D. paradisiaca* was considered as the earliest branching lineage in the *Dickeya* genus in previous evolution studies (Duprey et al., 2019). However, data on the genetic diversity of this species was scarce, and it was poorly characterized at the genomic level. Only two genome sequences were available, including those of the type strain CFBP 4178^T (Pritchard et al., 2013). Calculation of aligned fraction values between *Dickeya* and *Musicola* genomes showed that less than 33% of the genomes of these two genera could be aligned together (Hugouvieux-Cotte-Pattat et al., 2021).

A new *Musicola* strain was identified among poorly characterized strains of the CFBP collection. This strain, A3967 (CFBP 722), is related to *M. paradisiaca* CFBP 4178^T but showed atypical phenotypes for sugar assimilation. Genomic comparison (ANI and dDDH values of 96.21% and 68.3%, respectively) confirmed the divergence and justified the description of a novel species *Musicola keenii* (Hugouvieux-Cotte-Pattat et al., 2021). Since the main phenotypic differences between *M. keenii* and *M. paradisiaca* members concern sugar assimilation, a simple distinction between the two species can be obtained by testing the bacterial growth in the presence of myo-inositol, melibiose or raffinose as the sole carbon source (Table 8). Sequencing of the genomes of two other *Musicola* strains, CFBP 3477 and CFBP 3699, confirms their assignation to the species *M. paradisiaca*, as suggested by phenotypic analysis (Table 1).

Musicola strains are less equipped than *Dickeya* members in PCWDEs and other virulence factors. They lack genes encoding PelA, PelI, PnlH, PehN, Rhi, PemB, GanA and Prt (Table 9). The reduced number of PCWDE genes could explain the low pectinase activity and the absence of protease secretion observed for *Musicola* members (Table 8). While the number of T1SS, T3SS, T4SS and T6SS varies among *Dickeya* species, *Musicola* members have none of them. In addition, they are deprived of factors important to deal with the plant stress responses occuring during infection, such as the nitric oxide dioxygenase HmpX that detoxify nitric oxide produced by plants, the *suf* cluster involved in the repair of damaged Fe/S clusters, and the *ind* cluster encoding the ROS scavenging pigment indigoïdine. These dissimilarities suggest notable differences in the virulence strategies of *Dickeya* and *Musicola* members. Indeed, virulence tests showed that the *Musicola* strains have a weak maceration activity on potato tubers and chicory leaves, two dicot models classically used to evaluate the virulence of *Dickeya* strains (Hugouvieux-Cotte-Pattat et al., 2021). With a low pectate lyase activity, *Musicola* strains are less equipped than *Dickeya* strains to degrade the high pectin content of dicot cell

10.3389/fpls.2023.1168480

TABLE 3 Characterized strains of *D. dadantii*.

Strain designations	Origin: Country, year, plant/habitat	Identification criteria
D. dadantii		
Species authority: Brady et al., 2012		
D. dadantii subsp. *dadantii*		
DSM18020^T (NCPPB898^T, CFBP1269^T)	Comores 1960, Pelargonium	genome
3937 (CFBP3855)	France 1977, Saintpaulia	genome
NCPPB3537 (IPO598)	Peru 1985, potato	genome
BI3-1, Housui2-1, BI1-1	Japan 2016, apple tree	genome
Kousui1-1	Japan 2016, japanese pear tree	genome
Yana2-2, Aka1-1	Japan 2016, peach tree	genome
Kunimi-3	Japan 2018, peach tree	genome
CZ1501	PRC (China) 2016, sweet potato	genome
M2-3	PRC 2019, potato	genome
ICMP 9290	Papua New Guinea 2005, sweet potato	genome
CFBP1245	USA 1945, Philodendron	genes *dnaX, leuS, recA*
CFBP3695	Cuba 1987, corn	genes *dnaX, leuS, recA*
CFBP1443 (NCPPB2351)	USA 1969, Syngonium	genes *dnaX, leuS, recA*
CFBP1444	Honduras 1973, Syngonium	genes *dnaX, leuS, recA*
CFBP1449	USA 1971, Aglaonema	genes *dnaX, leuS, recA*
CFBP1613	France 1974, Euphorbia	genes *dnaX, leuS, recA*
CFBP1891	USA, tabaco	genes *dnaX, leuS, recA*
CFBP2014	France 1974, Dieffenbachiae	genes *dnaX, leuS, recA*
CFBP2593	Peru, potato	genes *dnaX, leuS, recA*
CFBP3694 (CFBP5649)	Cuba 1987, tomato	genes *dnaX, leuS, recA*
CFBP3697	Cuba 1987, sweet potato	genes *dnaX, leuS, recA*
CFBP3698	Cuba 1987, banana	genes *dnaX, leuS, recA*
CFBP3780	Italy, carnation	genes *dnaX, leuS, recA*
CFBP4152	Greece 1985, Philodendron	genes *dnaX, leuS, recA*
CFBP4177	Jamaica 1970, banana	genes *dnaX, leuS, recA*
MAFF301767	eggplant	genes *recA, dnaX, gyrB, rpoD*
SUPP877	carrot	genes *recA, dnaX, gyrB, rpoD*
SUPP2162	strawberry	genes *recA, dnaX, gyrB, rpoD*
Dri1	RC (Taiwan), Drimiopsis	genes *dnaA, dnaJ, dnaX, gyrB, recN*
PD598	Netherlands 1885, Kalanchoe	gene *recA*
PD1132	Netherlands 1985, Gymnocalicium	gene *recA*
PD552	Netherlands 1988, Scindapsus pictus	gene *recA*
NCPPB2477	Jamaica 1972, banana	gene *recA*
NCPPB3065	Brazil 1978, potato	gene *recA*
NCPPB3458	Hungary 1986, Dieffenbachia	gene *recA*
PD753	Netherlands 1986, Eryngium alpinum	gene *recA*

(Continued)

TABLE 3 Continued

Strain designations	Origin: Country, year, plant/habitat	Identification criteria
PD1713	Netherlands 1990, Euphorbia milii	gene *recA*
PD916	RC (Taiwan) 1987, Packera	gene *recA*
PD168	Netherlands 1979, Gymnocalicium	gene *recA*
NCPPB2958	USA 1977, sweet potato	gene *recA*
NCPPB3476	Papua New Guinea1986, sweet potato	gene *recA*
NCPPB4097	Denmark 2000, Euphorbia	gene *recA*
IPO1260	Germany, 2007, potato	gene *dnaX*
IPO2017	Netherlands, hyacinth	gene *dnaX*
D. dadantii subsp. *dieffenbachiae*		
NCPPB2976^T (CFBP2051^T)	USA 1957, Dieffenbachia	genome
CFBP1152	Italy 1962, Dieffenbachia	genes *dnaX, leuS, recA*
CFBP1237	Germany 1959, Dieffenbachia	genes *dnaX, leuS, recA*
CFBP1360	France 1970, Dieffenbachia	genes *dnaX, leuS, recA*
CFBP1870	Ivory Coast 1976, Dieffenbachia	genes *dnaX, leuS, recA*
CFBP2597	Switzerland 1963, Dieffenbachia	genes *dnaX, leuS, recA*
NCPPB2454	UK 1972, Dieffenbachia	gene *recA*
IPO1259	Germany, potato	gene *dnaX*
D. dadantii (unspecified subspecies)		
S3-1	RC (Taiwan) 2002, calla lily (arum)	genome
FZ06	Philippines 2018, banana	genome
A622-S1-A17	France 2017, water	genome

As they are too numerous, only a selection of strains is given, the complete list of *D. dadantii* strains and the latin name of the host plants are given en *Table S1*.

wall. *Musicola* strains may be better adapted to monocots such as *Poaceae* whose primary cell wall has a low pectin content (Jarvis et al., 1988).

Only 16 *Musicola* strains have been characterized up to now (Table 1). These strains were mainly isolated from banana and in a few cases from another monocot, corn, and from dicots of the *Solanaceae* family, potato and tomato. They were isolated between 1968 and 1987 (Table 1). Unfortunately, no *Musicola* strain has been isolated more recently.

The water species *D. aquatica* and *D. lacustris*, true *Dickeya* or members of another genus?

Some water isolates belong to phylogenetic groups differing from plant-related *Dickeya* species. The two species *D. aquatica* and *D. lacustris* form a clade distinct from the other *Dickeya* species in phylogenomic studies (Duprey et al., 2019; Hugouvieux-Cotte-Pattat et al., 2019) (Figure 1). Some *D. lacustris* strains were found associated to the rhizosphere of bittersweet nightshade (*Solanum dulcamara)*, a weed whose roots are in contact with water (Hugouvieux-Cotte-Pattat et al., 2019). Since water strains deserve less interest than pathogenic isolates, they were less studied. Only a few genomes have been sequenced, three for *D. aquatica* and one for *D. lacustris* (Table 2). Very recently, a new *D. lacustris* genome sequence (GCA_027571425.1) became available, it corresponds to strain isb1 isolated in Pakistan from Human stool. The surprising origin of this strain needs further investigation.

Although there is no formal definition of genus delineation on the basis of genome similarity, recent approaches used the genome aligned fraction to discriminate at genus level, showing that genus boundary corresponds to aligned fraction values around 60% (Barco et al., 2020). Indeed, for strains of the ten species *D. chrysanthemi, D. dadantii, D. dianthicola, D. fangzhongdai, D. oryzae, D. parazeae, D. poaceiphila, D. solani, D. undicola* and *D. zeae*, paired aligned fractions correspond to at least 58% of the genome lengths (Hugouvieux-Cotte-Pattat et al., 2021). These ten species constitute a coherent group corresponding to the "core *Dickeya* genus" (Figure 1). With aligned fractions of 73% between D. *lacustris* and *D. aquatica* genomes, these two species correspond to a homogeneous group. In contrast, the aligned fraction of *D. lacustris* and *D. aquatica* genomes is less than 41% with other *Dickeya* species (Hugouvieux-Cotte-Pattat et al., 2021). At the

10.3389/fpls.2023.1168480

TABLE 4 Characterized strains of *D. dianthicola* and *D. solani*.

Strain designations	Origin: Country, year, plant/habitat	Identification criteria
D. dianthicola		
Species authority: Samson et al., 2005		
NCPPB453^T(CFBP1200^T)	UK 1956, carnation	genome
NCPPB3534	Netherlands 1987, potato	genome
RNS04.9	France 2004, potato	genome
WV516	USA 2016, potato	genome
SS70	Pakistan 2017, potato	genome
ME23	USA, potato	genome
GBBC2039	Belgium, potato	genome
MIE34	Switzerland 2013, potato	genome
S4.16.03.P2.4	Morocco 2016, potato	genome
67.19	USA 2019, New Guinea Impatiens	genome
CFBP1805	Denmark 1977, Kalanchoe	genome
CFBP1984	France 1972, Dianthus	genome
CFBP2598	Switzerland, 1982, Kalanchoe	genome
CFBP2982	France 1978, Kalanchoe	genome
CFBP3706	Switzerland 1986, chicory	genome
CFBP6548	France 1994, chicory	genome
59W	USA 2016, water	genome
NY1528B	USA 2016, potato	genome
A260-S21-A16	France 2016, water	genome
Dd31	Serbia 2018, potato	genes *acnA, gapA, icdA, mdh*
MAFF302984	Japan, 1992, yacon	genes *recA, dnaX, gyrB, rpoD*
MAFF311149	Japan 1996, Kalanchoe	genes *recA, dnaX, gyrB, rpoD*
SUPP2525	Japan 2006, carnation	genes *recA, dnaX, gyrB, rpoD*
SUPP2565	Japan 2006, potato	genes *recA, dnaX, gyrB, rpoD*
CFBP1150	Italy 1967, carnation	genes *dnaX, leuS, recA*
CFBP1244 (NCPPB1956)	Netherlands 1966, Dahlia	genes *dnaX, leuS, recA*
CFBP1274 (NCPPB429)	UK 1956, carnation	genes *dnaX, leuS, recA*
CFBP1276 (NCPPB1385)	Romania 1962, Dahlia	genes *dnaX, leuS, recA*
CFBP1353	Netherlands 1969, Begonia	genes *dnaX, leuS, recA*
CFBP1358	France, 1970, Dahlia	genes *dnaX, leuS, recA*
CFBP3702	France, 1984, artichoke	genes *dnaX, leuS, recA*
D18-A1	Japan 2018, fleabane	genes *recA, dnaX*
D18-B1	Japan 2018, butterbur	genes *recA, dnaX*
D19-W1	Japan 2019, water	genes *recA, dnaX*
S4.16.03.P2.18	Morocco 2016, potato	gene *gapA*
CH85/54	Switzerland 1985, potato	gene *gapA*
MG717687	Australia 2017, potato	gene *recA*

(Continued)

10.3389/fpls.2023.1168480

TABLE 4 Continued

Strain designations	Origin: Country, year, plant/habitat	Identification criteria
NCPPB394	USA, 1957, Chrysanthemum	gene *recA*
NCPPB2421 (PD823)	Netherlands, 1969, Begonia	gene *recA*
PD554	Netherlands 1985, Kalanchoe	gene *recA*
PD788	Netherlands 1987, Chicory	gene *recA*
PD1325	Netherlands, 1989, Kalanchoe	gene *recA*
PD1077	Bangladeshs, 1988, potato	gene *recA*
IPO1302	Spain, potato	gene *dnaX*
IPO2096	Finland 2005, potato	gene *dnaX*
D. solani		
Species authority: Van der Wolf et al., 2014		
IPO2222^{T}(NCPPB4479^{T})	Netherlands 2007, potato	genome
Ds0432-1	Finland 2004, potato	genome
RNS 05.1.2A	France 2005, potato	genome
RNS 08.23.3.1.A (3337)	France 2008, potato	genome
RNS 07.7.3B	France 2007, potato	genome
GBBC 2040	Belgium 2007, potato	genome
MK16	UK (Scotland), water	genome
IPO2019	Netherlands 2009, hyacinth	genome
PPO 9019	Netherlands 2006, muscari	genome
PPO 9134	Netherlands 2008, hyacinth	genome
IFB0099	Poland 2005, potato	genome
IFB0158, IFB0167	Poland 2009, potato	genome
IFB0212	Poland 2010, potato	genome
IFB0221, IFB0223	Germany 2005, potato rhizosphere	genome
IFB0231	Finland 2008, potato	genome
IFB0311	Poland 2011, potato	genome
IFB0487	Poland 2013, potato	genome
IFB0695	Poland 2014, potato	genome
IFB0417, IFB0421	Portugal 2012, potato	genome
CH05026-1	Switzerland 2005, potato	genome
CH07044	Switzerland 2007, potato	genome
CH9635-1	Switzerland 1996, potato	genome
CH9918-774	Switzerland 1999, potato	genome
MIE35	Switzerland 2005, potato	genome
D12, F012	Russia 2010, potato	genome
M21a	France 2014, potato	genome
Am3a	France 2015, potato	genome
MK10	Israel, potato	genome
A623-S20-A17	France 2017, water	genome

(Continued)

TABLE 4 Continued

Strain designations	Origin: Country, year, plant/habitat	Identification criteria
CFBP7085	Spain 2002, potato	genes *dnaX, leuS, recA*
CFBP7373	Syria 2004, potato	genes *dnaX, leuS, recA*
CFBP5647	France (Guadeloupe), tomato	gene *gapA*
20711883	UK 2007, potato	gene *recA*
G-115	Israel 2007, potato	gene *recA*
IPO2093	Finland 2005, potato	gene *dnaX*

Only a selection of strains is given, the complete list of D.dianthicola and D. solani strains and the latin name of the host plants are given en Table S1.

TABLE 5 Characterized strains of *D. fangzhongdai*.

Strain designations	Origin: Country, year, plant/habitat	Identification criteria
D. fangzhongdai		
Species authority: Tian et al., 2016		
DSM101947^T(CFBP8607^T, JS5^T)	PRC (China) 2009, pear tree	genome, phenotype
B16 (CFBP8496)	Slovenia 2010, Phalaenopsis	genome, phenotype
S1	Slovenia 2012, Phalaenopsis	genome, phenotype
MK7	UK (Scotland), water	genome, phenotype
NCPPB3274	St. Lucia 1983, Aglaonema	genome, phenotype
PA1	PRC 2011, Phalaenopsis	genome
Onc5	PRC 2021	genome
M005	Malaysia 2013, waterfall	genome
M074	Malaysia 2013, waterfall	genome
ND14b	Malaysia 2013, waterfall	genome
908C	Canada 2020, market	genome
AP6	USA 2014, onion	genome
643b	USA 2020, Aglaonema	genome
LN1	PRC 2014, pear tree	genome
QZH3	PRC 2014, pear tree	genome
Secpp1600	PRC 2016, radish	genome
Ph1 to Ph29	RC (Taiwan), Phalaenopsis	genes *dnaA, dnaJ, dnaX, gyrB, recN*
CAS9, IAS4 and TAS1	RC, Welsh onion	genes *dnaA, dnaJ, dnaX, gyrB, recN*
SUPP40	Japan 1982, Welsh onion	genes *recA, dnaX, gyrB, rpoD*
SUPP420	Japan 1985, Clivia	genes *recA, dnaX, gyrB, rpoD*
SUPP1034	Japan 1988, Phalaenopsis	genes *recA, dnaX, gyrB, rpoD*
SUPP1152	Japan 1989, Oncidium	genes *recA, dnaX, gyrB, rpoD*
SUPP1164	Japan 1989, Vanda	genes *recA, dnaX, gyrB, rpoD*
SUPP1352	Japan 1990, Dracaena	genes *recA, dnaX, gyrB, rpoD*
SUPP1399	Japan 1990, Cattleya	genes *recA, dnaX, gyrB, rpoD*
SUPP1539	Japan 1992, Iris	genes *recA, dnaX, gyrB, rpoD*
SUPP2451	Japan 2004, Welsh onion	genes *recA, dnaX, gyrB, rpoD*

(Continued)

TABLE 5 Continued

Strain designations	Origin: Country, year, plant/habitat	Identification criteria
SUPP2586	Japan 2004, taro	genes *recA, dnaX, gyrB, rpoD*
SUPP2737	Japan 1989, Phalaenopsis	genes *recA, dnaX, gyrB, rpoD*
SUPP2738	Japan 1990, Oncidium	genes *recA, dnaX, gyrB, rpoD*
MAFF311172	Japan 1998, taro	genes *recA, dnaX, gyrB, rpoD*
PD813	Netherlands 1987, Phalaenopsis	gene *recA*
PD1750	Netherlands 1990, Yucca	gene *recA*
NCPPB2915	Panama 1977, banana	gene *recA*
NCPPB2929	Solomon Islands 1977, taro	gene *recA*
NCPPB3211	Sri Lanka 1982, orchid	gene *recA*
NCPPB3306	UK 1984, Polyscias	gene *recA*

Only a selection of strains is given, the complete list of D. fangzhongdai strains and the latin name of the host plants are given en Table S1.

TABLE 6 Characterized strains of *D. chrysanthemi*.

Strain designations	Origin: Country, year, plant/habitat	Identification criteria
D. chrysanthemi		
Species authority: Samson et al., 2005		
NCPPB402^{T} (CFBP2048^{T})	USA 1956, *Chrysanthemum morifolium*	genome
NCPPB516 (CFBP1270)	Danemark 1957, *Parthenium argentatum*	genome
Ech1591		genome
NCPPB 3533	USA 1985, *Solanum tuberosum*	genome
EC16, ATCC11662	USA 1956, *Chrysanthemum morifolium*	genome
L11	Malaysia 2014, water	genome
ws52	PRC 2017, *Nicotiana tabacum*	genome
A604-S21-A17	France 2017, water	genome
CH91/70-1	Switzerland 1991, *Solanum tuberosum*	gene *gapA*
CH93/38-317-4	Switzerland 1993, *Solanum tuberosum*	gene *gapA*
CH93/40-24-1	Switzerland 1993, *Solanum tuberosum*	gene *gapA*
CH98/10	Netherlands 1998, *Solanum tuberosum*	gene *gapA*
CFBP1236 (NCPPB1861)	USA 1945, *Parthenium argentatum*	genes *dnaA, dnaJ, dnaX, gyrB, recA*
CFBP1242 (NCPPB427)	USA 1957, *Chrysanthemum maximum*	genes *dnaA, dnaJ, dnaX, gyrB, recA*
CFBP1275 (NCPPB1111)	UK 1961, Dianthus caryophylus	genes *dnaA, dnaJ, dnaX, gyrB, recA*
CFBP 1346	Italy 1969, *Chrysanthemum maximum*	genes *dnaA, dnaJ, dnaX, gyrB, recA*
CFBP1347	Italy 1969, *Chrysanthemum maximum*	genes *dnaA, dnaJ, dnaX, gyrB, recA*
CFBP1348	Italy 1969, *Chrysanthemum maximum*	genes *dnaA, dnaJ, dnaX, gyrB, recA*
CFBP1441	USA, *Dianthus caryophylus*	genes *dnaA, dnaJ, dnaX, gyrB, recA*
CFBP3262	France 1981, *Cichorum intybus*	genes *dnaA, dnaJ, dnaX, gyrB, recA*
CFBP3263	France 1982, *Cichorum intybus*	genes *dnaA, dnaJ, dnaX, gyrB, recA*
CFBP3701	France 1981, *Lycopersicon esculantum*	genes *dnaA, dnaJ, dnaX, gyrB, recA*

(Continued)

TABLE 6 Continued

Strain designations	Origin: Country, year, plant/habitat	Identification criteria
CFBP3703	France 1986, *Helianthus annuus*	genes *dnaA, dnaJ, dnaX, gyrB, recA*
CFBP3704	France (La Réunion) 1986, *Cynara scolymus*	genes *dnaA, dnaJ, dnaX, gyrB, recA*
CFBP5847	Brazil 1994, *Daucus carota*	genes *dnaA, dnaJ, dnaX, gyrB, recA*
CFBP6689	France 2002, *Cichorum intybus*	genes *dnaA, dnaJ, dnaX, gyrB, recA*
CFBP7086	Spain 2003, *Solanum tuberosum*	genes *dnaA, dnaJ, dnaX, gyrB, recA*
NCPPB1849	USA 1966, *Parthenium argentatum*	gene *recA*
NCPPB2148	UK 1968, *Euphorbia pulcherrima*	gene *recA*
NCPPB2149	UK 1968, *Euphorbia pulcherrima*	gene *recA*
NCPPB2227	UK 1969, *Chrysanthemum morifolium*	gene *recA*
NCPPB2309	Italy, *Chrysanthemum morifolium*	gene *recA*
NCPPB2899	USA 1976, *Daucus carota*	gene *recA*
NCPPB3930	Brazil, *Lycopersicon esculentum*	gene *recA*
SUPP20	Japan 1983, *Chrysanthemum* sp.	gene *recA*
SUPP1844	Japan 1998, *Chrysanthemum* sp.	gene *recA*
MAFF302132	Japan 1989, *Solanum melongena*	gene *recA*
MAFF311043	Japan 1992, *Chrysanthemum* sp.	gene *recA*
MAFF311151	Japan 1990, *Cichorum intibus*	gene *recA*
IFB0284	Poland 2011, water	gene *recA*
IFB0320	Poland 2011, water	gene *recA*
IFB0336	Poland 2011, water	gene *recA*
PD720	*Kalanchoe*	gene *recA*
PD806		gene *recA*
IPO2117		gene *recA*
SD17-1 to SD17-11		gene *recA*

phenotypic level, D. *lacustris* and *D. aquatica* showed some metabolic particularities in comparison to the ten species of the "core *Dickeya* genus", such as the non-assimilation of xylose or mannitol (Table 8). However, their PCWDE equipment is quite similar to that of other *Dickeya* species. They lack a few accessory pectinases PnlG, PehN and PemB (Table 9), but they have the capacity to macerate different plants in laboratory conditions (Duprey et al., 2019). A notable difference is their ecology as *D. lacustris* and *D. aquatica* seem to inhabit only water. An exception could be an isolate from carrot in Northern Ireland which was putatively identified as *D. aquatica* on the basis of a partial *recA* sequence (Zaczek-Moczydłowska et al., 2019). However, phylogenetic analysis of the corresponding sequences (MH688057, MH688058) suggests that strain Ca3 is quite distant from *D. aquatica* (Figure 2). Further analysis will be required to clarify the classification of this strain. The isolation of new strains and sequencing of new genomes is essential in order to obtain more information on the phenotypic and genetic diversity of these water species.

Analysis of old strains from collections, the species *Dickeya poaceiphila*

The phenotypic and genetic analysis of poorly characterized strains from collections allowed the characterization of the species *Dickeya poaceiphila*, including a group of strains isolated in Australia from sugarcane and other *Poaceae* (commonly known as grasses) (Hugouvieux-Cotte-Pattat et al., 2020). Between 1955 and 1957, a plant disease affecting sugarcane in Australia was designated by bacterial mottle (Steindl, 1964). The symptoms consisted of chlorotic striping of the leaves which were heavily invaded by bacteria as were also the stems, causing severe stunting and wilting (Dowson and Hayward, 1960). Symptoms of chlorosis and wilting were also observed on various grasses occurring near sugarcane fields, such as *Pennisetum purpureum* (elephant grass), *Megathyrsus maximus* (Guinea grass), and *Brachiaria mutica* (para grass). The strain NCPPB 569^T was sampled during this outbreak in Australia; its genome sequence was reported in 2013 (Pritchard et al., 2013). Genomic comparisons indicated that this strain was a

10.3389/fpls.2023.1168480

TABLE 7 Characterized strains of the *Dickeya zeae* complex (*D. oryzae, D. parazeae, D. zeae*).

Strain designations	Origin: Country, year, plant/habitat	Identification criteria
D. oryzae		
Species authority: Wang et al., 2020		
ZYY5^T	PRC (China), rice	genome, phenotype
DZ2Q (CFBP8738)	Italy, rice	genome, phenotype
S20 (CFBP8715)	France 2017, water	genome, phenotype
FVG03	France 2017, water	genome, phenotype
NCPPB3531 (CFBP8729)	Australia, potato	genome, phenotype
EC1, EC2, ZJU1202	PRC, rice	genome
CSL RW192	UK, water	genome
BRIP64262	Australia	genome
A003-S1-M15	France 2015, water	genome
A642-S2-A17	France 2017, water	genome
NCPPB2547	India 1969, corn	gene *gapA*, phenotype
CFBP1271	Egypt 1961, corn	gene *gapA*, phenotype
CFBP3707	Israel 1986, water	gene *gapA*, phenotype
CFBP4148	Japan 1978, rice	gene *gapA*, phenotype
CH91/71-2	Switzerland 1991, potato	gene *gapA*
A10-S1-M15 + 6 st	France 2015, water	gene *gapA*
A223-S2-A16 + 3 st	France 2016, water	gene *gapA*
A443-S1-J17 + 9 st	France 2017, water	gene *gapA*
IFB0324, 0330, 0334	Poland 2011, water	gene *recA*
IPO648 + 3 st	Netherlands, potato	gene *recA*
SUPP410	Japan 1985, millet	gene *recA*
SUPP739	Japan 1977, rice	gene *recA*
MAFF106502	Japan 1984, rice	gene *recA*
SUPP3076	Japan 2014, rice	gene *recA*
BC2880	Korea, corn	gene *recA*
KFB414, 415, 417	Serbia 2019	gene *recA*
B1B2	Australia 2017	gene *recA*
DZ15SB01 + 3 st	Thailand 2015, corn	gene *recA*
IMI389157	India, aloe	gene *recA*
SR120	corn	gene *recA*
D. parazeae		
Species authority: Hugouvieux-Cotte-Pattat et al., 2021		
S31^T (CFBP8716^T, LMG8719^T)	France 2017, water	genome, phenotype
Ech586	USA, Philodendron	genome
A586-S18-A17	France 2017, water	genome
CFBP1531	USA 1966, corn	gene *gapA*
CFBP1596 (NCPPB3731)	France 1974, corn	gene *gapA*

(Continued)

TABLE 7 Continued

Strain designations	Origin: Country, year, plant/habitat	Identification criteria
NCPPB2540	USA, corn	gene *recA*
SUPP27	Japan 1980, corn	gene *recA*
MAFF311098	Japan 1990, corn	gene *recA*
PD1619		gene *recA*
D. zeae		
Species authority: Samson et al., 2005		
NCPPB2538^T (CFBP2052^T)	USA 1970, corn	genome, phenotype
NCPPB3532	Australia, potato	genome, phenotype
MK19	UK, water	genome
MS1	PRC 2009, banana	genome
MS2	PRC 2012, banana	genome
MS2014	PRC 2014, banana	genome
MS2018	PRC 2018, banana	genome
WH1	PRC 2021, rice roots	genome
A661-S21-A17	France 2017, water	genome
A5272	USA (Hawai)	genome
BRIP64263	Australia	genome
CFBP1268 (NCPPB1851)	USA 1966, corn	gene *gapA*
CFBP6466	France (Martinique) 1991, pineapple	gene *gapA*
CFBP7084	Spain 2005, water	gene *gapA*
MS3	PRC 2012, banana	gene *recA*
NCPPB2339 (CFBP4176)	USA, 1970, Chrysanthemum	gene *recA*
NCPPB2340	USA, 1970, *Chrysanthemum*	gene *recA*
NCPPB2347	Italy 1971, corn	gene *recA*
SUPP1158	Japan 1989, *Calanthe*	gene *recA*
IPO651	potato	gene *recA*
SR171	corn	gene *recA*
Potential new classification		
FVG08	France 2017, water	genome, phenotype
CE1	PRC, Canna	genome
JZL7	PRC 2017, Clivia	genome
PL65	USA (Hawai) 2018, taro	genome
A5410	USA (Hawai) 2007, pineapple	genome

Only a selection of strains is given, the complete list of strains and the latin name of the host plants are given en Table S1.

candidate for assignment to a novel *Dickeya* species (Pritchard et al., 2016; Duprey et al., 2019) and the species *D. poaceiphila* was recognized in 2020 (Hugouvieux-Cotte-Pattat et al., 2020). In addition to the type strain, it includes strain CFBP 2040 whose genome was also sequenced (dDDH values of 90.2%) and strain CFBP 1537 also isolated in Australia (Table 2).

The three *D. poaceiphila* strains showed substantial phenotypic differences compared to other *Dickeya* species. They produce a low level of pectinases and proteases and no cellulase activity (Table 8). This low secretion of PCWDEs is associated with a low capacity to macerate potato tubers and chicory leaves (Hugouvieux-Cotte-Pattat et al., 2020). The absence of extracellular cellulase activity

TABLE 8 Phenotypic comparison of the different *Dickeya* species.

		Carbon sources												Enzyme secretion			Temp.
Species	Strain	Dara	Mel	Mtl	Xyl	Clb	Ino	G6P	GluA	GalA	Dpsi	Ltart	PGA	Pel	Cel	Prt	39°C
D. dadantii ssp. *dad.*	3937	w	+	+	+	+	+	+	+	_	_	_	+	+	w	w	+
D. dadantii ssp. *dief.*	CFBP 2051^T	w	_	+	+	+	+	+	+	_	_	_	+	+	+	+	+
D. solani	IPO2222^T	w	+	+	+	w	+	+	+	+	_	_	+	+	+	+	+
D. dianthicola	CFBP 1200^T	_	+	+	+	+	+	+	+	+	_	_	+	+	+	w	_
D. fangzhongdai	DSM101947^T	w	+	+	+	+	+	+	+	_	w	w	+	+	+	+	+
D. undicola	2B12^T	w	+	+	+	ND	+	+	+	+	_	+	+	+	+	+	+
D. poaceiphila	NCPPB 569^T	w	+	+	+	_	_	_	_	_	+	_	_	w	_	w	+
D. oryzae	DZ2Q	w	+	+	+	+	+	+	w	_	w	_	+	+	+	+	+
D. parazeae	S31^T	w	+	+	+	_	+	+	w	_	_	w	+	+	+	w	+
D. zeae	NCPPB 2538^T	w	+	+	+	w	+	+	w	_	_	w	+	+	+	+	+
D. chrysanthemi	NCPPB 402^T	_	+	+	+	w	+	+	+		_	_	+	+	+	+	+
D. aquatica	174/2^T	_	+	_	_	_	+	ND	+	_	_	+	+	+	+	w	+
D. lacustris	S29^T	_	+	_	+	_	+	ND	+	_	_	+	+	+	+	+	+
M. paradisiaca	NCPPB 2511^T	w	+	_	_	_	_	_	+	_	_	_	+	w	+	_	+
M. keenii	CFBP 8732^T	w	_	_	+	_	+	+	+	_	+	_	+	w	+	_	+

For carbon source assimilation, the sign - indicates no growth at 72h; +, indicates growth at 24 h; w, indicates weak growth (visible after 48 or 72 h). Dara, D-arabinose; Mel, D-melibiose; Mtl, mannitol; Xyl, D-xylose; Clb, cellobiose; Ino, myo-inositol; G6P, glucose-6-phosphate; GalA, galactonic acid; GluA, gluconic acid; Dpsi, D-psicose; Ltart, L-tartaric acid; PGA, polygalacturonate (pectin backbone).
For PCWDE secretion: +, positive; -, negative (at 24 h). Pel, pectinase; Cel, cellulase; Prt, protease. +, positive; w, weak; -, negative. Growth at the temperature of 39°C was observed after 48 h in LB medium. ND, nt determined.

10.3389/fpls.2023.1168480

in *D. poaceiphila* results from the absence of the cellulase gene *celZ* present in all other *Dickeya* species (Table 9). The weak protease production could be due to the presence of a single *prt* gene in *D. poaceiphila*, while several *prt* genes are present in other *Dickeya* species (Table 9). Similarly, the low level of pectinase activity could be due to a low number of pectinase genes. *D. poaceiphila* has only two genes encoding secreted pectate lyases of the polysaccharide lyase family 1 (PL1), one of the *pelADE* cluster and one of the *pelBC* cluster. PL1 are responsible for the major pectate lyase activity of *Dickeya* (Hugouvieux-Cotte-Pattat et al., 2014) and the other *Dickeya* species contain 5 to 6 genes encoding PL1 pectate lyases (Table 9). *D. poaceiphila* is the only *Dickeya* species lacking the pectate lyase genes *pelL* and *pelZ*. It also lacks the accessory pectinase genes *pnlG*, *pnlH*, *pehK*, *pehN*, *pemB* and the galactanase gene *ganA*. It has only one polygalacturonase gene of the cluster *pehXVW* (Table 9). Several gene duplications leading to clusters of *pel*, *peh* or *prt* genes in other *Dickeya* species are not found in *D. poaceiphila*. This restricted number of PCWDE activities and genes could explain why *D. poaceiphila* strains are poorly effective in causing soft rot symptoms (Tables 8, 9) and instead produce other types of symptoms, such as stunting or wilting (Dowson and Hayward, 1960).

Additional phenotypic differences between *D. poaceiphila* and other *Dickeya* species were observed for sugar assimilation, including an absence of growth with D-gluconic acid, D-fructose-6-phosphate, D-glucose-1-phosphate, D-glucose-6-phosphate, *myo*-inositol, or polygacturonate (PGA), the pectin backbone (Table 8). The absence of growth of *D. poaceiphila* on pectin or polygalacturonate may result from the inactivation of *kduI*, a gene involved in the intracellular pectin catabolic pathway (Hugouvieux-Cotte-Pattat et al., 1996). This gene is annotated as a pseudogene in *D. poaceiphila* because it has an internal deletion of 555 bp. A defect in pectin assimilation is clearly a factor that could affect the bacterial growth in macerated plant tissues. It is less troublesome for a species

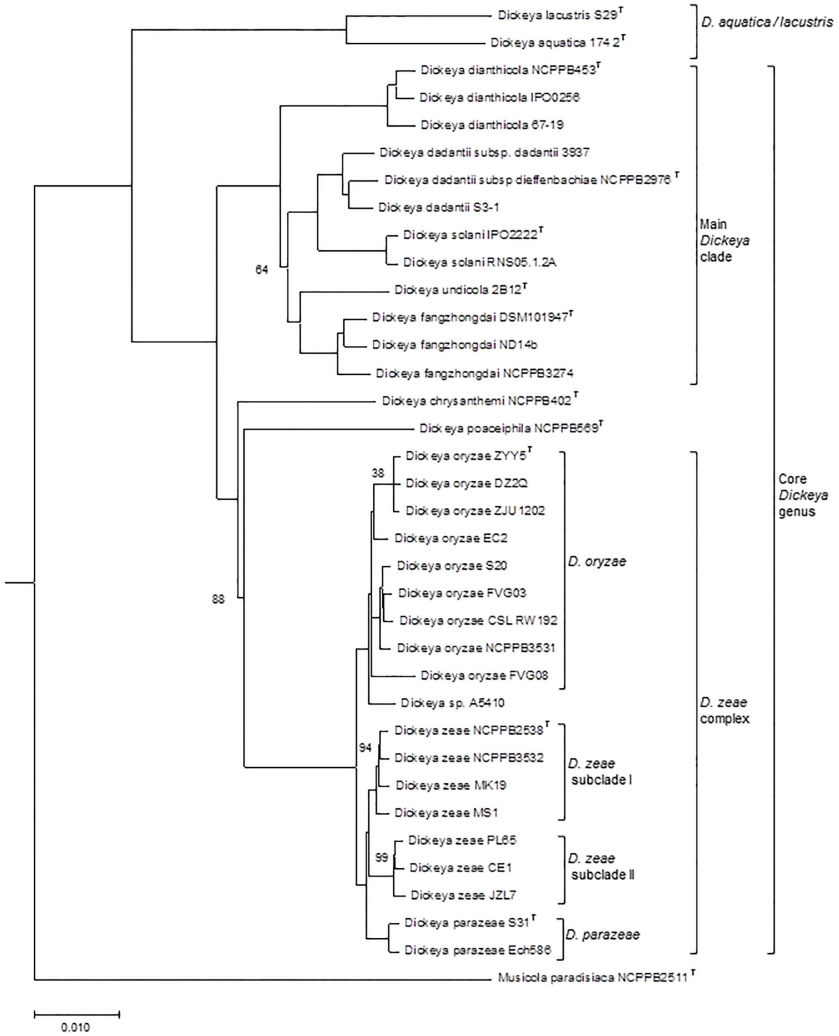

FIGURE 1
Phylogenomic tree of the *Dickeya* species. The phylogenetic tree, constructed from concatenated amino acid sequences of 963 unique homologous proteins (293566 sites), was computed using the BioNJ distance method. Two hundred bootstrap replicates were performed to assess the statistical support of each node. The tree includes 35 *Dickeya* genomes, representative of the different species and subclades discussed in the text. A *Musicola* genome was used as outgroup. Only boostrap values below 100 are indicated. T, type strain. The scale bar represents the average number of changes per nucleotide position.

that does not cause maceration of its host plants but other types of symptoms.

While *D. poaceiphila* strains show clear differences in phenotypic and genomic features from strains of the other characterized *Dickeya* species, phylogenomic studies confirmed that these strains clearly belong to the genus *Dickeya* (Hugouvieux-Cotte-Pattat et al., 2020). However, the *D. poaceiphila* genomes appear to be the smallest ones (4.22-4.32 Mb) among the *Dickeya* species and they have the lowest GC content (52.60-52.70%) (Table 10). A reduced genome size is consistent with the numerous gene losses observed in this species and suggests an evolution of these genomes towards an adaptation to a more restricted habitat. This could correspond to an adaptation to a specialized host range and type of symptom as *D. poaceiphila* has only been shown to cause wilt disease on monocot herbaceous plants of the *Poaceae* family.

Only three *D. poaceiphila* strains have been characterized and only two genome sequences have been reported (Table 2). Since the three strains were isolated from the same country, isolation and characterization of new strains from different origins will be necessary to access to the diversity of the species *D. poaceiphila* and to confirm its genomic divergence and potential specialization within the genus *Dickeya*.

The main *Dickeya* clade includes *D. dadantii, D. dianthicola, D. fangzhongdai, D. solani* and *D. undicola*

Using phylogenetic studies, two clades are observed in the core *Dickeya* genus (Figure 1). One includes *D. chrysanthemi*, *D. poaceiphila, D. oryzae, D. parazeae* and *D. zeae*. The other, called the "main *Dickeya* clade", regroups the five species *D. dadantii*, *D. dianthicola*, *D. fangzhongdai, D. solani* and *D. undicola* (Figure 1). These five species form a clade sharing high ANI values (89 to 94%) and share more than 50% of their protein families (around 2600) including most virulence genes (Pedron and Van Gijsegem, 2019). They have a large equipment in PCWDEs (Table 9). Their genomes encode at least ten pectate lyases (PelB, PelC, PelD, PelE, PelI, PelL, PelN, PelW, PelX and PelZ), the rhamnogalacturonate lyase RhiE, the predicted pectin lyase PnlG, the pectin acetyl esterases PaeX and PaeY, the feruloyl esterases FaeD and FaeT, and the two pectin methyl esterases PemA and PemB (Table 9). The arsenal of polygalacturonases is more variable, ranging from three to five, including at least PehN and PehX. All species of the main *Dickeya* clade produce the cellulase CelZ and the galactanase GanA. Their genome harbor at least two protease genes (Table 9). While the siderophore clusters *cbs* and *acs* belongs to the *Dickeya* core genome, most clusters encoding secondary metabolite biosynthesis are members of the *Dickeya* accessory genomes, as they variably distributed among species and sometimes among strains of the same species (Table 11).

Despite their high genetic proximity and sharing of virulence related genes, the closeness and host ranges of these five *Dickeya* species differ, ranging from narrow to wide host ranges and genomic diversities. The two species *D. dadantii* and *D. fangzongdai* are even able to cause tree diseases in orchards, such as the bleeding canker necrosis of pear trees (Tian et al., 2016) and the bacterial quick decline of apple trees (Fujikawa et al., 2019).

D. dadantii, a wide host range, the model strain 3937

Noticeably, the *D. dadantii* species includes the strain 3937 that has been used for a long time as a model of the genus *Dickeya* for genetic studies leading to the characterization of virulence factors, including the different enzymes constituting the PCWDE equipment, and the regulatory network controlling expression of the virulence genes (Hugouvieux-Cotte-Pattat et al., 1996;

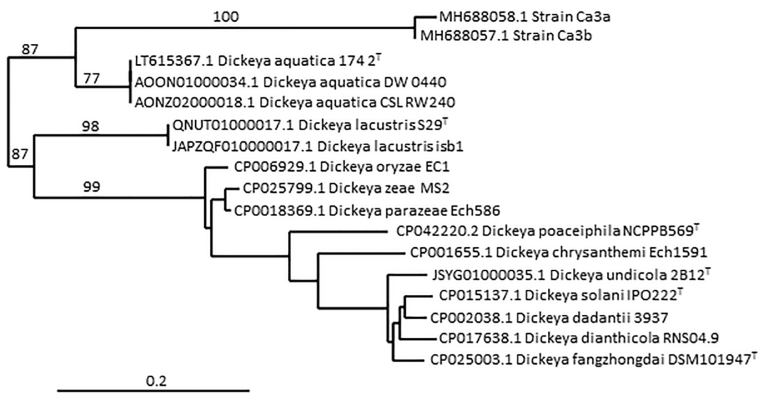

FIGURE 2
Phylogenetic position of strain Ca3a among the Dickeya species, based on partial recA gene sequences. The tree was constructed using the pipeline Phylogeny.fr (http://www.phylogeny.fr/phylogeny.cgi). The nucleotide sequences are aligned with MUSCLE, the phylogenetic tree is reconstructed using the maximum likelihood method implemented in the PhyML program and graphical representation is performed with TreeDyn. Numbers correspond to bootstrap values (500 replicates). The scale bar represents the average number of substitutions per site. The two strains Ca3a and Ca3b were isolated from carrots in Northern Ireland (Zaczek-Moczydłowska et al., 2019) and their partial recA gene sequences (MH688058 and MH688057, respectively) consisted of 503 nt.

TABLE 9 Repartition of the main PCWDEs in the different *Dickeya* species.

			Dickeya sp.												*Musicola* sp.	
Enzymatic activity	CAZY family	Gene name	Ddad	Dsol	Ddian	Dfang	Dund	Dpoa	Dor	Dpara	Dzeae	Dchrys	Daq	Dlac	Mparad	Mkeen
Pectin lyase	PL1	*pnlG*	1	1	1	1	1	0	1	0	1	0	0	0	0	0
		pnlH	0	0	1	0	0	0	0	0	0	1	0	1	1	1
Pectate lyase	PL1	*pelA/D/E*	3	3	2	3	3	1	3	3	3	2	2	3	2	2
		pelB/C	2	2	2	2	2	1	2	2	2	2	2	2	2	2
		pelZ	1	1	1	1	1	0	1	1	1	1	1	1	1	1
	PL2	*pelW*	1	1	1	1	1	1	1	1	1	1	1	1	1	1
	PL3	*pelI*	1	1	1	1	1	1	1	1	1	1	1	1	0	0
	PL9	*pelL*	1	1	1	1	1	0	1	1	1	1	1	1	1	1
		pelN	1	0	1	1	1	1	1	1	1	1	1	1	1	1
		pelX	1	1	1	1	1	1	1	1	1	1	1	1	1	1
	PL10	*pel10*	0	0	0	1	0	0	0	0	0	0	1	0	0	0
Rhamnogalacturonate	PL4	*rhiE*	1	1	1	1	1	0	0	0	1	1	0	1	0	0
lyase	PL26	*rhiF*	1	1	1	1	0	0	0	0	0	1	0	1	0	0
Polygalacturonase	GH28	*pehV/W/X*	3	3	2	1	1	1	1	1	1	2	1	1	1	1
		pehK	1	0	1	1	1	0	1	1	1	0	1	1	1	1
		pehN	1	1	1	1	1	0	0	0	1	1	0	0	0	0
Pectin methylesterase	CE8	*pemA*	1	1	1	1	1	1	1	1	1	1	1	1	1	1
		pemB	1	1	1	1	1	0	0	0	0	1	0	0	0	0
Pectin acetylesterase	CE10	*paeY*	1	1	1	1	1	0	1	1	1	1	1	1	1	1
	CE12	*paeX*	1	1	1	1	1	1	1	1	1	1	1	1	1	1
Ferruloyl esterase	CE10	*faeD*	1	1	1	1	1	1	1	1	1	1	1	1	1	1
		faeT	1	1	1	1	1	0	1	1	1	1	1	1	1	1
Cellulase	GH5	*celZ*	1	1	1	1	1	0	1	1	1	1	1	1	1	1
Galactanase	GH 53	*ganA*	1	1	1	1	1	0	1	1	1	1	1	1	0	0
Protease		*prtA/B/C*	3	3	2	3	3	1	3	3	3	3	3	3	0	0
		prtG	1	1	0	1	0	0	1	1	1	1	1	1	0	0

Data are given for the type strain of each species. The families of enzymes that degrade or modify polysaccharides are described in the CAZy database (http://www.cazy.org/) (Drula et al., 2022). GH, glycoside hydrolase; PL, polysaccharide lyase; CE, carbohydrate esterase.

10.3389/fpls.2023.1168480

TABLE 10 Range of genome size and GC% for the *Dickeya* and *Musicola* species.

Species	Genome number	Genome size (Mb)	GC%	Intraspecies ANI	Intraspecies dDDH
D. dadantii	17	4.66-5.35	55.90-56.50	>96.3	>68.9
D. solani	44	4.81-5.07	56.10-56.38	>98.7	>89.2
D. dianthicola	76	4.68-4.91	55.60-56.00	>97.3	>76.4
D. fangzhongdai	16	4.93-5.18	56.44-56.90	>96.1	>68.5
D. undicola	3	4.35-4.61	54.50	>98.9	>92.9
D. poaceiphila	2	4.02-4.32	52.60-52.80	98.8	90.3
D. oryzae	10	4.53-4.75	53.30-53.70	>96.0	>67.9
D. parazeae	3	4.71-4.82	53.60-53.70	>98.6	>88.1
D. zeae	21	4.56-4.93	53.30-53.70	>96.1	>68.3
D. chrysanthemi	8	4.62-4.81	54.19-54.51	>96.2	>68.9
D. aquatica	3	4.34-4.50	53.35-53.60	>99.9	>99.1
D. lacustris	2	4.30-4.31	53.10	100	100
M. paradisiaca	2	4.63-4.68	55.00	100	99.9
M. keenii	1	4.40	54.40	_	_

For each species, are given the number of available genomes, their size range and their GC% range (data from the NCBI genome database, February 2023) and the intraspecies ANI and dDDH values.

Hugouvieux-Cotte-Pattat et al., 2014; Reverchon et al., 2016). The 3937 genome was the first *Dickeya* genome to be sequenced (Glasner et al., 2011).

Among all *Dickeya* species, *D. dadantii* has the widest host range and geographical distribution. It was isolated in all continents, from several dicots and monocot plants. More than 100 strains have been isolated from at least 25 countries and 26 different plants, including apple, peach and pear trees, vegetables (potato, tomato, eggplant, carrot, sweet potato), and numerous ornamentals (*Aglaonema, Dieffenbachia, Drimiopsis*, *Euphorbia, Kalenchoe, Pelargonium, Phylodendron, Saintpaulia, Syngonium*, etc). It was occasionally found in corn (*Zea mays*), cactus (*Gymnocalicium*), alpine plants (*Erygium alpinum*) and water (Table 3; Table S1).

First described as a separate species, *D. dieffenbachiae* was included as a subspecies of *D. dadantii* (*D. dadantii* subsp. *dieffenbachiae*) since both species type strains shared 96.6 ANI and 71.4% dDDH values. The main *D. dadantii* clade was renamed *D. dadantii* subsp. *dadantii* (Brady et al., 2012). The main phenotypic difference between the two subspecies is the assimilation of melibiose (Table 8). *D. dadantii* subsp. *dieffenbachiae* strains were nearly all isolated from ornamentals of the genus *Dieffenbachia* (*Araceae* family). With the isolation of new Asiatic strains of *D. dadantii* (Fujikawa et al., 2019; Wei et al., 2021; Tan et al., 2022), the heterogeneity within this species may increase. The strain S3-1 isolated from an *Araceae* (*Zantedeschia aethiopica*) in Taiwan (Wei et al., 2021) is distinct from members of both *D. dadantii* subspecies, with 96.3-96.7 ANI values and 68-72% dDDH values. This raises the possibility of an additional *D. dadantii* subspecies including strains S3-1, FZ06 and A622-S1-A17 (Table 3, Figure 1). A classification at the subspecies level can be justified when each subspecies has a specific feature or is linked to a particular host. However, newly isolated strains are rarely classified at this level, except when there is a clear phenotypic difference between the subspecies. So far, no specific traits have been described for the three *D. dadantii* strains not assigned to a recognized subspecies. Nevertheless, with 17 genome sequences available (Table 3), the genomic diversity of the *D. dadantii* species is exemplified by the large range of genome sizes, from 4.66 to 5.35 Mb (Table 10).

Another intriguing type of diversity among *D. dadantii* members concerns the *vfm* cluster which is present in all *Dickeya* strains (Table 11). The VFM molecule plays a major role in intercellular communication by acting as a quorum sensing molecule (Nasser et al., 2013). However, differences in the enzymatic specificity of the proteins VfmO and VfmP generate the production of different analogs of the VFM molecule, which vary according to the strain (Hugouvieux-Cotte-Pattat et al., 2022). As these analogs are differentially recognized, signaling through the Vfm quorum sensing system is limited to strains belonging to compatible groups. For instance, the *D. dadantii* strains are divided in two groups and the production of two different VFM analogs affects the intra-species communication (Table 11).

D. dianthicola, a potato pathogen known since 1950s

The two species *D. dianthicola* and *D. solani* deserved special attention because they caused severe damages in the important crop potato. Most analyzed genomes are from strains isolated from diseased potatoes introducing a severe bias for diversity analyses. Despite its reputation of potato pathogen, *D. dianthicola* has a broad host range (van der Wolf et al., 2021). It was first described in

an outbreak on carnation in Europe in the 1950s. Nearly 300 strains have now been characterized, including about 80% potato isolates (Table 4; Table S1). Other isolates were reported from vegetables, such as chicory or artichoke, and ornamentals, frequently carnation, kalanchoe, begonia and dahlia (Table 4). Potato infections in Europe have been detected since the 1970s but losses caused by *D. dianthicola* remained generally low and sporadic (Toth et al., 2011) except in Switzeland and the Netherlands where *D. dianthicola* dominated till the advent of *D. solani* in the 2000s (Pedron et al., 2021; Pedron et al., 2022). Since 2015, *D. dianthicola* caused a severe blackleg outbreak in the US that originated from Maine and further spread in at least eighteen US states (Charkowski, 2018). *D. dianthicola* also caused a blackleg outbreak in Western Australia in 2017 (Wright et al., 2018).

All *D. dianthicola* genomes contain the cluster *ooc* involved in the biosynthesis of an oocydin A-like molecule that may contribute to the maintenance of these species in the potato environment, by favouring the competition with other microorganisms (Brual et al., 2023). At the genomic level, *D. dianthicola* has a truncated pectate lyase gene *pelA* and lacks two protease genes (Table 9). At the phenotypic level, it is the sole member of the main *Dickeya* clade unable to grow with D-arabinose as the sole carbon source and it is the sole *Dickeya* species unable to grow at 39°C (Table 8). Such phenotypic differences could reflect a divergent adaptation of *D. dianthicola* to environmental conditions.

Due to the large interest for this potato pathogen, more than 70 *D. dianthicola* genome sequences are now available (Tables 4, 10). Most show strong relatedness illustrated by ANI values greater than 99% and clonal origin of the strains isolated during the US potato outbreak (Ge et al., 2021). Analysis of additional genomes highlights the diversity in *D. dianthicola*, with two strains isolated from potato in the Netherlands in 1975 and from impatiens in the US in 2019 (Liu et al, 2021) (Table 4), sharing 97 to 98% ANI values with other *D. dianthicola* genomes (Pedron et al., 2022). A recent report of *D. dianthicola* presence in *Asteraceae* weeds (fleabane and butterbur) close to potato fields points to another possible route of transmission from weeds to potato through surface water flow (Aono et al., 2022).

D. solani, a potato pathogen emerging in the 2000s

In contrast to *D. dianthicola, D. solani* has a narrow host range, it was recognized as the agent of a potato outbreak in Europe in the 2000s (Slawiak et al., 2009; van der Wolf et al., 2014), then it spread in Asia (Israel, Syria, Turkey, Georgia, oriental Russia), North Africa (Morocco) and Latin America (Brazil) (van der Wolf et al., 2021). On 65 *D. solani* characterized strains so far (Table 4; Table S1), only two other hosts have been identified apart to potato, the ornamentals muscari (one strain) and hyacinth (2 strains), and two strains were isolated from water (Table 4). A large majority of *D. solani* isolates collected in Europe and the Mediterranean Basin are clonal (Khayi et al., 2015; Golanowska et al., 2018; Blin et al., 2021). Even strains isolated more than 20 years apart are highly related, indicating a high genomic stability (Pedron et al., 2021). Genomic variations in *D. solani* genomes consist mainly in the presence of genes related to phages and even complete prophages (Golanowska et al., 2018; Khayi et al., 2022). The first exception was observed with strain RNS05.1.2A isolated from potato in France, which showed an ANI value of only 98% with other *D. solani* genomes (Khayi et al., 2015). Recently, two other French strains, RNS10-105-1A and A623S-20A-17, isolated from potato and surface water respectively, were shown to belong to the same rare subclade (Khayi et al., 2022). The other genetic variations observed in *D. solani* results from horizontal gene transfers leading to gene replacement. A few potato strains collected in France (RNS07.7.3B, RNS13-30-1A, RNS13-31-1A and RNS13-48-1A) acquired genomic regions related to the RNS05.1.2A subclade (Khayi et al., 2022). Two *D. solani* strains isolated from ornamentals (PPO9019 and PPO9134) acquired gene clusters from *D. dianthicola*. The strain PPO9019 also possesses a 45 kb plasmid identical to a plasmid of *Burholderia ambifaria* (Khayi et al., 2015). Interestingly, *D. solani* and *B. ambifaria* beside sharing an identical plasmid, exhibit similarities in the O-polysaccharide compositions that both contain 6-deoxyaltropyranose (Ossowska et al., 2017). Even if divergences remain rather limited, the *D. solani* strains from ornamentals or water seem to show more diversity than the potato isolates. Strains showing genomic variations were collected in The Netherlands and France and it would be interesting to further analyze the potential *D. solani* diversification in other countries.

A genomic comparison revealed the presence of three genomic regions encoding NRPS, PKS and associated proteins which are present in all *D. solani* genomes but absent in *D. dadantii* 3937 (Garlant et al., 2013; Pedron et al., 2014). First described for some *D. oryzae* strains (Zhou et al., 2011), the cluster *zms* is found in all *D. solani* and *D. fangzhongdai* genomes (Table 11). It encodes proteins involved in the biosynthesis of toxins of the zeamine family. The zeamine produced by *D. solani* is involved in antibacterial activity (Effantin et al., 2021; Brual et al., 2023). The *D. solani* cluster *ooc* comprises genes involved in the biosynthesis of an oocydin A-like molecule, a compound inhibiting *Ascomycetes* growth (Effantin et al., 2021; Brual et al., 2023). This cluster is also found in all the *D. dianthicola* genomes and some strains of *D. fangzongdai, D. oryzae, D. chryanthemi* and *D. aquatica* (Table 11). The cluster *sol* (or *ssm*) produces an antifungal compound recently named solanimycin (Matilla et al., 2022). Solanimycin is active against a broad range of plant-pathogenic fungi and the human pathogen *Candida albicans* (Effantin et al., 2021; Matilla et al., 2022; Brual et al., 2023). The *sol* cluster is conserved in most *Dickeya* species, including all the genomes of *D. fangzongdai*, *D. poaceiphila*, *D. parazeae* and *D. zeae* and in some strains of *D. dadantii, D. undicola* and *D. oryzae* (Table 11). The presence of the *sol* cluster appears to be correlated with signs of horizontal genetic transfer (Matilla et al., 2022).

D. fangzhongdai, a tree and orchid pathogen

D. fangzhongdai was the first *Dickeya* species found to infect trees, where it causes bleeding canker necrosis (Tian et al., 2016).

Most *D. fangzhongdai* isolates originated from Asia (Table 5, Table S1), but the species was also identified in Europe, mainly in orchids (Alic et al., 2017). Analysis of old bacterial collections showed that *D. fangzhongdai* was introduced to Europe as early as 1985, through the propagation of ornamental plants (Parkinson et al., 2009; Van Vaerenbergh et al., 2012; Suharjo et al., 2014; Alic et al., 2018). Beside pear trees, *D. fangzhongdai* is able to cause soft rot on orchids (*Phalenopsis, Oncidium, Vanda, Cattleya*), and it is also found in water (Alic et al., 2018) (Table 5). Unlike other members of the main *Dickeya* clade, *D. fangzhongdai* strains are able to assimilate the rare sugar D-psicose (Table 8). The D-psicose catabolic pathway was not yet characterized but this capacity was also observed for *D. oryzae* and *D. poaceiphila* (Table 8). Genome mining in the three *Dickeya* species able to utilize D-psicose demonstrates the correlation between the presence of the gene cluster *alsRBACDEKS* and the bacterial utilization of D-psicose (Figure 3A). The importance of this pathways during pathogenesis is unknown but D-psicose was shown to induce some plant defense genes, conferring plant resistance to diseases (Kano et al., 2011).

When analyzed for their maceration ability in laboratory conditions, *D. fangzhongdai* members appear to be more efficient than any other *Dickeya* species (Alic et al., 2018). In addition to classical PCWDE equipment, the *D. fangzhongdai* genome contains a gene encoding a pectate lyase of the rare family PL10 (Table 9). PL10 enzymes exhibit catalytic properties similar to those of pectate lyases of the PL1 family such as an alkaline optimal pH, a Ca2+ requirement and a preference for low methylated pectin as substrate (Hugouvieux-Cotte-Pattat et al., 2014). They adopt an (α/α)3 barrel topology in place of the parallel β-helix topology found for PL1 pectate lyases, but the catalytic machinery used by PL10 and PL1 displays a striking resemblance, presumably due to convergent evolution (Charnock et al., 2002).

D. fangzhongdai clearly shows intra-species diversity with ANI values ranging from 96 to 99% between its members. The *D. fangzhongdai* strains are distributed in three clades in phylogenetic trees (Figure 1). One strain, NCPPB3274, is at the limit of being part of the species, with ANI values of ~96% and dDDH values of 68.6-70.5% with other *D. fangzhongdai* isolates. The *D. fangzhongdai* strain S1 carries a 23 kb plasmid similar to an *Acidovorax* plasmid. Besides genes involved in plasmid replication, stabilization and conjugative transfer, this plasmid contains two streptomycin kinase genes responsible for the resistance to the antibiotic streptomycin (Alic et al., 2019).

D. fangzhongdai is particularly well armed in secondary metabolites. In addition to the clusters *zms* and *sol* involved in the biosynthesis of the antibiotic zeamine and the antifungal compound solanimycin, respectively (Table 11), all the *D. fangzhongdai* genomes possess additional NRPS/PKS clusters (Alic et al., 2019; Van Gijsegem et al., 2021). Two of them are predicted to be involved in the biosynthesis of cyanobactin-related and thiopeptide-related metabolites, respectively. The atypical strain NCPPB3274 harbours the cluster *ooc* involved in the biosynthesis of an oocydin A-like molecule.

D. undicola, only a water species?

The species *D. undicola* was only recently described after isolation of three strains from surface waters, one from a lake in Malaysia and two from an irrigation canal in the South of France (Oulghazi et al., 2019) (Table 2). Phylogenetic analyses identified *D. fangzhongdai* as the closest *Dickeya* species (Figure 1). Carbon sources utilization analysis identified galactonic acid as a potential discriminative character for distinguishing between these two species (Table 8). The PCWDE repertoire of *D. undicola* is identical to that of *D. dadantii*, except that it produces only one polygalacturonase of the *pelXVW* cluster (Table 9). The genes involved in resistance to stresses encountered during plant infection are shared by all species of the main *Dickeya* clade, except that *D. undicola* harbors a truncated flavohemoglobin gene *hmpX* (Van Gijsegem et al., 2021). *D. undicola* genomes contain the *car* locus involved in the synthesis of the β-lactam antibiotic, 1-carbapen-2-em-3-carboxylic acid (carbapenem) as well as genes encoding the carbapenem immunity proteins. This cluster is also found in the water species *D. aquatica* and *D. lacustris*, some strains of *D. chrysanthemi*, *D. oryzae* and *D. zeae* (Table 11) and some *Pectobacterium* species (Van Gijsegem et al., 2021).

Despite they were isolated from far regions, the three *D. undicola* strains are closely related as they shared ANI and dDDH values higher than 99 and 92%, respectively, but each genome carries hundreds of specific genes (Pedron and Van Gijsegem, 2019). The low number of genomes sequenced, only three, remains insufficient to relate the closeness of the accessory genomes to the geographical origin. Recently, a new *D. undicola* strain was isolated from carrot in Taiwan (Wei et al., 2021) and we identified as *D. undicola* a strain from the CFBP collection isolated from onion in 2005 in Spain (Table 2). These two isolates suggest that *D. undicola* is not only a water species but can also infect plants, perhaps after irrigation with contaminated water. To better understand the *D. undicola* diversity and habitat, it will clearly be interesting to analyze new strains and to sequence the genomes of isolates from diverse origins.

D. chrysanthemi, the type species of the genus *Dickeya*

The species *D. chrysanthemi* is the type species of the genus *Dickeya* (Samson et al., 2005). The type strain was isolated in 1956 from *Chrysanthemum morifolium* displaying signs of soft rot and wilt. Other members of the species have been isolated from various plants, mostly *Chrysanthemum* sp., *Parthenium argentatum*, carnation, sunflower, tobacco, and from several vegetables including potato, tomato, carrot, eggplant, chicory, and artichoke. Several members were also isolated from surface water (Table 6).

At the phenotypic level, *D. chrysanthemi* is unable to grow with D-arabinose as the sole carbon source, a feature shared by a few other *Dickeya* species such as *D. dianthicola*, *D. aquatica*, and *D.*

TABLE 11 Clusters encoding secondary metabolites in the *Dickeya* species.

				Dickeya sp.												*Musicola* sp.	
Cluster	Gene nbr	Product	Activity	Ddad	Dsol	Ddian	Dfang	Dund	Dpoa	Dor	Dpara	Dzeae	Dchrys	Daq	Dlac	Mparad	Mkeen
vfm	26	VFM molecule	quorum-sensing	+	+	+	+	+	+	+	+	+	+	+	+	+	+
		VFM group (s)	VFM analogs	I, IV	III, IV	I	I, III, IV	III, IV	V	II, III	III, IV	III, IV	II, III, IV	IV	IV	VI	VI
cbs	16	chrysobactin	siderophore	+	+	+	+	+	+	+	+	+	+	+	+	+	+
acs	6	achromobactin	siderophore	+	+	+	+	+	+	+	+	+	+	+	+		
ind	3	indigoidin	antioxidant	+	+	+	+	+	+	+	+	+	+	+	_	_	_
sol/ssm	11	solanimycin	antifungal	**v+**	+	_	+	**v+**	+	**v+**	+	+	_	+	_	_	_
ooc	20	oocydin A	antifungal	_	+	+	**v-**	_	_	**v**	_	_	**v**	**v-**	_	+	_
zms	17	zeamine	phytotoxin, antibiotic	_	+	_	+	_	_	**v-**	_	_	_	_	_	_	_
car	8	carbapenem	antibiotic	**v-**	_	_	_	+	_	**v-**	_	**v**	**v+**	+	+	_	_
cfa	10	coronafacic acid	phytotoxin	**v-**	_	_	_	_	+	_	_	_	_	_	_	_	_
cluster A	16	unknown	unknown	_	_	_	_	_	_	_	_	_	_	+	_	_	_
cluster B	9	unknown	unknown	_	_	_	_	_	_	_	_	_	_	_	_	+	_
cluster C	37	unknown	unknown	_	_	_	_	_	_	_	_	_	_	_	_	+	_

Data are given for the sequenced genomes of each species. +, present; - absent; v, variable; v+, variable but mostly present; v- variable but mostly absent.

10.3389/fpls.2023.1168480

*lacus*tris (Table 8). The *D. chrysanthemi* PCWDE equipment is quite typical of the genus *Dickeya*; the genome just lacks the secondary pectinase genes *pnlG* and *pehK*, one *pel* gene of the cluster *pelADE* and the protease gene *prtG* (Table 9).

Phylogenomic data suggest that the species *D. chrysanthemi* contains at least two subclades. Since dDDH values of 69%–70% were observed between most distant members, at the border of the species delimitation; this species clearly includes a high genetic diversity (Table 10). However, although this species has been known for a long time, only eight *D. chrysanthemi* genome sequences are currently available (Table 6); this is insufficient to propose a new classification in this heterogeneous species.

The *Dickeya zeae* complex: *D. oryzae, D. parazeae, D. zeae* and maybe others

Since classification of the strains previously classified as *D. zeae* has recently evolved, the term "*D. zeae* complex" was used to describe all these isolates (Hugouvieux-Cotte-Pattat and Van Gijsegem, 2021). In addition to the species *D. zeae*, the *D. zeae* complex comprises the species *D. oryzae*, initially described for a rice isolate (Wang et al., 2020), and *D. parazeae* whose type strain is a water isolate (Hugouvieux-Cotte-Pattat and Van Gijsegem, 2021). Several genome sequences of strains belonging to the *D. zeae* complex are avaible in public databases but most of the corresponding strains have not been deposited in collections and are not publicly available for phenotypic analyses, restraining their microbiological characterization.

A high diversity was noticed within genomes of the *D. zeae* complex which form distinct clades in phylogenetic analyses (Pedron and Van Gijsegem, 2019). The two main clades includes a group of genomes clustering with the *D. zeae* type strain, and another group clustering with the *D. oryzae* type strain (Figure 1). It should be noted that the majority of strains previously classified as *D. zeae* are reclassified as *D. oryzae* (Table 7; Table S1). In addition, a separate branch is formed by strains of the species D. *parazeae*. The strain CE1 clusters with the strains PL65 and JZL7 isolated from taro and clivia, respectively (Hu et al., 2018; Boluk et al., 2021) (subclade II, Figure 1). These three strains share dDDH values of about 90%, and values of ~68%, ~65% and ~56% with *D. zeae* subclade I (Figure 1), *D. parazeae* and *D. oryzae*, respectively. Thus, they may correspond to a novel species of the *D. zeae* complex and, indeed, strain PL65 was recently proposed as the type strain of a new species, *Dickeya colocasiae* (Boluk et al., 2022), but this classification is not officially recognized. The *D. zeae* strain

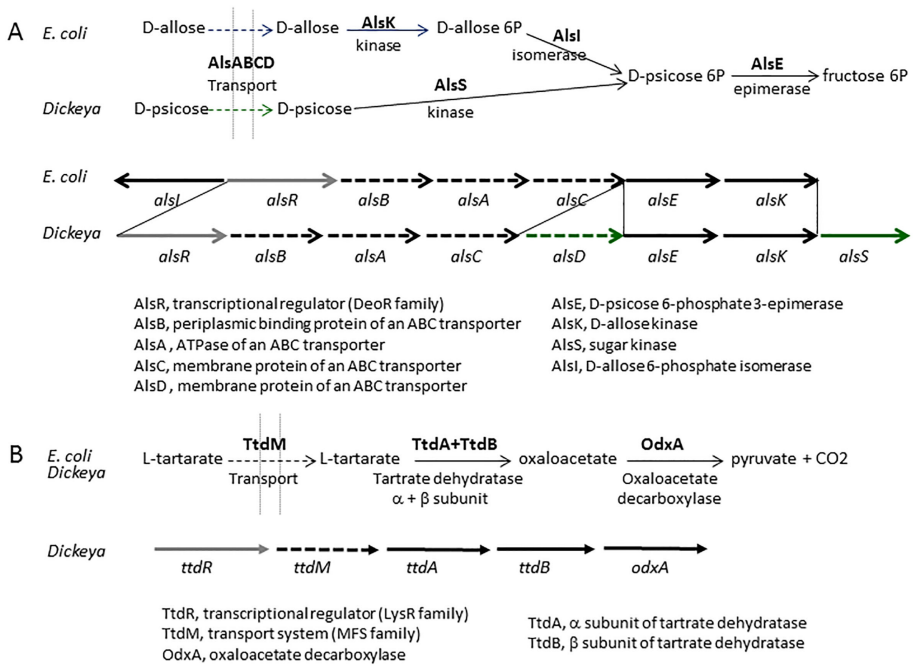

FIGURE 3
The *Dickeya* clusters involved in D-pscicose and L-tartarate catabolism. **(A)** Comparison of the pathways and gene clusters involved in D-allose and D-pscicose utilization in *E. coli* and *Dickeya*, respectively. The *E. coli* cluster involved in D-allose utilization contains the additional gene *alsI*, encoding the isomerase necessary for D-allose assimilation. The *Dickeya* cluster involved in D-pscicose utilization includes two additional genes, encoding a second permease (AlsD) and a second sugar kinase (AlsS). The cluster *alsRBACDEKS* is found in the three *Dickeya* species able to utilize D-pscicose, *D. fangzhongdai, D. oryzae*, and *D. poaceiphila*. **(B)** The L-tartarate catabolic pathway and the *Dickeya* cluster involved in L-tartarate utilization. The three-step pathway of L-tartarate assimilation is biochemically similar in *E. coli* and *Dickeya*. The genes *ttdA* and *ttdB* encode the two subunits of tartrate dehydratase. The *Dickeya* genes *ttdR, ttdM* and *odxA* encode a regulator, a transporter and a decarboxylase which belong to different protein families but are predicted to have similar functions. The cluster *ttdRMABodxA* is found in the different *Dickeya* species able to utilize L-tartarate, namely *D. aquatica, D. fangzhongdai, D. parazeae, D. undicola* and *D. zeae*.

A5410, which was isolated from pineapple (Boluk et al., 2021), also forms a separate branch (Figure 1); it shares dDDH similarities of 66–70% to *D. oryzae*, and 57-58% to *D. zeae* and *D. parazeae*. Strain FVG08, isolated from water is another example of strains not clearly positionned in the phylogenetic tree (Figure 1); it is at the limit of belonging to the species *D. oryzae* with dDDH values of 67.1-69.2% with other *D. oryzae* strains. These examples highlight the residual heterogeneity of the *D. zeae* complex. Interesting, the different *D. oryzae* subclades show some host preference, suggesting an evolution towards host adaptation. The rice strains form a homogeneous subclade also including a millet strain. A second *D. oryzae* branch brings together mostly maize strains. A third branch includes isolates from water and potato; these later may result from contaminations of potato crops by irrigation water (Hugouvieux-Cotte-Pattat and Van Gijsegem, 2021).

The *D. oryzae*, *D. parazeae* and *D. zeae* strains exhibit high secreted pectinase, protease and cellulase activities (Table 8). Their repertoire of PCWDEs is similar to those of the main *Dickeya* clade (Table 9). Differences were observed only for accessory pectinases; the genes encoding PnlH, PemB and RhiF are absent in all genomes of the *D. zeae* complex. The genes encoding PehN and RhiE are absent in *D. parazeae* and *D. oryzae*. Some differences in their virulence equipment disclose particularities of rice strains among *D. oryzae* members. The *D. oryzae* rice strains possess the zeamine cluster *zms*, the gene *pnlG*, and the genes *cyt* encoding entomotoxins but not the glycopeptidase gene *avrL*. In contrast, the other *D. oryzae* strains possess *avrL* but not *zms*, *pnlG*, or *cyt*. The toxin zeamine was shown to be involved in the rice foot rot disease caused by *D. oryzae* (Zhou et al., 2011). Despite its name, zeamine is not produced by *D. zeae* but by *D. solani*, *D. fangzhondai* and some *D. oryzae* strains isolated from rice (Table 11).

A phenotypic difference was observed between *D. oryzae* and *D. zeae* for the assimilation of L-tartarate, a compound abundant in many fruits (Table 8) (Hugouvieux-Cotte-Pattat and Van Gijsegem, 2021). Genomic comparison allowed the identification of the gene cluster *ttdRMAB-odxA* encoding the L-tartarate catabolic pathway in *Dickeya* (Figure 3B). This pathway was previously described in *Salmonella typhimurium* and *Escherichia coli* (Hurlbert and Jakoby, 1965), but the *Dickeya* cluster encodes proteins of different families sharing the same function, indicating a convergent evolution among *Enterobacterales*. The six species *D. zeae*, *D. parazeae D. fangzhongdai*, *D. aquatica*, *D. lacustris* and *D. undicola* are able to assimilate L-tartarate (Table 8). Their genome contains the cluster *ttdRMAB-odxA*, confirming the correlation between phenotypic and genomic data.

To reassign strains previously classified as *D. zeae*, we took advantage of the many available *recA* sequences and we sequenced the *gapA* gene from available strains (Table 7). This study also gives information into the host range or habitat of each species. Most *D. oryzae* isolates come from corn and they are frequently found in potato, rice and water. Most of the *D. zeae* isolates originate from corn, banana, potato, and water. Similarly, the *D. parazeae* strains were mostly isolated from corn and water (Table 7). Thus, members of the *D. zeae* complex are noticeably most common on monocots (corn, rice, banana, pineapple), but also frequent in surface water and in a few dicots, such as potato.

Conclusion

Since the definition of the genus *Dickeya* and the six first historic species *D. chrysanthemi, D. dadantii*, *D. dianthicola, D. dieffenbachiae*, *D. paradisiaca*, and *D. zeae* (Samson et al., 2005), mainly based on phenotypes and 16S rRNA comparison, we recently faced numerous assignation modifications and new species occurrence due to sharp genomic comparisons of known *Dickeya* members, new disease outbreaks, data mining in old collections and enlargement of habitat surveys. Genomic analyses resulted in the re-assignation of *D. paradisiaca* to the new genus *Musicola*. They also led to the split of *D. zeae* into three species and putatively more, given the high diversity among the *D. zeae* members. The severe outbreak in potato crops in Europe in the 2000s led to the identification of the new species *D. solani*. Similarly, *D. fangzhongdai* was described in 2016 after outbreaks in apple trees and in orchids. The atypical species *D. poaceiphila* was described after analysis of the diversity of old strains present in collections. Surveys of surface waters allowed the characterization of three new species, *D. aquatica*, *D. lacustris* and *D. undicola*, absent or rarely present on plants. New investigations in other environments such as soils but also alternative hosts such as insects or nematodes could also expand the range of *Dickeya* diversity. It should also be noted that, apart from the *Musicola* strains isolated almost exclusively in Latin America, international bacterial collections contain very few isolates from Central and South America or Central Africa. Given their climatic particularities, investigations in these underscored geographical locations should also broaden our vision of the *Dickeya* diversity.

Even if they are usually described as pathogens presenting a large host range, some *Dickeya* species seem to have a preference for herbaceous monocots. For instance, *D. poaceiphila* was only isolated from *Poaceae* and members of *D. oryzae*, *D. parazeae* and *D. zeae* were more often isolated from monocots than from dicots (Tables 2, 7). Similarly, *Musicola* members were mostly identified on monocots (banana trees) (Table 1). Pectate lyases are critical virulence factors for causing the soft rot symptoms; as these enzymes have no strict substrate specificity (Hugouvieux-Cotte-Pattat et al, 2014) they allow *Dickeya* to attack a large range of plants. Adaptation to a preferential host may depend on the variety and abundance of PCWDEs. For instance, *D. poaceiphila* has the poorest PCWDE repertoire among *Dickeya* members and shows a low production of pectate lyases that would disfavor the breakdown of the cell walls rich in pectin. *D. poaceiphila* is less well equipped to degrade the high pectin content of dicot cell wall and may be better adapted to monocots whose primary cell wall has low pectin content, such as *Poaceae* (Jarvis et al., 1988). The inactivation of pectin catabolism in *D. poaceiphila* is also a strong argument indicating that pectin degradation has become a secondary virulence factor for this species that produces mostly symptoms of chlorosis and wilting.

Genomic analyses are powerful but not suitable to the first screening of a large number of isolates as they need sequencing facilities and remains costly in time and resources. Thus, the phenotypic analysis of simple growth traits should not be forgotten for a preliminary strain classification (Table 8). In addition, the

sequencing of a quality marker gene, such as *recA* or *gapA* is recommended in order to obtain a reliable taxonomic assignation of newly isolated strains. In any case, a correct classification of phytopathogenic bacteria in genera and species requires many strains of various origins (in terms of host plants, habitats and countries), a phenotypic analysis of these strains and a sufficient number of sequenced genomes to propose a solid phylogeny.

Data availability statement

The original contributions presented in the study are included in the article/Supplementary Material. Further inquiries can be directed to the corresponding author.

Author contributions

NH-C-P – conceptualization of the study, phenotypic analysis, writing, reviewing, and editing of the manuscript. JP – comparative genomics, phylogenetic analysis. FV – genome analysis, writing, reviewing, and editing of the manuscript. All authors contributed to the article and approved the submitted version.

Funding

The work was financially supported by funding of CNRS, University Lyon 1, and INSA Lyon to UMR 5240.

Acknowledgments

We thank Veronique Utzinger for medium preparation and contribution to phenotypic analysis, and the members of the team MTSB (MAP, UMR 5240) for sharing of unpublished information. We also thank Sebastien Santini (CNRS UMR7256) and the PACA Bioinfo platform for the availability and management of the phylogeny.fr website used to construct the *recA* tree.

Conflict of interest

The authors declare that the research was conducted in the absence of any commercial or financial relationships that could be construed as a potential conflict of interest.

Publisher's note

Supplementary material

The Supplementary Material for this article can be found online at: https://www.frontiersin.org/articles/10.3389/fpls.2023.1168480/full#supplementary-material

SUPPLEMENTARY TABLE 1
Complete list of *D. dadantii, D. dianthicola, D. solani, D. fangzhongdai D. oryzae*, and *D. zeae* strains.

SUPPLEMENTARY TABLE 2
List of the genome sequences used in this study with their accession numbers and references.

References

Adeolu, M., Alnajar, S., Naushad, S., and Gupta, R. S. (2016). Genome based phylogeny and taxonomy of the '*Enterobacteriales*': proposal for enterobacterales ord. nov. divided into the families *Enterobacteriaceae, erwiniaceae* fam. nov., *Pectobacteriaceae* fam. nov., *Yersiniaceae* fam. nov., *Hafniaceae* fam. nov., *Morganellaceae* fam. nov., and *Budviciaceae* fam. nov. *Int. J. Syst. Evol. Microbiol.* 66, 5575–5599. doi: 10.1099/ijsem.0.001485

Alic, S., Pedron, J., Dreo, T., and Van Gijsegem, F. (2019). Genomic characterisation of the new dickeya fangzhongdai species regrouping plant pathogens and environmental isolates. *BMC Genomics* 20, 34. doi: 10.1186/s12864-018-5332-3

Alic, S., Tusek-Znidaric, M., Peterka, M., Ravnikar, M., and Dreo, T. (2017). Putative new species of the genus dickeya as major soft rot pathogens in *Phalaenopsis* orchid production. *Plant Pathol.* 66, 1357–1368. doi: 10.1111/ppa.12677

Alic, S., Van Gijsegem, F., Pedron, J., Ravnikar, M., and Dreo, T. (2018). Diversity within the novel dickeya fangzhongdai sp., isolated from infected orchids, water and pears. *Plant Pathol.* 67, 1612–1620. doi: 10.1111/ppa.12866

Aono, Y., Nakayama, T., Ogawa, S., Fujimoto, T., Ohki, T., Oka, N., et al. (2022). *Asteraceae* weeds may be an alternative host of dickeya dianthicola, a causal agent of potato blackleg in Japan. *Eur. J. Plant Pathol.* 63, 257–268. doi: 10.1007/s10658-022-02474-1

Barco, R. A., Garrity, G. M., Scott, J. J., Amend, J. P., Nealson, K. H., and Emerson, D. (2020). A genus definition for bacteria and archaea based on a standard genome relatedness index. *mBio* 11 (1), e02475–e02419. doi: 10.1128/mBio.02475-19

Ben Moussa, H., Bertrand, C., Rochelle-Newall, E., Fiorini, S., Pedron, J., and Barny, M. A. (2022). The diversity of soft rot *Pectobacteriaceae* along the durance river stream in the south-east of France revealed by multiple seasonal surveys. *Phytopathology* 112 (8), 1676–1685. doi: 10.1094/phyto-12-21-0515-r

Blin, P., Robic, K., Khayi, S., Cigna, J., Munier, E., Dewaegeneire, P., et al. (2021). Pattern and causes of the establishment of the invasive bacterial potato pathogen *Dickeya solani* and of the maintenance of the resident pathogen d. *dianthicola. Mol. Ecol.* 30, 608–624. doi: 10.1111/mec.15751

Boluk, G., Arizala, D., Dobhal, S., Zhang, J., Hu, J., Alvarez, A. M., et al. (2021). Genomic and phenotypic biology of novel strains of dickeya zeae isolated from pineapple and taro in Hawaii: insights into genome plasticity, pathogenicity, and virulence determinants. *Front. Plant Sci.* 12, 663851. doi: 10.3389/fpls.2021.663851

Boluk, G., Dobhal, S., Arizala, D., Alvarez, A. M., and Arif, M. (2022). Dickeya colocasiae sp. nov. isolated from wetland taro, *Colocasia esculentum*. *bioRxiv*. doi: 10.1101/2022.01.14.476417

Brady, C. L., Cleenwerck, I., Denman, S., Venter, S. N., Rodríguez-Palenzuela, P., Coutinho, T. A., et al. (2012). Proposal to reclassify *Brenneria quercina* (Hildebrand & schroth 1967) hauben et al. 1999 into a novel genus, *Lonsdalea* gen. nov., as *Lonsdalea quercina* comb. nov., descriptions of *Lonsdalea quercina* subsp. *quercina* comb. nov., *Lonsdalea quercina* subsp. *iberica* subsp. nov., and *Lonsdalea quercina* subsp. *britannica* subsp. nov., emendation of the description of the genus *Brenneria*, reclassification of *Dickeya dieffenbachiae* as *Dickeya dadantii* subsp. *dieffenbachiae* comb. nov., and emendation of the description of *Dickeya dadantii*. *Int. J. Syst. Evol. Microbiol.* 62, 1592–1602. doi: 10.1099/ijs.0.035055-0

Broders, K., Aspin, A., Bailey, J., Chapman, T., Portier, P., and Weir, B. S. (2022). Building more resilient culture collections: a call for increased deposits of plant-associated bacteria. *Microorganisms* 10, 741. doi: 10.3390/microorganisms10040741

Brual, T., Effantin, G., Baltenneck, J., Attaiech, L., Grosbois, C., Royer, M., et al. (2023). A natural single nucleotide mutation in the small regulatory RNA ArcZ of dickeya solani switches off the antimicrobial activities against yeast and bacteria. *PloS Genet.* 19 (4), e1010725. doi: 10.1371/journal.pgen.1010725

Charkowski, A. O. (2018). The changing face of bacterial soft-rot diseases. *Annu. Rev. Phytopathol.* 56, 269–288. doi: 10.1146/annurev-phyto-080417-045906

Charkowski, A., Blanco, C., Condemine, G., Expert, D., Franza, T., Hayes, C., et al. (2012). The role of secretion systems and small molecules in soft-rot *Enterobacteriaceae* pathogenicity. *Annu. Rev. Phytopathol.* 50, 425–449. doi: 10.1146/annurev-phyto-081211-173013

Charnock, S. J., Brown, I. E., Turkenburg, J. P., Black, G. W., and Davies, G. J. (2002). Convergent evolution sheds light on the anti-beta -elimination mechanism common to family 1 and 10 polysaccharide lyases. *Proc. Natl. Acad. Sci. U. S. A.* 99, 12067–12072. doi: 10.1073/pnas.182431199

Cigna, J., Dewaegeneire, P., Beury, A., Gobert, V., and Faure, D. (2017). A *gapA* PCR-sequencing assay for identifying the dickeya and *Pectobacterium* potato pathogens. *Plant Dis.* 101, 1278–1282. doi: 10.1094/PDIS-12-16-1810-RE

Criscuolo, A., and Gascuel, O. (2008). Fast NJ-like algorithms to deal with incomplete distance matrices. *BMC Bioinf.* 9, 166. doi: 10.1186/1471-2105-9-166

Delcher, A. L., Phillippy, A., Carlton, J., and Salzberg, S. L. (2002). Fast algorithms for large-scale genome alignment and comparison. *Nucleic Acids Res.* 30, 2478–2483. doi: 10.1093/nar/30.11.2478

Dereeper, A., Guignon, V., Blanc, G., Audic, S., Buffet, S., Chevenet, F., et al. (2008). Phylogeny.fr: robust phylogenetic analysis for the non-specialist. *Nucleic Acids Res.* 36, W465–W469. doi: 10.1093/nar/gkn180

Dickey, R. S., and Victoria, J. I. (1980). Taxonomy and emended description of strains of erwinia isolated from *Musa paradisiaca* lineaus. *Int. J. Syst. Bacteriol.* 30, 129–134. doi: 10.1099/00207713-30-1-129

Dowson, W. J., and Hayward, A. C. (1960). The bacterial mottle pathogen of Queensland sugar cane. *Intern. Sugar J.* 62, 275.

Drula, E., Garron, M. L., Dogan, S., Lombard, V., Henrissat, B., and Terrapon, N. (2022). The carbohydrate-active enzyme database: functions and literature. *Nucleic Acids Res.* 50 (D1), D571–D577. doi: 10.1093/nar/gkab1045

Duprey, A., Taib, N., Leonard, S., Garin, T., Flandrois, J. P., Nasser, W., et al. (2019). The phytopathogenic nature of *Dickeya aquatica* 174/2 and the dynamic early evolution of dickeya pathogenicity. *Environ. Microbiol.* 21, 2809–2835. doi: 10.1111/1462-2920.14627

Edgar, R. C. (2004). MUSCLE: a multiple sequence alignment method with reduced time and space complexity. *BMC Bioinf.* 32, 1792–1797. doi: 10.1186/1471-2105-5-113

Effantin, G., Brual, T., Rahbé, Y., Hugouvieux-Cotte-Pattat, N., and Gueguen, E. (2021). Dickeya solani d s0432-1 produces an arsenal of secondary metabolites with anti-prokaryotic and anti-eukaryotic activities against bacteria, yeasts, fungi, and aphids. *bioRxiv*. doi: 10.1101/2021.07.19.452942

Fujikawa, T., Ota, N., Sasaki, M., Nakamura, T., and Iwanami, T. (2019). Emergence of apple bacterial quick decline caused by *Dickeya dadantii* in Japan. *J. Gen. Plant Pathol.* 85, 314–319. doi: 10.1007/s10327-019-00852-y

Garlant, L., Koskinen, P., Rouhiainen, L., Laine, P., Paulin, L., Auvinen, P., et al. (2013). Genome sequence of dickeya solani, a new soft rot pathogen of potato, suggests its emergence may be related to a novel combination of non-ribosomal peptide/polyketide synthetase clusters. *Diversity* 5, 824–842. doi: 10.3390/d5040824

Ge, T., Jiang, H., Tan, E. H., Johnson, S. B., Larkin, R. P., Charkowski, A. O., et al. (2021). Pangenomic analysis of dickeya dianthicola strains related to the outbreak of blackleg and soft rot of potato in USA. *Plant Dis.* 105, 3946–3955. doi: 10.1094/PDIS-03-21-0587-RE

Glasner, J. D., Yang, C. H., Reverchon, S., Hugouvieux-Cotte-Pattat, N., Condemine, G., Bohin, J. P., et al. (2011). Genome sequence of the plant-pathogenic bacterium dickeya dadantii 3937. *J. Bacteriol.* 193, 2076–2077. doi: 10.1128/JB.01513-10

Golanowska, M., Potrykus, M., Motyka-Pomagruk, A., Kabza, M., Bacci, G., Galardini, M., et al. (2018). Comparison of highly and weakly virulent *Dickeya solani* strains, with a view on the pangenome and panregulon of this species. *Front. Microbiol.* 9, 1940. doi: 10.3389/fmicb.2018.01940

Goris, J., Konstantinidis, K. T., Klappenbach, J. A., Coenye, T., Vandamme, P., and Tiedje, J. M. (2007). DNA–DNA Hybridization values and their relationship to whole genome sequence similarities. *Int. J. Syst. Evol. Microbiol.* 57, 81–91. doi: 10.1099/ijs.0.64483-0

Guindon, S., and Gascuel, O. (2003). A simple, fast and accurate algorithm to estimate larges phylogenies by maximum likelihood. *Syst. Biol.* 52, 696–704. doi: 10.1080/10635150390235520

Hélias, V., Hamon, P., Huchet, E., van der Wolf, J., and Andrivon, D. (2012). Two new effective semiselective crystal violet pectate media for isolation of pectobacterium and *Dickeya*: isolating pectolytic bacteria on CVP. *Plant Pathol.* 61, 339–345. doi: 10.1111/j.1365-3059.2011.02508.x

Hu, M., Li, J., Chen, R., Li, W., Feng, L., Shi, L., et al. (2018). Dickeya zeae strains isolated from rice, banana and clivia rot plants show great virulence differentials. *BMC Microbiol.* 18, 136. doi: 10.1186/s12866-018-1300-y

Hugouvieux-Cotte-Pattat, N., Brochier-Armanet, C., Flandrois, J. P., and Reverchon, S. (2020). Dickeya poaceaphila sp. nov., a plant-pathogenic bacterium isolated from sugar cane (*Saccharum officinarum*). *Int. J. Syst. Evol. Microbiol.* 70, 4508–4514. doi: 10.1099/ijsem.0.004306

Hugouvieux-Cotte-Pattat, N., Condemine, G., Nasser, W., and Reverchon, S. (1996). Regulation of pectinolysis in erwinia chrysanthemi. *Annu. Rev. Microbiol.* 50, 213–257. doi: 10.1146/annurev.micro.50.1.213

Hugouvieux-Cotte-Pattat, N., Condemine, G., and Shevchik, V. E. (2014). Bacterial pectate lyases, structural and functional diversity. *Environ. Microbiol. Rep.* 6, 427–440. doi: 10.1111/1758-2229.12166

Hugouvieux-Cotte-Pattat, N., des-Combes, C. J., Briolay, J., and Pritchard, L. (2021). Proposal for the creation of a new genus musicola gen. nov., reclassification of *Dickeya paradisiaca* (Samson et al. 2005) as *Musicola paradisiaca* comb. nov. and description of a new species *Musicola keenii* sp. nov. *Int. J. Syst. Evol. Microbiol.* 71, 005037. doi: 10.1099/ijsem.0.005037

Hugouvieux-Cotte-Pattat, N., Jacot-des-Combes, C., and Briolay, J. (2019). Dickeya lacustris sp. nov., a water-living pectinolytic bacterium isolated from lakes in France. *Int. J. Syst. Evol. Microbiol.* 69, 721–726. doi: 10.1099/ijsem.0.003208

Hugouvieux-Cotte-Pattat, N., Royer, M., Gueguen, E., Le Guen, P., Süssmuth, R. D., Reverchon, S., et al. (2022). Allelic variations within the vfm locus define quorum sensing specificity groups in plant pathogenic bacteria of the genus *Dickeya*. *Environ. Microbiol.* 24, 1467–1483. doi: 10.1111/1462-2920.15889

Hugouvieux-Cotte-Pattat, N., and Van Gijsegem, F. (2021). Diversity within the *Dickeya* zeae complex, identification of dickeya zeae and *Dickeya oryzae* members, proposal of the novel species *Dickeya parazeae* sp. nov. *Int. J. Syst. Evol. Microbiol.* 71, 005059. doi: 10.1099/ijsem.0.005059

Hurlbert, R. E., and Jakkoby, W. B. (2022). Tartaric acid metabolism. I. Subunits of L (+)-tartaric acid dehydrase. *J. Biol. Chem.* 240, 2772–2777. doi: 10.1016/0926-6569(64)90298-6

Jarvis, M. C., Forsyth, W., and Duncan, H. J. (1988). A survey of the pectic content of nonlignified monocot cell walls. *Plant Physiol.* 88, 309–314. doi: 10.1104/pp.88.2.309

Kano, A., Hosotani, K., Gomi, K., Yamasaki-Koduko, Y., Shirakawa, C., Fukumoto, T., et al. (2011). D-psicose induces upregulation of defense-related genes and resistance in rice against bacterial blight. *J. Plant Physiol.* 168, 1852–1857. doi: 10.1016/j.jplph.2011.04.003

Khayi, S., Blin, P., Pedron, J., Chong, T. M., Chan, K. G., Moumni, M., et al. (2015). Population genomics reveals additive and replacing horizontal gene transfers in the emerging pathogen *Dickeya solani*. *BMC Genom.* 16, 788. doi: 10.1186/s12864-015-1997-z

Khayi, S., Chan, K. G., and Faure, D. (2022). Patterns of genomic variations in the plant pathogen dickeya solani. *Microorganisms* 10, 2254. doi: 10.3390/microorganisms10112254

Liu, Y., Tyler, C., Helmann, T. C., Stodghill, P., and Filiatrault, M. J. (2021). Complete genome sequence resource for the necrotrophic plant pathogenic bacterium *Dickeya dianthicola* 67-19 isolated from new Guinea impatiens. *Plant Dis.* 105, 1174–1176. doi: 10.1094/PDIS-09-20-1968-A

Mansfield, J., Genin, S., Magori, S., Citovky, V., Sriariyanum, M., Ronald, P., et al. (2012). Top 10 plant pathogenic bacteria in molecular plant pathology. *Mol. Plant Pathol.* 13, 614–629. doi: 10.1111/j.1364-3703.2012.00804.x

Matilla, M. A., Monson, R. E., Murphy, A., Schicketanz, M., Rawlinson, A., Duncan, C., et al. (2022). Solanimycin: biosynthesis and distribution of a new antifungal antibiotic regulated by two quorum-sensing systems. *mBio* 13 (6), e0247222. doi: 10.1128/mbio.02472-22

Meier-Kolthoff, J. P. M., Auch, A. F., Klenk, H. P., and Göker, M. (2013). Genome sequence-based species delimitation with confidence intervals and improved distance functions. *BMC Bioinf.* 14, 60. doi: 10.1186/1471-2105-14-60

Nasser, W., Dorel, C., Wawrzyniak, J., Van Gijsegem, F., Groleau, M. C., Déziel, E., et al. (2013). Vfm a new quorum sensing system controls the virulence of *Dickeya dadantii*. environ. *Microbiol* 15, 865–880. doi: 10.1111/1462-2920.12049

Ossowska, K., Czerwicka, M., Sledz, W., Zoledowska, S., Motyka, A., Golanowska, M., et al. (2017). The uniform structure of O-polysaccharides isolated from dickeya solani strains of different origin. *Carbohydr. Res.* 445, 40–43. doi: 10.1016/j.carres.2017.04.001

Oulghazi, S., Pedron, J., Cigna, J., Lau, Y. Y., Moumni, M., Van Gijsegem, F., et al. (2019). Dickeya undicola sp. nov., a novel species for pectinolytic isolates from surface waters in Europe and Asia. *Int. J. Syst. Evol. Microbiol.* 69, 2440–2444. doi: 10.1099/ijsem.0.003497

Parkinson, N., DeVos, P., Pirhonen, M., and Elphinstone, J. (2014). Dickeya aquatica sp. nov., isolated from waterways. *Int. J. Syst. Evol. Microbiol.* 64, 2264–2266. doi: 10.1099/ijs.0.058693-0

Parkinson, N., Stead, D., Bew, J., Heene, J., Tsror Lahkim, L., and Elphinstone, J. (2009). *Dickeya* species relatedness and clade structure determined by comparison of *recA* sequences. *Int. J. Syst. Evol. Microbiol.* 59, 2388–2393. doi: 10.1099/ijs.0.009258-0

Pedron, J., Mondy, S., Raoul des Essarts, Y., Van Gijsegem, F., and Faure, D. (2014). Genomic and metabolic comparison with *Dickeya dadantii* 3937 reveals the emerging dickeya solani potato pathogen to display distinctive metabolic activities and T5SS/T6SS-related toxin repertoire. *BMC Genom.* 15, 283. doi: 10.1186/1471-2164-15-283

Pedron, J., Schaerer, S., Kellenberger, I., and Van Gijsegem, F. (2021). Early emergence of dickeya solani revealed by analysis of *Dickeya* diversity of potato blackleg and soft rot causing pathogens in Switzerland. *Microorganisms* 9, 1187. doi: 10.3390/microorganisms9061187

Pedron, J., van der Wolf, J. M., Portier, P., Caullireau, E., and Van Gijsegem, F. (2022). The broad host range plant pathogen dickeya dianthicola shows a high genetic diversity. *Microorganisms* 10, 1024. doi: 10.3390/microorganisms10051024

Pedron, J., and Van Gijsegem, F. (2019). Diversity in the bacterial genus dickeya grouping plant pathogens and waterways isolates. *OBM Genet.* 3 (4), 098. doi: 10.21926/obm.genet.1904098

Portier, P., Pedron, J., Taghouti, G., Dutrieux, C., and Barny, M.-A. (2020). Updated taxonomy of pectobacterium genus in the CIRM-CFBP bacterial collection: when newly described species reveal "old" endemic population. *Microorganisms* 8, 1441. doi: 10.3390/microorganisms8091441

Potrykus, M., Golanowska, M., Sledz, W., Zoledowska, S., Motyka, A., Kolodziejska, A., et al. (2016). Biodiversity of dickeya spp. isolated from potato plants and water sources in temperate climate. *Plant Dis.* 100, 408–417. doi: 10.1094/PDIS-04-15-0439-RE

Pritchard, L., Glover, R. H., Humphris, S., Elphinstone, J. G., and Toth, I. K. (2016). Genomics and taxonomy in diagnostics for food security: soft-rotting enterobacterial plant pathogens. *Anal. Methods* 8, 12–24. doi: 10.1039/C5AY02550H

Pritchard, L., Humphris, S., Saddler, G. S., Elphinstone, J. G., Pirhonen, M., and Toth, I. K. (2013). Draft genome sequences of 17 isolates of the plant pathogenic bacterium *Dickeya*. *Genome Announc* 1 (6), e00978–e00913. doi: 10.1128/genomeA.00978-13

Reverchon, S., Muskhelisvili, G., and Nasser, W. (2016). Virulence program of a bacterial plant pathogen: the dickeya model. *Prog. Mol. Biol. Transl. Sci.* 142, 51–92. doi: 10.1016/bs.pmbts.2016.05.005

Richter, M., and Rosselló-Móra, R. (2009). Shifting the genomic gold standard for the prokaryotic species definition. *Proc. Natl. Acad. Sci. U.S.A.* 106, 19126–19131. doi: 10.1073/pnas.0906412106

Samson, R., Legendre, J. B., Christen, R., Fischer-Le Saux, M., Achouak, W., and Gardan, L. (2005). Transfer of *Pectobacterium chrysanthemi* (Burkholder et al 1953) Brenner et al. 1973 and *Brenneria paradisiaca* to the genus *Dickeya* gen. nov. as *Dickeya chrysanthemi* comb. nov. and *Dickeya paradisiaca* comb. nov. and delineation of four novel species, *Dickeya dadantii* sp. nov., *Dickeya dianthicola* sp. nov., *Dickeya dieffenbachiae* sp. nov. and *Dickeya zeae* sp. nov. *Int. J. Syst. Evol. Microbiol.* 55, 1415–1427. doi: 10.1099/ijs.0.02791-0

Slawiak, M., van Beckhoven, J. R. C. M., Speksnijde, A. G. C. L., Czajkowski, R. L., Grabe, G., and van der Wolf, J. M. (2009). Biochemical and genetical analysis reveal a new clade of biovar 3 dickeya spp. strains isolated from potato in Europe. *Eur. J. Plant Pathol.* 125, 245–261. doi: 10.1007/s10658-009-9479-2

Steindl, D. R. L. (1964). "Bacterial mottle," in *Sugar cane diseases of the world*. Eds. C. G. Hughes, E. V. Abbott and C. A. Wismer (New York: Elsevier Publishing Company) 2, 2–11.

Suharjo, R., Sawada, H., and Takikawa, Y. (2014). Phylogenetic study of Japanese dickeya spp. and development of new rapid identification methods using PCR–RFLP. *J. Gen. Plant Pathol.* 80, 237–254. doi: 10.1007/s10327-014-0511-9

Tan, C., Li, C., Hu, M., Hu, A., Xue, Y., Zhou, X., et al. (2022). Comparative pathogenomic analysis of two banana pathogenic *Dickeya* strains isolated from China and the Philippines. *Int. J. Mol. Sci.* 23, 12758. doi: 10.3390/ijms232112758

Tian, Y., Zhao, Y., Yuan, X., Yi, J., Fan, J., Xu, Z., et al. (2016). *Dickeya fangzhongdai* sp. nov., a plant-pathogenic bacterium isolated from pear trees (*Pyrus pyrifolia*). *Int. J. Syst. Evol. Microbiol.* 66, 2831–2835. doi: 10.1099/ijsem.0.001060

Toth, I. K., Barny, M., Brurberg, M. B., Condemine, G., Czajkowski, R., Elphinstone, J. G., et al. (2021). "Pectobacterium and dickeya: environment to disease development," in *Plant diseases caused by dickeya and pectobacterium species*. Eds. F. Van Gijsegem, J. M. van der Wolf and I. K. Toth (Cham, Switzerland: Springer International Publishing), 39–84.

Toth, I. K., van der Wolf, J. M., Saddler, G., Lojkowska, E., Hélias, V., Pirhonen, M., et al. (2011). Dickeya species: an emerging problem for potato production in Europe. *Plant Pathol.* 60, 385–399. doi: 10.1111/j.1365-3059.2011.02427.x

van der Wolf, J., Acuña, I., De Boer, S. H., Brurberg, M. B., Cahill, G., Charkowski, A. O., et al. (2021). "Diseases caused by pectobacterium and dickeya species around the world," in *Plant diseases caused by dickeya and pectobacterium species*. Eds. F. Van Gijsegem, J. M. van der Wolf and I. K. Toth (Cham, Switzerland: Springer International Publishing), 215–270.

van der Wolf, J. M., Nijhuis, E. H., Kowalewska, M. J., Saddler, G. S., Parkinson, N., Elphinstone, J. G., et al. (2014). *Dickeya solani* sp. nov., a pectinolytic plant-pathogenic bacterium from potato (*Solanum tuberosum*). *Int. J. Syst. Evol. Microbiol.* 64, 768–774. doi: 10.1099/ijs.0.052944-0

Van Gijsegem, F., Hugouvieux-Cotte-Pattat, N., Kraepiel, Y., Lojkowska, E., Moleleki, L. N., Gorshkov, V., et al. (2021). "Molecular interactions of pectobacterium and dickeya with plants," in *Plant diseases caused by dickeya and pectobacterium species*. Eds. F. Van Gijsegem, J. M. van der Wolf and I. K. Toth (Cham, Switzerland: Springer International Publishing), 85–147.

Van Vaerenbergh, J., Baeyen, S., De Vos, P., and Maes, M. (2012). Sequence diversity in the dickeya fliC gene: phylogeny of the *Dickeya* genus and TaqMan PCR for '*D. solani*', new biovar 3 variant on potato in Europe. *PloS One* 7, e35738. doi: 10.1371/journal.pone.0035738

Wang, X., He, S. W., Guo, H. B., Han, J. G., Thin, K. K., Gao, J. S., et al. (2020). *Dickeya oryzae* sp. nov., isolated from the roots of rice. *Int. J. Syst. Evol. Microbiol.* 70, 4171–4178. doi: 10.1099/ijsem.0.004265

Wei, X.-Y., Deng, W.-L., and Chu, C.-C. (2021). Phylogenetic and phenotypic analyses on dickeya spp. isolated from different host plants in Taiwan. *J. Phytopathol.* 169, 678–691. doi: 10.1111/jph.13038

Wright, D., Bwye, A., Banovic, M., Baulch, J., Wang, C., Hair, S., et al. (2018). First report of dickeya dianthicola in potatoes in Australia. *Plant Dis.* 102, 2029. doi: 10.1094/PDIS-01-18-0094-PDN

Zaczek-Moczydłowska, M. A., Fleming, C. C., Young, G. K., Campbell, K., and Hanlon, R. O. (2019). *Pectobacterium* and *Dickeya* species detected in vegetables in northern Ireland. *Eur. J. Plant Pathol.* 154, 635–647. doi: 10.1007/s10658-019-01687-1

Zhou, J., Zhang, H., Wu, J., Liu, Q., Xi, P., Lee, J., et al. (2011). A novel multidomain polyketide synthase is essential for zeamine production and the virulence of dickeya zeae. *Mol. Plant Microbe Interact.* 24, 1156–1164. doi: 10.1094/MPMI-04-11-0087

frontiers | Frontiers in Plant Science

TYPE Original Research
PUBLISHED 05 July 2023
DOI 10.3389/fpls.2023.1197706

OPEN ACCESS

EDITED BY
Prem Lal Kashyap,
Indian Institute of Wheat and Barley Research (ICAR), India

REVIEWED BY
Rikky Rai,
University of Allahabad, India
Satyendra Pratap Singh,
National Botanical Research Institute (CSIR), India
Yasmina Jaufeerally Fakim,
University of Mauritius, Mauritius

*CORRESPONDENCE
Chiaraluce Moretti
chiaraluce.moretti@unipg.it
Theo H. M. Smits
theo.smits@zhaw.ch

RECEIVED 31 March 2023
ACCEPTED 19 June 2023
PUBLISHED 05 July 2023

CITATION
Orfei B, Pothier JF, Fenske L, Blom J, Moretti C, Buonaurio R and Smits THM (2023) Race-specific genotypes of *Pseudomonas syringae* pv. tomato are defined by the presence of mobile DNA elements within the genome. *Front. Plant Sci.* 14:1197706. doi: 10.3389/fpls.2023.1197706

Race-specific genotypes of *Pseudomonas syringae* pv. tomato are defined by the presence of mobile DNA elements within the genome

Benedetta Orfei[1], Joël F. Pothier[2], Linda Fenske[3], Jochen Blom[3], Chiaraluce Moretti[1]*, Roberto Buonaurio[1] and Theo H. M. Smits[2]*

[1]Dipartimento di Scienze Agrarie, Alimentari e Ambientali (DSA3), Università degli Studi di Perugia, Perugia, Italy, [2]Environmental Genomics and Systems Biology Research Group, Institute of Natural Resource Sciences (IUNR), Zurich University of Applied Sciences ZHAW, Wädenswil, Switzerland, [3]Bioinformatics and Systems Biology, Justus-Liebig University Giessen, Giessen, Germany

Pseudomonas syringae pv. tomato is the causal agent of bacterial speck of tomato, an important disease that results in severe crop production losses worldwide. Currently, two races within phylogroup 01a (PG01a) are described for this pathogen. Race 0 strains have avirulence genes for the expression of type III system-associated effectors AvrPto1 and AvrPtoB, that are recognized and targeted by the effector-triggered immunity in tomato cultivars having the *pto* race-specific resistance gene. Race 1 strains instead lack the *avrPto1* and *avrPtoB* genes and are therefore capable to aggressively attack all tomato cultivars. Here, we have performed the complete genome sequencing and the analysis of *P. syringae* pv. tomato strain DAPP-PG 215, which was described as a race 0 strain in 1996. Our analysis revealed that its genome comprises a 6.2 Mb circular chromosome and two plasmids (107 kb and 81 kb). The results indicate that the strain is phylogenetically closely related to strains Max13, K40, T1 and NYS-T1, all known race 1 strains. The chromosome of DAPP-PG 215 encodes race 1-associated genes like *avrA* and *hopW1* and lacks race 0-associated genes like *hopN1*, giving it a race 1 genetic background. However, the genome harbors a complete ortholog of *avrPto1*, which allows the strain to display a race 0 phenotype. Comparative genomics with several PG01a genomes revealed that mobile DNA elements are rather involved in the evolution of the two different races.

KEYWORDS

***Pseudomonas avellanae*, *Pseudomonas syringae* pv. tomato, comparative genomics, AvrPto1, AvrPtoB, race shift**

1 Introduction

Bacterial speck is one of the most widespread and economically important disease of tomato (Schneider & Grogan, 1977). Its symptoms affect leaves, flowers, fruits and stems of the plant and consist in small, irregular dark brown to black necrotic spots (Goode & Sasser, 1980). Usually surrounded by a yellow halo (green in the fruit), these spots can converge in the leaves as they appear, increasing the necrotic area of the foliage, and thus leading to plant death. Yield losses for outbreaks of this disease could be around 20-25% for tomato seedlings and up to 75% for tomato fruits (Yunis et al., 1980; Basim et al., 2004). The causative agent of the disease is *Pseudomonas syringae* pv. tomato, a Gram-negative, rod-shaped bacteria ubiquitously widespread in all tomato crop growing areas. It is a member of the *P. syringae* species complex, one of the most relevant groups of phytopathogenic bacteria (Mansfield et al., 2012) with its 15 species assigned to 13 different phylogroups (PGs) (Berge et al., 2014). *P. syringae* pv. tomato falls into one of the two clades of the phylogroup 01 (PG01a), while in the other clade (PG01b), *Pseudomonas avellanae* and *P. syringae* pv. actinidiae are included.

In order to begin its cycle of infection and cause disease, *P. syringae* pv. tomato can occur as a consequence of natural phenomena like rain and wind, water irrigation, and also due to the use of contaminated seeds. As an epiphyte, *P. syringae* pv. tomato can survive and grow on the surface of the leaves and the seeds. Then, when the environmental conditions are favorable, it can rapidly increase its population and enter the host plant trough natural openings or wounds exploiting its polar flagella.

Inside the plant, the apoplast is the niche used by *P. syringae* pv. tomato for its colonization and subsequentially infection (Melotto et al., 2008). Pathogenicity and virulence of *P. syringae* pv. tomato largely rely on the use of the Hrp (hypersensitive response and pathogenicity) Type III Secretion System (T3SS) and its Type III Effectors (T3Es) like Hop (Hrp outer protein) or Avr (avirulence) proteins, as well as the production of the phytotoxin coronatine. In *P. syringae* pv. tomato DC3000, the genes *hopM1* and *avrE1* are both required for the establishment of an aqueous environment in the apoplast that promotes growth and thus colonization of the pathogen, while *avrPto1* and *avrPtoB* suppress the pattern-triggered immunity (PTI) of the plant, usually elicited by a structural component of the bacteria flagellum, flagellin, encoded by *fliC* (He et al., 2016).

The discovery and subsequent cloning in cultivated tomato strains of the *pto* gene, encoding a serine-threonine kinase capable of recognizing both the AvrPto1 and AvrPtoB protein effectors and activating the effector-triggered immunity (ETI) of the host (Xiao et al., 2007; Kunkeaw et al., 2010), allowed some control of the disease for a few decades. However, the emergence of *P. syringae* pv. tomato strains lacking functioning AvrPto1 and AvrPtoB effectively rendered the protection offered by Pto ineffective and allowed the establishment of a new race (race 1) of *P. syringae* pv. tomato capable of causing disease even in plants that carries the *pto* gene. Even today, the capability to cause disease in resistant tomato plants is the basis of the race assignment process for *P. syringae* pv. tomato, although there are useful genotypic markers to differentiate between the two different races (Jones et al., 2015). Moreover, strains of *P. syringae* pv. tomato expressing an intermediate phenotype between race 0 and race 1 strains have been characterized as well (Kraus et al., 2017).

P. syringae pv. tomato strain DAPP-PG 215 was obtained by isolation from an individual lesion on a diseased tomato plant, randomly selected from a field with tomato cultivar 'Erminia F1' (Petoseed) in Pontenure (Piacenza, Italy) in 1995 by Buonaurio et al. (1996) and described as race 0 following inoculation on resistant Ontario 7710 plants. In this study, the sequencing and genome analysis of this strain was performed and, according to the *in silico* results, we propose a different base for *P. syringae* pv. tomato race determination.

2 Materials and methods

2.1 Bacterial strain and growth conditions

Pseudomonas syringae pv. tomato strain DAPP-PG 215 belongs to the bacterial collection of the Plant Protection Unit, Department of Agricultural, Food and Environmental Sciences, University of Perugia, Italy, where it is stored in a -80°C ultrafreezer as glycerol stocks in 50% (*vol*/*vol*) King's broth (King et al., 1954). For genome sequencing, strain DAPP-PG 215 was transferred on Luria-Bertani (LB) agar plates (Miller, 1972) and incubated at 28°C overnight; then, an isolated colony was streaked onto the same medium and grown in the same manner. Bacterial strains used for screening were instead grown on nutrient agar (NA) plates and then incubated at 27°C for 12 h.

2.2 Whole genome sequencing, assembly, and annotation

For genomic DNA (gDNA) extraction, *P. syringae* pv. tomato strain DAPP-PG 215 was inoculated in LB broth (Miller, 1972) from single colony of a pure bacterial culture on a LB plate and incubated overnight at 28°C. The following day, whole gDNA extraction was performed using the NucleoSpin tissue kit (Macherey-Nagel, Düren, Germany) according to the manufacturer's protocol with the following specifications: elution buffer was preheated at 70°C before use, and the gDNA was eluted in 60 µL. The gDNA was quantified using a high sensitivity double-stranded DNA (dsDNA) assay (DeNovix, Wilmigton, DE) with a Fluo-100B fluorometer (Allsheng, Hangzhou, China).

Library preparation for short-read sequencing was done using the Nextera XT DNA library prep kit (Illumina, San Diego, CA) following the manufacturer's instructions. Sequencing was performed on a MiSeq Illumina sequencer with 2×300-bp paired-end reads using a MiSeq reagent kit version 3 (Illumina, San Diego, CA) according to the manufacturer's instructions.

For long-read sequencing, the Gentra PureGene Yeast/Bact kit protocol (Qiagen, Hilden, Germany) was used on an overnight bacterial culture for the gDNA extraction. The gDNA was quantified as described above. Library preparation and

sequencing were performed with the ligation sequencing kit (catalog no. SQK-LSK109; Oxford Nanopore Technologies, Oxford, United Kingdom) and run on an R9.4.1 Flongle Flow Cell with a MinION sequencer. The native barcoding expansion kit (catalog no. XP-NBD114; Oxford Nanopore Technologies, Oxford, United Kingdom) was used for multiplexing. Base calling was performed using Guppy version 5.0.11.

A hybrid assembly using the MiSeq and MinION reads was conducted with Unicycler version 0.4.9 (Wick et al., 2017). The genome was then annotated using Bakta version 1.2.4 (Schwengers et al., 2021) and the database version 3.0. All tools were run with default parameters unless otherwise specified. The BioCircos tool (Cui et al., 2016) was used to have a circular visualization of genomic data.

2.3 Identification of mobile regions

The genome of *P. syringae* pv. tomato strain DAPP-PG 215 was checked for the presence of potential prophage regions using the search tool PHASTER (Zhou et al., 2011; Arndt et al., 2016). It was thus possible to identify the prophage regions contained in the genome and to have them classified according to their level of completeness into incomplete, questionable, and intact. Genomic island (GI) prediction was carried out using IslandViewer 4 (Bertelli et al., 2017). The homology search of the proteins localized in these regions was performed by BLAST+ v. 2.13.0 (Camacho et al., 2009) using the National Center for Biotechnology Information (NCBI) database.

2.4 Selection of genome sequences and comparative analysis

Comparative genome analyses were performed on a total of 72 genomes taken from the *P. syringae* species complex and representatives of seven phylogroups according to Berge et al. (2014), plus *P. syringae* PDD-32b-74 and *P. syringae* pv. tomato DAPP-PG 215 (Table S1). Genome sequences were taken from the NCBI RefSeq database (http://www.ncbi.nlm.nih.gov) and added to an EDGAR 3.0 database (Dieckmann et al., 2021). Through the EDGAR platform, the core genome phylogenetic tree was constructed. Briefly, for the core genome of the 74 selected genomes, the EDGAR pipeline made an alignment for each of the 1,969 gene sets of the core genome using the MUSCLE software (Edgar, 2004). The resulting alignments for 145,706 genes in total were then concatenated into one multiple alignment of 753,574 AA-residues per genome, 55,764,476 AA-residues in total. This large alignment was submitted as input to FastTree 2 software (Price et al., 2010) within EDGAR 3.0, which processed a maximum likelihood phylogenetic tree and verified the tree topology using the Shimodaira-Hasegawa test.

Based on the phylogenetic tree obtained by comparing the core genomes of all strains in Table S1, the genomes belonging to PG01a were divided into five different subgroups (Figure 1). Using the subroutine in EDGAR 3.0, five meta-core genomes representing the core genome of all strains included in each subgroup were defined. Subsequently, the EDGAR pipeline was used to perform a comparison of the different meta-core genomes, in order to reveal the presence of orthologous genes for each subgroup. Protein

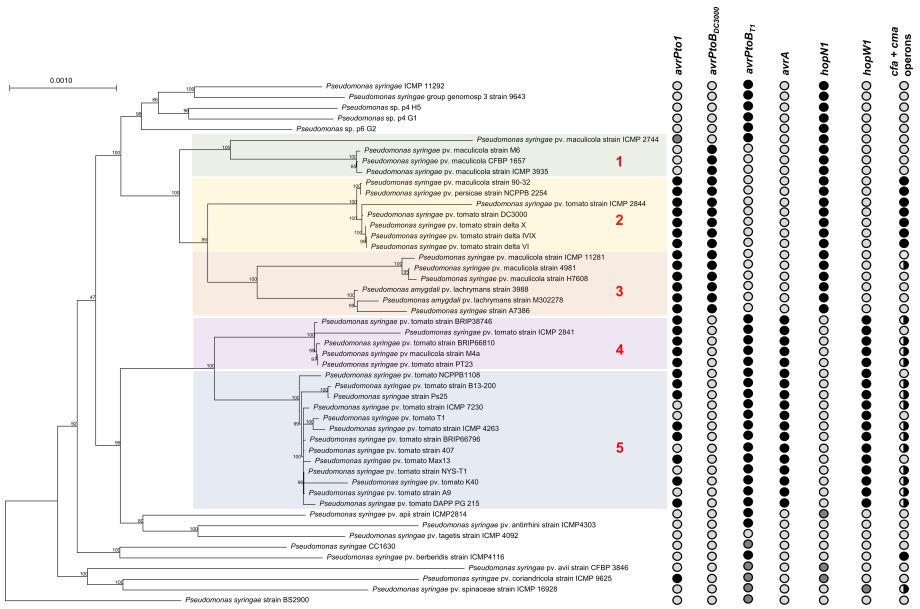

FIGURE 1
Subgroups defined according to core phylogeny for later comparative analysis. The green branch represents the first subgroup; the yellow branch represents the second subgroup; the orange branch represents the third subgroup; the pink branch represents the fourth subgroup; the blue branch represents the fifth subgroup. Dots in the right part of the figure are meant to show the absence or the presence of avirulence (*avr*) and Hrp-dependent outer protein (*hop*) genes *avrPto1*, *avrPtoB*$_{DC3000}$, *avrPtoB*$_{T1}$, *avrA*, *hopN1* and *hopW1*, and of coronatine synthesis genes belonging to the *cfa* and *cma* clusters. Dot filling indicates the presence with high sequence identity (black), the presence with low sequence identity (dark grey) and absence of the genes (white); half-filled dots for the coronatine genes indicates presence of these genes with a plasmid origin.

sequences resulting from all the comparisons were then displayed in a Venn diagram.

2.5 Distribution of avirulence gene *avrPto1* and *avrPtoB*

To test whether there was a different distribution of the *avrPto1* and *avrPtoB* genes in the selected genomes, a pan-genome analysis of all strains was performed in EDGAR 3.0. Annotation gaps were checked using BLASTX (Altschul et al., 1990) and compared to a database of bacterial reference proteins (Refseq_proteins) restricted to "*Pseudomonas syringae* group (taxid:136849)". Standard settings were used for all other parameters. Nucleotide sequences corresponding to each identified gene were used to analyze the phylogenetic relationship existing between the selected genomes and those containing *avrPto1* and *avrPtoB* genes. The resulting phylogenetic trees were carried out with Molecular Evolutionary Genetics Analysis v11 (MEGA11) software (Tamura et al., 2021), according to the neighbor-joining method (Saitou & Nei, 1987). To model rates amongst sites, a gamma distribution ($\alpha = 5$) was used and a partial deletion consisting in a 95% cut-off of the site coverage was applied to gaps and missing data. Furthermore, alignments from the MUSCLE algorithm were also checked for protein identity and coverage with NCBI Multiple Sequence Alignment Viewer 1.22.2 (MSA) using *P. syringae* pv. tomato DAPP-PG 215 sequences as anchor.

The presence of potential prophages was also assessed for all the strains carrying the gene *avrPto1* using PHASTER (Zhou et al., 2011; Arndt et al., 2016) and visualized with MAUVE v2.4.0 (Darling et al., 2004).

2.6 Data availability

The genome sequence of *P. syringae* pv. tomato DAPP-PG 215 were submitted to EMBL and received the Assembly accession number GCA_949769235. Additional genome sequences analyzed within this study are available in the NCBI GenBank/DDJ/EMBL database under the accession numbers detailed in Table S1. The original contributions presented in the study are publicly available. This data can be found here: NCBI, PRJEB59188, OX458335-7.

3 Results

3.1 Whole genome general features

The complete genome of *P. syringae* pv. tomato DAPP-PG 215 consists of a 6,218,123 bp circular chromosome and two circular plasmids of 106,705 bp (p107) and 80,902 bp (p81), with a GC content of 59%, 58% and 57%, respectively (Figure 2). The 6.2 Mb chromosome comprises of 5,595 protein coding sequences (CDS), while plasmids p107 and p81 have 103 and 92 CDS, respectively. In the whole genome, 642 CDS were identified as hypothetical proteins, and 72 predicted tRNAs and 5 rRNA operons were found. Among the most prominent genomic features for the characterization of strain DAPP-PG 215 is the presence of the avirulence genes *avrPto1* and *avrPtoB*, but also of the effector genes *hopW1* and *avrA*, which are considered as diagnostic markers for race 1 (Jones et al., 2015), while the *hopN1* gene (a diagnostic marker for race 0 strains), was missing (Figure 1). Gene clusters for the biosynthesis of coronafacic acid and coronamic acid, precursors of the phytotoxin coronatine, *hopK1* and a type VI Hcp1 effector gene were detected within plasmid p107, while in plasmid p81, effector genes *avrD1*, *hopD1* and *hopQ1-1* were found.

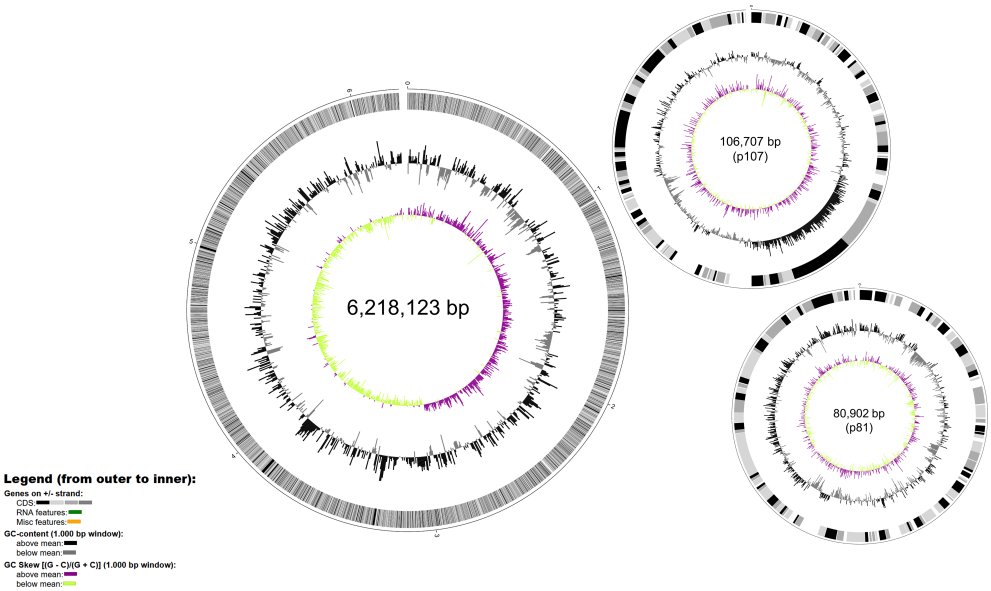

FIGURE 2
Map of the genome of *Pseudomonas syringae* pv. tomato DAPP-PG 215 generated with BioCircos. In the outermost ring, identified CDS are in grey, RNA features in green and miscellaneous features are in orange. In the intermediate ring GC content in grey and the innermost ring represents the GC skew above the mean in purple and GC skew below the mean in green.

Analysis of the DNA mobile regions using PHASTER indicated a total of nine prophages in the chromosome and two in plasmid p107. Information related to their size and their completeness level can be found in Table S2. Most of the prophages detected were taxonomically similar to phage families belonging to the class *Caudoviricetes* such as *Myoviridae*, *Podoviridae* and *Siphoviridae* (Iwasaki et al., 2018). Within prophage region 9 (PR-9, from position 5,843,821 to 5,884,716), the *avrPto1* gene is located. Genomic islands (GIs), clusters of genes obtained by horizontal gene transfer, were also found in both the chromosome and the plasmids of strain DAPP-PG 215. In the chromosome, a total of 44 GIs were detected by IslandViewer 4 (with the SIGI-HMM prediction method); while two and a single GIs were predicted for plasmids p107 and p81, respectively (Table S2). Most of the GIs contained transposases, integrases, phage-related genes and hypothetical protein-coding genes. However, genes for protein effectors associated with the type III secretion system were annotated within the first GI on plasmid p81 and in six GIs on the chromosome. More specifically, effector genes *hopD1* and *hopQ1-1* within both GI-10 and GI-46, *hop-T1* in GI-13, *hopF2* in GI-16, *hopC1* in GI-23, *hopAF1* in GI-32, *hopT1-2* and *hopS* in GI-35 were predicted. Genes associated with arsenic resistance such as *arsC* and *arsN1* were found within GI-6, while in GI-4 the algorithm detected the presence of two fluoride exporters (*eriC* and *crcB*).

3.2 Phylogenomic analysis

Phylogenomic analysis conducted using the core genomes of the 74 strains listed in Table S1 has confirmed the correctness of the phylogroup clustering made by Berge et al. (2014) and revealed that strain DAPP-PG 215 is part of the PG01a, as well as the other *P. syringae* pv. tomato strains used for the comparison (Figure S1). Furthermore, looking more closely at the clustering of PG01a, it is possible to see that the *P. syringae* pv. tomato strains are divided into two different subgroups: in the first group, race 0 strain DC3000 was found along with strain ICMP 2844, *P. syringae* pv. persicae NCPPB 2254, *P. syringae* A7386 and a few strains of *P. syringae* pv. maculicola and *P. amygdali* pv. lachrymans while in the second group, several known strains of *P. syringae* pv. tomato race 1 such as strains T1, NYS-T1, Max13, K40 and NCPPB 1108, but also *P. syringae* pv. maculicola M4a, were identified. Strain DAPP-PG 215 was included within the second subgroup. This finding confirms again the greater genotypic proximity of this strain to race 1 P. *syringae* pv. tomato strains.

3.3 Comparative genomics

By comparing the five representative meta-core genomes of the subgroups defined in Figure 1, it was possible to identify which and how many orthologous genes were shared among the different subgroups and which genes were instead distinctive for each of them (Figure 3). A total number of 5,496 CDS were retrieved from the analysis, of which 3,177 (57.8%), 1,642 (29.9%) and 677 (12.3%) were assigned as core genome, disposable and singleton components, respectively. Among the latter, the distinctive proteins for each subset ranged from 74 (subgroup 1) to 269 (subgroup 4). Mostly, the singletons for each subgroup were hypothetical proteins and transposable elements. However, within

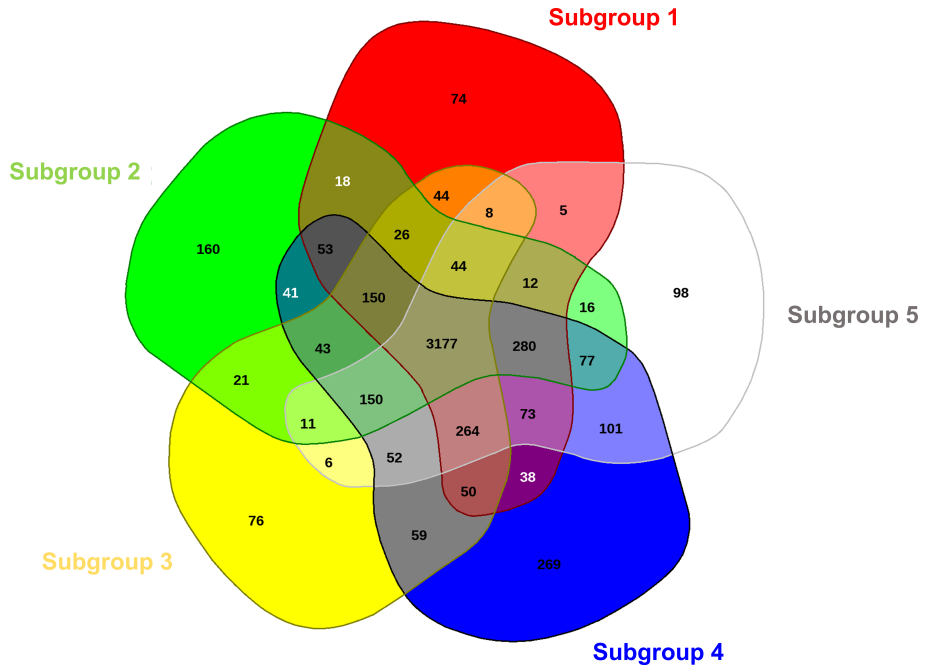

FIGURE 3
Comparative analysis of the meta-core-genomes of five different defined groups in PG01a. The Venn diagram, constructed with EDGAR 3.0, shows unique and shared genome components for all the five groups.

the core genome of specific subgroups, distinctive genes were also found coding for: (a) the virulence effectors HopAD1 and HopK1, a TonB-dependent siderophore receptor, the coronafacic acid biosynthetic enzymes, and the proteins for biosynthesis of a putative bacteriocin in subset 2; (b) the virulence effector HopO1-3 in subgroup 3; (c) various ABC transporters, arsenic-resistance proteins (ArsB, ArsC, ArsH), the virulence effector AvrPphD, and colicin immunity protein in subset 4; and (d) copper resistance proteins (CopB, CopC and CopD) in subset 5. It is important to mention as well that the *avrPtoB* gene was observed to be one of the 3,177 core genes shared among all the subgroups.

3.4 Avirulence gene *avrPto1* is located in a prophage

Since the *avrPto1* gene in *P. syringae* pv. tomato DAPP-PG 215 was found within an intact prophage region (PR-12, *Pseudomonas* phage *phi3*), the same analysis was also performed on all genomes that were part of the subgroups defined above (Figure 1). For all strains having the *avrPto1* gene, PHASTER detected the presence of *Pseudomonas* phage *phi3* prophage in the genome (Table 1). Despite the different degree of completeness of the region, for all strains, it was in a position overlapping with that of the *avrPto1* gene. Strains lacking *avrPto1* such as *P. syringae* pv. *tomato* race 1 strains A9, T1, NYS-T1, BRIP 66796 and 407, on the other hand, also did not have *Pseudomonas* phage *phi3*. It also appears that this *avrPto1*-containing prophage is located at different locations in the genome. Whereas in *P. syringae* pv. tomato DAPP-PG 215, it is inserted in the chromosome, between another prophage (Vibrio_vB_VpaM_MAR_NC_019722) and two contiguous transposons of the IS*Psy4* family transposase, flanked by *attL* and *attR* sites of 11 bp (CCACGTAACAAG), in *P. syringae* DC3000, it is located in the chromosome as well, but about 1.35 Mb upstream of the attachment site *attL* of *P. syringae* pv. tomato DAPP-PG 215, flanked by different 11 bp *attL* and *attR* sites (CCTGACGATGAA).

3.5 Distribution of the avirulence gene *avrPto1* in genome sequences

A BLASTX search was performed using as queries the *avrPto1* and *avrPtoB* sequences of *P. syringae* pv. tomato DAPP-PG 215 obtained with the aim of determining the evolutionary relationship existing between this specific strain and the other strains included in PG01a concerning these two avirulence genes. The BLASTX analysis revealed the presence of *avrPto1* in 28 out of 49 strains within PG01a, while *avrPtoB* was found in 46 out of 49 genomes.

Comparing the dendrogram based on the presence or absence of *avrPto1* with the core genome phylogeny, it was observed that although some of the major subgroups defined in PG01a by the phylogenetic analysis were confirmed, their positioning in the structure of these trees was not consistent (Figure S2). For AvrPto1, the sequence of *P. syringae* pv. tomato DAPP-PG 215 was found to cluster with those of strains of subgroup IV and V, in a branch of the tree that was only slightly distinct from subgroup II (98.82% protein identity, due to two substitutions: V49L and Y156A) and a part of subgroup III (*P. syringae* A7386 and *P. amygdali* pv. lachrymans strains 3988 and M302278), while the *P. syringae* pv. maculicola strains from subgroup III (ICMP 11281, 4981 and H7608, respectively) clustered together more distantly from the two groups (68.67% protein identity). The only strain of subgroup I carrying *avrPto1* was *P. syringae* pv. maculicola ICMP 2744, the protein sequence of which was very distant to the AvrPto1 sequences of the other strains mentioned above (33.94% protein identity with *P. syringae* pv. tomato DAPP-PG 215). An AvrPto1 ortholog was also found in *P. syringae* pv. coriandricola ICMP 9625 (96.45% protein identity with *P. syringae* pv. tomato DAPP-PG 215). Among the five amino acid changes between the AvrPto1 protein sequences of *P. syringae* pv. coriandricola ICMP 9625 and *P. syringae* pv. tomato DAPP-PG 215 (I4M, D29G, A44S, Y90F and G97R), the fifth is occurring inside the GINP loop, a region known to be responsible for the interaction with plant Pto (Shan et al., 2000; Chang et al., 2001; Wulf et al., 2004). Lastly, it was observed that, unlike subgroups II and III, the *avrPto1* gene was not observed in subgroups I and V: *P. syringae* pv. tomato race 1 strains T1, ICMP 7230, 407, NYS-T1 and A9 and *P. syringae* pv. maculicola strains M6, CFBP 1657 and ICMP 3935 were all lacking it.

3.6 Distribution of the avirulence gene *avrPtoB* in genome sequences

For orthologs of *avrPtoB*, there are two distinct major clades in the dendrogram (Figure S3). In the first clade, gene sequences from all strains included in the subgroups I, II and III were clustering together. However, subgroup III was divided with the *P. syringae* pv. maculicola strains and the *P. syringae* A7386 and *P. amygdali* pv. lachrymans3988 and M302278 positioned in two different parts of the subtree. In the other cluster, gene sequences from strains of subgroups IV and V were clustering together alongside *P. syringae* ICMP 11292, *P. syringae* group genomosp. 3 strain 9643, *Pseudomonas* sp. p4.H5, *Pseudomonas* sp. p4.G1, *Pseudomonas* sp. p6.G2, *P. syringae* pv. antirrhini ICMP 4303, *P. syringae* pv. apii ICMP 2814, *P. syringae* BS2900 and *P. syringae* CC1630. The tree also showed that strain *P. syringae* pv. avii CFBP 3846 also has an ortholog of *avrPtoB*, but it was found to be quite distinct from all other *avrPtoB* gene sequences. The existence of two major groups was consistent with previous discovery of *P. syringae* pv. tomato DC3000 *avrPtoB* orthologs with lower sequence identity in *P. syringae* pv. tomato PT23 ($avrPtoB_{PT23}$) and T1 ($avrPtoB_{T1}$) strains (Lin et al., 2006). The clear separation of race 0 and race 1 strains could again not be confirmed, as the *avrPtoB* sequence of *P. syringae* pv. tomato DAPP-PG 215 was observed to cluster with *P. syringae* pv. tomato T1 and PT23, rather than with race 0 strain *P. syringae* pv. tomato DC3000. From the amino acid alignment, *avrPtoB* of *P. syringae* pv. tomato DAPP-PG 215 resulted to have an almost identical amino acid sequence as the proteins of *Pseudomonas* sp. p6.G2 (99.64%), *P. syringae* pv. berberidis ICMP4116 and subgroup IV strains (99.29%); while its identity with the other major cluster with subgroups I, II and III strains was around 72.83%. Lower amino acid sequence identities were found

10.3389/fpls.2023.1197706

TABLE 1 PHASTER predictions of prophage Pseudo_phi3_NC_030940 locations in all *Pseudomonas syringae* pv. tomato strains used in this study and all the PG01a strains carrying avrPto1 in comparison with avrPto1 locations for each of these strains.

		PHAGE_Pseudo_phi3_NC_030940			*avrPto1*	
Subgroup	Strain	+/-	Locus	Region	Locus	Region
1	*P. syringae* pv. maculicola ICMP 2744	+	NZ_RBQA01000301.1	108-35161	NZ_RBQA01000301.1	1135-1635
2	*P. syringae* pv. maculicola 90-32	+	LGLH01000007.1	41073-62385	LGLH01000007.1	40462-40956
2	*P. syringae* pv. persicae NCPPB 2254	+	LAZV01000025.1	1-23807	LAZV01000025.1	1547-2041
2	*P. syringae* pv. tomato ICMP 2844	+	LJRN01000253.1[1]	1-8438[1]	LJRN01000253.1	1099-1593
2	*P. syringae* pv. tomato DC3000	+	NC_004578.1	4505488-4530373	NC_004578.1	4514766-4515260
2	*P. syringae* pv. tomato delta X	+	NZ_CP047073.1	4505480-4530365	NZ_CP047073.1	4514758-4515252
2	*P. syringae* pv. tomato delta IV, IX	+	NZ_CP047072.1	4505481-4530366	NZ_CP047072.1	4514759-4515253
2	*P. syringae* pv. tomato delta VI	+	NZ_CP047071.1	4505477-4530362	NZ_CP047071.1	4514755-4515249
3	*P. syringae* pv. maculicola ICMP 11281	+	NZ_RBUQ01000113.1	274-18458	NZ_RBUQ01000164.1	1061-1555
			NZ_RBUQ01000164.1[2]			
3	*P. syringae* pv. maculicola ICMP 4981	+	NZ_RBOO01000069.1	35873-59467	NZ_RBOO01000069.1	37554-38048
3	*P. syringae* pv. maculicola H7608	+	NZ_LGLG01000401.1	10054-33648	NZ_LGLG01000401.1	11735-12229
3	*P. amygdali* pv. lachrymans 3988	+	NZ_LGLJ01000049.1	83427-129946	NZ_LGLJ01000049.1	94628-95122
3	*P. amygdali* pv. lachrymans M302278	+	NZ_GL385206.1	88977-127163	NZ_GL385206.1	91352-91846
3	*P. syringae* A7386	+	NZ_RBOB01000082.1	2233-36720	NZ_RBOB01000082.1	33794-34288
4	*P. syringae* BRIP38746	+	NZ_SNVG01000016.1	73880-108746	NZ_SNVG01000016.1	76255-76749
4	*P. syringae* pv. tomato ICMP 2841	+	NZ_RBUK01000087.1	3203-24750	NZ_RBUK01000087.1	9618-10112
4	*P. syringae* pv. tomato BRIP66810	+	NZ_SNVE01000036.1	1-34047	NZ_SNVE01000036.1	1556-2050
4	*P. syringae* pv. maculicola M4a	+	NZ_LGLE01000008.1	1006002-1040868	NZ_LGLE01000008.1	1008377-1008871
4	*P. syringae* pv. tomato PT23	+	NZ_MSDS01000023.1	464-35330	NZ_MSDS01000023.1	2839-3333
5	*P. syringae* pv. tomato NCPPB 1108	+	NZ_ADGA01000002.1	7121-41975	NZ_ADGA01000002.1	39117-39611
5	*P. syringae* pv. tomato B13-200	+	NZ_CP019871.1	5938347-5973213	NZ_CP019871.1	5940722-5941216
5	*P. syringae* Ps25	+	NZ_CP034558.1	926805-962874	NZ_CP034558.1	960016-960510
5	*P. syringae* pv. tomato ICMP 7230	+	NZ_RBRI01000207.1	439-35293	NZ_RBRI01000207.1	32435-32929
5	*P. syringae* pv. tomato T1	–	–	–	–	–
5	*P. syringae* pv. tomato ICMP 4263	+	NZ_RBRJ01000006.1	439-35293	NZ_RBRJ01000006.1	32435-32929
5	*P. syringae* pv. tomato BRIP66796	–	–	–	–	–
5	*P. syringae* pv. tomato 407	–	–	–	–	–
5	*P. syringae* pv. tomato Max13	+	NZ_ADFZ01000218.1	21015-55880	NZ_ADFZ01000218.1	23390-23884
5	*P. syringae* pv. tomato NYS-T1	–	–	–	–	–
5	*P. syringae* pv. tomato K40	+	NZ_ADFY01000134.1	280-21260	NZ_ADFY01000134.1	2485-2979
5	*P. syringae* pv. tomato A9	–	–	–	–	–
5	*P. syringae* pv. tomato DAPP-PG 215	+	GCA_949769235	5852865-5887730	GCA_949769235	5855240-5855734
–	*P. syringae* pv. coriandricola ICMP 9625	+	NZ_RBRV01000199.1	2567-25399	NZ_RBRV01000199.1	1956-2450

[1]Prophage presence for this strain was identified with MAUVE software.
[2]Part of the prophage in this strain was found in NZ_RBUQ01000113.1, and the other in NZ_RBUQ01000164.1 (MAUVE software).

with the AvrPtoB orthologs from *P. syringae* CC1630 (58.36% identity, 75.09% coverage), *P. syringae* BS2900 (36.30% identity, 75.98% coverage) and *P. syringae* pv. avii CFBP 3846 (44.84% identity, 89.32% coverage).

3.7 Localization of coronatine genes is divergent within PG01a

Coronatine (COR) is a phytotoxin produced by several pathovars of *P. syringae*, and consists in the conjunction of coronafacic acid (CFA) and coronamic acid (CMA), synthetized by the homonymous clusters. Because the presence of the *cfa* and *cma* clusters in plasmids has been observed in different pathovars of *P. syringae* (Bender et al., 1991), we made a comparison among the PG01a strains gene sequences of the *cfa* cluster (*cfa1-9*, and the *cfl* gene coding for coronofactate ligase), the *cma* cluster (the *cmaABCDET* cluster and *cmaU*) and the COR regulatory region (*corRSP*). Phylogenetic analysis of the sequences for these twenty genes, obtained using EDGARs ortholog retrieval function, allowed us to observe two different PG01a strains having the necessary clusters for coronatine production groups (Figure S4). Resuming the division made previously above (Figure 1), a first group includes all the strains from subgroup 4 except *P. syringae* pv. tomato ICMP 2841 and all the strains from subgroup 5 except *P. syringae* pv. tomato NCPPB 1108, T1 and Max13, but also *P. syringae* pv. maculicola ICMP 4891 (subgroup 3) and *P. syringae* pv. spinaceae ICMP 16928. A second group, on the other hand, contains the entire subgroup 2, and *P. syringae* pv. berberidis ICMP 4116. More specifically, the nucleotide sequences of *P. syringae* pv. tomato DAPP-PG 215 have approximately 96% identity with the group containing *P. syringae* pv. tomato DC3000 (90% with *P. syringae* pv. maculicola 90-32), 90% with *P. syringae* pv. berberidis ICMP 4116, 98% with *P. syringae* pv. maculicola ICMP 4891, and 99% with *P. syringae* pv. spinaceae ICMP 16928. Significant deletions (>50 bp) were observed in some genes carried by *P. syringae* pv. tomato K40 (*cfa6*, *cfl*, *cmaT* and *corR*), *P. syringae* pv. tomato NYS-T1 (*cfa6*, *cmaT* and *corR*), *P. syringae* pv. maculicola 90-32 (*cfa4* and *cmaT*) and *P. syringae* pv. maculicola M4a (*cfa4* and *cmaT*). In addition, it was possible to observe that both clusters plus the COR regulatory region were located on plasmid regions regarding strains *P.* syringae Ps25 (pPs252, RefSeq: NZ_CP034559.1) and P. syringae pv. tomato B13-200 (pB13-200A, RefSeq: NZ_CP019872.1). Moreover, checking the sequence upstream of cfl, the presence of a CorR-binding site identical to that found in *P. syringae* pv. glycinea PG4180 (Liyanage et al., 1995; Peñaloza-Vázquez & Bender, 1998) and considered to be essential for transcription of genes involved in coronatine synthesis was observed in *P. syringae* pv. tomato DAPP-PG 215.

4 Discussion

P. syringae pv. tomato DAPP-PG 215 was described as a race 0 strain (Buonaurio et al., 1996) based on its phenotype expressed upon inoculation on susceptible tomato plants cv. 'Bonny Best' (+/+) and resistant cv. 'Ontario 7710' (*pto*/*pto*). From the analysis of its genome reported here, it rather possesses the marker genes *avrA* and *hopW1* used to distinguish race 1 from race 0 strains, and instead lacks the *hopN1* gene, which is characteristic for race 0 strains (Jones et al., 2015). The presence of a race 1 genotypic background for *P. syringae* pv. tomato strain DAPP-PG 215 is also supported by the phylogenomic analysis of its core genome in comparison with other PG01a strains, in which it clustered with strains described as race 1, such as *P. syringae* pv. tomato T1 rather than with strains described as race 0, such as *P. syringae* pv. tomato DC3000, and by the sequence analysis of the *avrPtoB* gene, found to be identical to that possessed by strain T1.

Resistance to bacterial speck disease caused by *P. syringae* pv. tomato is due to the occurrence of the *pto* gene in the tomato plant. This genes encodes the protein Pto that is involved in recognition of the type III effectors AvrPto1 and AvrPtoB (HopAB2) expressed by the pathogen (Salmeron et al., 1996; Lin & Martin, 2007). Although it was long assumed that the presence or absence of the two genes was sufficient to distinguish a strain of *P. syringae* pv. tomato race 0 from a race 1, it was recently observed that specific mutations in the *avrPto1* gene prevent the AvrPto1 protein effector from Pto-mediated recognition (Xing et al., 2007). On the other hand, some strains expressing a race 1 phenotype, such as *P. syringae* pv. tomato T1, are capable to evade recognition because they have orthologous *avrPtoB* genes that are weakly transcribed (Lin et al., 2006; Kunkeaw et al., 2010). However, an intact *avrPto1* avirulence gene was also found in *P. syringae* pv. tomato DAPP-PG 215, which could be responsible for the expression of the target of Pto and therefore the reason for the race 0 phenotype expressed by this strain. This hypothesis is in agreement with what was reported by Kraus et al. (2017) who observed the presence of *avrPto1* in some strains of *P. syringae* pv. tomato race 1 and noticed in these strains a growth profile *in planta* intermediate between a race 0 and a race 1. According to what was reported so far, therefore, *P. syringae* pv. tomato DAPP-PG 215 would result in a race 1 genotype and a race 0 strain for its expressed phenotype.

In addition, the detection of the *avrPto1* gene within a prophage in *P. syringae* pv. tomato DAPP-PG 215 and in all other strains belonging to PG01a used in this work possessing this avirulence gene was only reported in this study. Prophages (viral DNA integrated within bacterial genome) are mobile genetic elements that can be responsible for horizontal gene transfer in bacteria. The presence within prophages of genes encoding for virulence effectors of the bacterium is well documented (Fortier & Sekulovic, 2013; Varani et al., 2013), however, since our results suggest that the *avrPto1* gene is associated with this type of mobile regions, the genotype-based criterion for distinguishing race in *P. syringae* pv. tomato appears unstable and unreliable.

Since strains of *P. syringae* pv. tomato having *avrPto1* express a race-typical 0 phenotype even when they carry a low expressed *avrPtoB* homologue such as $avrPtoB_{T1}$ (Kraus et al., 2017), it is possible to advance a hypothesis that the phenotype expressed by *P. syringae* pv. tomato will result in a race 1 if the strain lacks a functioning *avrPto1* and instead has the *avrPtoB* ortholog

avrPtoB$_{T1}$, capable of escaping the Pto recognition, and a race 0 if the *P. syringae* pv. tomato strain meets either of the two following conditions: (a) it lacks a functioning *avrPto1* but has an *avrPtoB*$_{DC3000}$ (Lin et al., 2006), which results in a normal expression of AvrPtoB; (b) it has a functioning *avrPto1*, which, regardless of which *avrPtoB* gene is present in its genome, will be recognized by Pto.

Another difference between strains having a race 0 genomic background and those having a race 1 is the type of coronatine biosynthesis genes. Coronatine is a phytotoxin that interferes with stomata closure in response to pathogen-associated molecular patterns (PAMPs) and salicylic acid-mediated plant defense, also contributing to the development of chlorotic spots on plant leaves (Geng et al., 2014). Produced by strains of various pathovars of *P. syringae*, such as the pathovars atropurpurea, glycinea, maculicola, morsprunorum, and tomato (Bereswill et al., 1994), the genes involved in its synthesis are either located on plasmids or integrated in the chromosome (Preston, 2000). More specifically, the *cfa* and *cma* clusters, required for the synthesis of coronafacic acid and coronamic acid, respectively, and the regulatory region separating them containing the three genes *corP*, *corS*, and *corR*, are found in the chromosome in several strains of *P. syringae* pv. maculicola (including ICMP 2744) and in *P. syringae* pv. tomato DC3000, while in other strains such as *P. syringae* pv. tomato PT23 and *P. syringae* pv. maculicola 4981, they are found on a plasmid (Bender et al., 1989; Cuppels & Ainsworth, 1995).

From our analyses, genes for coronatine were also found on a plasmid in strains *P. syringae* Ps25, *P. syringae* pv tomato B13-200, and *P. syringae* pv tomato DAPP-PG 215. In addition, between the latter named strains and *P. syringae* pv. tomato DC3000, the *cfa* and *cma* clusters have about 96% identity at the nucleotide level, a finding in agreement with what was observed by in *P. syringae* pv. glycinea PG4180, which also had the genes for coronatine located in a plasmid (Wang et al., 2002). The subdivision in the phylogenetic analysis showed that all strains having the coronatine genes in the plasmid mentioned earlier clustered in one group, while *P. syringae* pv. tomato DC3000, which has the genes on the chromosome, was part of the other group. Although it has not been possible to verify for *P. syringae* pv. maculicola ICMP 2744 belonging to the same group as *P. syringae* pv. tomato DC3000, it is possible to assume that all strains belonging to the group with *P. syringae* pv. tomato DAPP-PG 215, B13-200, PT23, *P. syringae* Ps25 and *P. syringae* pv. maculicola 4981 have the genes for coronatine located on a plasmid, while *P. syringae* pv. tomato ICMP 2844, *P. syringae* pv. persicae NCPPB 2254 and *P. syringae* pv. maculicola 90-32 have them on the chromosome. Although it is currently unclear what the implications are for having the gene clusters for coronatine located on the plasmid rather than on the chromosome, a different regulatory mechanism for the synthesis of this phytotoxin was proposed for *P. syringae* pv. tomato DC3000 (Fouts et al., 2002), which lacks the CorR-binding site upstream *cfl* (Wang et al., 2002).

The results of this study confirm what has been previously observed regarding the distribution of genes for coronatine in some strains of *P. syringae* pv. tomato and *P. syringae* pv. maculicola and proposes new hypotheses in the distinction between strains carrying the coronatine biosynthetic genes on plasmids or on chromosomes, although molecular investigations are needed to better understand the significance of this difference. The existence of strains of *P. syringae* pv. tomato having an intermediate phenotype between a race 0 and a race 1 is also confirmed. Subsequent studies that can estimate the ability of the respective strains to grow *in planta* and the severity of the disease on tomato plants in comparison with other non-intermediate strains are required to understand the role of *avrPto1* in the various genomic assets. Lastly, the presence of the *avrPto1* gene in a prophage may result in a different awareness of the concept of race in *P. syringae* pv. tomato, which is therefore, on a phenotypic basis, to be intended as potentially less permanent.

Whereas the race concept may thus become obsolete, it still needs to be commented that strains of both races were and will remain pathogens of tomato, irrespective of their genetic background.

Data availability statement

The datasets presented in this study can be found in online repositories. The names of the repository/repositories and accession number(s) can be found in the article/Supplementary Material.

Author contributions

BO and TS have conceptualized and designed the study. JP has carried out the bacterial cultivation, DNA extraction and NGS sequencing. JP, LF, JB and TS have performed the bioinformatic and software analysis. CM conducted the molecular investigations. RB and TS provided the resources needed for the analysis. BO and TS have prepared the original draft preparation. RB, CM and TS have contributed to the funding acquisition. All authors contributed to the article and approved the submitted version.

Funding

JP and TS were supported by the Department of Life Sciences and Facility Management of the Zurich University of Applied Sciences (ZHAW) in Wädenswil. The EDGAR platform is funded by the BMBF grant FKZ031A533 within the de.NBI network. CM and RB were supported by the research fund “Ricerca di Base” of Department of Agricultural, Food and Environmental Sciences (DSA3) of the University of Perugia, Italy.

Acknowledgments

We thank Dr. M. Orfei and Mr. L. Bonciarelli (DSA3, University of Perugia) for technical assistance. The authors would also like to thank the HPC team of the School for Life Sciences and Facility Management at ZHAW for providing computing resources and support.

Conflict of interest

The authors declare that the research was conducted in the absence of any commercial or financial relationships that could be construed as a potential conflict of interest.

Publisher's note

All claims expressed in this article are solely those of the authors and do not necessarily represent those of their affiliated organizations, or those of the publisher, the editors and the reviewers. Any product that may be evaluated in this article, or claim that may be made by its manufacturer, is not guaranteed or endorsed by the publisher.

Supplementary material

The Supplementary Material for this article can be found online at: https://www.frontiersin.org/articles/10.3389/fpls.2023.1197706/full#supplementary-material

References

Altschul, S. F., Gish, W., Miller, W., Myers, E. W., and Lipman, D. J. (1990). Basic local alignment search tool. *J. Mol. Biol.* 215, 403–410. doi: 10.1016/S0022-2836(05)80360-2

Arndt, D., Grant, J. R., Marcu, A., Sajed, T., Pon, A., Liang, Y., et al. (2016). PHASTER: a better, faster version of the PHAST phage search tool. *Nucleic Acids Res.* 44, W16–W21. doi: 10.1093/nar/gkw387

Basim, H., Basim, E., Yilmaz, S., Dickstein, E. R., and Jones, J. B. (2004). An outbreak of bacterial speck caused by *Pseudomonas syringae* pv. tomato on tomato transplants grown in commercial seedling companies located in the western mediterranean region of Turkey. *Plant Dis.* 88, 1050. doi: 10.1094/PDIS.2004.88.9.1050A

Bender, C. L., Malvick, D. K., and Mitchell, R. E. (1989). Plasmid-mediated production of the phytotoxin coronatine in *Pseudomonas syringae* pv. tomato. *J. Bacteriol.* 171, 807–812. doi: 10.1128/jb.171.2.807-812.1989

Bender, C. L., Young, S. A., and Mitchell, R. E. (1991). Conservation of plasmid DNA sequences in xoronatine-producing pathovars of *Pseudomonas syringae*. *Appl. Environ. Microbiol.* 57, 993–999. doi: 10.1128/aem.57.4.993-999.1991

Bereswill, S., Bugert, P., Völksch, B., Ullrich, M., Bender, C. L., and Geider, K. (1994). Identification and relatedness of coronatine-producing *Pseudomonas syringae* pathovars by PCR analysis and sequence determination of the amplification products. *Appl. Environ. Microbiol.* 60, 2924–2930. doi: 10.1128/aem.60.8.2924-2930.1994

Berge, O., Monteil, C. L., Bartoli, C., Chandeysson, C., Guilbaud, C., Sands, D. C., et al. (2014). A user's guide to a data base of the diversity of *Pseudomonas syringae* and its application to classifying strains in this phylogenetic complex. *PLoS One* 9, e105547. doi: 10.1371/journal.pone.0105547

Bertelli, C., Laird, M. R., Williams, K. P., Fraser, S., Lau, B. Y., Hoad, G., et al. (2017). IslandViewer 4: expanded prediction of genomic islands for larger-scale datasets. *Nucleic Acids Res.* 45, W30–W35. doi: 10.1093/nar/gkx343

Buonaurio, R., Stravato, V. M., and Cappelli, C. (1996). Occurrence of *Pseudomonas syringae* pv. tomato race 1 in Italy on *Pto* gene-bearing tomato plants. *J. Phytopathol.* 144, 437–440. doi: 10.1111/j.1439-0434.1996.tb00320.x

Camacho, C., Coulouris, G., Avagyan, V., Ma, N., Papadopoulos, J., Bealer, K., et al. (2009). BLAST+: architecture and applications. *BMC Bioinf.* 10, 421. doi: 10.1186/1471-2105-10-421

Chang, J. H., Tobias, C. M., Staskawicz, B. J., and Michelmore, R. W. (2001). Functional studies of the bacterial avirulence protein AvrPto by mutational analysis. *Mol. Plant-Microbe Interact.* 14, 451–459. doi: 10.1094/MPMI.2001.14.4.451

Cui, Y., Chen, X., Luo, H., Fan, Z., Luo, J., He, S., et al. (2016). BioCircos.js: an interactive circos JavaScript library for biological data visualization on web applications. *Bioinformatics* 32, 1740–1742. doi: 10.1093/bioinformatics/btw041

Cuppels, D. A., and Ainsworth, T. (1995). Molecular and physiological characterization of *Pseudomonas syringae* pv. tomato and *Pseudomonas syringae* pv. maculicola strains that produce the phytotoxin coronatine. *Appl. Environ. Microbiol.* 61, 3530–3536. doi: 10.1128/aem.61.10.3530-3536.1995

Darling, A. C. E., Mau, B., Blattner, F. R., and Perna, N. T. (2004). Mauve: multiple alignment of conserved genomic sequence with rearrangements. *Genome Res.* 14, 1394–1403. doi: 10.1101/gr.2289704

Dieckmann, M. A., Beyvers, S., Nkouamedjo-Fankep, R. C., Hanel, P. H. G., Jelonek, L., Blom, J., et al. (2021). EDGAR3.0: comparative genomics and phylogenomics on a scalable infrastructure. *Nucleic Acids Res.* 49, W185–W192. doi: 10.1093/nar/gkab341

Edgar, R. C. (2004). MUSCLE: multiple sequence alignment with high accuracy and high throughput. *Nucleic Acids Res.* 32, 1792–1797. doi: 10.1093/nar/gkh340

Fortier, L.-C., and Sekulovic, O. (2013). Importance of prophages to evolution and virulence of bacterial pathogens. *Virulence* 4, 354–365. doi: 10.4161/viru.24498

Fouts, D. E., Abramovitch, R. B., Alfano, J. R., Baldo, A. M., Buell, C. R., Cartinhour, S., et al. (2002). Genomewide identification of *Pseudomonas syringae* pv. tomato DC3000 promoters controlled by the HrpL alternative sigma factor. *Proc. Natl. Acad. Sci. U. S. A.* 99, 2275–2280. doi: 10.1073/pnas.032514099

Geng, X., Jin, L., Shimada, M., Kim, M. G., and Mackey, D. (2014). The phytotoxin coronatine is a multifunctional component of the virulence armament of *Pseudomonas syringae*. *Planta* 240, 1149–1165. doi: 10.1007/s00425-014-2151-x

Goode, M. J., and Sasser, M. (1980). Prevention-the key to controlling bacterial spot and bacterial speck of tomato. *Plant Dis.* 64, 831. doi: 10.1094/PD-64-831

He, D., Zhan, J., and Xie, L. (2016). Problems, challenges and future of plant disease management: from an ecological point of view. *J. Integr. Agric.* 15, 705–715. doi: 10.1016/S2095-3119(15)61300-4

Iwasaki, T., Yamashita, E., Nakagawa, A., Enomoto, A., Tomihara, M., and Takeda, S. (2018). Three-dimensional structures of bacteriophage neck subunits are shared in *Podoviridae*, *Siphoviridae* and *Myoviridae*. *Genes Cells Devoted Mol. Cell. Mech.* 23, 528–536. doi: 10.1111/gtc.12594

Jones, L. A., Saha, S., Collmer, A., Smart, C. D., and Lindeberg, M. (2015). Genome-assisted development of a diagnostic protocol for distinguishing high virulence *Pseudomonas syringae* pv. tomato strains. *Plant Dis.* 99, 527–534. doi: 10.1094/PDIS-08-14-0833-RE

King, E. O., Ward, M. K., and Raney, D. E. (1954). Two simple media for the demonstration of pyocyanin and fluorescin. *J. Lab. Clin. Med.* 44, 301–307.

Kraus, C. M., Mazo-Molina, C., Smart, C. D., and Martin, G. B. (2017). *Pseudomonas syringae* pv. tomato strains from new York exhibit virulence attributes intermediate between typical race 0 and race 1 strains. *Plant Dis.* 101, 1442–1448. doi: 10.1094/PDIS-03-17-0330-RE

Kunkeaw, S., Tan, S., and Coaker, G. (2010). Molecular and evolutionary analyses of *Pseudomonas syringae* pv. *tomato* race 1. *Mol. Plant-Microbe Interact.* 23, 415–424. doi: 10.1094/MPMI-23-4-0415

Lin, N.-C., Abramovitch, R. B., Kim, Y. J., and Martin, G. B. (2006). Diverse AvrPtoB homologs from several *Pseudomonas syringae* pathovars elicit pto-dependent resistance and have similar virulence activities. *Appl. Environ. Microbiol.* 72, 702–712. doi: 10.1128/AEM.72.1.702-712.2006

Lin, N.-C., and Martin, G. B. (2007). Pto- and prf-mediated recognition of AvrPto and AvrPtoB restricts the ability of diverse *Pseudomonas syringae* pathovars to infect tomato. *Mol. Plant-Microbe Interact.* 20, 806–815. doi: 10.1094/MPMI-20-7-0806

Liyanage, H., Palmer, D. A., Ullrich, M., and Bender, C. L. (1995). Characterization and transcriptional analysis of the gene cluster for coronafacic acid, the polyketide component of the phytotoxin coronatine. *Appl. Environ. Microbiol.* 61, 3843–3848. doi: 10.1128/aem.61.11.3843-3848.1995

Mansfield, J., Genin, S., Magori, S., Citovsky, V., Sriariyanum, M., Ronald, P., et al. (2012). Top 10 plant pathogenic bacteria in molecular plant pathology. *Mol. Plant Pathol.* 13, 614–629. doi: 10.1111/j.1364-3703.2012.00804.x

Melotto, M., Underwood, W., and He, S. Y. (2008). Role of stomata in plant innate immunity and foliar bacterial diseases. *Annu. Rev. Phytopathol.* 46, 101–122. doi: 10.1146/annurev.phyto.121107.104959

Miller, J. H. (1972). *Experiments in molecular genetics* (Cold Spring Harbor, N.Y: Cold Spring Harbor Laboratory).

Peñaloza-Vázquez, A., and Bender, C. L. (1998). Characterization of CorR, a transcriptional activator which is required for biosynthesis of the phytotoxin coronatine. *J. Bacteriol.* 180, 6252–6259. doi: 10.1128/JB.180.23.6252-6259.1998

Preston, G. M. (2000). *Pseudomonas syringae* pv. tomato: the right pathogen, of the right plant, at the right time. *Mol. Plant Pathol.* 1, 263–275. doi: 10.1046/j.1364-3703.2000.00036.x

Price, M. N., Dehal, P. S., and Arkin, A. P. (2010). FastTree 2 – approximately maximum-likelihood trees for large alignments. *PLoS One* 5, e9490. doi: 10.1371/journal.pone.0009490

Saitou, N., and Nei, M. (1987). The neighbor-joining method: a new method for reconstructing phylogenetic trees. *Mol. Biol. Evol.* 4, 406–425. doi: 10.1093/oxfordjournals.molbev.a040454

Salmeron, J. M., Oldroyd, G. E. D., Rommens, C. M. T., Scofield, S. R., Kim, H.-S., Lavelle, D. T., et al. (1996). Tomato prf is a member of the leucine-rich repeat class of plant disease resistance genes and lies embedded within the pto kinase gene cluster. *Cell* 86, 123–133. doi: 10.1016/S0092-8674(00)80083-5

Schneider, R. W., and Grogan, R. G. (1977). Bacterial speck of tomato: sources of inoculum and establishment of a resident population. *Phytopathology* 67, 388–394. doi: 10.1094/Phyto-67-388

Schwengers, O., Jelonek, L., Dieckmann, M. A., Beyvers, S., Blom, J., and Goesmann, A. (2021). Bakta: rapid and standardized annotation of bacterial genomes via alignment-free sequence identification. *Microb. Genomics* 7, 000685. doi: 10.1099/mgen.0.000685

Shan, L., Thara, V. K., Martin, G. B., Zhou, J.-M., and Tang, X. (2000). The *Pseudomonas* AvrPto protein is differentially recognized by tomato and tobacco and is localized to the plant plasma membrane. *Plant Cell* 12, 2323–2337. doi: 10.1105/tpc.12.12.2323

Tamura, K., Stecher, G., and Kumar, S. (2021). MEGA11: molecular evolutionary genetics analysis version 11. *Mol. Biol. Evol.* 38, 3022–3027. doi: 10.1093/molbev/msab120

Varani, A. M., Monteiro-Vitorello, C. B., Nakaya, H. I., and Van Sluys, M.-A. (2013). The role of prophage in plant-pathogenic bacteria. *Annu. Rev. Phytopathol.* 51, 429–451. doi: 10.1146/annurev-phyto-081211-173010

Wang, X., AlarcÓn-Chaidez, F., PeÑaloza-VÁzquez, A., and Bender, C. L. (2002). Differential regulation of coronatine biosynthesis in *Pseudomonas syringae* pv. tomato DC3000 and *P. syringae* pv. glycinea PG4180. *Physiol. Mol. Plant Pathol.* 60, 111–120. doi: 10.1006/pmpp.2002.0382

Watson, M. (2018) *Indels are not ideal: quick test for interrupted ORFs in bacterial/microbial*. Available at: https://github.com/mw55309/ideel.

Wick, R. R., Judd, L. M., Gorrie, C. L., and Holt, K. E. (2017). Unicycler: resolving bacterial genome assemblies from short and long sequencing reads. *PLoS Comput. Biol.* 13, e1005595. doi: 10.1371/journal.pcbi.1005595

Wulf, J., Pascuzzi, P. E., Fahmy, A., Martin, G. B., and Nicholson, L. K. (2004). The solution structure of type III effector protein AvrPto reveals conformational and dynamic features important for plant pathogenesis. *Structure* 12, 1257–1268. doi: 10.1016/j.str.2004.04.017

Xiao, F., He, P., Abramovitch, R. B., Dawson, J. E., Nicholson, L. K., Sheen,, et al. (2007). The n-terminal region of *Pseudomonas* type III effector AvrPtoB elicits pto-dependent immunity and has two distinct virulence determinants. *Plant J.* 52, 595–614. doi: 10.1111/j.1365-313X.2007.03259.x

Xing, W., Zou, Y., Liu, Q., Liu, J., Luo, X., Huang, Q., et al. (2007). The structural basis for activation of plant immunity by bacterial effector protein AvrPto. *Nature* 449, 243–247. doi: 10.1038/nature06109

Yunis, H., Bashan, Y., Okon, Y., and Henis, Y. (1980). Weather dependence, yield losses, and control of bacterial speck of tomato caused by *Pseudomonas tomato*. *Plant Dis.* 64, 937–939. doi: 10.1094/PD-64-937

Zhou, Y., Liang, Y., Lynch, K. H., Dennis, J. J., and Wishart, D. S. (2011). PHAST: a fast phage search tool. *Nucleic Acids Res.* 39, W347–W352. doi: 10.1093/nar/gkr485

frontiers | Frontiers in Plant Science

TYPE Original Research
PUBLISHED 31 July 2023
DOI 10.3389/fpls.2023.1198160

OPEN ACCESS

EDITED BY
Prem Lal Kashyap,
Indian Institute of Wheat and Barley Research (ICAR), India

REVIEWED BY
Junjie Yue,
Beijing Institute of Biotechnology, China
Paul Stodghill,
Robert W. Holley Center for Agriculture and Health, Agricultural Research Service (USDA), United States

*CORRESPONDENCE
Priya Gupta
gupta.priya719@gmail.com

†Deceased

‡These authors have contributed equally to this work

RECEIVED 31 March 2023
ACCEPTED 10 July 2023
PUBLISHED 31 July 2023

CITATION
Geraffi N, Gupta P, Wagner N, Barash I, Pupko T and Sessa G (2023) Comparative sequence analysis of pPATH pathogenicity plasmids in *Pantoea agglomerans* gall-forming bacteria.
Front. Plant Sci. 14:1198160.
doi: 10.3389/fpls.2023.1198160

Comparative sequence analysis of pPATH pathogenicity plasmids in *Pantoea agglomerans* gall-forming bacteria

Naama Geraffi[1‡], Priya Gupta[1*‡], Naama Wagner[2], Isaac Barash[1], Tal Pupko[2] and Guido Sessa[1†]

[1]School of Plant Sciences and Food Security, George S. Wise Faculty of Life Sciences, Tel Aviv University, Tel Aviv, Israel, [2]The Shmunis School of Biomedicine and Cancer Research, George S. Wise Faculty of Life Sciences, Tel Aviv University, Tel Aviv, Israel

Acquisition of the pathogenicity plasmid pPATH that encodes a type III secretion system (T3SS) and effectors (T3Es) has likely led to the transition of a non-pathogenic bacterium into the tumorigenic pathogen *Pantoea agglomerans*. *P. agglomerans* pv. *gypsophilae* (*Pag*) forms galls on gypsophila (*Gypsophila paniculata*) and triggers immunity on sugar beet (*Beta vulgaris*), while *P. agglomerans* pv. *betae* (*Pab*) causes galls on both gypsophila and sugar beet. Draft sequences of the *Pag* and *Pab* genomes were previously generated using the MiSeq Illumina technology and used to determine partial T3E inventories of *Pab* and *Pag*. Here, we fully assembled the *Pab* and *Pag* genomes following sequencing with PacBio technology and carried out a comparative sequence analysis of the *Pab* and *Pag* pathogenicity plasmids $pPATH_{pag}$ and $pPATH_{pab}$. Assembly of *Pab* and *Pag* genomes revealed a ~4 Mbp chromosome with a 55% GC content, and three and four plasmids in *Pab* and *Pag*, respectively. $pPATH_{pag}$ and $pPATH_{pab}$ share 97% identity within a 74% coverage, and a similar GC content (51%); they are ~156 kb and ~131 kb in size and consist of 198 and 155 coding sequences (CDSs), respectively. In both plasmids, we confirmed the presence of highly similar gene clusters encoding a T3SS, as well as auxin and cytokinins biosynthetic enzymes. Three putative novel T3Es were identified in *Pab* and one in *Pag*. Among T3SS-associated proteins encoded by *Pag* and *Pab*, we identified two novel chaperons of the ShcV and CesT families that are present in both pathovars with high similarity. We also identified insertion sequences (ISs) and transposons (Tns) that may have contributed to the evolution of the two pathovars. These include seven shared IS elements, and three ISs and two transposons unique to *Pab*. Finally, comparative sequence analysis revealed plasmid regions and CDSs that are present only in $pPATH_{pab}$ or in $pPATH_{pag}$. The high similarity and common features of the pPATH plasmids support the hypothesis that the two strains recently evolved into host-specific pathogens.

KEYWORDS

***Pantoea agglomerans*, sugar beet, gypsophila, type 3 secretion system, type 3 secreted effectors, plasmid, genome assembly, gall-forming**

1 Introduction

Pantoea agglomerans is a Gram-negative facultative anaerobic bacterium of the Erwineaceae family (Adeolu et al., 2016). It is widespread in nature and found in association with many plant species as an epiphyte and endophyte (Manulis and Barash, 2003; Sulja et al., 2022). Strains of *P. agglomerans* have evolved into tumorigenic pathogens displaying host specificity on various plants by acquiring a pathogenicity plasmid, which is designated as pPATH. Two *P. agglomerans* pathogenic pathovars can be distinguished: *P. agglomerans* pv. *gypsophilae* (*Pag*), which induces galls on gypsophila and triggers an immune response on sugar beet, and *P. agglomerans* pv. *betae* (*Pab*), which causes galls on both beet and gypsophila (Weinthal et al., 2007; Barash and Manulis-Sasson, 2009). Pathogenicity of both pathovars is dependent on a type III secretion system (T3SS) and effectors (T3Es), and on auxin and cytokinins biosynthetic pathways that are all encoded in the pathogenicity plasmids $pPATH_{pag}$, in *Pag*, and $pPATH_{pab}$, in *Pab* (Manulis and Barash, 2003). The extensively characterized $pPATH_{pag}$ plasmid has a size of ~131 kb and contains a pathogenicity island (PAI) of ~75 kb that harbors genes encoding T3SS structural, regulatory and effector proteins, and plasmid maintenance determinants, and carries multiple insertion sequences (IS) (Lichter et al., 1996; Guo et al., 2002; Weinthal et al., 2007). The PAI structure, composition and location on the plasmid support a recent evolution of pathogenesis (Manulis and Barash, 2003).

The inventory of T3Es in *Pab* and *Pag* bacteria was previously determined based on draft genome sequences in combination with a machine-learning approach and translocation assays into beet roots, where eight and nine plasmid-borne effectors were identified in *Pab* and *Pag* strains, respectively (Nissan et al., 2018). Five of them (DspA/E, HopX2, HopAY1, HopAF1, and HrpK) are in common between *Pag* and *Pab*, and shared with other phytopathogenic bacteria (Lindeberg et al., 2005; Petnicki-Ocwieja et al., 2005; Boureau et al., 2006; Washington et al., 2016; Saint-Vincent et al., 2020). HopD1 was also reported in other bacteria (Block et al., 2014) but it is only present in *Pag*. Conversely, four T3Es (HsvB, HsvG, PthG and PseB) were only identified in *Pag* and *Pab* strains. HsvG and HsvB are putative transcription factors which may contribute to host specificity in gypsophila and beet, respectively (Valinsky et al., 1998; Nissan et al., 2006; Nissan et al., 2012). PthG is present only in *Pag* and triggers an immune response in beet species, while PseB is present only in *Pab* and its function is still unknown (Nissan et al., 2018). The small repertoire and plasmid location of T3Es in the two pathovars are consistent with recent evolution of *P. agglomerans* pathogenesis and limited functional redundancy between effectors. Remarkably, transformation of HsvG and PthG or HsvB and PseB was found to convert nonpathogenic bacteria into host-specific gall-forming pathogens on gypsophila and beet, respectively (Nissan et al., 2019).

Draft genome sequences of the *Pab* 4188 and *Pag* 824-1 strains were previously generated using MiSeq second-generation sequencing technology and partially assembled into 79 and 55 contigs for *Pab* and *Pag*, respectively (Nissan et al., 2018). In this study, we employed Pacific Biosciences (PacBio) third-generation sequencing technology, which provides longer reads than MiSeq (Bachall, 2009), to sequence and completely assemble the *Pab* and *Pag* genomes. Comparative sequence analysis of the newly assembled $pPATH_{pag}$ and $pPATH_{pab}$ pathogenicity plasmids identified common and unique genes involved in plasmid housekeeping and bacterial virulence that may have shaped the evolution of the *Pag* and *Pab* pathogenic pathovars.

2 Materials and methods

2.1 Bacterial strains and growth conditions

The bacterial strains used are *Pantoea agglomerans* pv. *betae* strain 4188 (*Pab*) (Burr et al., 1991) and *Pantoea agglomerans* pv. *gypsophilae* strain 824-1 (*Pag*) (Manulis et al., 1991). These strains were grown at 28°C in Lysogeny Broth (LB) medium supplemented with Rifampicin (100 µg/ml). The same strains were sequenced before (Nissan et al., 2018). The strains used for both sequencing efforts (MiSeq, PacBio) were drawn from the same stock, which was kept frozen in -80°C. Thus, it is unlikely that mutations have accumulated between the two sequencing efforts.

2.2 PacBio library construction and DNA sequencing

Bacteria were grown overnight in LB liquid medium, and bacterial genomic DNA was isolated as described by Chen and Kuo (1993). The DNA was sent to Macrogen (Seoul, South Korea) for sequencing. PacBio/single-molecule real-time (SMRT) sequencing was used to sequence the genome of the *Pag* and *Pab* strains. Samples were prepared according to standard instructions for SMRTbell templates for sequencing on the PacBio RS System, and were sequenced using SMRT® sequencing. In *Pag*, the sequencing yielded 82,397 reads (692,414,886 read bases). The read N50 was 12,640 bp and the average read length was 8,748 bp. In *Pab*, the sequencing yielded 81,985 reads (706,785,250 read bases). The read N50 was 12,688 bp and the average read length was 8,906 bp.

2.3 Genome assembly and correction

The PacBio reads were used to complete the assembly of the bacterial genomes. These reads are long, and thus allow achieving longer contigs, and in bacterial genomes even the full chromosome sequence. Nevertheless, they are prone to more errors than Illumina reads. In order to obtain a more accurate assembly, previously published draft genome sequences from MiSeq data (Nissan et al., 2018) were used to correct the assembly done using PacBio reads. The PacBio reads were used as input to Canu v1.7 (Koren et al., 2017) to generate the draft complete assembly, with the following parameters: -pacbio-raw corMhapSensitivity=high genomeSize= 5m. The average coverage was assessed by mapping corrected and trimmed reads obtained by Canu v1.7 against the assembly using

BWA v0.7.17 (Li and Durbin, 2009; Li and Durbin, 2010), calculating the alignment depth using SAMtools v1.3.3 (Danecek et al., 2021), and the average depth per molecule using awk. Next, we used Circlator (Hunt et al., 2015) to convert the linear contigs into a circular sequence. To run Circlator, the following additional programs were used: BWA v0.7.17 (Li and Durbin, 2009; Li and Durbin, 2010), Prodigal v2.6.3 (Hyatt et al., 2010), Canu v1.7 (Koren et al., 2017), SAMtools v1.3.3 (Danecek et al., 2021), and MUMmer v3.23 (Kurtz et al., 2004). Following this step, we used the abovementioned Illumina reads to polish the assembly using Pilon v1.22 (Walker et al., 2014). To this end, we mapped the Illumina reads to the draft genome using BWA v0.7.17 (Li and Durbin, 2009; Li and Durbin, 2010), converted the output SAM file to BAM file and sorted it using SAMtools v1.3.3 (Danecek et al., 2021), and finally used it to correct the assembly using Pilon with the default parameters values and including –changes to keep track of the corrections done in the assembly. We repeated this process until no further corrections were introduced to the assembly. Two and three rounds were required to fully correct *Pab* and *Pag* assemblies, respectively. The average coverage of the Illumina reads was assessed in the same manner as assessed for the PacBio reads.

2.4 Genome annotation and alignment

Genomes were annotated using two different programs: (i) Prokka v1.13.3 (Seemann, 2014) with default parameter values; (ii) RAST: a webserver that was used with default settings (Aziz et al., 2008; Overbeek et al., 2014; Brettin et al., 2015). Finally, ISFinder (Siguier et al., 2006) was used to find and locate ISs and Tns in the plasmids. Whole genome alignment was performed using Mugsy-1.2.2. (Angiuoli and Salzberg, 2011). CDSs were aligned using Emboss Needle global alignment (Rice et al., 2000).

3 Results

3.1 Assembly of *Pab* and *Pag* genome sequences

Draft genome sequences of the *Pab* 4188 and *Pag* 824-1 strains (~5 Mb) (NCBI accession no. ASM166202v1 and ASM166198v1) were previously generated by MiSeq second-generation sequencing technologies and partially assembled into 79 contigs for *Pab* and 55 for *Pag* (Nissan et al., 2018). In this study, PacBio third-generation sequencing technology, which provides longer reads than MiSeq (Bachall, 2009), was employed to sequence the *Pab* and *Pag* genomes. The newly sequenced data (NCBI accession no.: ASM166202v2 and ASM166198v2), as well as the previously sequenced MiSeq sequencing data, were used to assemble the genome, aiming that the short-read data would correct errors introduced to the assemblies using the long-read data. Both the sequencing data and the final assemblies were deposited to NCBI and can be found under BioProject PRJNA320975.

Assembly of the *Pab* and *Pag* PacBio reads revealed four and five circular contigs respectively, representing the chromosome for each strain, three plasmids for *Pab*, and four plasmids for *Pag* (Table 1). The chromosomes have a similar length of ~4 Mb with a 55% GC content and each consists of ~4,000 CDSs. Among the plasmids, the previously identified pPATH pathogenicity plasmids *Pab* and *Pag* ($pPATH_{pab}$ and $pPATH_{pag}$; Manulis and Barash, 2003), have a length of ~156 kb and ~131 kb, respectively, a 51% GC content, and consist of 163 and 138 CDSs, respectively. Two other homologous plasmids were identified in the two pathovars: Plasmid 02 with a length of ~540 kb in *Pab* and ~580 kb in *Pag*, and Plasmid 03 with a length of ~180 kb in *Pab* and ~140 kb in *Pag*. Plasmid 02 and 03 have a GC content ranging between 52% and 54%, and they consist of ~600 and ~200 CDSs, respectively. An additional ~79 kb plasmid, Plasmid 04, was detected in *Pag*. It has a 52% GC content and consists of ~80 CDSs. In a BLASTn search, Plasmid 04 was found to be homologous to plasmid pAR1aD of the *P. agglomerans* strain AR1a (accession no. CP059087) with 67% coverage and 99.8% identity, and to the pEM02 plasmid of *Erwinia* spp. (accession no. LN907829) with 44% coverage and 98% identity.

3.2 Comparative analysis of the $pPATH_{pab}$ and $pPATH_{pag}$ plasmids

Next, detailed comparative analysis was carried out for proteins encoded in the $pPATH_{pab}$ and $pPATH_{pag}$ pathogenicity plasmids (Barash and Manulis-Sasson, 2009). This analysis detected proteins that are involved in plasmid housekeeping and plant pathogenicity, including proteins required for plasmid maintenance, structural and regulatory proteins of the T3SS, T3Es, Type 3 chaperons (T3Cs), harpins, and enzymes of biosynthetic pathways of plant growth hormones. Homologous proteins encoded in the $pPATH_{pab}$ and $pPATH_{pag}$ plasmids were compared and their closest homolog in other bacteria was determined. The obtained data were used to generate an updated map of $pPATH_{pag}$ (Figure 1) and the first map of $pPATH_{pab}$ (Figure 2).

To examine if other bacterial strains have plasmids with similar structures as observed in $pPATH_{pab}$ and $pPATH_{pag}$, we conducted a small-scale comparative genomics analysis with publicly available *P. agglomerans* genomes. Specifically, we searched for genes related to the T3SS, which in *Pantoea* are known to be encoded on plasmids. We have blasted (tblastn) the protein sequences of the T3SS regulators and components listed in Tables 2, 3 versus all the fully assembled genomes of *P. agglomerans* available in NCBI. To consider the presence of each of the components, an E-value lower than 10^{-10} and percentage of identical matches higher than 50% were required. Interestingly, a full cluster was found in one genome – *P. agglomerans* strain DAPP-PG734, on plasmid P2. This cluster was not identified in any other genome. In addition to the T3SS, we also searched for the effectors HsvB and HsvG using tblastn. These effectors were found only on pPATH plasmid of *Pag* and *Pab*. These results suggest that the presence of a T3SS and associated effectors is a derived state that characterizes a few specific strains rather than an ancestral state that characterizes the entire *P. agglomerans* species.

10.3389/fpls.2023.1198160

TABLE 1 Features of *Pab* and *Pag* genomes following sequencing with PacBio, assembly with Canu, polishing with Pilon, and annotation with PGAP.

Pab				
Feature	Chromosome	pPAB02	pPAB03	pPATHpab
Size (bp)	4,165,783	541,337	178,621	156,057
No. of circular contigs	1	1	1	1
No. of CDSs	3,810	516	156	163
G+C content (%)	55.4	53.4	52.4	50.8
Pac-bio average coverage	39X	34X	21X	37X
Illumina average coverage	606X	614X	660X	1,259X
No. of tRNA genes	77	0	0	0

Pag					
Feature	Chromosome	pPAG02	pPAG03	pPATHpag	pPAG04
Size (bp)	4,098,036	582,658	143,524	131,449	78,538
No. of circular contigs	1	1	1	1	1
No. of CDSs	3,748	572	127	138	83
G+C content (%)	55.3	53.1	53.5	50.7	52
Pac-bio average coverage	41.3X	22.8X	21.9X	31.5X	18.5X
Illumina average coverage	734X	735X	788X	1,372X	1,319X
No. of tRNA genes	77	0	0	0	0

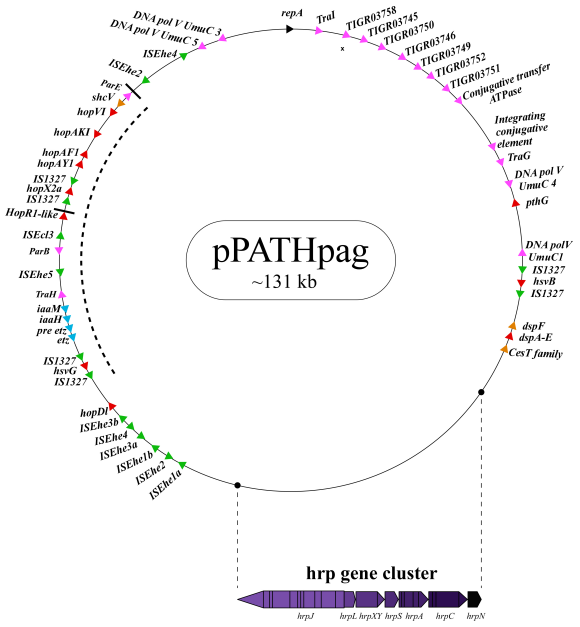

FIGURE 1
Schematic representation of the pPATH$_{pag}$ plasmid. The plasmid contains the *hrp* gene cluster, genes encoding validated and putative T3SS effector proteins (red), a gene cluster encoding indole-3-acetic acid (IAA) and cytokinins (CK) biosynthetic genes (blue), insertion sequence (IS) elements (green), plasmid maintenance genes (pink), T3C (orange) and the *repA* gene (black). Arrows indicate gene orientation. A cluster of effector genes is marked by thick bars, and an inversion fragment by a dotted line.

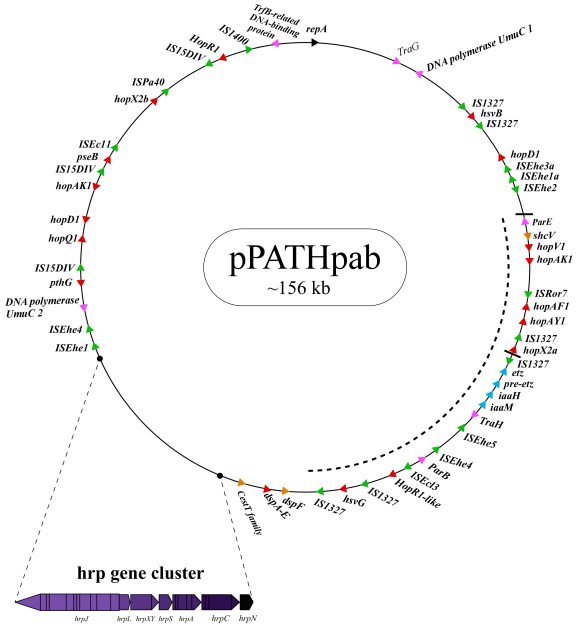

FIGURE 2
Schematic representation of the pPATH$_{pab}$ plasmid. The plasmid contains the *hrp**hrc* gene cluster, genes encoding validated and putative T3SS effector proteins (red), a gene cluster encoding indole-3-acetic acid (IAA) and cytokinins (CK) biosynthetic genes (blue), insertion sequence (IS) elements (green), plasmid maintenance genes (pink), T3C (orange) and the *repA* gene (black). Arrows indicate gene orientation. A cluster of effector genes is marked by thick bars, and an inversion fragment by a dotted line.

TABLE 2 *Pab* and *Pag* regulatory Hrp proteins.

Protein	[a]*Pab**Pag* Identity (%)	[b]Species with Closest Homolog	Function	Source
HrpY	100	*Erwinia psidii* (86%)	Transcription factor Activates HrpS Acts as response regulator of HrpX	(Wei et al., 2000b; Nizan-Koren et al., 2003)
HrpX	100	*Erwinia mallotivora* (85%)	PAS domain S-box protein Function as sensor	(Wei et al., 2000b; Nizan-Koren et al., 2003)
HrpS	100	*E. mallotivora* (84%)	Transcriptional factor of the NtrC family Activates HrpL	(Nizan-Koren et al., 2003)
HrpL	100	*E. psidii* (82%)	Alternative sigma factor. Activates genes containing "hrp box" promoter	(Nizan-Koren et al., 2003)
HrpT	100	*E. psidii* (69%)	Downregulates T3SS gene expression independent of HrpV	(Ortiz-Martín et al., 2010)
HrpG	100	*E. mallotivora* (68%)	Inhibitor of HrpV; regulates HrpC operon; chaperon-like	(Gazi et al., 2015)
HrpV	100	*Erwinia pyriflorinigrans* (63%)	Interacts with HrpS to diminish the activation of T3SS genes	(Gazi et al., 2015)

[a]Percentage of identity is based on alignment of Pab and Pag protein sequences obtained using BLASTp.
[b]The closest homolog was determined by using the Pag protein sequence as query in BLASTp searches.

TABLE 3 *Pab* and *Pag* structural Hrp\Hrc proteins.

Protein	[a]*Pab**Pag* Identity (%)	[b]Species with Closest Homolog	Activity/Function	Source
HrcC	100	*E. psidii* (85%)	Outer membrane ring subunit	(Portaliou et al., 2016)
HrpF	100	*Erwinia pyrifoliae* (86%)	Stabilizes HrpA prior to formation of pilus interacts with HrpG and downregulates T3SS expression	(Huang et al., 2016)
HrpE	100	*E. mallotivora* (73%)	Stator protein stabilizes HrcN to the membrane in *P. syringae*. Act as pilus subunit in *Xanthomonas*	(Weber and Koebnik, 2006; Portaliou et al., 2016)
HrpD	100	*E. mallotivora* (69%)	ATPase co-factor	(Portaliou et al., 2016)
HrcJ	100	*E. psidii* (85%)	Inner membrane ring lipoprotein	(Portaliou et al., 2016)
HrpB	99	*E. mallotivora* (75%)	Inner rod Positive regulator of virulence pathways	(Genin et al., 1992; Occhialini et al., 2005; Portaliou et al., 2016)
HrpA	100	*E. mallotivora* (80%)	Pilus/Injectisome	(Wei et al., 2000a; Portaliou et al., 2016)
HrpJ	99	*E. mallotivora* (79%)	Gatekeeper subunit Interacts with chaperone-effector complex and prevents effector secretion	(Portaliou et al., 2016)
HrcV	100	*E. mallotivora* (89%)	Export apparatus subunit	(Portaliou et al., 2016)
HrpQ	100	*E. mallotivora* (74.11%)	Inner membrane ring	(Portaliou et al., 2016)
HrcN	100	*E. mallotivora* (89%)	ATPase	(Portaliou et al., 2016)
HrpO	99	*E. tracheiphila* (68%)	Stalk	(Portaliou et al., 2016)
HrcQa	100	*E. psidii* (66%)	Cytoplasmic ring protein	(Portaliou et al., 2016)
HrcQb	100	*E. mallotivora* (69%)	Cytoplasmic ring protein	(Portaliou et al., 2016)
HrcR	100	*E. psidii* (95%)	Export apparatus subunit	(Portaliou et al., 2016)
HrcS	100	*Erwinia tracheiphila* (98%)	Export apparatus subunit	(Portaliou et al., 2016)

(Continued)

TABLE 3 Continued

Protein	[a]*Pab\Pag* Identity (%)	[b]Species with Closest Homolog	Activity/Function	Source
HrcT	100	*E. tracheiphila* (85%)	Export apparatus subunit	(Portaliou et al., 2016)
HrcU	100	*E. psidii* (86%)	Export apparatus subunit	(Portaliou et al., 2016)

[a]Percentage of identity is based on alignment of Pab and Pag protein sequences obtained by using BLASTp.
[b]The closest homolog was determined by using the Pag protein sequence as query in BLASTp searches.

3.2.1 Housekeeping proteins

Proteins involved in plasmid maintenance, replication, and transfer were found to be encoded in the $pPATH_{pab}$ and $pPATH_{pag}$ plasmids (Table 4). Within this group of proteins is RepA that in *Pseudomonas* was shown to initiate plasmid replication by binding to the origin of replication (Díaz-López et al., 2003; Weinthal et al., 2007), which is yet to be determined in $pPATH_{pab}$ and $pPATH_{pag}$. Several proteins of the partition system that assures equal segregation of chromosome and plasmids were also detected (Bignell and Thomas, 2001; Funnell, 2016). We also found a transcriptional repressor and toxin which are involved in plasmid maintenance. These include a TrfB-related

TABLE 4 Housekeeping proteins.

Protein	[a]*Pab\Pag* identity (%)	[b]Species with closest homolog	Function	Source
ParB partition protein	100	*Chimaeribacter arupi* (76%)	Helps in plasmid and chromosome partition/ DNA binding protein	(Bignell and Thomas, 2001)
ParA family protein	Only *Pag*	*Chimaeribacter arupi* (90%)	Helps in plasmid and chromosome partition/ Membrane-associated ATPase	(Bignell and Thomas, 2001)
RepA	100	*Klebsiella pneumoniae* (95%)	Replication initiation protein	(Spiers and Bergquist, 1992)
DNA polymerase V UmuC 1 (152 aa)	100	*Serratia marcescens* (82%)	Involved in translesion DNA synthesis	(Wang, 2001)
DNA polymerase V UmuC 2 (265 aa)	Only *Pab*	*Klebsiella pneumoniae* (95%)	Involved in translesion DNA synthesis	(Wang, 2001)
DNA polymerase V UmuC 3 (40 aa)	Only *Pag*	*Klebsiella pneumoniae* (100%)	Involved in translesion DNA synthesis	(Wang, 2001)
DNA polymerase V UmuC 4 (130aa)	Only *Pag*	*Erwinia oleae* (86%)	Involved in translesion DNA synthesis	(Wang, 2001)
DNA polymerase V UmuC 5 (340 aa)	Only *Pag*	*Erwinia rhapontici* (98%)	Involved in translesion DNA synthesis	(Wang, 2001)
TraH	100	*Salmonella enterica* (86%) *E. mallotivora* (86%)	Pilus assembly	(Zatyka and Thomas, 1998)
TraG	100	*Klebsiella pneumoniae* (100%)	Pilus assembly	(Zatyka and Thomas, 1998)
Integrating conjugative element	Only *Pag*	*Klebsiella pneumoniae* (99%)	Unknown function	(Baltrus et al., 2022)
TIGR03758 family integrating conjugative element	Only *Pag*	*Dryocola clanedunensis* (53%)	Unknown function	(Baltrus et al., 2022)
TIGR03745 family integrating conjugative element	Only *Pag*	*Klebsiella oxytoca* (60%)	virB2/iceB2 (Precursor for conjugative pilus)	(Daveri et al., 2023)
TIGR03750 family conjugal transfer protein	Only *Pag*	*Kalamiella piersonii* (67%)	Unknown function	(Baltrus et al., 2022)
TIGR03746 family integrating conjugative element	Only *Pag*	*Erwinia rhapontici* (88%)	Unknown function	(Baltrus et al., 2022)
TIGR03749 family integrating conjugative element	Only *Pag*	*Duffyella gerundensis* (88%)	Unknown function	(Baltrus et al., 2022)

(Continued)

TABLE 4 Continued

Protein	[a]*Pab**Pag* identity (%)	[b]Species with closest homolog	Function	Source
TIGR03752 family integrating conjugative element	Only *Pag*	*Duffyella gerundensis* (90%)	virB10/part of Type IV component	(Voth et al., 2012)
TIGR03751 family conjugal transfer lipoprotein	Only *Pag*	*Duffyella gerundensis* (96%)	Outer membrane protein	(Daveri et al., 2023)
TraI	Only *Pag*	*Erwinia rhapontici* (94%)	Putative DNA helicase	(Matson and Ragonese, 2005)
Conjugative transfer ATPase	Only *Pag*	*Duffyella gerundensis* (93%)	Unknown	(Baltrus et al., 2022)
TrfB-related DNA-binding protein	99	*Duffyella gerundensis* (93%)	Transcriptional repressor	(Thomas and Smith, 1986)
ParE family toxin	100	*Pseudomonas* sp. *T1.Ur* (85%)	Inhibit DNA gyrase	(Jiang et al., 2002; Kamruzzaman and Iredell, 2019)

[a]Percentage of identity is based on alignment of Pab and Pag protein sequences obtained by using BLASTp.
[b]The closest homolog was determined by using the Pag protein sequence as query in BLASTp searches.

DNA binding protein (transcriptional repressor of genes involved in plasmid inheritance) (Thomas and Smith, 1986), and ParA and ParB partitioning proteins (Bignell and Thomas, 2001; Funnell, 2016). The ParE toxin is predicted to inhibit DNA gyrase to stop replication during stress conditions (Jiang et al., 2002), and to be involved in plasmid maintenance via post segregation killing of plasmid free daughter cells using toxin antitoxin systems (Engelberg-Kulka and Glaser, 1999). ParA is only present in $pPATH_{pag}$, while ParB and ParE are present in both pathovars. In addition, we found two and four copies of polymerase V in *Pab* and *Pag*, respectively. Polymerase V participates in DNA repair (Wang, 2001). Interestingly, proteins involved in the conjugative transfer of integrative conjugative elements (ICEs) are present in $pPATH_{pag}$. ICEs are self-transmissible mobile genetic elements that encode the machinery for conjugation, as well as regulatory systems to control their excision and conjugative transfer (Baltrus et al., 2022; Daveri et al., 2023). They include six integrating conjugative element proteins, a conjugal transfer protein, a conjugal transfer lipoprotein, and a conjugative transfer ATPase. In addition, we found two proteins, TraH (contains an ATP binding motif) and TraG (NTPase), encoded in pPATH of both pathovars, whose homologs in other bacteria participate in pilus synthesis and assembly (Zatyka and Thomas, 1998). Finally, a TraI domain containing protein, which plays a putative function as DNA helicase/relaxase, was detected in $pPATH_{pag}$ in the proximity of RepA and can be a part of relaxosome that facilitates plasmid transfer (Matson and Ragonese, 2005).

3.2.2 Structural and regulatory proteins of the type III secretion system

The T3SS is a syringe-like structure that delivers effector proteins inside the plant cell (Galán and Collmer, 1999). It is a complex of proteins encoded by *hrp* (hypersensitive response and pathogenicity) and *hrc* (hypersensitive response and conserved) genes (Alfano and Collmer, 1997). Structure and function of the *Pag* T3SS were extensively characterized in previous studies (Nizan et al., 1997; Mor et al., 2001). Here, we identified and compared structural and regulatory T3SS proteins of $pPATH_{pab}$ and $pPATH_{pag}$ and determined their closest homologs in other bacteria (Tables 2, 3). All Hrp\Hrc proteins are identical in the two pathovars. They display 63%-98% sequence similarity to proteins in different *Erwinia* spp., most commonly *Erwinia mallotivora* and *Erwinia psidii*. As schematically shown in Figure 3, the *hrp\hrc* gene cluster consists of four operons: *hrpJ, hrpA, hrpC, hrpXY*, and three single genes: *hrpL*, *hrpS* and *hrpN*. The genetic arrangement of these operons was found to be the same as in *Pag* (Mor et al., 2001). Operons *hrpJ, hrpA* and *hrpC* mainly encode T3SS structural components, while the *hrpXY* operon encodes regulatory proteins (Tables 2, 3). The *hrpJ* operon is the largest and consists of 11 genes (*hrpJ*, *hrcV*, *hrpQ*, *hrcN*, *hrpO*, *hrcQa*, *hrcQb*, *hrcR*, *hrcS*, *hrcT* and *hrcU*), all encoding structural proteins of the T3SS basal body, except HrcN which is an ATPase and HrpJ that acts as a gatekeeper protein that regulates translocator and effector secretion (Portaliou et al., 2016). *hrpA* is a smaller operon and consists of five genes (*hrpA*, *hrpB*, *hrcJ*, *hrpD* and *hrpE*) encoding pilus/injectisome (HrpA, HrpB and HrcJ) components, an ATPase cofactor (HrpD) and a stator protein (HrpE) to stabilize HrcN. The last structural operon is *hrpC* consisting of five genes (*hrpF*, *hrpG*, *hrcC*, *hrpT* and *hrpV*) with different functions. Homologs of *hrpT*, *hrpV* and *hrpG* in *Pseudomonas syringae* and *Erwinia amylovora* were shown to have a regulatory role (Ortiz-Martín et al., 2010; Gazi et al., 2015). They act in concert to control *hrp/hrc* gene expression which should be coupled with the assembly and function of the T3SS under inducing condition (Ortiz-Martín et al., 2010). The *hrpXY* two-gene operon together with hrpS and hrpL is responsible for regulation of T3SS genes that contain a hrp box in their promoter (Tables 2, 3).

3.2.3 Type III effectors

T3Es are secreted through the T3SS directly inside the plant cell and manipulate host cellular processes to promote bacterial growth in the apoplast (Macho, 2016). Previous reports identified nine effectors in *Pag* (HsvG, HsvB, DspA/E, HopAY1, HopX2, HopAF1,

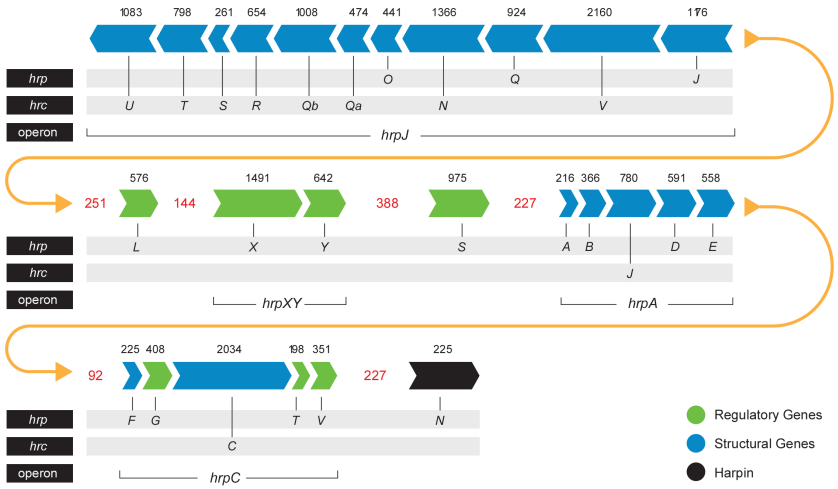

FIGURE 3
Pab and *Pag hrp\hrc* gene cluster. Arrows indicate gene orientation. Black numbers denote the gene size (base pairs). Red numbers denote the distance (base pairs) between operons\genes. Yellow arrows represent the continuity of the gene cluster.

HrpK, PthG, and HopD1) and eight in *Pab* (HsvG, HsvB, PseB, DspA/E, HopAY1, HopX2, HopAF1 and HrpK) (Nissan et al., 2018). Truncated forms of PthG and HopD1 were found in *Pab*, and a truncated HopAY1 was found in *Pag*. In addition, homologs of HopV1 and HopR1 effectors, which are known to be functional in other bacteria (Wei et al., 2007), were found, but their translocation was not assessed by secretion assays (Nissan et al., 2018). Notably, in our analysis, HrpK was not retrieved in any of the pathovar assemblies. The composition of the *Pab* and *Pag* T3E pools was further refined by the identification of three new candidate effectors in $pPATH_{pab}$ and one in $pPATH_{pag}$. One of these candidate T3Es was named HopR1-like, based on its similarity to HopR1 of *Pab* (47%). HopR1-like is present and identical in the two pathovars and represents a new member of the AvrE-family of T3Es displaying 96% similarity to a transducer protein in *E. psidii* (Table 5). Two additional newly identified candidate effectors present in *Pab* are HopQ1 and HopX2b. HopQ1 displays high sequence similarity (98%) to HopQ1 of *P. syringae* pv. *tomato* DC3000 and to XopQ of *Xanthomonas euvesicatoria* (63%) (Giska et al., 2013; Teper et al., 2014). HopX2a (previously reported as HopX2) is present in both pathovars. Another CDS (HopX2b) which is more closely related (98%) to HopX2 of *P. syringae*, was found only in *Pab* (Table 5). HopX2b displays 70% identity to HopX2a and they both belong to XopE/AvrPphe family. However, translocation of HopR1-like, HopX2b and HopQ1 into plant cells and their contribution to bacterial virulence is yet to be determined.

T3Es of the two pathovars, either in full-length or truncated, display a high degree of sequence similarity (91%-100%). The majority of them display high sequence similarity to effectors of other bacteria, mainly of *Pseudomonas* spp. (73%-97%) (Table 5). Remarkably, in this study we found a homolog in *P. syringae* pv. *coryli* (87.91%) for PthG that, along with HsvB, HsvG and PseB, has not been previously detected in any other bacteria. Most of the effector genes are distributed throughout the $pPATH_{pab}$ and $pPATH_{pag}$ plasmids, with the exception of a gene cluster including the HopV1, HopAF1, HopAY1, and HopX2a effector genes, and the HopAKI harpin (Figures 1, 2). Putative functions of the effectors are listed in Table 5.

3.2.4 Harpins

Harpins represent a class of proteins secreted through the T3SS that facilitate translocation of T3Es into plant cells (Li et al., 2019a). Our analysis confirmed the presence of the previously reported harpins HrpN and HopAK1 in both pathovars (Nissan et al., 2018), and identified an additional homolog of HopAK1 in $pPATH_{pab}$ (HopAK1-1). Sequence comparison revealed that HrpN of *Pab* and *Pag* are almost identical (99%), while HopAK1 homologs of the two pathovars display 91% similarity. Closest homologs of HopAK1 and HrpN were found in *P. syringae* (86%) and *E. psidii* (65%), respectively. In terms of location of the genes within the pPATH plasmids, *hrpN* is at the edge of the *hrp\hrc* cluster in both pathovars, while *hopAK1* is located within a cluster of effector genes (Figures 1, 2). *Pab hopAK1-1* encodes a harpin, which has its closest homolog in *P. syringae* (64%) and is located upstream of the *PseB* effector gene.

3.2.5 Type 3 chaperons

T3Cs are small (15-20 kDa), cytoplasmic, and acidic proteins that play roles in T3Es secretion, such as prevention of T3E premature aggregation and cytoplasmic proteolysis (Lohou et al., 2013). Our analysis detected three T3Cs that are encoded in both pPATH plasmids: DspF, ShcV and CesT (Table 6). DspF was previously reported to be present in *Pag* (Mor et al., 2001) and shares relatively high sequence similarity to DspF of *E. piriflorinigrans* (74%). In *E. amylovora* it was shown to facilitate translocation of the DspA/E T3E by interacting with its N-terminus through a predicted β-sheet helix-binding groove (Gaudriault et al., 2002; Triplett et al., 2009). ShcV displays the highest similarity to its *Pseudomonas coronafaciens* homolog (88%). ShcV was reported to interact with and assist the translocation of HopPtoV effector in

TABLE 5 *Pab* and *Pag* T3Es.

Effector	[a]*Pab**Pag* Identity (%)	[b]Species with closest homolog	Putative function\target	[c]Translocation	Source
HsvB	91	none	Transcription factor\gall elicitation in beet	+	(Nissan et al., 2006)
HsvG	98	none	Transcription factor\gall elicitation in gypsophila	+	(Nissan et al., 2006)
DspA/E	100	*E. mallotivora* (73%)	Cell-death inducer	+	(Boureau et al., 2006)
HopAF1	98	*Pseudomonas amygdali* (94%)	Inhibits ethylene biosynthesis	+	(Washington et al., 2016)
HopX2a (327 aa)	100	*P. syringae* (80%)	Cysteine protease	+	(Nissan et al., 2018)
HopR1-like	100	*E. psidii* (96%)	Possibly cytoplasmic arginine transducer	ND	(Storch et al., 1999)
*PthG	28	*P. syringae* pv. *coryli* (88%)	Gall elicitation in gypsophila\HR in beet	+	(Ezra et al., 2004)
*HopD1	57	*P. syringae* (93%)	Suppression of effector-triggered immunity	+	(Block et al., 2014)
*HopAY1	67	*P. syringae* (85%)	Cysteine-type endopeptidase activity	+	(Nissan et al., 2018)
HopQ1	Only *Pab*	*P. syringae* pv. *tomato* DC3000 (98%)	14-3-3 protein binding	ND	(Giska et al., 2013)
HopX2b (353 aa)	Only *Pab*	*P. syringae* (98%)	Cysteine protease (70% similarity to HopX2a)	ND	
PseB	Only *Pab*	none	Gall elicitation in beet	+	(Nissan et al., 2019)
○HopR1	Only *Pab*	*Pseudomonas caricapapayae* (96%)	Possibly suppresses callose formation	–	(Kvitko et al., 2009)
○HopV1	100	*Pseudomonas coronafaciens* (89%)	Contributes to virulence but not to growth	–	(Wei et al., 2007)

[a]Percentage of identity based on an alignment of Pab and Pag protein sequences obtained by using pairwise sequence alignment (https://www.ebi.ac.uk/Tools/psa/emboss_needle/)
[b]The closest homolog for proteins present in both pathovars was determined by using the Pag protein sequence as a query in a BLASTp search.
[c]Translocation ability as reported by Nissan et al. (2018).
*Truncated or possibly truncated effectors in one pathovar.
○Proteins with effector-like features whose translocation was tested, but not detected by Nissan et al. (2018).
ND, Not determined.

P. syringae. This effector-chaperon interaction is also supported by the genomic location of these two proteins: the CDS for the ShcV T3C and the HopPtoV T3E are adjacent to each other (Wehling et al., 2004). In $pPATH_{pab}$ and $pPATH_{pag}$, ShcV and DspF are encoded by CDS adjacent to the *HopV1* and *DspA/E* T3E genes, respectively (Figures 1, 2) in support of the hypothesis that they play a function as chaperones of the encoded T3Es. An additional T3C encoded in both *Pab* and *Pag* is a member of the CesT family of chaperons that were shown to assist in the recruitment of multiple T3Es to the T3SS (Thomas et al., 2005). It shares a relatively low sequence similarity to a protein in *E. psidii* (53%) and its location upstream to the *DspA/E* CDS suggests its involvement in folding and\or secretion of this effector.

3.2.6 Biosynthetic enzymes of plant hormones

Galls formation may be caused by interference of the bacteria with the hormone balance of the plant, in particular with the ratio between auxin and cytokinin concentrations. We identified four plant hormone biosynthetic genes (*iaaM*, *iaaH*, *etz* and *pre-etz*) in both the pPATH plasmids, as previously reported for $pPATH_{pag}$

TABLE 6 Type III chaperones.

Chaperon	[a]*Pab**Pag* identity (%)	[b]Species with closest homolog	Putative function\target	Source
ShcV	100	*Pseudomonas coronafaciens* (88%)	HopPtoV secretion and translocation	(Wehling et al., 2004)
DspF	99	*E. piriflorinigrans* (74%)	DspE stability and secretion	(Triplett et al., 2010)
CesT family	99	*E. psidii* (53%)	Multi effector chaperon	(Thomas et al., 2005)

[a]Percentage of identity based on an alignment of *Pab* and *Pag* protein sequences obtained by using globular alignment emboss needle.
[b]The closest homolog was determined by using the *Pag* protein sequence as query in BLASTp search.

TABLE 7 Biosynthetic enzymes of plant hormones.

Enzyme	[a]*Pab**Pag* identity (%)	[b]Species with closest homolog	Hormone synthesized
Tryptophan 2-monooxygenase iaaM	96	Bacteria symbiont BFo1 of *Frankliniella occidentalis* (99%)	Auxin
Indoleacetamide hydrolase iaaH	96	Bacteria symbiont BFo1 of *Frankliniella occidentalis* (98%)	Auxin
Pre-Etz	96	–	Cytokinin
Etz	97	*E. tracheiphila* (57%)	Cytokinin

[a]Percentage of identity is based on alignment of *Pab* and *Pag* protein sequences obtained by using BLASTp.
[b]The closest homolog was determined by using the *Pag* protein sequence as query in BLASTp searches.

(Table 7) (Lichter et al., 1995; Manulis et al., 1998). IaaM and IaaH are enzymes participating in auxin synthesis through the indole-3-acetamide pathway (Morris, 1986). The operon for cytokinin biosynthesis consists of two genes: *pre-etz* and *etz*. The function of *pre-etz* is unknown, while *etz* encodes the enzyme isopentenyl transferase (Guo et al., 2001). The similarity of these genes in the two pathovars is high (96%-97%), and all enzymes, except pre-Etz, are very similar to homologs in *Erwinia* spp. No putative homologs have been found for pre-Etz. All four genes are clustered together in the $pPATH_{pag}$ and $pPATH_{pab}$ plasmids (Figures 1, 2).

3.2.7 Mobile transposable elements

TEs, including ISs and Tns, are major determinants in the evolution of pathogenic bacteria (Siguier et al., 2014; Nicolas et al., 2015). Tns differ from ISs because in addition to the transposase, they carry passenger/cargo genes, which are not involved in catalysis or regulation of the TE movement (Siguier et al., 2014). ISs belong to diverse families and groups based on the type of transposase, number of CDSs, size, conserved terminal base pairs at the end, number of base pairs present in direct repeats produced at the target site after transposition, and mechanism of transposition

TABLE 8 Insertional sequences and transposons present in $pPATH_{pab}$ and $pPATH_{pag}$.

IS/Tn	IS Family	Group	Size range (bp)	*DR (bp)	Ends	[#]No of CDSs	[@]Chemistry of the enzyme	Mechanism	Origin	Copies in *Pab*	Copies in *Pag*	Comments	Accession No (ISfinder)
ISEhe*5*	IS*1*		740-1180	8-9	GGnnnTG	2	DDE	Copy and paste Co-integrate	*P. agglomerans*	1	1		AY665723
ISEhe*4*	IS*3*	IS*407*	1100-1400	4	TG	2	DDE	Copy and paste	*P. agglomerans*	2	2		AF324174
ISEhe*3*	IS*3*	IS*51*	1000-1400	3-4	TG	2	DDE	Copy and paste	*P. agglomerans*	1	1	Disrupted (in 2 parts in *Pag*; only first part in *Pab*)	AF327445
ISEhe*2*	IS*5*	IS*427*	800-1000	2-4	Ga/g	2	DDE	–	*P. agglomerans*	1	2		AF327444
IS*1327*	IS*6*	-	700-900	8	GG	1	DDE	Co-integrate	*P. agglomerans*	6	6		X87144
ISEhe*1*	IS*630*	-	1000-1400	2		1 or 2	DDE	–	*P. agglomerans*	1	1	Disrupted (in 2 parts in *Pag*; only first part in *Pab*)	AF326767
IS*1400*	IS*3*	IS*407*	1100-1400	4	TG	2	DDE	Copy and paste	*Y. enterocolitica*	1	–	Host- *Yersinia pseudotuberculosis* IP32938 *Yersinia enterocolitica* O5 *Yersinia enterocolitica* O13 *Yersinia enterocolitica* Ye 8081 *Yersinia pseudotuberculosis* IP32954	X94452
ISEcl*1*	IS3	IS*2*	1300-1400	5	TG	2	DDE	Copy and paste	*E. cloacae*	1	–		AF342826
ISEcl*3*	IS*5*	IS*903*	950-1150	9	TG	1	DDE	–	*Enterobacter cloacae*	1	1		AY780889
IS*15DIV*	IS*6*	–	700-900	8	GG	1	DDE	Co-integrate	*Salmonella typhimurium*	3	–		X13616
ISRor*7*	Tn*3*		3150	0		1	DDE	–	*Raoultella ornithinolytica*	1	–	Host-*Raoultella ornithinolytica* 170602815 plasmid p602815-NR	MN310380
ISPa*40*/ TnPa*40*	Tn*3*		6592	0		5	DDE	–	*P. aeruginosa*	1	–	Host-*Pseudomonas aeruginosa* DK2	–

All the information was obtained by using ISFinder. All ISs have terminal inverted repeats. *DR-Direct repeats formed after transposition at the target site.
[#]CDS-coding sequence for transposase enzyme except ISPa40 which has passenger and accessory genes in addition to transposase.
[@]DDE represents the common acidic triad of aspartate (D), aspartate, glutamate (E); presumed to be part of the active site of the transposase.

(Mahillon and Chandler, 1998). Previous studies detected the presence of ISEhe*1*, ISEhe*2*, ISEhe*3*, ISEhe*4*, ISEhe*5*, IS*1327* (six copies) in pPATH$_{pag}$ (Lichter et al., 1996; Guo et al., 2002). Information about the presence of ISs and Tns in *Pab* was not reported earlier.

In this study, we used the ISFinder tool to retrieve TE sequences in pPATH$_{pab}$ and pPATH$_{pag}$, and sequences with the highest significance were analyzed for their location in the plasmid and number of copies. This analysis identified ten types of ISs and two Tns (ISPa*40* and ISRor*7*) in pPATH$_{pab}$ and seven ISs in pPATH$_{pag}$. Seven of all the identified ISs are common to both pathovars (ISEhe*1*, ISEhe*2*, ISEhe*3*, ISEhe*4*, ISEhe*5*, IS*1327*, ISEcl*3*) and belong to diverse IS families: IS1, IS3, IS5, IS6 and IS630. Exclusively present in *Pab* are the ISs IS*1400*, ISEcl*1* and IS*15DIV* and the Tns ISRor*7* and ISPa*40*. In *Pag* we found an additional copy of ISEhe*2* and ISEhe*4*, and new IS ISEcl*3* (Table 8). The presence of such diverse ISs indicates massive horizontal gene transfer (HGT) (Barash and Manulis-Sasson, 2009).

Homologs of ISPa*40*, IS*1400* and IS*15DIV* were found in plant and animal pathogenic bacteria, such as *P. aeruginosa*, *Yersinia enterocolitica* and *Salmonella typhimurium*. In contrast, ISEhe*1*, *3*, *5* and IS*1327*, display very little similarity to proteins in other bacteria (Lichter et al., 1996; Guo et al., 2002). As previously reported by Guo et al. (2002), ISEhe*3* and ISEhe*1* are separated into two parts in *Pag* due to the insertion of ISEhe*4* and ISEhe*2*, respectively. Conversely in *Pab*, we found only the first fragment of ISEhe*3* and ISEhe*1*. It is likely that the second fragment of ISEhe*3* and ISEhe*1* has been lost during evolution of pPATH$_{pab}$ (Figures 1, 2).

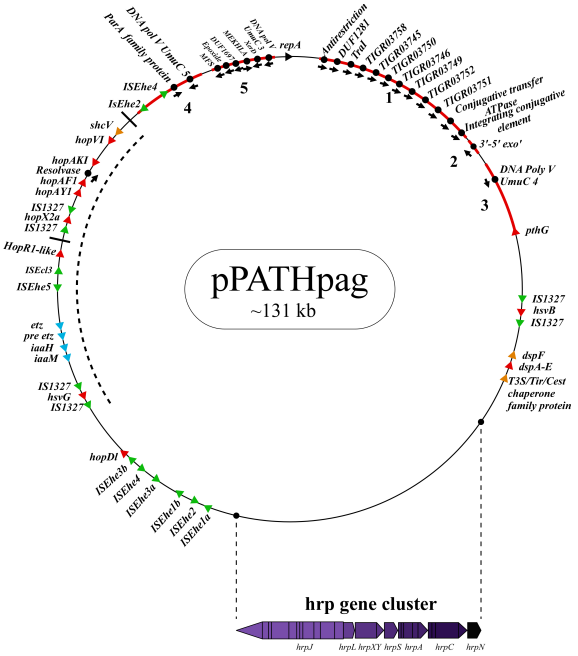

FIGURE 4
Unique sequences of the pPATH$_{pag}$ plasmid. Sequences that are present in pPATH$_{pag}$, but not in pPATH$_{pab}$, are marked in red and numbered from 1 to 5. Genes located on these unique sequences and present in pPATH$_{pag}$, but not in pPATH$_{pab}$, are indicated with black dots. Color code for arrows for rest of the genes are similar to Figure 1.

All ISs are quite dispersed throughout the pPATH plasmid in both pathovars, though in pPATH$_{pag}$ there is a typical clustering of ISEhe*1-4* downstream to the T3SS cluster (Figures 1, 2).

3.2.8 Unique CDSs

To investigate differences between pPATH$_{pab}$ and pPATH$_{pag}$, we aligned the two plasmids and analyzed the CDSs in all the unaligned fragments. Sequences that are present in pPATH$_{pag}$, but not in pPATH$_{pab}$, are indicated in Figure 4 (fragments 1-5). Three unique sequences are located downstream to the *repA* gene: the first (~15 kb) contains a CDS encoding an antirestriction protein, DUF1281 with unknown function, six integrating conjugative element protein, TIGR03750 family conjugal transfer protein, and TIGR03751 family conjugal transfer lipoprotein (Figure 4, fragment 1). The second fragment (261 bp) encodes a 3'-5' exonuclease (Figure 4, fragment 2). The third one (1,524 bp) contains a CDS that encodes a polymerase V (Figure 4, fragment 3). Fragment 4 (2,131 bp) contains CDSs encoding two ISs (ISEhe2 and ISEhe4), a membrane-associated ATPase (ParA family protein), and two polymerase V (Figure 4). Fragment 5 of the unique area (5,930 bp) ends closely to *repA*. It contains seven CDSs that are unique to *Pag* and encode: MFS (major facilitator superfamily) transporter, which has a role in resistance to toxic compounds, epoxide hydrolase, DUF1697, a protein containing a MEKHLA domain, tyrosine recombinase XerC that is involved in transposition, polymerase V, and peptidase (Figure 4). The vast majority of these CDSs display high sequence similarity to genes present in genomes of *Erwinia* spp. (85%-96%) (Table 9).

Sequences that are present in pPATH$_{pab}$ but not in pPATH$_{pag}$ are indicated in Figure 5. There are two consecutive unique sequences in the first ~16 kb downstream to repA (Figure 5, fragments 1 and 2). Fragment 1 contains four CDSs encoding ArdC-like ssDNA-binding domain-containing protein/DUF1738 (antirestriction protein), STY4534 family ICE replication protein/DUF3577 (unknown function), DUF4160 (unknown function) and a pilL protein involved in pilus assembly. Fragment 2 encodes a resolvase I gene involved in recombination processes, and an ATPase gene involved in the zeta toxin\antitoxin system. An additional unique sequence of ~5,400 bp is located within the T3E cluster (Figure 4, fragment 3); it includes a resolvase II gene and the transposon ISRor*7*, which belongs to the Tn3 family. There is also a ~20 kb unique sequence upstream to repA (Figure 5, fragment 4) that includes a copy of HopD1 and HopAKI, and CDSs encoding four effectors present only in pPATH$_{pab}$ (HopQ1, PseB, HopX2b and HopR1). In addition, throughout this region, there are the ISs IS*15DIV* (three copies), ISEcl*1*, IS*1400* and the Tn ISPa*40*. Other unique CDSs within fragment 4 encode proteins involved in type II toxin\antitoxin two components system, which enhances bacteria fitness, antibiotics resistance and maintenance. A CDS next to the truncated PthG encoding polymerase is also unique to *Pab* (Table 10).

4 Discussion

Sequencing of the *Pag* and *Pab* genomes by PacBio technology allowed their complete assembly and disclosed the structure and composition of the pPATH$_{pab}$ and pPATH$_{pag}$ pathogenicity

TABLE 9 Unique CDS in *Pag*.

Protein	[a]Species with closest homolog	Category	Putative function\target	Source
zincin-like metallopeptidase domain-containing protein/ Antirestriction protein	*Duffyella gerundensis* (97%)	General	Protects the DNA from host endonucleases during conjugation	(González-Montes et al., 2020)
DUF1281	*Klebsiella pneumoniae* (99%)	General	Unidentified protein	
TraI	*Erwinia rhapontici* (94%)	Plasmid mobility	Putative DNA helicase	(Matson and Ragonese, 2005)
Integrating conjugative element	*Klebsiella pneumoniae* (99%)	Present on integrative conjugative elements (ICEs)	Unknown	(Baltrus et al., 2022)
TIGR03758 family integrating conjugative element	*Dryocola clanedunensis* (53%)	Present on integrative conjugative elements (ICEs)	Unknown	(Baltrus et al., 2022)
TIGR03745 family integrating conjugative element	*Klebsiella oxytoca* (60%)	Present on integrative conjugative elements (ICEs)	virB2/iceB2 (Precursor for conjugative pilus)	(Daveri et al., 2023)
TIGR03750 family conjugal transfer protein	*Kalamiella piersonii* (67%)	Present on integrative conjugative elements (ICEs)	Unknown	(Baltrus et al., 2022)
TIGR03746 family integrating conjugative element	*Erwinia rhapontici* (88%)	Present on integrative conjugative elements (ICEs)	Unknown	(Baltrus et al., 2022)
TIGR03749 family integrating conjugative element	*Duffyella gerundensis* (88%)	Present on integrative conjugative elements (ICEs)	Unknown	(Baltrus et al., 2022)
TIGR03752 family integrating conjugative element	*Duffyella gerundensis* (90%)	Present on integrative conjugative elements (ICEs)	virB10/part of Type IV component	(Daveri et al., 2023)
TIGR03751 family conjugal transfer lipoprotein	*Duffyella gerundensis* (96%)	Present on integrative conjugative elements (ICEs)	Outer membrane protein	(Daveri et al., 2023)
Conjugative transfer ATPase	*Duffyella gerundensis* (93%)	Present on integrative conjugative elements (ICEs)	Unknown	(Baltrus et al., 2022)
3'-5' exonuclease	*E. hormaechei* (89%)	General	DNA proofreading	(Shevelev and Hübscher, 2002)
DNA polymerase V UmuC 4 (130aa)	*Erwinia oleae* (86%)	DNA repair	Involved in translesion DNA synthesis	(Wang, 2001)
ParA family protein	*Chimaeribacter arupi* (90%)	Plasmid partition	Helps in plasmid and chromosome partition/ Membrane-associated ATPase	(Bignell and Thomas, 2001)
Error-prone, lesion bypass DNA polymerase; UmuC 5 (340 aa)	*Erwinia rhapontici* (98%)	DNA repair	Involved in translesion DNA synthesis	(Wang, 2001)

(Continued)

TABLE 9 Continued

Protein	[a]Species with closest homolog	Category	Putative function\target	Source
DNA polymerase V; UmuC 3 (40aa)	*Klebsiella pneumoniae* (100%)	DNA repair	Involved in translesion DNA synthesis	(Wang, 2001)
XerD/site specific integrase	*E. rhapontici* (92%)	Mobility accessory	site-specific recombinase Functions in circular chromosome separation	(Subramanya et al., 1997)
MFS Transporter	*P. seleniipraecipitans* (55%)	Resistance	Resistance to various toxic compounds and antibiotics	(Vela-Corcía et al., 2019)
Epoxide hydrolase	*P. seleniipraecipitans* (75%)	General	Detoxification of xenobiotics, regulation of signalling pathways and mediation of virulence Hydrolyze epoxides	(Morisseau and Hammock, 2013; Archelas et al., 2016; Bahl et al., 2016; Stojanovski et al., 2020)
MKHLA domain containing protein	*Erwinia* sp. *AG740* (63%)	General	Putative bacterial sensor histidine kinases	(Mukherjee and Bürglin, 2006)
DUF1697	*Microvirga* sp. *3-52* (66%)	General	Unidentified protein	
Resolvase	*P. amygdali* pv *mori* (66%)	Transposon mobility	Resolving the cointegrate (Fusion of donor having Tn3 family transposons and target DNA molecule) in site-specific recombination	(Nicolas et al., 2015)

[a]Species with closest homolog were determined by using BLASTp.

plasmids. Sequence analysis of $pPATH_{pab}$ and $pPATH_{pag}$ allows to formulate hypotheses about their evolutionary origin. The high similarity (97%) between $pPATH_{pab}$ and $pPATH_{pag}$ supports the notion that these plasmids evolved from a common ancestor plasmid. CDSs of the ~20 kb *hrp\hrc* gene cluster, which is highly conserved in *Pab* and *Pag* (>99% identity), display high similarity to *hrp\hrc* genes of *Erwinia* spp. This suggests that the ancestor *P. agglomerans* strain, which were possibly non-pathogenic, may have acquired the *hrp\hrc* gene cluster from a pathogenic *Erwinia* strain and thereby turned into a new pathogenic strain. In support of this hypothesis, copies of the T3E *DspA/E* are located in *Pag* and *Pab* at the edge of the *hrp\hrc* cluster, as similarly observed in *Erwinia* spp. (Siamer et al., 2011), and it is likely that *DspA/E* has been transferred from *Erwinia* to *P. agglomerans* along with the *hrp\hrc* cluster. Recently, a T3SS has also been reported in endophytic *P. agglomerans* DAPP-PG 734 and, *P. agglomerans* BAV 2934 but it is distantly related to *Pab* and *Pag* T3SS suggesting different origin of T3SS in different *Pantoea* strains (Moretti et al., 2021; Sulja et al., 2022). It is possible that pPATH was introduced into a *P. agglomerans* population by a conjugative or mobilizable plasmid. *P. agglomerans* may have acquired the entire pPATH plasmid or the PAI was incorporated in a pre-existing plasmid (Barash and Manulis-Sasson, 2009). In either one of these cases, horizontal gene transfer (HGT) appears as a major evolutionary force that drove pPATH generation. Large mobile elements, such as Tns and ISs, are key players in HGT (Nicolas et al., 2015). The wide genetic interchange between *P. agglomerans* and other bacterial strains manifests itself in the large repertoire of IS elements occurring in $pPATH_{pab}$ and $pPATH_{pag}$, and in the presence of T3E genes common to other phytopathogenic bacteria, and particularly widespread among *P. syringae* pathovars (Guo et al., 2002; Manulis and Barash, 2003).

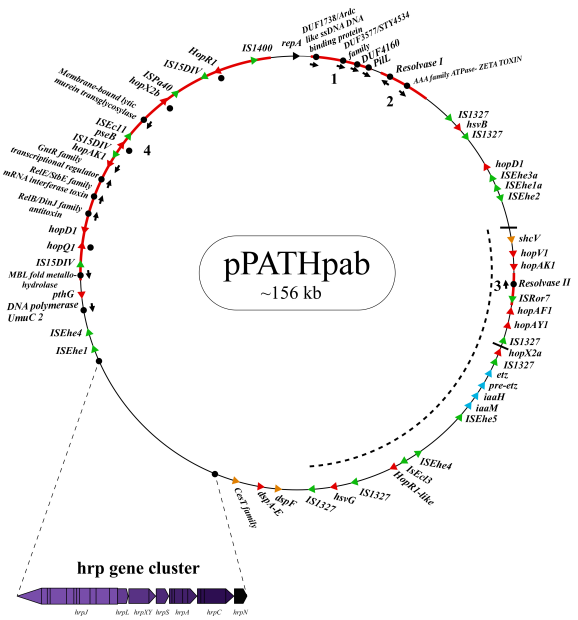

FIGURE 5
Unique sequences of the $pPATH_{pab}$ plasmid. Sequences that are present in $pPATH_{pab}$, but not in $pPATH_{pag}$, are marked in red and numbered from 1 to 4. Genes located on these unique sequences and present in $pPATH_{pab}$, but not in $pPATH_{pag}$, are indicated with black dots. Color code for arrows for rest of the genes are similar to Figure 2.

Several lines of evidence indicate that *P. agglomerans* pathogenic strains are in an early stage of evolution. First, *P. agglomerans* pathovars have their T3SS gene cluster and effector genes in a plasmid, which suggests that the pPATH plasmids have been acquired recently, and the PAI has not been yet incorporated in the *P. agglomerans* chromosome, as observed in other pathogens (Hacker et al., 1997). In addition, comparison between corresponding plasmids of the two pathovars revealed a high identity (96%-97%) and similarity coverage (73%-74%) suggesting

TABLE 10 Unique CDS in *Pab*.

Protein	[a]Species with closest homolog	Category	Putative function\target	Source
ArdC-like ssDNA-binding domain-containing protein/ DUF1738	*Klebsiella pneumoniae* (98%)	Antirestriction protein	Exported during conjugation to recipient cell and protects the DNA from host endonucleases	(González-Montes et al., 2020)
STY4534 family ICE replication protein/DUF3577	*Duffyella gerundensis* (98%)	–	Unknown	(Seth-Smith et al., 2012)
DUF4160	*Klebsiella pneumoniae* (99%)	General	Unknown	
PilL	*Duffyella gerundensis* (98%)	Type IV	Pilus biosynthesis	(Srimanote et al., 2002)
Resolvase - recombinase family protein 1	*Duffyella gerundensis* (96%)	Transposon mobility	Resolving the cointegrate (Fusion of donor having Tn3 family transposons and target DNA molecule) in site-specific recombination	(Nicolas et al., 2015)
AAA family ATPase - ZETA TOXIN	*Curtobacterium plantarum* (69%)	Toxin\anti-toxin system	Targets cell wall formation Arrests growth in an ATP dependent manner	(Jaén-Luchoro et al., 2017)
Resolvase - recombinase family protein 2	*Klebsiella aerogenes* (98%)	Transposon mobility	Resolving the cointegrate (Fusion of donor having Tn3 family transposons and target DNA molecule) in site-specific recombination	(Nicolas et al., 2015)
HopAKI02	*P. syringae* (86%)	Harpin	Pectate lyase	(Kvitko et al., 2007)
HopX2b	*P. syringae* (98%)	Effector	Cysteine proteases	This study
HopQ1	*P. syringae* pv. *tomato* DC3000 (98%)	Effector	14-3-3 protein binding	(Giska et al., 2013)
HopR1	*P. caricapapayae* (96%)	Effector	Possibly suppresses callose formation	(Kvitko et al., 2009)
PseB	–	Effector	Gall elicitation in *Beta vulgaris*	(Nissan et al., 2019)
Membrane-bound lytic murein transglycosylase	*E. psidii* (97%)	Cell wall recycling	Murein-degrading enzyme	(Lee et al., 2013)
GntR family transcriptional regulator	*Pseudomonas* sp. *ES3-33* (55%)	Transcription factor	Involved in many biological processes like cell motility, glucose metabolism, bacterial resistance, pathogenesis expression of multiple sugar transporter and biofilm formation	(Suvorova et al., 2015; Li et al., 2019b; Liu et al., 2021)
RelB/DinJ family antitoxin	*Erwinia persicina* (78%)	Type II toxin-antitoxin system	Antitoxin	(Kamruzzaman and Iredell, 2019)
RelE/StbE family mRNA interferase toxin	*Cronobacter dublinensis* (86%)	Type II toxin-antitoxin system	mRNA cleavage Inhibits translation	(Keren et al., 2004)
MBL fold metallo-hydrolase	*Salmonella enterica* (64%)	Resistance	Resistance to β-lactam antibiotics	(Pettinati et al., 2016)
DNA polymerase V UmuC 2 (265 aa)	*Klebsiella pneumoniae* (95%)	DNA repair	Involved in translesion DNA synthesis	(Wang, 2001)

[a]Species with closest homolog were determined using BLASTp.

that pPATH, plasmid 02 and plasmid 03 were all present in the common ancestor strain before its splitting into two distinct pathovars. Finally, the repertoire of T3Es of the two pathovar is limited as compared to other pathogens. Based on our refined analysis, seven effectors are present in both pathovars (HsvG, HsvB, DspA/E, HopX2a, HopAF1, HopV1 and HopR1-like). In addition, HopD1 and PthG are present only in *Pag*, while PseB, HopQ1, HopAY1, HopR1 and HopX2b are exclusive to *Pab* and are located in a region of ~20 kb that is unique to $pPATH_{pab}$ (Figure 3).

Introduction of pathoadaptive mutations represents an important mechanism that may contribute to evolution of a new pathogen (Sokurenko et al., 1999; Bartoli et al., 2016). In support of the involvement of pathoadaptive mutations in the evolution of *Pag* and *Pab*, truncated variants of T3Es are present in the two

pathovars: HopAY1 is truncated in *Pag*, while PthG and HopD1 are truncated in *Pab*. These genes acquired mutations that interrupted their CDSs, possibly contributing to the formation of the two distinct pathovars. Truncation of these effectors may have allowed bacteria to escape recognition by newly appeared resistance proteins of the host plant. Generation of PthG in *Pag* may be the result of pathoadaptive changes that occurred randomly and were preserved due to their beneficial effect. One possible scenario is that *Pab* evolved from *Pag* by a genetic modification that resulted in truncation of the PthG CDS and evasion of beet recognition and immunity (Ezra et al., 2000; Manulis and Barash, 2003; Ezra et al., 2004). Typically, these are mutations causing a functional modification or elimination of genes that confer enhanced pathogenicity to the bacteria (Sokurenko et al., 1999).

A 20 kb region which is perfectly mirrored in $pPATH_{pab}$ and $pPATH_{pag}$ is present in the two plasmids. This segment includes the cluster of plant hormone biosynthetic genes, the clustered effector genes, the *hsvG* gene, and the *hopR1-like* candidate effector gene. The inversion must have occurred sometime after the splitting into two pathovars and could have happened spontaneously or due to a replication-transcription conflict that resulted in DNA rearrangement (Merrikh et al., 2012; Merrikh and Merrikh, 2018). It has been known that head-on orientation genes can be beneficial to the bacteria due to their high mutation frequency (Merrikh and Merrikh, 2018). Altogether, we conclude that genetic rearrangements and mutations in the ancestor pathogenic plasmid supposedly shaped $pPATH_{pag}$ and $pPATH_{pab}$ resulting in the generation of two pathogenic strains with different host specificities.

Data availability statement

The datasets presented in this study can be found in online repositories. The names of the repository/repositories and accession number(s) can be found below: https://www.ncbi.nlm.nih.gov/, BioProject PRJNA320975.

Author contributions

Conceptualization, GS, IB and TP. Software, TP and NW. Formal Analysis, NG, PG and NW. Investigation, NG and PG. Data Curation, NG and PG. Writing – Original Draft Preparation, NG, PG, GS and IB. Writing – Review and Editing, TP and NW. Supervision, GS, TP and IB. Project Administration, GS. Funding Acquisition, GS and IB. All authors contributed to the article and approved the submitted version.

Funding

This research was supported by the Israel Science Foundation (ISF) under grant number 488/19.

In Memoriam

This paper is dedicated to Guido-Sessa (19642023), a scientist, a mentor, and a friend.

Conflict of interest

The authors declare that the research was conducted in the absence of any commercial or financial relationships that could be construed as a potential conflict of interest.

Publisher's note

References

Adeolu, M., Alnajar, S., Naushad, S., and Gupta, R. S. (2016). Genome-based phylogeny and taxonomy of the "Enterobacteriales": proposal for *Enterobacterales* ord. nov. divided into the families *Enterobacteriaceae*, *Erwiniaceae* fam. nov., *Pectobacteriaceae* fam. nov., *Yersiniaceae*. *Int. J. Syst. Evol. Microbiol.* 66, 5575–5599. doi: 10.1099/IJSEM.0.001485

Alfano, J. R., and Collmer, A. (1997). The type III (Hrp) secretion pathway of plant pathogenic bacteria: trafficking harpins, Avr proteins, and death. *J. Bacteriol.* 179, 5655–5662. doi: 10.1128/jb.179.18.5655-5662.1997

Angiuoli, S. V., and Salzberg, S. L. (2011). Mugsy: fast multiple alignment of closely related whole genomes. *Bioinformatics* 27, 334–342. doi: 10.1093/bioinformatics/btq665

Archelas, A., Iacazio, G., and Kotik, M. (2016). "Epoxide hydrolases and their application in organic synthesis," in *Green Biocatalysis*, 179–229. doi: 10.1002/9781118828083.ch8

Aziz, R. K., Bartels, D., Best, A. A., DeJongh, M., Disz, T., Edwards, R. A., et al. (2008). The RAST Server: rapid annotations using subsystems technology. *BMC Genomics* 9, 75. doi: 10.1186/1471-2164-9-75

Bachall, O. (2009). Pac bio sequencing. *Nat. Genet.* 41, 147–148.

Bahl, C. D., Hvorecny, K. L., Morisseau, C., Gerber, S. A., and Madden, D. R. (2016). Visualizing the mechanism of epoxide hydrolysis by the bacterial virulence enzyme Cif. *Biochemistry* 55, 788–797. doi: 10.1021/acs.biochem.5b01229

Baltrus, D. A., Feng, Q., and Kvitko, B. H. (2022). Genome context influences evolutionary flexibility of nearly identical type III effectors in two phytopathogenic *Pseudomonads*. *Front. Microbiol.* 13. doi: 10.3389/fmicb.2022.826365

Barash, I., and Manulis-Sasson, S. (2009). Recent evolution of bacterial pathogens: the gall-forming *Pantoea agglomerans* case. *Annu. Rev. Phytopathol.* 47, 133–152. doi: 10.1146/annurev-phyto-080508-081803

Bartoli, C., Roux, F., and Lamichhane, J. R. (2016). Molecular mechanisms underlying the emergence of bacterial pathogens: an ecological perspective. *Mol. Plant Pathol.* 17, 303–310. doi: 10.1111/mpp.12284

Bignell, C., and Thomas, C. M. (2001). The bacterial ParA-ParB partitioning proteins. *J. Biotechnol.* 91, 1–34. doi: 10.1016/s0168-1656(01)00293-0

Block, A., Toruño, T. Y., Elowsky, C. G., Zhang, C., Steinbrenner, J., Beynon, J., et al. (2014). The *Pseudomonas syringae* type III effector HopD1 suppresses effector-triggered immunity, localizes to the endoplasmic reticulum, and targets the *Arabidopsis* transcription factor NTL9. *New Phytol.* 201, 1358–1370. doi: 10.1111/nph.12626

Boureau, T., ElMaarouf-Bouteau, H., Garnier, A., Brisset, M.-N., Perino, C., Pucheu, I., et al. (2006). DspA/E, a type III effector essential for *Erwinia amylovora* pathogenicity and growth in planta, induces cell death in host apple

and nonhost tobacco plants. *Mol. Plant Microbe Interact.* 19, 16–24. doi: 10.1094/MPMI-19-0016

Brettin, T., Davis, J. J., Disz, T., Edwards, R. A., Gerdes, S., Olsen, G. J., et al. (2015). RASTtk: a modular and extensible implementation of the RAST algorithm for building custom annotation pipelines and annotating batches of genomes. *Sci. Rep.* 58365. doi: 10.1038/srep08365

Burr, T. J., Katz, B. H., Abawi, G. S., and Crosier, D. (1991). Comparison of tumorigenic strains of *Erwinia herbicola* isolated from table beet with *E. h.* gypsophilae. *Plant Dis.* 75, 855–858. doi: 10.1094/PD-75-0855

Chen, W., and Kuo, T. (1993). A simple and rapid method for the preparation of gram-negative bacterial genomic DNA. *Nucleic Acids Res.* 212260. doi: 10.1093/nar/21.9.2260

Danecek, P., Bonfield, J. K., Liddle, J., Marshall, J., Ohan, V., Pollard, M. O., et al. (2021). Twelve years of SAMtools and BCFtools. *Gigascience* 10, giab008. doi: 10.1093/gigascience/giab008

Daveri, A., Benigno, V., and van der Meer, J. R. (2023). Characterization of an atypical but widespread type IV secretion system for transfer of the integrative and conjugative element (ICEclc) in Pseudomonas putida. *Nucleic Acids Res.* 51, 2345–2362. doi: 10.1093/nar/gkad024

Díaz-López, T., Lages-Gonzalo, M., Serrano-López, A., Alfonso, C., Rivas, G., Díaz-Orejas, R., et al. (2003). Structural changes in RepA, a plasmid replication initiator, upon binding to origin DNA. *J. Biol. Chem.* 278, 18606–18616. doi: 10.1074/jbc.M212024200

Engelberg-Kulka, H., and Glaser, G. (1999). Addiction modules and programmed cell death and antideath in bacterial cultures. *Annu. Rev. Microbiol.* 53, 43–70. doi: 10.1146/annurev.micro.53.1.43

Ezra, D., Barash, I., Valinsky, L., and Manulis, S. (2000). The dual function in virulence and host range restriction of a gene isolated from the pPATH (Ehg) plasmid of *Erwinia herbicola* pv. gypsophilae. *Mol. Plant Microbe Interact.* 13, 683–692. doi: 10.1094/MPMI.2000.13.6.683

Ezra, D., Barash, I., Weinthal, D. M., Gaba, V., and Manulis, S. (2004). pthG from *Pantoea agglomerans* pv. gypsophilae encodes an avirulence effector that determines incompatibility in multiple beet species. *Mol. Plant Pathol.* 5, 105–113. doi: 10.1111/j.1364-3703.2004.00211.x

Funnell, B. E. (2016). ParB partition proteins: complex formation and spreading at bacterial and plasmid centromeres. *Front. Mol. Biosci.* 3. doi: 10.3389/fmolb.2016.00044

Galán, J. E., and Collmer, A. (1999). Type III secretion machines: bacterial devices for protein delivery into host cells. *Science* 284, 1322–1328. doi: 10.1126/science.284.5418.1322

Gaudriault, S., Paulin, J.-P., and Barny, M.-A. (2002). The DspB/F protein of *Erwinia amylovora* is a type III secretion chaperone ensuring efficient intrabacterial production of the Hrp-secreted DspA/E pathogenicity factor. *Mol. Plant Pathol.* 3, 313–320. doi: 10.1046/j.1364-3703.2002.00124.x

Gazi, A. D., Charova, S., Aivaliotis, M., Panopoulos, N. J., and Kokkinidis, M. (2015). HrpG and HrpV proteins from the type III secretion system of *Erwinia amylovora* form a stable heterodimer. *FEMS Microbiol. Lett.* 362, 1–8. doi: 10.1093/femsle/fnu011

Genin, S., Gough, C. L., Zischek, C., and Boucher, C. A. (1992). Evidence that the hrpB gene encodes a positive regulator of pathogenicity genes from *Pseudomonas solanacearum*. *Mol. Microbiol.* 6, 3065–3076. doi: 10.1111/j.1365-2958.1992.tb01764.x

Giska, F., Lichocka, M., Piechocki, M., Dadlez, M., Schmelzer, E., Hennig, J., et al. (2013). Phosphorylation of HopQ1, a type III effector from *Pseudomonas syringae*, creates a binding site for host 14-3-3 proteins. *Plant Physiol.* 161, 2049–2061. doi: 10.1104/pp.112.209023

González-Montes, L., Del Campo, I., Garcillán-Barcia, M. P., de la Cruz, F., and Moncalián, G. (2020). ArdC, a ssDNA-binding protein with a metalloprotease domain, overpasses the recipient hsdRMS restriction system broadening conjugation host range. *PloS Genet.* 16, e1008750–e1008750. doi: 10.1371/journal.pgen.1008750

Guo, M., Manulis, S., Barash, I., and Lichter, A. (2001). The operon for cytokinin biosynthesis of *Erwinia herbicola* pv. gypsophilae contains two promoters and is plant induced. *Can. J. Microbiol.* 47, 1126–1131. doi: 10.1139/cjm-47-12-1126

Guo, M., Manulis, S., Mor, H., and Barash, I. (2002). The presence of diverse IS elements and an avrPphD homologue that acts as a virulence factor on the pathogenicity plasmid of *Erwinia herbicola* pv. gypsophilae. *Mol. Plant Microbe Interact.* 15, 709–716. doi: 10.1094/MPMI.2002.15.7.709

Hacker, J., Blum-Oehler, G., Mühldorfer, I., and Tschäpe, H. (1997). Pathogenicity islands of virulent bacteria: structure, function and impact on microbial evolution. *Mol. Microbiol.* 23, 1089–1097. doi: 10.1046/j.1365-2958.1997.3101672.x

Huang, Y.-C., Lin, Y.-C., Wei, C.-F., Deng, W.-L., and Huang, H.-C. (2016). The pathogenicity factor HrpF interacts with HrpA and HrpG to modulate type III secretion system (T3SS) function and T3SS expression in *Pseudomonas syringae* pv. averrhoi. *Mol. Plant Pathol.* 17, 1080–1094. doi: 10.1111/mpp.12349

Hunt, M., De Silva, N., Otto, T. D., Parkhill, J., Keane, J. A., and Harris, S. R. (2015). Circlator: automated circularization of genome assemblies using long sequencing reads. *Genome Biol.* 16, 1–10. doi: 10.1186/S13059-015-0849-0

Hyatt, D., Chen, G.-L., LoCascio, P. F., Land, M. L., Larimer, F. W., and Hauser, L. J. (2010). Prodigal: prokaryotic gene recognition and translation initiation site identification. *BMC Bioinf.* 11, 119. doi: 10.1186/1471-2105-11-119

Jaén-Luchoro, D., Aliaga-Lozano, F., Gomila, R. M., Gomila, M., Salvà-Serra, F., Lalucat, J., et al. (2017). First insights into a type II toxin-antitoxin system from the clinical isolate Mycobacterium sp. MHSD3, similar to epsilon/zeta systems. *PloS One*, 12, e0189459. doi: 10.1371/journal.pone.0189459

Jiang, Y., Pogliano, J., Helinski, D. R., and Konieczny, I. (2002). ParE toxin encoded by the broad-host-range plasmid RK2 is an inhibitor of *Escherichia coli* gyrase. *Mol. Microbiol.* 44, 971–979. doi: 10.1046/j.1365-2958.2002.02921.x

Kamruzzaman, M., and Iredell, J. (2019). A ParDE-family toxin antitoxin system in major resistance plasmids of *Enterobacteriaceae* confers antibiotic and heat tolerance. *Sci. Rep.* 9, 9872. doi: 10.1038/s41598-019-46318-1

Keren, I., Shah, D., Spoering, A., Kaldalu, N., and Lewis, K. (2004). Specialized persister cells and the mechanism of multidrug tolerance in *Escherichia coli*. *J. Bacteriol.* 186, 8172–8180. doi: 10.1128/JB.186.24.8172-8180.2004

Koren, S., Walenz, B. P., Berlin, K., Miller, J. R., Bergman, N. H., and Phillippy, A. M. (2017). Canu: scalable and accurate long-read assembly via adaptive k-mer weighting and repeat separation. *Genome Res.* 27, 722–736. doi: 10.1101/GR.215087.116

Kurtz, S., Phillippy, A., Delcher, A. L., Smoot, M., Shumway, M., Antonescu, C., et al. (2004). Versatile and open software for comparing large genomes. *Genome Biol.* 5, 1–9. doi: 10.1186/GB-2004-5-2-R12

Kvitko, B. H., Park, D. H., Velásquez, A. C., Wei, C.-F., Russell, A. B., Martin, G. B., et al. (2009). Deletions in the repertoire of *Pseudomonas syringae* pv. tomato DC3000 Type III secretion effector genes reveal functional overlap among Effectors. *PloS Pathog.* 5, e1000388. doi: 10.1371/journal.ppat.1000388

Kvitko, B. H., Ramos, A. R., Morello, J. E., Oh, H.-S., and Collmer, A. (2007). Identification of harpins in *Pseudomonas syringae* pv. tomato DC3000, which are functionally similar to HrpK1 in promoting translocation of type III secretion system effectors. *J. Bacteriol.* 189, 8059–8072. doi: 10.1128/JB.01146-07

Lee, M., Hesek, D., Llarrull, L. I., Lastochkin, E., Pi, H., Boggess, B., et al. (2013). Reactions of all *Escherichia coli* lytic transglycosylases with bacterial cell wall. *J. Am. Chem. Soc* 135, 3311–3314. doi: 10.1021/ja309036q

Li, H., and Durbin, R. (2009). Fast and accurate short read alignment with Burrows–Wheeler transform. *Bioinformatics* 25, 1754–1760. doi: 10.1093/bioinformatics/btp324

Li, H., and Durbin, R. (2010). Fast and accurate long-read alignment with Burrows–Wheeler transform. *Bioinformatics* 26, 589–595. doi: 10.1093/bioinformatics/btp698

Li, Z., Xiang, Z., Zeng, J., Li, Y., and Li, J. (2019b). A GntR family transcription factor in streptococcus mutans regulates biofilm formation and expression of multiple sugar transporter genes. *Front. Microbiol.* 9. doi: 10.3389/fmicb.2018.03224

Li, P., Zhang, L., Mo, X., Ji, H., Bian, H., Hu, Y., et al. (2019a). Rice aquaporin PIP1;3 and harpin Hpa1 of bacterial blight pathogen cooperate in a type III effector translocation. *J. Exp. Bot.* 70, 3057–3073. doi: 10.1093/jxb/erz130

Lichter, A., Barash, I., Valinsky, L., and Manulis, S. (1995). The genes involved in cytokinin biosynthesis in *Erwinia herbicola* pv. gypsophilae: characterization and role in gall formation. *J. Bacteriol.* 177, 4457–4465. doi: 10.1128/jb.177.15.4457-4465.1995

Lichter, A., Manulis, S., Valinsky, L., Karniol, B., and Barash, I. (1996). IS1327, a new insertion-like element in the pathogenicity-associated plasmid of Erwinia herbicola pv. gypsophilae. *Mol. Plant Microbe Interact.* 9, 98–104. doi: 10.1094/MPMI-9-0098

Lindeberg, M., Stavrinides, J., Chang, J. H., Alfano, J. R., Collmer, A., Dangl, J. L., et al. (2005). Proposed guidelines for a unified nomenclature and phylogenetic analysis of type III hop effector proteins in the plant pathogen *Pseudomonas syringae*. *Mol. Plant-Microbe Interact.* 18, 275–282. doi: 10.1094/MPMI-18-0275

Liu, G. F., Wang, X. X., Su, H. Z., and Lu, G. T. (2021). Progress on the GntR family transcription regulators in bacteria. *Yi Chuan = Hered.* 43, 66–73. doi: 10.16288/j.yczz.20-245

Lohou, D., Lonjon, F., Genin, S., and Vailleau, F. (2013). Type III chaperones & Co in bacterial plant pathogens: a set of specialized bodyguards mediating effector delivery. *Front. Plant Sci.* 4. doi: 10.3389/fpls.2013.00435

Macho, A. P. (2016). Subversion of plant cellular functions by bacterial type-III effectors: beyond suppression of immunity. *New Phytol.* 210, 51–57. doi: 10.1111/nph.13605

Mahillon, J., and Chandler, M. (1998). Insertion sequences. *Microbiol. Mol. Biol. Rev.* 62, 725–774. doi: 10.1128/MMBR.62.3.725-774.1998

Manulis, S., and Barash, I. (2003). *Pantoea agglomerans* pvs. gypsophilae and betae, recently evolved pathogens? *Mol. Plant Pathol.* 4, 307–314. doi: 10.1046/j.1364-3703.2003.00178.x

Manulis, S., Gafni, Y., Clark, E., Zutra, D., Ophir, Y., and Barash, I. (1991) Identification of a plasmid DNA probe for detection of strains of *Erwinia herbicola* pathogenic on *Gypsophila paniculata Phytopathol.* 81, 54–57. doi: 10.1094/Phyto-81-54

Manulis, S., Haviv-Chesner, A., Brandl, M. T., Lindow, S. E., and Barash, I. (1998). Differential involvement of indole-3-acetic acid biosynthetic pathways in pathogenicity and epiphytic fitness of *Erwinia herbicola* pv. gypsophilae. *Mol. Plant Microbe Interact.* 11, 634–642. doi: 10.1094/MPMI.1998.11.7.634

Matson, S. W., and Ragonese, H. (2005). The F-plasmid TraI protein contains three functional domains required for conjugative DNA strand transfer. *J. Bacteriol.* 187, 697–706. doi: 10.1128/JB.187.2.697-706.2005

Merrikh, C. N., and Merrikh, H. (2018). Gene inversion potentiates bacterial evolvability and virulence. *Nat. Commun.* 9, 4662. doi: 10.1038/s41467-018-07110-3

Merrikh, H., Zhang, Y., Grossman, A. D., and Wang, J. D. (2012). Replication-transcription conflicts in bacteria. *Nat. Rev. Microbiol.* 10, 449–458. doi: 10.1038/nrmicro2800

Mor, H., Manulis, S., Zuck, M., Nizan, R., Coplin, D. L., and Barash, I. (2001). Genetic organization of the hrp gene cluster and dspAE/BF operon in *Erwinia herbicola* pv. gypsophilae. *Mol. Plant Microbe Interact.* 14, 431–436. doi: 10.1094/MPMI.2001.14.3.431

Moretti, C., Rezzonico, F., Orfei, B., Cortese, C., Moreno-Pérez, A., van den Burg, H. A., et al. (2021). Synergistic interaction between the type III secretion system of the endophytic bacterium *Pantoea agglomerans* DAPP-PG 734 and the virulence of the causal agent of olive knot *Pseudomonas savastanoi* pv. savastanoi DAPP-PG 722. *Mol. Plant Pathol.* 22, 1209–1225. doi: 10.1111/MPP.13105

Morisseau, C., and Hammock, B. D. (2013). Impact of soluble epoxide hydrolase and epoxyeicosanoids on human health. *Annu. Rev. Pharmacol. Toxicol.* 53, 37–58. doi: 10.1146/annurev-pharmtox-011112-140244

Morris, R. O. (1986). Genes specifying auxin and cytokinin biosynthesis in phytopathogens. *Annu. Rev. Plant Physiol.* 37, 509–538. doi: 10.1146/annurev.pp.37.060186.002453

Mukherjee, K., and Bürglin, T. R. (2006). MEKHLA, a novel domain with similarity to PAS domains, is fused to plant homeodomain-leucine zipper III proteins. *Plant Physiol.* 140, 1142–1150. doi: 10.1104/pp.105.073833

Nicolas, E., Lambin, M., Dandoy, D., Galloy, C., Nguyen, N., Oger, C. A., et al. (2015). The Tn3-family of replicative transposons. *Microbiol. Spectr.* 3. doi: 10.1128/microbiolspec.MDNA3-0060-2014

Nissan, G., Chalupowicz, L., Sessa, G., Manulis-Sasson, S., and Barash, I. (2019). Two *Pantoea agglomerans* type III effectors can transform nonpathogenic and phytopathogenic bacteria into host-specific gall-forming pathogens. *Mol. Plant Pathol.* 20, 1582–1587. doi: 10.1111/mpp.12860

Nissan, G., Gershovits, M., Morozov, M., Chalupowicz, L., Sessa, G., Manulis-Sasson, S., et al. (2018). Revealing the inventory of type III effectors in *Pantoea agglomerans* gall-forming pathovars using draft genome sequences and a machine-learning approach. *Mol. Plant Pathol.* 19, 381–392. doi: 10.1111/mpp.12528

Nissan, G., Manulis-Sasson, S., Chalupowicz, L., Teper, D., Yeheskel, A., Pasmanik-Chor, M., et al. (2012). The type III effector HsvG of the gall-forming *Pantoea agglomerans* mediates expression of the host gene HSVGT. *Mol. Plant Microbe Interact.* 25, 231–240. doi: 10.1094/MPMI-06-11-0173

Nissan, G., Manulis-Sasson, S., Weinthal, D., Mor, H., Sessa, G., and Barash, I. (2006). The type III effectors HsvG and HsvB of gall-forming *Pantoea agglomerans* determine host specificity and function as transcriptional activators. *Mol. Microbiol.* 61, 1118–1131. doi: 10.1111/j.1365-2958.2006.05301.x

Nizan, R., Barash, I., Valinsky, L., Lichter, A., and Manulis, S. (1997). The presence of hrp genes on the pathogenicity-associated plasmid of the tumorigenic bacterium *Erwinia herbicola* pv. gypsophilae. *Mol. Plant-Microbe Interact.* 10, 677–682. doi: 10.1094/MPMI.1997.10.5.677

Nizan-Koren, R., Manulis, S., Mor, H., Iraki, N. M., and Barash, I. (2003). The regulatory cascade that activates the Hrp regulon in *Erwinia herbicola* pv. gypsophilae. *Mol. Plant Microbe Interact.* 16, 249–260. doi: 10.1094/MPMI.2003.16.3.249

Occhialini, A., Cunnac, S., Reymond, N., Genin, S., and Boucher, C. (2005). Genome-wide analysis of gene expression in *Ralstonia solanacearum* reveals that the hrpB gene acts as a regulatory switch controlling multiple virulence pathways. *Mol. Plant Microbe Interact.* 18, 938–949. doi: 10.1094/MPMI-18-0938

Ortiz-Martín, I., Thwaites, R., Mansfield, J. W., and Beuzón, C. R. (2010). Negative regulation of the Hrp type III secretion system in *Pseudomonas syringae* pv. phaseolicola. *Mol. Plant Microbe Interact.* 23, 682–701. doi: 10.1094/MPMI-23-5-0682

Overbeek, R., Olson, R., Pusch, G. D., Olsen, G. J., Davis, J. J., Disz, T., et al. (2014). The SEED and the Rapid Annotation of microbial genomes using Subsystems Technology (RAST). *Nucleic Acids Res.* 42, D206–D214. doi: 10.1093/nar/gkt1226

Petnicki-Ocwieja, T., Van Dijk, K., and Alfano, J. R. (2005). The hrpK operon of *Pseudomonas syringae* pv. tomato DC3000 encodes two proteins secreted by the type III (Hrp) protein secretion system: HopB1 and HrpK, a putative type III translocator. *J. Bacteriol.* 187, 649–663. doi: 10.1128/JB.187.2.649-663.2005

Pettinati, I., Brem, J., Lee, S. Y., McHugh, P. J., and Schofield, C. J. (2016). The chemical biology of human metallo-β-lactamase fold proteins. *Trends Biochem. Sci.* 41, 338–355. doi: 10.1016/j.tibs.2015.12.007

Portaliou, A. G., Tsolis, K. C., Loos, M. S., Zorzini, V., and Economou, A. (2016). Type III secretion: building and operating a remarkable nanomachine. *Trends Biochem. Sci.* 41, 175–189. doi: 10.1016/j.tibs.2015.09.005

Rice, P., Longden, L., and Bleasby, A. (2000). EMBOSS: the European molecular biology open software suite. *Trends Genet.* 16, 276–277. doi: 10.1016/S0168-9525(00)02024-2

Saint-Vincent, P. M. B., Ridout, M., Engle, N. L., Lawrence, T. J., Yeary, M. L., Tschaplinski, T. J., et al. (2020). Isolation, characterization, and pathogenicity of two Pseudomonas syringae pathovars from Populus trichocarpa seeds. *mdpi.com* 8, 1137. doi: 10.3390/microorganisms8081137

Seemann, T. (2014). Prokka: rapid prokaryotic genome annotation. *Bioinformatics* 30, 2068–2069. doi: 10.1093/bioinformatics/btu153

Seth-Smith, H. M. B., Fookes, M. C., Okoro, C. K., Baker, S., Harris, S. R., Scott, P., et al. (2012). Structure, diversity, and mobility of the *Salmonella pathogenicity* island 7 family of integrative and conjugative elements within *Enterobacteriaceae*. *J. Bacteriol.* 194, 1494–1504. doi: 10.1128/JB.06403-11

Shevelev, I. V., and Hübscher, U. (2002). The 3' 5' exonucleases. *Nat. Rev. Mol. Cell Biol.* 3, 364–376. doi: 10.1038/nrm804

Siamer, S., Patrit, O., Fagard, M., Belgareh-Touzé, N., and Barny, M.-A. (2011). Expressing the *Erwinia amylovora* type III effector DspA/E in the yeast *Saccharomyces cerevisiae* strongly alters cellular trafficking. *FEBS Open Bio* 1, 23–28. doi: 10.1016/j.fob.2011.11.001

Siguier, P., Gourbeyre, E., and Chandler, M. (2014). Bacterial insertion sequences: their genomic impact and diversity. *FEMS Microbiol. Rev.* 38, 865–891. doi: 10.1111/1574-6976.12067

Siguier, P., Perochon, J., Lestrade, L., Mahillon, J., and Chandler, M. (2006). ISfinder: the reference centre for bacterial insertion sequences. *Nucleic Acids Res.* 34, D32–D36. doi: 10.1093/nar/gkj014

Sokurenko, E. V., Hasty, D. L., and Dykhuizen, D. E. (1999). Pathoadaptive mutations: gene loss and variation in bacterial pathogens. *Trends Microbiol.* 7, 191–195. doi: 10.1016/S0966-842X(99)01493-6

Spiers, A. J., and Bergquist, P. L. (1992). Expression and regulation of the RepA protein of the RepFIB replicon from plasmid P307. *J. Bacteriol.* 174, 7533–7541. doi: 10.1128/jb.174.23.7533-7541.1992

Srimanote, P., Paton, A. W., and Paton, J. C. (2002). Characterization of a novel type IV pilus locus encoded on the large plasmid of locus of enterocyte effacement-negative Shiga-toxigenic *Escherichia coli* strains that are virulent for humans. *Infect. Immun.* 70, 3094–3100. doi: 10.1128/IAI.70.6.3094-3100.2002

Stojanovski, G., Dobrijevic, D., Hailes, H. C., and Ward, J. M. (2020). Identification and catalytic properties of new epoxide hydrolases from the genomic data of soil bacteria. *Enzyme Microb. Technol.* 139, 109592. doi: 10.1016/j.enzmictec.2020.109592

Storch, K. F., Rudolph, J., and Oesterhelt, D. (1999). Car: a cytoplasmic sensor responsible for arginine chemotaxis in the archaeon *Halobacterium salinarum*. *EMBO J.* 18, 1146–1158. doi: 10.1093/emboj/18.5.1146

Subramanya, H. S., Arciszewska, L. K., Baker, R. A., Bird, L. E., Sherratt, D. J., and Wigley, D. B. (1997). Crystal structure of the site-specific recombinase, XerD. *EMBO J.* 16, 5178–5187. doi: 10.1093/emboj/16.17.5178

Sulja, A., Pothier, J. F., Blom, J., Moretti, C., Buonaurio, R., Rezzonico, F., et al. (2022). Comparative genomics to examine the endophytic potential of *Pantoea agglomerans* DAPP-PG 734. *BMC Genomics* 23, 1–15. doi: 10.1186/S12864-022-08966-Y

Suvorova, I. A., Korostelev, Y. D., and Gelfand, M. S. (2015). GntR family of bacterial transcription factors and their DNA binding motifs: structure, positioning and co-evolution. *PloS One* 10, e0132618. doi: 10.1371/journal.pone.0132618

Teper, D., Salomon, D., Sunitha, S., Kim, J.-G., Mudgett, M. B., and Sessa, G. (2014). *Xanthomonas euvesicatoria* type III effector XopQ interacts with tomato and pepper 14-3-3 isoforms to suppress effector-triggered immunity. *Plant J.* 77, 297–309. doi: 10.1111/tpj.12391

Thomas, N. A., Deng, W., Puente, J. L., Frey, E. A., Yip, C. K., Strynadka, N. C. J., et al. (2005). CesT is a multi-effector chaperone and recruitment factor required for the efficient type III secretion of both LEE- and non-LEE-encoded effectors of enteropathogenic *Escherichia coli*. *Mol. Microbiol.* 57, 1762–1779. doi: 10.1111/j.1365-2958.2005.04802.x

Thomas, C. M., and Smith, C. A. (1986). The trfB region of broad host range plasmid RK2: the nucleotide sequence reveals incC and key regulatory gene trfB/korA/korD as overlapping genes. *Nucleic Acids Res.* 14, 4453–4469. doi: 10.1093/nar/14.11.4453

Triplett, L. R., Melotto, M., and Sundin, G. W. (2009). Functional analysis of the N terminus of the *Erwinia amylovora* secreted effector DspA/E reveals features required for secretion, translocation, and binding to the chaperone DspB/F. *Mol. Plant Microbe Interact.* 22, 1282–1292. doi: 10.1094/MPMI-22-10-1282

Triplett, L. R., Wedemeyer, W. J., and Sundin, G. W. (2010). Homology-based modeling of the *Erwinia amylovora* type III secretion chaperone DspF used to identify amino acids required for virulence and interaction with the effector DspE. *Res. Microbiol.* 161, 613–618. doi: 10.1016/j.resmic.2010.05.015

Valinsky, L., Manulis, S., Nizan, R., Ezra, D., and Barash, I. (1998). A pathogenicity gene isolated from the pPATH plasmid of *Erwinia herbicola* pv. gypsophilae determines host specificity. *Mol. Plant Microbe Interact.* 11, 753–762. doi: 10.1094/MPMI.1998.11.8.753

Vela-Corcía, D., Aditya, D.Srivastava, Dafa-Berger, A., Rotem, N., Barda, O., and Levy, M. (2019). MFS transporter from *Botrytis cinerea* provides tolerance to glucosinolate-breakdown products and is required for pathogenicity. *Nat. Commun.* 10, 2886. doi: 10.1038/s41467-019-10860-3

Voth, D. E., Broederdorf, L. J., and Graham, J. G. (2012). Bacterial type IV secretion systems: versatile virulence machines. *Future Microbiol.* 7, 241–257. doi: 10.2217/fmb.11.150

Walker, B. J., Abeel, T., Shea, T., Priest, M., Abouelliel, A., Sakthikumar, S., et al. (2014). Pilon: an integrated tool for comprehensive microbial variant detection and genome assembly improvement. *PloS One* 9, e112963. doi: 10.1371/JOURNAL.PONE.0112963

Wang, Z. (2001). Translesion synthesis by the UmuC family of DNA polymerases. *Mutat. Res.* 486, 59–70. doi: 10.1016/s0921-8777(01)00089-1

Washington, E. J., Mukhtar, M. S., Finkel, O. M., Wan, L., Banfield, M. J., Kieber, J. J., et al. (2016). *Pseudomonas syringae* type III effector HopAF1 suppresses plant immunity by targeting methionine recycling to block ethylene induction. *Proc. Natl. Acad. Sci. U. S. A.* 113, E3577–E3586. doi: 10.1073/pnas.1606322113

Weber, E., and Koebnik, R. (2006). Positive selection of the Hrp pilin HrpE of the plant pathogen *Xanthomonas*. *J. Bacteriol.* 188, 1405–1410. doi: 10.1128/JB.188.4.1405-1410.2006

Wehling, M. D., Guo, M., Fu, Z. Q., and Alfano, J. R. (2004). The *Pseudomonas syringae* HopPtoV protein is secreted in culture and translocated into plant cells via the type III protein secretion system in a manner dependent on the ShcV type III chaperone. *J. Bacteriol.* 186, 3621–3630. doi: 10.1128/JB.186.11.3621-3630.2004

Wei, Z., Kim, J. F., and Beer, S. V. (2000b). Regulation of hrp genes and type III protein secretion in Erwinia amylovora by HrpX/HrpY, a novel two-component system, and HrpS. *Mol. Plant Microbe Interact.* 13, 1251–1262. doi: 10.1094/MPMI.2000.13.11.1251

Wei, C.-F., Kvitko, B. H., Shimizu, R., Crabill, E., Alfano, J. R., Lin, N.-C., et al. (2007). A *Pseudomonas syringae* pv. tomato DC3000 mutant lacking the type III effector HopQ1-1 is able to cause disease in the model plant *Nicotiana benthamiana*. *Plant J.* 51, 32–46. doi: 10.1111/j.1365-313X.2007.03126.x

Wei, W., Plovanich-Jones, A., Deng, W. L., Jin, Q. L., Collmer, A., Huang, H. C., et al. (2000a). The gene coding for the Hrp pilus structural protein is required for type III secretion of Hrp and Avr proteins in *Pseudomonas syringae* pv. tomato. *Proc. Natl. Acad. Sci. U. S. A.* 97, 2247–2252. doi: 10.1073/pnas.040570097

Weinthal, D. M., Barash, I., Panijel, M., Valinsky, L., Gaba, V., and Manulis-Sasson, S. (2007). Distribution and replication of the pathogenicity plasmid pPATH in diverse populations of the gall-forming bacterium *Pantoea agglomerans*. *Appl. Environ. Microbiol.* 73, 7552–7561. doi: 10.1128/AEM.01511-07

Zatyka, M., and Thomas, C. M. (1998). Control of genes for conjugative transfer of plasmids and other mobile elements. *FEMS Microbiol. Rev.* 21, 291–319. doi: 10.1111/j.1574-6976.1998.tb00355.x

frontiers | Frontiers in Plant Science

TYPE Original Research
PUBLISHED 13 September 2023
DOI 10.3389/fpls.2023.1254107

OPEN ACCESS

EDITED BY
Vittoria Catara,
University of Catania, Italy

REVIEWED BY
Alessandro Passera,
University of Milan, Italy
Massimiliano Morelli,
National Research Council (CNR), Italy

*CORRESPONDENCE
Monika Kałużna
monika.kaluzna@inhort.pl
Joël F. Pothier
joel.pothier@zhaw.ch

RECEIVED 06 July 2023
ACCEPTED 18 August 2023
PUBLISHED 13 September 2023

CITATION
Kałużna M, Prokić A, Obradović A, Weldon WA, Stockwell VO and Pothier JF (2023) Specific and sensitive detection tools for *Xanthomonas arboricola* pv. corylina, the causal agent of bacterial blight of hazelnut, developed with comparative genomics.
Front. Plant Sci. 14:1254107.
doi: 10.3389/fpls.2023.1254107

Specific and sensitive detection tools for *Xanthomonas arboricola* pv. corylina, the causal agent of bacterial blight of hazelnut, developed with comparative genomics

Monika Kałużna[1]*, Andjelka Prokić[2], Aleksa Obradović[2], William A. Weldon[3], Virginia O. Stockwell[4] and Joël F. Pothier[5]*

[1]The National Institute of Horticultural Research, Skierniewice, Poland, [2]University of Belgrade, Faculty of Agriculture, Belgrade, Serbia, [3]Valent BioSciences, Libertyville, IL, United States, [4]United States Department of Agriculture, Agricultural Research Service, Horticultural Crops Disease and Pest Management Research Unit, Corvallis, OR, United States, [5]Environmental Genomics and Systems Biology Research Group, Institute for Natural Resource Sciences, Zurich University of Applied Sciences (ZHAW), Wädenswil, Switzerland

Xanthomonas arboricola pv. corylina (*Xac*; formerly *Xanthomonas campestris* pv. corylina) is the causal agent of the bacterial blight of hazelnuts, a devastating disease of trees in plant nurseries and young orchards. Currently, there are no PCR assays to distinguish *Xac* from all other pathovars of *X. arboricola*. A comparative genomics approach with publicly available genomes of *Xac* was used to identify unique sequences, conserved across the genomes of the pathogen. We identified a 2,440 bp genomic region that was unique to *Xac* and designed identification and detection systems for conventional PCR, qPCR (SYBR® Green and TaqMan™), and loop-mediated isothermal amplification (LAMP). All PCR assays performed on genomic DNA isolated from eight *X. arboricola* pathovars and closely related bacterial species confirmed the specificity of designed primers. These new multi-platform molecular diagnostic tools may be used by plant clinics and researchers to detect and identify *Xac* in pure cultures and hazelnut tissues rapidly and accurately.

KEYWORDS

***Corylus* spp., *Corylus avellana*, diagnosis, PCR, LAMP, qPCR**

1 Introduction

Xanthomonas arboricola pv. corylina (*Xac*; formerly *Xanthomonas campestris* pv. corylina; Vauterin et al., 1995) is a Gram-negative plant pathogenic bacterium of the *Lysobacteraceae* family (earlier synonym of *Xanthomonadaceae*) (Saddler and Bradbury, 2005; Tindall, 2014). *Xac* is the causal agent of the bacterial blight of hazelnut (*Corylus avellana* L.). Other *Corylus* spp., including *C. pontica*, *C. maxima* and *C. colurna*, also can

be infected by *Xac* (OEPP/EPPO, 1986; OEPP/EPPO, 2004). Bacterial blight of hazelnut is a devastating disease that is commonly observed in plant nurseries and young orchards, causing significant plant mortality (Miller et al., 1949; Moore, 2002; OEPP/EPPO, 2004; Lamichhane and Varvaro, 2014; Webber et al., 2021). The disease also can be seen in established production orchards, especially on susceptible cultivars. The main disease symptoms include angular necrotic lesions on leaves and the involucres of shells, as well as shoot necrosis and cankers. Lesions on the stalk and top of nuts results in reduced nut quality. Dieback of nut-bearing branches causes measurable yield reduction. Over time, bacterial blight of hazelnut reduces tree health and results in poor tree structure and continued yield losses (Obradović et al., 2010; Kałużna et al., 2021).

Xac has been a regulated pathogen and placed on the European and Mediterranean Plant Protection Organization (EPPO) list A2 of quarantine pathogens, but it was recently reclassified as a Regulated Non-Quarantine Pest (RNQP) (European Union, 2016; European Union, 2019). Currently, bacterial blight caused by *Xac* has been reported in nearly every hazelnut-producing country (OEPP/EPPO, 2004; Kałużna et al., 2021; Osdaghi, 2022). Identification of *Xac* is currently a tedious, multistep process, which is described below and can take several days to return a diagnostic result. Difficulty in identification arises largely because it is closely related to seven other pathovars of *X. arboricola*, including pv. pruni (*Xap*), pv. juglandis (*Xaj*), pv. fragariae, pv. celebensis, pv. arracaciae, pv. poinsettiicola and pv. zantedeschiae (Vauterin et al., 1995; Janse et al., 2001; Fischer-Le Saux et al., 2015; Kałużna et al., 2021). Two former *X. arboricola* pathovars were recently elevated to the species rank as *X. guizotiae* and *X. populina* (Zarei et al., 2022).

The diagnostic procedures for *Xac* as recommended by EPPO rely on the observation of disease symptoms, microscopic examination of the symptomatic tissues, isolation of the pathogen from the plant material on common microbiological media for xanthomonads (Schaad et al., 2001), observation of colony morphology, biochemical, phenotypic, and pathogenicity assays (Lelliott and Stead, 1987; OEPP/EPPO, 2004). *Xac* also can be identified with serological methods following the procedures described in EPPO protocols (OEPP/EPPO, 2010b).

Molecular tools for rapid diagnosis of *Xac* colonies currently include methods specific for the genus *Xanthomonas* (Maes, 1993) and for the species *X. arboricola* (Pothier et al., 2011a). To identify *X. arboricola* isolates to the pathovar level, rep-PCR and partial sequence alignments are generally used (Tuang et al., 1999; Schaad et al., 2001; Scortichini et al., 2002; Parkinson et al., 2007; Young et al., 2008; Calić et al., 2009; OEPP/EPPO, 2010a; Puławska et al., 2010; Webber et al., 2020). Moreover, it was reported that primers designed for identification of *X. arboricola* pv. pruni (XapY17-F/XapY17-R) can also generate amplicons of some *Xac* strains (Pothier et al., 2011a; Webber et al., 2020).

Currently, there are no rapid and sensitive diagnostic tools for *Xac* (Prokić et al., 2012; Kałużna et al., 2021). The conventional methods are too labor-intensive and slow for routine detection and diagnosis, as complete diagnostic protocols can take several days. Additionally, the symptoms of bacterial blight of hazelnuts may be confused with anthracnose, a fungal disease caused by *Piggotia coryli* (Roberge ex Desm.) B. Sutton (Syn. *Gloeosporium coryli* (Roberge ex Desm.) Sacc.). Disease misidentification can lead to applying ineffective management methods and use of unwarranted chemical applications.

Recently, next-generation sequencing (NGS) and comparative genomics have developed as effective methods to provide information on pathogen population structures, create species specific markers, and characterize virulence or antibiotic resistance genes. The genomes and/or plasmids of several pathovars of *X. arboricola*, including *Xac*, have been sequenced (Pothier et al., 2011b; Pothier et al., 2011c; Ibarra Caballero et al., 2013; Garita-Cambronero et al., 2014; Cesbron et al., 2015; Higuera et al., 2015; Ignatov et al., 2015; Garita-Cambronero et al., 2016a; Garita-Cambronero et al., 2016b; Garita-Cambronero et al., 2016c; Harrison et al., 2016; López-Soriano et al., 2016; Garita-Cambronero et al., 2017; Retamales et al., 2017; Fernandes et al., 2018; Fu et al., 2018; Gétaz et al., 2018; Nuñez Cerda et al., 2021; Teixeira et al., 2021; Cuesta-Morrondo et al., 2022; D'Amico-Willman et al., 2022; Herbert et al., 2022; Kałużna and Pothier, 2022; Pothier et al., 2022). The available sequence data and the needs of the grower community and diagnostic laboratories prompted us to develop rapid, accurate and sensitive tools for the bacterial blight of hazelnut causal agent. We developed molecular tools for identification of *Xac* that could be used with several platforms, including conventional PCR, qPCR, and Loop-mediated isothermal AMPlification (LAMP), to facilitate adoption based on available laboratory equipment. We validated each of the tools using genomic DNA isolated from pure cultures of *Xac* and DNA isolated from artificially inoculated and field-infected plant material. These fast and accurate identification and detection methods will aid in the diagnosis and management of bacterial blight of hazelnut in nursery stock tissues, nurseries, and in both young and established orchards.

2 Materials and methods

2.1 Bacterial strains

Xac isolates and strains collected from different geographical regions (n = 60) were tested to validate all diagnostic assays. Additionally, a collection of type and non-type strains of all pathovars of *X. arboricola* species, other closely related *Xanthomonas* species (n = 30), and microorganisms (bacteria and fungi) isolated from symptomatic hazelnut and walnut tissues, i.e. *Pseudomonas* spp., *Pseudomonas avellanae*, *Sphingomonas* spp. and *Xanthomonas campestris* (n = 46) were included in assays (Table 1, Supplementary Table S1).

Xanthomonads were grown on yeast extract nutrient agar (YNA) or yeast extract dextrose calcium carbonate (YDC; Schaad et al., 2001) and pseudomonads were cultured on King's B medium (King et al., 1954) at 28°C for 24 to 48 h. The nine fungal isolates were grown on PDA (potato dextrose agar; Becton Dickinson, Sparks, MD, USA) at 24°C with an 8 h light and 16 h dark photoperiod.

10.3389/fpls.2023.1254107

TABLE 1 Summary of *in vitro* primers specificity with the different *Xanthomonas arboricola* pv. corylina detection tools developed in this study.

Organism or material type	No. ...	Conventional PCR						qPCR[1]						LAMP		
		Xac2.4-1	Xac2.4-4	XacPPU-1	Xac45-1	Xac45	XacPPU54630	Xac2.4-2RT	Xac45-1RT	Xac45-2RT	Xac2.4-3RT	Xac-PPU54630	Xac-reg45	XacPPU-1	NewXac2.4-1	NewXac2.4-2
X. arboricola pv. corylina (*n* = 60)	tested	42	42	42	42	36	36	28	28	28	28	23	23	23	23	23
	positive	*42*	*42*[2]	*42*[3]	*42*	*36*	*36*	*28*	*28*	*28*	*28*	*23*	*23*	*23*	*23*	*23*
Other *X. arboricola* pathovars (*n* = 27)	tested	22	22	22	22	6	6	22	23	22	22	17	17	22	22	22
	positive	*0*	*0*	*0*	*0*	*0*	*0*	*0*	*0*	*0*	*0*	*0*	*0*	*0*	*0*	*0*
Former *X. arboricola* pathovars (*n* = 3)	tested	2	2	2	2	1	1	2	2	2	2	2	2	2	2	2
	positive	0	0	0	0	0	0	0	0	0	0	0	0	0	0	0
Pseudomonas avellanae (*n* = 2)	tested	2	2	2	2	-[4]	–	2	2	2	2	2	2	2	2	2
	positive	*0*	*0*	*0*	*0*			*0*	*0*	*0*	*0*	*0*	*0*	*0*	*0*	*0*
HR[5] negative *Pseudomonas* isolates from hazelnut (*n* = 9)	tested	8	8	8	8	–	–	8	8	8	8	2	2	8	8	8
	positive	*0*	*0*	*0*	*0*			*0*	*0*	*0*	*0*	*0*	*0*	*0*	*0*	*0*
Sphingomonas sp. non-pathogenic on hazelnut (*n* = 1)	tested	1	1	1	1	1	1	–	–	–	–	–	–	–	–	–
	positive	*0*	*0*	*0*	*0*	*0*	*0*									
Xanthomonas campestris non-pathogenic on hazelnut (*n* = 1)	tested	1	1	1	1	1	1	–	–	–	–	–	–	–	–	–
	positive	*0*	*0*	*0*	*0*	*0*	*0*									
HR positive *Pseudomonas* from walnut (*n* = 3)	tested	3	3	3	3	–	–	2	2	2	2	–	–	1	1	1
	positive	*0*	*0*	*0*	*0*			*0*	*0*	*0*	*0*			*0*	*0*	*0*
HR negative *Pseudomonas* and other hazelnut isolates (*n* = 8)	tested	7	7	7	7	–	–	8	8	8	8	–	–	8	8	8
	positive	*0*	*0*	*0*	*0*			*0*	*0*	*0*	*0*			*0*	*0*	*0*
HR negative *Pseudomonas* and other walnut isolates (*n* = 8)	tested	8	8	8	8	–	–	8	8	8	8	–	–	8	8	8
	positive	*0*	*0*	*0*	*0*			*0*	*0*	*0*	*0*			*0*	*0*	*0*
DNA from healthy plants (*n* = 5)	tested	5	5	5	5	–	–	5	5	5	5	–	–	5	5	5
	positive	*0*	*0*	*0*	*0*			*0*	*0*	*0*	*0*			*0*	*0*	*0*
Fungi isolated from diseased hazelnut (*n* = 4)	tested	4	4	4	4	–	–	4	4	4	4	–	–	–	–	–
	positive	*0*	*0*	*0*	*0*			*0*	*0*	*0*	*0*					
Fungi isolated from diseased walnut (*n* = 5)	tested	5	5	5	5	–	–	5	5	5	5	–	–	–	–	–
	positive	*0*	*0*	*0*	*0*			*0*	*0*	*0*	*0*					

[1]The first five columns for qPCR correspond to assays performed with SYBR® Green I whereas the last column corresponds to a TaqMan™ assay.
[2]A smaller amplicon of 900 bp was observed with one strain instead of the 1,455 bp expected amplicon.
[3]Larger amplicons of 1,150 bp and 1,450 bp were observed with two strains instead of the 385 bp expected amplicon.
[4]"-" denotes not tested.
[5]HR: hypersensitivity reaction on tobacco leaves cv. 'Samsun'.

2.2 DNA isolation from bacterial and fungal cultures

Genomic bacterial DNA was isolated using the Genomic Mini bacterial DNA Purification Kit (A&A Biotechnology, Poland), the DNeasy Mericon Food Kit (Qiagen, Hilden, Germany) or Whole Blood and Tissue kit (Qiagen, Germantown, MD, USA), according to the manufacturer's instructions. The total fungal DNA was extracted from 100 mg of mycelia scraped from 10-day-old PDA cultures with the GeneMatrix Plant & Fungi DNA Purification Kit (EURx, Gdańsk, Poland) according to the manufacturer's instructions. The quality and total DNA concentration was estimated with a NanoDrop ND-100 or NanoDrop 2000c (ThermoFisherScientific, Waltham, MA, USA).

2.3 Genome-informed target identification

DNA sequences from three *Xac* whole genome shotgun sequencing projects (WGS) (CFBP 1159^{PT}, CFBP 2565 and NCCB 100457; GenBank WGS prefixes MDEA01, MDSJ01 and APMC02, respectively) was used for comparative genomic analysis. A 'dual-BLASTn' comparative genomics pipeline was applied to select 300-bp regions shared among these three target WGS (Schneeberger et al., 2017). After segmentation into 300 bp length fragments, duplicates were removed and *Xac* unique sequences were selected using BLASTn+ v.2.8.1 (Altschul et al., 1990; Camacho et al., 2009) analysis against the database derived from the three genomes. Regions obtained from this workflow were further checked for *Xac* specificity using online BLASTn searches against the *nr*/*nt* and *X. arboricola* and *Xanthomonas* WGS NCBI databases (accessed in July 2019). Finally, *Xac*-specific DNA markers were also confirmed in three recently released *Xac* complete genomes (CFBP 1159^{PT}, CFBP 6600 and Xac 301; GenBank assemblies GCA_905220785.1, GCA_905220805.1, and GCA_905220715.1, respectively; Pothier et al., 2022).

2.4 Primer design and synthesis

Three *Xac*-specific regions and their associated primers were given 'in-house' names during analyses, the genome context of the regions is illustrated in Figure 1. These regions were used to design primers for: 1) conventional PCR, 2) qPCR (SYBR® Green and TaqMan™), and 3) LAMP. The primers for conventional PCR and qPCR were designed using the PrimerSelect program of the LASERGENE package v.9 (DNASTAR, Madison, WI, USA) and Primer3Web v.4.1.0. (Untergasser et al., 2012). LAMP primers were designed using the online platform PrimerExplorer v.5 (Eiken Chemical Co., Ltd, Tokyo, Japan, http://primerexplorer.jp/lampv5e/

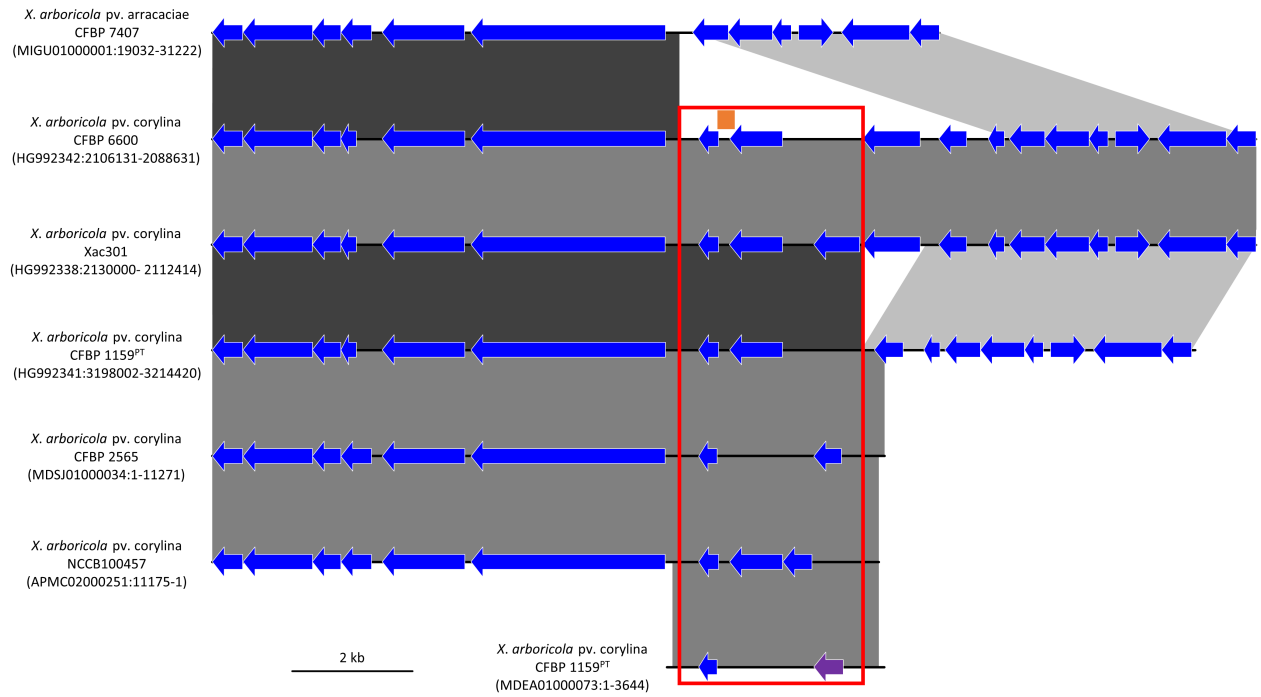

FIGURE 1
Comparison of the genetic environment of the *Xanthomonas arboricola* pv. corylina (*Xac*) specific DNA targets in six *Xac* draft and complete genomes and one draft *X. arboricola* pv. arracaciae draft genome. The 300 bp *Xac*-specific region called "target 45" is represented by an orange bar, the XaxcyCFBP1159_22010 singleton encoding the hypothetical protein "PPU54630" is displayed by a purple arrow, and the 2.4 kb region called "region 2.4" identified by comparative genomics is indicated by the red frame. Other CoDing Sequence (CDS) are shown with blue arrows, which do not denote any shared identity among the genomes. Regions with high DNA sequence identity between the genomes are represented with blocks using a black to grey scale with black representing the highest identity. The strain name is followed by the GenBank accession number and the location of the genomic region displayed.

index.html) also including loop primers (i.e. in total six primers) to speed up the LAMP reaction (Nagamine et al., 2002). Based on the regions selected (Figure 1), ten candidate primer sets were designed for conventional PCR (5, 2 and 3 primer sets based on the "region 2.4", "PPU54630", and "target 45" *Xac*-specific DNA markers, respectively), six for SYBR® Green I qPCR (3, 1 and 2 primer sets based on the "region 2.4", "PPU54630", and "target 45" *Xac*-specific DNA markers, respectively), two for TaqMan™ qPCR (one primer pair based on the "region 2.4" and one based on the "target 45" *Xac*-specific DNA markers), and three for LAMP (two primer pairs based on the "region 2.4" and one based on the "PPU54630" *Xac*-specific DNA markers). The primers for the TaqMan™ qPCR were purchased HPLC purified since this effectively increases the melting temperature (T_m) for shorter sequences, allowing for an overall shorter amplicon while remaining within temperature requirements. The TaqMan™ probes were designed with a 5′ FAM reporter dye and a 3' BHQ-1 non-fluorescent quencher. Initially, the specificity of the primers, the TaqMan™ probe, and predicted amplicons to *Xac* were tested *in silico* with BLASTn searches against the *nr/nt* and WGS NCBI databases (accessed in July 2019). All these primer sets were then tested *in vitro* for specificity, sensitivity, and reproducibility during screening. Depending on the research institutions, primers were synthesized at Genomed S.A. (Warszawa, Poland), Invitrogen (ThermoFisherScientific, Waltham, MA, USA) and MilliporeSigma (Burlington, MA., USA).

2.5 Primer selection based on *in vitro* specificity analysis

The *in vitro* specificity of all primers was tested with purified genomic DNA of the bacteria and fungi listed in Table 1 (detailed in Supplementary Table S1).

To exclude potential non-specific amplification of plant genomic DNA with the primers, total plant DNA was isolated from clean asymptomatic leaves of five hazelnut cultivars (cv. 'Cosford', cv. 'Merveille de Bollwiller', cv. 'Garibaldi', cv. 'Webb's Prize Cob' and cv. 'Hall's Giant') grown in a greenhouse. Total plant DNA was isolated from leaves using the GeneMATRIX Plant & Fungi DNA Purification Kit (EURx, Gdańsk, Poland), as well as the Genomic Mini DNA Extraction Kit (A&A Biotechnology, Gdynia, Poland) to isolate bacterial DNA. Both kits were used according to the manufacturer's instructions with the following specifications concerning the starting material. To isolate plant DNA: 100 mg from hazelnut leaves were homogenized in liquid nitrogen in a cooled mortar and pestle and transferred to a 2 ml tube before addition of 400 µl lysis buffer L. For bacterial DNA isolation: 100 mg of crushed or cut leaf tissue was placed in 20 ml of PBS buffer, incubated for 1 h at 26°C with shaking (150 rpm), pelleted by centrifugation (5 min at 12,000 × *g*), and then re-suspended in 100 µl Tris EDTA (TE) buffer.

Three labs participated in the specificity validation of the assays: two assay development laboratories (Poland and Serbia) and one assay testing laboratory (USA).

The reactions were conducted according to the protocols established based on the optimization of all reagents and temperature gradient analysis performed separately for each primer pair. The amplification conditions for all the primers pairs/sets are listed in Table 2.

Amplification reactions with the four selected primer pairs for conventional PCR were conducted in a Biometra T3000 thermocycler (Biometra, Göttingen, Germany) in Poland, in a Thermo Cycler 2720 (Applied Biosystems, USA) in Serbia, and a Veriti 96-well Thermal Cycler 9902 (Applied Biosystems, USA) in the USA. The total amplification reaction mixtures for primers in 15 µl of volume included: 10 to 15 ng of DNA, 0.4 U of DreamTaq DNA Polymerase (ThermoFisherScientific, Waltham, MA, USA), 1× reaction DreamTaq Green buffer, 0.15 mM each dNTPs and 0.7 mM of each primer. The amplicons obtained in individual reactions for each primer pair were separated in 1.5% agarose gels in 0.5× TBE buffer (0.045 M Tris-boric acid, 0.001 M EDTA, pH 8.0) (Sambrook et al., 1989). To confirm the size of the obtained product O'GeneRuler100-bp DNA Ladder Plus (ThermoFisherScientific, Waltham, MA, USA) was used. Gels were stained in an ethidium bromide solution (0.5 µg ml^{-1}) and obtained products were visualized under UV irradiation.

SYBR® Green I qPCRs were conducted in a Bio-Rad CFX96 (Bio-Rad, Hercules, CA, USA) with SsoAdvanced™ Universal SYBR® Green Supermix (Bio-Rad, Hercules, CA, USA) in Poland or a Mic qPCR Cycler (Bio Molecular Systems, Australia) in Serbia. The reaction mixture in 20 µl of total volume included 1× reaction SYBR® Green Supermix and 0.5 mM of each primer from the following primer sets: Xac2.4-2RT, Xac45-1RT, Xac45-2RT, Xac2.43RT, and 10 ng of DNA. The PCR programs for all above-listed primers are given in Table 3. The specificity of amplification products was verified by a melting curve analysis using a progressive denaturation of products at a rising temperature (Table 3). Specific melting temperatures observed are indicated in Table 2.

The validation of the TaqMan™ qPCR was also done in Poland. The sequence of probes and primers are indicated in Table 2. Reactions were conducted in a Bio-Rad CFX96 (Bio-Rad, Hercules, CA, USA) using the amplification conditions in Table 3. The TaqMan™ qPCR assays were carried out in a 10 µl total reaction mixture containing 1 µl of template DNA, 0.25 µl of primers Xac-PPU54630-F and Xac-PPU54630-R (0.25 µM final concentration of each), 0.15 µl of probe Xac-PPU54630-P (0.15 µM final concentration), 1× TaqMan™ Fast Universal PCR Master Mix (Applied Biosystems, USA).

Loop-mediated isothermal amplifications were performed on a Bio-Rad CFX96 (Bio-Rad, Hercules, CA, USA) in Poland. The reactions mixture carried out in a total volume of 20 µl contained 1× Isothermal Mastermix (OptiGene, Horsham, UK) and primers at the final concentrations as follows: outer primers F3/B3 0.2 µM each, inner primers FIB/BIP 0.8 µM each and loop primers 0.4 µM each. Fluorescence was detected on the FAM channel. The LAMP reaction mixtures were run according to conditions detailed in Table 3.

2.6 Limits of detection of DNA- and crude bacterial cell-based assays

The limits of detection (LoD) of all the DNA-template based assays were tested with 10-fold dilutions series prepared in TE

10.3389/fpls.2023.1254107

TABLE 2 Nucleotide sequences of specific primers developed in this study for the detection of *Xanthomonas arboricola* pv. corylina.

Assay target or code name[1]	Primer info[2]	Primer sequence 5′-3′	Amplicon length[3] (bp)	MCA T_m[4] (°C)
Conventional PCR				
Xac2.4-1	F	CCGCCACCATTTAGTACACGAGGAG	794	NA
	R	GGAGCCCGCGGAGATAGTTGC		
Xac2.4-4	F	TAATTCCAACTCCCCAAGCGTATC	1,455[5]	NA
	R	AATGAATTGGAGTGGTTGTTTAGG		
XacPPU-1	F	TCCCAACACTAAGTCTTCAACATC	385[6]	NA
	R	GGTGCAGGTGGGAGGTGGTAAC		
Xac45-1	F	TTCCTCAATGCGGGCCAGTAATGTC	197	NA
	R	ATAGTGATAATGAGGTGGCAGTCG		
Xac45	F	CCAGTCTCACCCAACGTCAGA	198	NA
	R	TGTCGTGGAATCAACCTGATGTG		
XacPPU54630	F	CACCAGAAAAGCAGGGCCATAAC	159	NA
	R	GGCAATGGAAGGACGTCTAGG		
qPCR SYBR® Green I				
Xac2.4-2RT	F	AGCAGGGCCATAACTTCTTG	170	81.5
	R	ATATACACCCCTTTTTGGATGG		
Xac45-1RT	F	CTTGCCCAGCCCCCAGTC	104	84.5
	R	TATGAACAACGTACCGCAGATG		
Xac45-2RT	F	AAGTGCTTGCAAATAATAAATC	88	81.5
	R	TGTCGTGGAATCAACCTG		
Xac2.4-3RT	F	GCCACCATTTAGTACACGAGGAGTTC	102	81.0
	R	TATTTCGGTAGAGCTAGTCGGTTGTC		
qPCR TaqMan™				
Xac-reg45	F	CCAGTCTCACCCAACGTCAGA	198	NA
	R	TGTCGTGGAATCAACCTGATGTG		
	P	FAM-CATGATCATTCCTCAATGCG-BHQ-1		
Xac-PPU54630	F	CACCAGAAAAGCAGGGCCATAAC	159	NA
	R	GGCAATGGAAGGACGTCTAGG		
	P	FAM-TAATTAACCAAGCCATCGCC-BHQ-1		
LAMP				
XacPPU-1	F3	CGAAAAAAATAAGGAAACTTCACC	(214)[7]	84
	B3	ATTCATAGCGCCACGATA		
	FIP	GGATGGCAATGGAAGGACGTCACCCCCTATCTCCCTC		
	BIP	TAGAAAAGAAAGAAAGCTATCCGCTAAATGAATTGGAGTGGTTGTT		
	LF	AGGTTAGCCCTTCAGGTACTC		
	LB	ACTAGGCTCATCTATTACCCTAGTT		

(Continued)

10.3389/fpls.2023.1254107

TABLE 2 Continued

Assay target or code name[1]	Primer info[2]	Primer sequence 5′-3′	Amplicon length[3] (bp)	MCA T_m[4] (°C)
Xac2.4-1	F3	CGAAAAAAATAAGGAAACTTCACC	(214)	83.5
	B3	ATTCATAGCGCCACGATA		
	FIP	TACACCCCTTTTTGGATGGCAATCCCTATCTCCCTCATGAGTAC		
	BIP	TAGAAAAGAAAGAAAGCTATCCGCTAAATGAATTGGAGTGGTTGTT		
	LF	GAAGGACGTCTAGGTTAGCCCTTCA		
	LB	ACTAGGCTCATCTATTACCCTAGTT		
Xac2.4-2	F3	ATTCCTGAGGACTAGGCACT	(186)	87.5
	B3	CTTTGAGACGCGCTGTCG		
	FIP	TTGTGGTGAAGAACCGCCGTATCTGATCATCGAGGGACCCG		
	BIP	GCAAGGAAACTCTGGCAACGGATGCGCTAGGCATATTTGGTG		
	LF	GGAGGTGGTCTTTATAATGCTGG		
	LB	AAAGTTTCAGCCGAGGCAAA		

[1]Primer names begin with Xac45, Xac2.4, or XacPPU to indicate targeted genomic regions (target 45, region 2.4, or PPU54630, respectively) shown in Figure 1. RT at the end of the primer code name stands for real-time.
[2]Primer information is abbreviated as follows, F, forward primer; R, reverse primer; P, probe; F3, forward outer primer; B3, backward outer primer; FIP, forward inner primer; BIP, backward inner primer; LF, forward loop primer; LB, backward loop primer.
[3]Expected amplicon length based on the complete genome of *X. arboricola* pv. corylina CFBP 1159^{PT} (GenBank accession number HG992341) and amplicon size commonly observed during *in vitro* tests. Depending on the assay, a few strains produced an amplicon with a different size as indicated below in footnotes 5 and 6, and with more details in Supplementary Table S1.
[4]Specific melting temperature observed during melting curve analysis. NA, not applicable.
[5]A smaller amplicon of 900 bp was observed with one strain.
[6]Larger amplicons of 1,150 bp and 1,450 bp were observed with two strains.
[7]Parentheses indicate the predicted size (bp) of the region targeted by the F3 and B3 primers in LAMP assays.

TABLE 3 Amplification conditions for the primers pairs/sets designed and used in this study.

Detection tool	Assay target	Reaction conditions
Conventional PCR	Xac2.4-1	95°C for 4 min, 30× (94°C for 35 s, 63°C for 45 s, 72°C for 1 min), 72°C for 10 min
	Xac2.4-4	95°C for 4 min, 35× (94°C for 35 s, 58°C for 45 s, 72°C for 1 min), 72°C for 10 min
	XacPPU-1	95°C for 4 min, 30× (94°C for 30 s, 61°C for 40 s, 72°C for 55 s), 72°C for 10 min
	Xac45-1	95°C for 4 min, 30× (94°C for 25 s, 61°C for 35 s, 72°C for 50 s), 72°C for 7 min
	Xac45	95°C for 2 min, 30× (94°C for 30 s, 53°C for 30 s, 68°C for 45 s), 68°C for 5 min
	XacPPU54630	95°C for 2 min, 30× (95°C for 30 s, 53°C for 30 s, 68°C for 45 s), 68°C for 5 min
qPCR SYBR® Green I	all primer pairs	98°C for 2 min, 35× (95°C for 10 s, 60°C for 20 s), 65→95°C with +0.01°C s^{-1}
qPCR TaqMan™	all primer sets	95°C for 10 min, 40× (95°C for 10 s, 55°C for 40 s)
LAMP	all primer sets	50× (63°C for 30 s), 65→95°C with +0.01°C s^{-1}

buffer using bacterial genomic DNA isolated from pure cultures of CFBP 1159^{PT} and Xac 301. The dilution series ranged from ~10 ng µl^{-1} to 0.1 fg µl^{-1} based on the initial concentrations determined with a NanoDrop ND-100 (ThermoFisherScientific, Waltham, MA, USA). Additionally, bacterial genomic DNA was independently extracted from pure bacterial cultures of these two same strains using known bacterial concentrations ranging from ~10^8 to 10^0 CFU ml^{-1} as described in Kałużna et al. (2016).

For the crude bacterial cell-template based assays, 100 µl of different concentrations of aqueous suspensions of strain Xac 301 were added to 100 mg of crushed/cut fragments of leaves or stems. Then DNA was isolated from these 'heterogeneous suspensions' according to the methodology described by Kałużna et al. (2016).

For the PCR-based assays, the efficiency (E) was calculated from the slope (S) of the standard curve generated for each run using the following equation $E = 10^{(-1/S)}$ with $E = 2$ corresponding to 100% efficiency (Ramakers et al., 2003).

2.7 Validation of assays on artificially and naturally infected hazelnuts

To test the usefulness of designed primers, positive controls for *in planta* detection were obtained from artificially inoculated hazelnut cvs. 'Cosford' and 'Merveille de Bollwiller' (two samples from each cultivar) maintained in a greenhouse, as well as from naturally infected material obtained from orchards (two samples). For artificial inoculation of the hazelnut cultivars, a 48-h culture of Xac 301 grown on YNA medium was suspended in sterile water (10^8 and 10^7 CFU ml^{-1}) and infiltrated into hazelnut leaves with a needleless syringe and/or injected into green shoots using a hypodermic needle (0.7×30mm) attached to a syringe. Four to six weeks post-inoculation, symptomatic plant tissue was harvested. Leaf samples were rubbed for 10 s on both sides with a cotton-swab soaked in 70% ethanol. A sample consisting of three 1-cm^2 segments including the lesion border was collected, crushed, and suspended in 1 to 2 ml sterile PBS for 15 min. We then tested two DNA extraction methods on the tissue macerate. In the first one, 10 µl of the plant macerate was added to 190 µl of TE buffer, boiled for 10 min at 100°C, and then centrifuged for 5 min at 9,500 × *g*. In the second approach, 10 µl of the plant macerate was added to 90 µl of TE buffer and total DNA was isolated using the Genomic Mini DNA Extraction Kit (A&A Biotechnology Gdynia, Poland) according to the manufacturer's instructions. The boiled extract and purified DNA extract were used as templates in molecular assays. To confirm the infection by *Xac*, especially from naturally infected plant material, bacterial colony isolation was done simultaneously by plating on YNA medium.

3 Results

3.1 Genome-informed *Xac*-specific targets

The *in silico* analysis resulted in the detection of a highly conserved, *Xac*-specific sequence of 300 bp called "target 45" that had no hit with other bacteria in the database. A 2,440 bp genomic region called "region 2.4" encompassing "target 45" was identified after performing the comparative genomic analysis of target 45 in the six *Xac* whole genomes available (Figure 1). Region 2.4 located on the chromosome corresponds to an insertion in *Xac* that was not present in other *X. arboricola* pathovars, such as pv. arracacia (Figure 1). The annotations for this region varied slightly between the different *Xac* genomes, but the region contains between two and three singletons that encode hypothetical proteins. A 494 bp singleton located within "region 2.4" in *Xac* CFBP 1159^{PT} (locus_tag XaxcyCFBP1159_22010) and annotated as encoding the hypothetical protein PPU54630 was used for the further development of *Xac*-specific assays.

3.2 Candidate primer sets and *Xac* assays development

Out of the candidate primer sets designed for all three detection techniques, a few sets were discarded from further analysis due to the presence of non-specific products that persisted, even after adjusting annealing temperatures. After initial laboratory testing, we focused on validation and testing of six primer pairs for conventional PCR, four primer pairs for qPCR with SYBR® Green I, two primer pairs for TaqMan™ qPCR, and three primer pairs for LAMP. The sequences of these primer sets are reported in Table 2. A primer BLASTn analysis of selected primers showed no full similarity to any sequences of bacterial plant pathogens in GenBank in July 2019. This *in silico* result was also confirmed on 15 May 2023 with a final primer check performed in the course of writing this article.

3.3 Primers specificity for *Xac* in conventional, qPCR and LAMP *in vitro* and *in planta*

The genomic DNA of the 60 *Xac* strains was selectively amplified with all the primers developed for the different assays. No amplification was observed for the bacterial and fungal genomic DNA not belonging to the *Xac* pathovar (Table 1). Similarly, no amplification was observed with DNA templates obtained from clean, asymptomatic leaves of five hazelnut cultivars using two DNA extraction kits.

The PCR assays using primers designed for conventional PCR gave amplicons ranging from 197 bp to 1,455 bp depending on the primer pairs used (Table 2, Supplementary Table S1). The six primer sets designed for conventional PCR generated a single amplicon of the size predicted by genome analyses for nearly all the 60 strains of *Xac* evaluated (Table 1). Although, during validation of conventional PCR reactions on the JL26xx strains of *Xac* collected in Oregon, amplicons with an unexpected size were observed with *Xac* strain JL2600 with primers Xac2.4-4 and XacPPU-1. For *Xac* strain JL2600, the amplicon observed for primer pair for Xac2.4-4 was 1,166 bp instead of 1,455 bp and the amplicon for the primer pair for XacPPU-1 was 1,450 bp instead of

390 bp. The other conventional PCR primer pairs generated the predicted amplicon size for *Xac* strain JL2600. Conventional PCR reactions for all the other *Xac* strains in the JL26xx series (Supplementary Table S1) returned the expected amplicon size for each of the primer pairs.

In the SYBR® Green I qPCR assays, DNA from the *Xac* strains resulted in a positive reaction. However, non-specific, false-positive results after 28 cycles for a few bacteria not belonging to the *Xanthomonas* genus were observed when using the primers Xac45-1. Nonetheless, these non-specific amplicons were excluded based on the results of melting curve analysis i.e., having different melting temperature than the target product. The amplicons ranged from 88 bp to 170 bp and melting curve analysis performed on these specific products revealed a single peak characteristic of their already introduced line 492 T_m as reported in Table 2.

In the TaqMan™ qPCR, two primer sets designed resulted in a positive reaction for the tested DNA from the *Xac* strains tested (Table 1, Supplementary Table S1) and no product were observed in case of testing of bacterial and fungal genomic DNA not belonging to the *Xac* pathovar nor DNA templates obtained from clean, asymptomatic leaves of five hazelnut cultivars.

In the LAMP assays, DNA of the *Xac* strains gave a positive reaction as expected and no amplification was observed with DNA of other isolates. The T_m of products amplified using the LAMP primers are provided in Table 2.

Specificity, sensitivity, and efficiency of the *Xanthomonas arboricola* pv. corylina specific assays based on the organisms evaluated in this study are reported in Table 4.

The LAMP and both qPCR assays confirmed identity of verified *Xac* strains. Results for LAMP and qPCR platforms were obtained in less than 1 h.

3.4 Limits of detection of DNA- and crude bacterial cell-based assays

The sensitivity and detection limit of the *Xac* target DNA varies not only between the detection systems developed but also depending on the primer sets used. For four primer pairs designed for conventional PCR, 100 fg of genomic DNA generated a visible amplicon with primer pairs Xac2.4-4, and XacPPU-1; ~1 pg genomic DNA for primer pair Xac2.4-1; and 10 pg was detected with primer set Xac45-1. When crude, boiled bacterial cell templates were tested, the LoD was 1.8×10^1 CFU per reaction for Xac2.4-1 and XacPPU-1 primer sets, 1.8×10^0 CFU per reaction for Xac2.4-4 primer sets, 1.8×10^2 CFU per reaction for XacPPU54630 primer sets, and 1.8×10^3 CFU per reaction for Xac45-1 primer sets.

The LoD was lowered by 10^1 when using the primer pairs Xac2.4-1, Xac2.4-4, and XacPPU-1 to detect *Xac* in plant tissue macerates that contained the pathogen; for the primer pairs XacPPU54630 and Xac45-1 the LoD remained the same with or without plant tissues.

Among qPCR primers designed for SYBR® Green I, two primer sets (Xac2.4-3RT and Xac45-1RT) detected 1 fg of *Xac* genomic DNA (Figure 2), however the two other primer sets (Xac2.4-2RT and Xac45-2RT) detected about 10 fg of *Xac* genomic DNA. When crude boiled bacterial templates were tested, the limit of detection was 1×10^0 CFU per reaction. The same decrease of sensitivity as noticed for conventional PCR (lowered by 10^1) for boiled bacterial preparations and in combinations of plant tissues and bacteria. Parameters of the four qPCR SYBR® Green I assays are reported in Table 5.

For TaqMan™ qPCR, the primer sets Xac-reg45 and Xac-PPU54630 detected 80 and 8 pg of *Xac* genomic DNA, respectively. When crude boiled bacterial templates were tested, the limit of detection was 2×10^1 CFU per reaction for primer set Xac-PPU54630 and 2×10^3 CFU per reaction for primer set Xac-reg45.

When determining the sensitivity of LAMP primers, we detected 1 pg of purified genomic DNA from *Xac* isolates. When boiled bacterial cell templates were tested, the LoD was 1×10^0 CFU per reaction for the XacPPU-1 primer set and 1×10^1 CFU per reaction for the Xac2.4-1 and Xac2.4-2 primer sets. In purified DNA isolated from plant material combined with bacteria, the LoD was 1×10^3 CFU per reaction for all the primers tested.

3.5 Performance of the different detection tools on tissues from artificially inoculated and naturally infected hazelnuts

The detection of *Xac* in artificially inoculated plant material was done with four conventional primer sets (Xac2.4-1, Xac2.4-4, XacPPU-1 and Xac45-1), all SYBR® Green I qPCR (n = 4) and all LAMP primer sets (n = 3). All the primer sets used in the different platforms returned positive results for detection of *Xac* when the DNA was isolated using the kit procedure. Nonetheless, when the volume of the template of purified genomic DNA (µl or concentration per reaction) significantly increased, detection was decreased. Correspondingly, a one-tenth dilution of the purified genomic DNA template added to plant tissues allowed for consistent detection of *Xac*.

With all four conventional PCR primer sets, *Xac* was not detected when the assays were performed on DNA templates obtained *via* the boiling procedure of plant macerate (plants artificially or naturally infected). Because this was not the case with templates consisting of purified genomic DNA, we suspect that the boiling procedure did not eliminate possible plant inhibitors. The assays also remained negative when a tenfold dilution of the extracts was tested. For the SYBR® Green I qPCR primer sets, *Xac* was detected in DNA isolated with both procedures independent of the template DNA concentration. With the LAMP XacPPU-1, Xac2.4-1 and Xac2.4-2 primer sets, *Xac* was always detected with purified genomic DNA preparations. In case of DNA extracted by boiling, templates with only 0.5 and 1 µl of undiluted extract was detected.

4 Discussion

Based on a comparative genomics approach using five publicly available *Xac* genomes (Ibarra Caballero et al., 2013; Merda et al.,

TABLE 4 Specificity, sensitivity, and efficiency of the *Xanthomonas arboricola* pv. corylina specific assays based on the organisms evaluated in this study.

	Conventional PCR						qPCR[1]						LAMP		
	Xac2.4-1	Xac2.4-4	XacPPU-1	Xac45-1	Xac45	XacPPU54630	Xac2.4-2RT	Xac45-1RT	Xac45-2RT	Xac2.4-3RT	Xac-PPU54630	Xac-reg45	XacPPU-1	NewXac2.4-1	NewXac2.4-2
N[2]	110	110	110	110	45	45	94	95	94	94	46	46	79	79	79
N_{TP}	42	42	42	42	36	36	28	28	28	28	23	23	23	23	23
N_{TN}	68	68	68	68	9	9	66	67	66	66	23	23	56	56	56
N_{FP}	0	0	0	0	0	0	0	0	0	0	0	0	0	0	0
N_{FN}	0	0	0	0	0	0	0	0	0	0	0	0	0	0	0
Assay sensitivity (%)	100	100	100	100	100	100	100	100	100	100	100	100	100	100	100
Assay specificity (%)	100	100	100	100	100	100	100	100	100	100	100	100	100	100	100
Test efficiency (%)	100	100	100	100	100	100	100	100	100	100	100	100	100	100	100

[1]The first five columns for qPCR correspond to assays performed with SYBR® Green I whereas the last qPCR column corresponds to a TaqMan™ assay.
[2]N, total number of samples tested; N_{TP}, true positive samples; N_{TN}, true negative samples; N_{FP}, false positives and N_{FN}, false negatives.

2017; Pothier et al., 2022) and several bacterial genomes from NCBI GenBank, we successfully identified unique DNA targets and designed highly specific tools capable of identifying *Xac* in pure culture and culture-independent *in planta* detection. We developed four different systems for conventional PCR and qPCR, as well as a LAMP protocol for the rapid and specific detection of *Xac*. This ensures a wide application of the developed detection methods, depending on the equipment or preferences of scientists, diagnosticians, inspectors, and producers. In addition, these methods offer an advantage over conventional testing as bacteria do not need to be cultured prior to detection (Palacio-Bielsa et al., 2009). This could prove especially useful in the context of screening nursery material for latent infections, which would otherwise go undetected and become a source of primary infection in the field. For regions where new hazelnut acreage is rapidly increasing, such as Serbia and Chile (Lamichhane et al., 2012; Obradović et al., 2010), disease-free planting material is a critical first step to keep *Xac* disease pressure low.

Historically, hazelnut bacterial blight diagnostics have relied upon a combination of classical microbiology, serology, and molecular techniques (Schaad et al., 2001; OEPP/EPPO, 2004; Pothier et al., 2011a; Prokić et al., 2012; Kałużna et al., 2021). While recommended by EPPO, these methods are time consuming and risk misdiagnosis (Prokić et al., 2012). Moreover, none of them provide a LoD. For example, the biochemical features of Polish strains differ from those described in the EPPO standard. As a result, the recommended phenotype testing methods are not applicable to strains from the Polish climatic zone (Puławska et al., 2010). Similar issues have emerged when conducting the recommended procedure of sequencing housekeeping genes to identify pathovars within *X. arboricola*. The multilocus sequence analysis within this species showed that using a restricted number of housekeeping gene loci did not have sufficient discriminatory power to differentiate isolates of *Xaj* and *Xac* into unique groupings. Moreover, the use of partial *gyrB* sequences alone cannot discriminate *Xaj* and *Xac* from *Xap* (Kałużna et al., 2014; Fischer-Le Saux et al., 2015; Webber et al., 2020). The molecular tools reported herein overcome these sub-species diagnostic shortcomings.

The success of our work is based on comparing the genomes of all *X. arboricola* pathovars and related *Xanthomonas* species (Zarei et al., 2022), which allowed for the selection of a highly specific regions for *Xac*. The specificity of the region identified within the six genomes used for *in silico* development (three WGS and three complete genomes from five *Xac* strains) also was confirmed when tested with BLASTn analysis against three additional complete *Xac* genomes released after our assay development (namely: A7, assembly ASM1814170v1; IVIA 3978, assembly ASM2337497v1; CFBP 1846, assembly ASM2337499v1; data not shown). The success of our approach likely benefitted from the large number of genomes available for the *X. arboricola* species (about 100 genomes at the time of *in silico* development) thus allowing the development of assays at a sub-species level. The designed diagnostic tools allowed the detection of *Xac* genotypes from different worldwide geographical origins. A total of 60 *Xac* strains originating from eight countries in two continents and collected over 20 different years spanning the period 1939-2020 was tested successfully. The only exception was a result for the conventional PCR primer set Xac2.4-4 and XacPPU-1 when screening a set of *Xac* isolates from the United States. *Xac* isolate JL2600 amplified successfully, which indicates a *Xac* positive result, but the resulting amplicon was larger than expected. This result is particularly surprising because the dendrogram constructed using the concatenated partial sequences of *rpoD* and *gyrB* (Webber et al., 2020), had strain JL2600 clustered together with strain JL2606, an

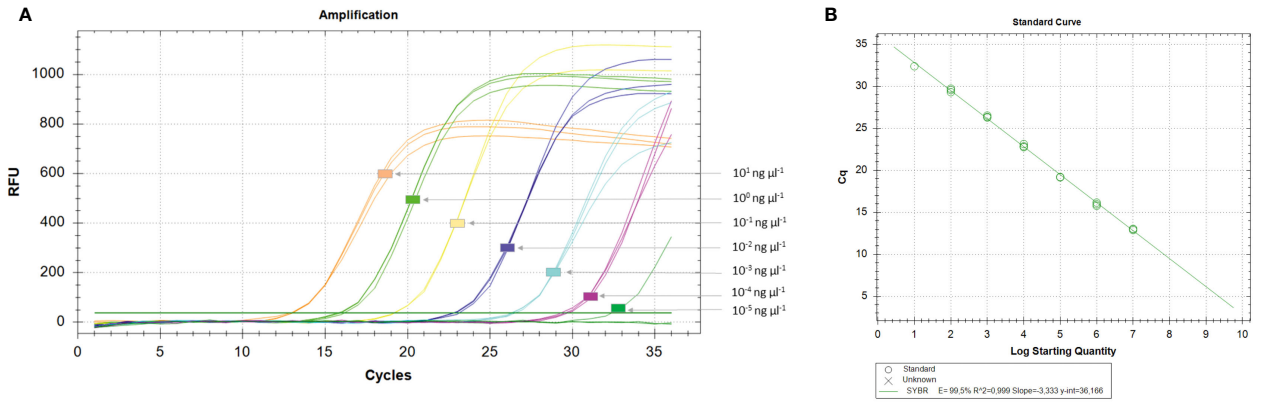

FIGURE 2
Determination of the limit of detection (LoD) of the *Xanthomonas arboricola* pv. corylina (*Xac*) qPCR SYBR® Green I assay **(A)** and standard curve **(B)**. The representative amplifications were obtained with the Xac2.4-3RT SYBR® Green I assay using 10-fold dilutions (three technical replicates) of genomic DNA of known concentrations isolated from pure cultures of strain Xac 301. The efficacy reaction *E*, coefficient of determination (R^2), slope and regression curve equations (*y*) were evaluated using the CFX Manager Software v.3.1 (Bio-Rad, Hercules, CA, USA).

TABLE 5 Parameters of the four qPCR SYBR® Green I assays evaluated through the analysis of standard curves generated with serial dilutions of genomic DNA extracts from *X. arboricola* pv. corylina CFBP 1159^{PT} and Xac 301 as templates.

qPCR code name	*E* (%)[1]	R^{2}[2]	*S*[3]	*Y* = *int*[4]
Xac2.4-2RT	101.9	0.996	-3.276	35.671
Xac45-1RT	102.6	0.991	-3.261	36.210
Xac45-1RT	99.7	0.998	-3.330	36.915
Xac2.4-3RT	99.5	0.999	-3.333	36.166

[1]*E* stands for PCR efficiency.
[2]R^2 is a measure of data linearity among technical replicates (n = 3) of serial dilutions.
[3]The slope (*S*) of the log–linear phase of the amplification reaction is a measure of reaction efficiency.
[4]*Y* = *int* represents the cycle threshold (C_t) value where the curve crosses the *y*-axis.

isolate for which the expected amplicon size was obtained. All other *Xac* strains (e.g., JL2610) belonging to the other *Xac* cluster described in the work by Webber et al. (2020) gave the expected amplicon size. This result reaffirms that validation testing of a comprehensive collection of strains, preferentially in different laboratories, is very important when developing novel identification and detection systems. Importantly, *Xac* specificity was confirmed by all detection assays and none of the non-*X. arboricola* pathovars tested returned a positive amplicon, which has happened in previous studies (Palacio-Bielsa et al., 2011; Pothier et al., 2011a; Fernandes et al., 2017). Also, none of the genomic DNA of *Pseudomonas*, other plant pathogenic and nonpathogenic bacteria, or fungi isolated from hazelnut and walnut gave a positive signal in the assays. In addition, no amplification was observed from DNA isolated from asymptomatic plants of different *C. avellana* cultivars, which means that the designed primers did not react with the hazelnut genome or its microbiota.

The methods and tools developed here can be applied for specific, reliable detection of *Xac* in infected plant material. Not having to first isolate and purify the pathogen significantly shortens the time required for diagnosis. All methods presented in this study allow for direct amplification of *Xac* DNA present in plant material. However, we observed that direct detection of DNA templates extracted by boiling can give false negative results, most likely due to the presence of inhibitory compounds. This phenomenon has already been observed with culture-independent detection of other pathogens *in planta* (De Boer et al., 1995; López et al., 2009; Palacio-Bielsa et al., 2009; Gétaz et al., 2017) and did not occur with the qPCR assays. The use of a DNA extraction kit eliminated putative DNA polymerase inhibitors and supports the finding of López et al. (2009) that the purification methods used should be evaluated for each combination of tested pathogen and plant before establishing and recommending the procedure for routine detection. Therefore, a DNA extraction kit is recommended for detection of *Xac* DNA in hazelnut tissues.

The LoD of the different assays was satisfactory for all the primer sets and allowed detection of between 1 pg to 10 fg per reaction or 1×10^{0} to 1×10^{3} CFU per reaction, with the highest sensitivity obtained for qPCRs. The qPCR procedure turned out to be the fastest of the protocols developed, with the whole reaction and melting curve analysis taking about 1 hour. The high sensitivity of these assays is especially important in the case of naturally infected plant material with low populations of the pathogen. LoD values, similar to the ones obtained in this study were

observed previously during the development of detection methods for other *X. arboricola* pathovars (Palacio-Bielsa et al., 2011; Pothier et al., 2011a; Fernandes et al., 2017), as well as for diagnostics of other plant pathogenic bacteria from other species or genus, e.g., *Pseudomonas morsprunorum* race 1 and 2 (Kałużna et al., 2016), *P. syringae* pv. actinidiae (Gallelli et al., 2014), *X. campestris* pv. campestris (Eichmeier et al., 2019).

The *Xac* detection systems developed allow for quick and reliable determination of host plant infection without the requirement for isolation of the bacterial pathogen. These assays also can be used to improve our knowledge of this pathogen, such as exploration of other host plants and natural reservoir(s). Even in the presence of potential plant inhibitors, the sensitivity of the assays remained high and sample-to-result times ranged from 5 to 6 hours for conventional PCR down to 1 to 2 hours for qPCR and LAMP assays. So far, this group of molecular assays is the first such methods available for rapid detection of the *Xac* pathogen directly from plant material.

Data availability statement

Publicly available datasets were analyzed in this study. This data can be found here: https://www.ncbi.nlm.nih.gov/datasets/genome/GCF_002939845.1, https://www.ncbi.nlm.nih.gov/datasets/genome/GCA_002940125.1, https://www.ncbi.nlm.nih.gov/datasets/genome/GCA_000355635.2, https://www.ncbi.nlm.nih.gov/bioproject/PRJEB42844.

Author contributions

MK: conceptualization, funding-acquisition, investigation, methodology, visualization, writing-original-draft, writing-review-editing. AP: investigation, software, writing-review-editing. AO: funding-acquisition, writing-review-editing. WW: investigation, writing-review-editing. VS: investigation, writing-review-editing, funding-acquisition. JP: conceptualization, funding-acquisition, software, visualization, writing-original-draft, writing-review-editing.

Funding

This study was partly financed by the National Science Centre, Poland (Narodowe Centrum Nauki), grant UMO- 2017/26/M/NZ9/01024 granted to MK. AP was granted a Short-Term Scientific Mission by the European Cooperation in Science and Technology COST Action CA16107 EuroXanth to conduct some analysis in Wädenswil (Switzerland). AO and AP were supported by the Ministry of Science, Technological Development and Innovation, Republic of Serbia and the Faculty of Agriculture contract number 451-03-47/2023-01/200116. VS and WW were supported by base funds of USDA ARS Project 2072-22000-045-000D and a 2020 USDA ARS HQ Administrator-funded Postdoctoral Award. Support was also provided to JP by the Department of Life Sciences and Facility Management of the Zurich University of Applied Sciences (ZHAW) in Wädenswil. The open access article processing charges of this publication were funded by the National Science Centre, Poland (grant UMO- 2017/26/M/NZ9/01024).

Acknowledgments

The authors would like to thank the HPC team of the School for Life Sciences and Facility Management at ZHAW for providing computing resources and support. They also want to acknowledge Dr. Jan Nechwatal from Bavarian State Research Center for Agriculture (DE) for supplying *Xac* strains and Prof. Ewa Zalewska from University of Life Sciences in Lublin (PL) as well as all Polish producers for providing diseased plant material. This article is based upon work from COST Action CA16107 EuroXanth, supported by COST (European Cooperation in Science and Technology).

Conflict of interest

Author WW was employed by USDA-ARS as a Postdoctoral Fellow during this project. All authors declare that the research was conducted in the absence of any commercial or financial relationships that could be construed as a potential conflict of interest.

Mention of trade names or commercial products in this publication is solely for the purpose of providing specific information and does not imply recommendation or endorsement by the U.S. Department of Agriculture.

Publisher's note

Supplementary material

The Supplementary Material for this article can be found online at: https://www.frontiersin.org/articles/10.3389/fpls.2023.1254107/full#supplementary-material

References

Altschul, S. F., Gish, W., Miller, W., Myers, E. W., and Lipman, D. J. (1990). Basic local alignment search tool. *J. Mol. Biol.* 215 (3), 403–410. doi: 10.1006/jmbi.1990.9999

Calić, A., Gašić, K., Ivanović, M., Obradović, A., Ferrante, P., and Scortichini, M. (2009). "New occurence of *Xanthomonas arboricola* pv. *corylina* on European hazelnut in Serbia," in *Proceedings of the Annual COST 873 Meeting*, Vol. 89, 89.

Camacho, C., Coulouris, G., Avagyan, V., Ma, N., Papadopoulos, J., Bealer, K., et al. (2009). BLAST+: architecture and applications. *BMC Bioinf.* 10 (1), 421. doi: 10.1186/1471-2105-10-421

Cesbron, S., Briand, M., Essakhi, S., Gironde, S., Boureau, T., Manceau, C., et al. (2015). Comparative genomics of pathogenic and nonpathogenic strains of *Xanthomonas arboricola* unveil molecular and evolutionary events linked to pathoadaptation. *Front. Plant Sci.* 6. doi: 10.3389/fpls.2015.01126

Cuesta-Morrondo, S., Redondo, C., Palacio-Bielsa, A., Garita-Cambronero, J., and Cubero, J. (2022). Complete genome sequence resources of six strains of the most virulent pathovars of *Xanthomonas arboricola* using long- and short-read sequencing approaches. *Phytopathology* 112 (8), 1808–1813. doi: 10.1094/phyto-10-21-0436-a

D'Amico-Willman, K. M., Joglekar, P., Luna, E. K., Ritchie, D. F., Fagen, J., and Huerta, A. I. (2022). Complete genome sequence of *Xanthomonas arboricola* pv. *pruni* strain Xcp1 isolated in 1984 from a bacterial spot spring canker on *Prunus persica* var. *nucipersica* cv. "Redgold". *Microbiol. Resour. Announc.* 11 (12), e00209–e00222. doi: 10.1128/mra.00209-22

De Boer, S. H., Ward, L. J., Li, X., and Chittaranjan, S. (1995). Attenuation of PCR inhibition in the presence of plant compounds by addition of BLOTTO. *Nucleic Acids Res.* 23 (13), 2567–2568. doi: 10.1093/nar/23.13.2567

Eichmeier, A., Peňázová, E., Pokluda, R., and Vicente, J. G. (2019). Detection of *Xanthomonas campestris* pv. *campestris* through a real-time PCR assay targeting the *Zur* gene and comparison with detection targeting the *hrpF* gene. *Eur. J. Plant Pathol.* 155 (3), 891–902. doi: 10.1007/s10658-019-01820-0

European Union (2016). Regulation (EU) 2016/2031 of the European Parliament of the Council of 26 October 2016 on protective measures against pests of plants, amending Regulations (EU) No 228/2013, (EU) No 652/2014 and (EU) No 1143/2014 of the European Parliament and of the Council and repealing Council Directives 69/464/EEC, 74/647/EEC, 93/85/EEC, 98/57/EC 2000/29/EC 2006/91/EC and 2007/33/EC. *Off. J. Eur. Union* L317, 4–104.

European Union (2019). Commission implementing directive (EU) 2019/2072 of 28 november 2019 establishing uniform conditions for the implementation of regulation (EU) 2016/2031 of the European Parliament and the Council, as regards protective measures against pests of plants, and repealing commission regulation (EC) no 690/2008 and amending commission implementing regulation (EU) 2018/2019. *Off. J. Eur. Union* L319, 1–278.

Fernandes, C., Albuquerque, P., Sousa, R., Cruz, L., and Tavares, F. (2017). Multiple DNA markers for identification of *Xanthomonas arboricola* pv. *juglandis* isolates and its direct detection in plant samples. *Plant Dis.* 101 (6), 858–865. doi: 10.1094/PDIS-10-16-1481-RE

Fernandes, C., Blom, J., Pothier, J. F., and Tavares, F. (2018). High-quality draft genome sequence of *Xanthomonas arboricola* pv. juglandis CPBF 1521, isolated from leaves of a symptomatic walnut tree in Portugal without a past of phytosanitary treatment. *Microbiol. Resour. Announc.* 7 (16), e00887–e00818. doi: 10.1128/mra.00887-18

Fischer-Le Saux, M., Bonneau, S., Essakhi, S., Manceau, C., and Jacques, M.-A. (2015). Aggressive emerging pathovars of *Xanthomonas arboricola* represent widespread epidemic clones that are distinct from poorly pathogenic strains, as revealed by multilocus sequence typing. *Appl. Environ. Microbiol.* 81 (14), 4651–4688. doi: 10.1128/aem.00050-15

Fu, B., Chen, Q., Wei, M., Zhu, J., Zou, L., Li, G., et al. (2018). Complete genome sequence of *Xanthomonas arboricola* pv. juglandis strain DW3F3, isolated from a *Juglans regia* L. bacterial blighted fruitlet. *Genome Announc.* 6 (8), e00023–e00018. doi: 10.1128/genomeA.00023-18

Gallelli, A., Talocci, S., Pilotti, M., and Loreti, S. (2014). Real-time and qualitative PCR for detecting *Pseudomonas syringae* pv. *actinidiae* isolates causing recent outbreaks of kiwifruit bacterial canker. *Plant Pathol.* 63, 264–276. doi: 10.1111/ppa.12082

Garita-Cambronero, J., Palacio-Bielsa, A., López, M. M., and Cubero, J. (2016a). Comparative genomic and phenotypic characterization of pathogenic and non-pathogenic strains of *Xanthomonas arboricola* reveals insights into the infection process of bacterial spot disease of stone fruits. *PloS One* 11 (8), e0161977. doi: 10.1371/journal.pone.0161977

Garita-Cambronero, J., Palacio-Bielsa, A., López, M. M., and Cubero, J. (2016b). Draft genome sequence for virulent and avirulent strains of *Xanthomonas arboricola* isolated from *Prunus* spp. in Spain. *Stand. Genomic Sci.* 11 (1), 1–10. doi: 10.1186/s40793-016-0132-3

Garita-Cambronero, J., Palacio-Bielsa, A., López., M. M., and Cubero, J. (2016c). Draft genome sequence of two strains of *Xanthomonas arboricola* isolated from *Prunus persica* which are dissimilar to strains that cause bacterial spot disease on *Prunus* spp. *Genome Announc.* 4 (5), e00974–e00916. doi: 10.1128/genomeA.00974-16

Garita-Cambronero, J., Palacio-Bielsa, A., López, M. M., and Cubero, J. (2017). Pan-genomic analysis permits differentiation of virulent and non-virulent strains of *Xanthomonas arboricola* that cohabit *Prunus* spp. and elucidate bacterial virulence factors. *Front. Microbiol.* 8 (573). doi: 10.3389/fmicb.2017.00573

Garita-Cambronero, J., Sena-Vélez, M., Palacio-Bielsa, A., and Cubero, J. (2014). Draft genome sequence of *Xanthomonas arboricola* pv. *pruni* strain Xap33, causal agent of bacterial spot disease on almond. *Genome Announc.* 2 (3), e00440–e00414. doi: 10.1128/genomeA.00440-14

Gétaz, M., Baeyen, S., Blom, J., Maes, M., Cottyn, B., and Pothier, J. F. (2018). High-quality draft genome sequences of five *Xanthomonas arboricola* pv. fragariae isolates. *Genome Announc.* 6 (7), e01585–e01517. doi: 10.1128/genomeA.01585-17

Gétaz, M., Bühlmann, A., Schneeberger, P. H. H., Van Malderghem, C., Duffy, B., Maes, M., et al. (2017). A diagnostic tool for improved detection of *Xanthomonas fragariae* using a rapid and highly specific LAMP assay designed with comparative genomics. *Plant Pathol.* 66 (7), 1094–1102. doi: 10.1111/ppa.12665

Harrison, J., Grant, M. R., and Studholme, D. J. (2016). Draft genome sequences of two strains of *Xanthomonas arboricola* pv. *celebensis* isolated from banana plants. *Genome Announc.* 4 (1), e01705–e01715. doi: 10.1128/genomeA.01705-15

Herbert, A., Hancock, C. N., Cox, B., Schnabel, G., Moreno, D., Carvalho, R., et al. (2022). Oxytetracycline and streptomycin resistance genes in *Xanthomonas arboricola* pv. *pruni*, the causal agent of bacterial spot in peach. *Front. Microbiol.* 13. doi: 10.3389/fmicb.2022.821808

Higuera, G., González-Escalona, N., Véliz, C., Vera, F., and Romero, J. (2015). Draft genome sequences of four *Xanthomonas arboricola* pv. juglandis strains associated with walnut blight in Chile. *Genome Announc.* 3 (5), e01160–e01115. doi: 10.1128/genomeA.01160-15

Ibarra Caballero, J., Zerillo, M. M., Snelling, J., Boucher, C., and Tisserat, N. (2013). Genome sequence of *Xanthomonas arboricola* pv. *corylina*, isolated from turkish filbert in Colorado. *Genome Announc.* 1 (3), e00246–e00213. doi: 10.1128/genomeA.00246-13

Ignatov, A. N., Kyrova, E. I., Vinogradova, S. V., Kamionskaya, A. M., Schaad, N. W., and Luster, D. G. (2015). Draft genome sequence of *Xanthomonas arboricola* strain 3004, a causal agent of bacterial disease on barley. *Genome Announc.* 3 (1), e01572–e01514. doi: 10.1128/genomeA.01572-14

Janse, J. D., Rossi, M. P., Gorkink, R. F. J., Derks, J. H. J., Swings, J., Janssens, D., et al. (2001). Bacterial leaf blight of strawberry (*Fragaria (×) ananassa*) caused by a pathovar of *Xanthomonas arboricola*, not similar to *Xanthomonas fragariae* Kennedy & King. Description of the causal organism as *Xanthomonas arboricola* pv. *fragariae* (pv. nov., comb. nov.). *Plant Pathol.* 50 (6), 653–665. doi: 10.1046/j.1365-3059.2001.00644.x

Kałużna, M., Albuquerque, P., Tavares, F., Sobiczewski, P., and Puławska, J. (2016). Development of SCAR markers for rapid and specific detection of *Pseudomonas syringae* pv. *morsprunorum* races 1 and 2, using conventional and real-time PCR. *Appl. Microbiol. Biotechnol.* 100 (8), 3693–3711. doi: 10.1007/s00253-016-7295-0

Kałużna, M., Fischer-Le Saux, M., Pothier, J. F., Jacques, M.-A., Obradović, A., Tavares, F., et al. (2021). *Xanthomonas arboricola* pv. *juglandis* and pv. *corylina*: brothers or distant relatives? Genetic clues, epidemiology, and insights for disease management. *Mol. Plant Pathol.* 22 (12), 1481–1499. doi: 10.1111/mpp.13073

Kałużna, M., and Pothier, J. F. (2022). Complete genome sequence data of two *Xanthomonas arboricola* strains isolated from blueberry plants displaying bacterial leaf blight in Poland. *Phytopathology* 112 (8), 1814–1818. doi: 10.1094/phyto-11-21-0484-a

Kałużna, M., Pulawska, J., Waleron, M., and Sobiczewski, P. (2014). The genetic characterisation of *Xanthomonas arboricola* pv. *juglandis*, the causal agent of walnut blight in Poland. *Plant Pathol.* 63 (6), 1404–1416. doi: 10.1111/ppa.12211

King, E. O., Ward, M. K., and Raney, D. E. (1954). Two simple media for the demonstration of pyocyanin and fluorescin. *J. Lab. Clin. Med.* 44 (2), 301–307.

Lamichhane, J. R., Grau, P., and Varvaro, L. (2012). Emerging hazelnut cultivation and the severe threat of bacterial blight in Chile. *J. Phytopathol.* 160, 752–754. doi: 10.1111/jph.12004

Lamichhane, J. R., and Varvaro, L. (2014). *Xanthomonas arboricola* disease of hazelnut: current status and future perspectives for its management. *Plant Pathol.* 63, 243–254. doi: 10.1111/ppa.12152

Lelliott, R. A., and Stead, D. E. (1987). *Methods for the diagnosis of bacterial diseases of plants*. (Oxford, UK: Blackwell Scientific Publications).

López, M. M., Llop, P., Olmos, A., Marco-Noales, E., Cambra, M., and Bertolini, E. (2009). Are molecular tools solving the challenges posed by detection of plant pathogenic bacteria and viruses? *Curr. Issues Mol. Biol.* 11, 13–46. doi: 10.21775/cimb.011.013

López-Soriano, P., Boyer, K., Cesbron, S., Morente, M. C., Peñalver, J., Palacio-Bielsa, A., et al. (2016). Multilocus variable number of tandem repeat analysis reveals multiple introductions in Spain of *Xanthomonas arboricola* pv. *pruni*, the causal agent of bacterial spot disease of stone fruits and almond. *PloS One* 11 (9), e0163729. doi: 10.1371/journal.pone.0163729

Maes, M. (1993). Fast classification of plant-associated bacteria in the *Xanthomonas* genus. *FEMS Microbiol. Lett.* 113 (2), 161–165. doi: 10.1111/j.1574-6968.1993.tb06508.x

Merda, D., Briand, M., Bosis, E., Rousseau, C., Portier, P., Barret, M., et al. (2017). Ancestral acquisitions, gene flow and multiple evolutionary trajectories of the type

three secretion system and effectors in *Xanthomonas* plant pathogens. *Mol. Ecol.* 26 (21), 5939–5952. doi: 10.1111/mec.14343

Miller, P., Bollen, W., and Simmons, J. (1949). *Filbert bacteriosis and its control. Technical bulletin 16.* (Corvallis: Agricultural Experiment Station).

Moore, L. W. (2002). "Bacterial blight," in *Compendium of nut crop diseases in temperate zones*. Eds. B. L. Teviotdale, T. J. Michailides and J. W. Pscheidt (St Paul, MN: APS Press), 249–257.

Nagamine, K., Hase, T., and Notomi, T. (2002). Accelerated reaction by loop-mediated isothermal amplification using loop primers. *Mol. Cell. Probes* 16 (3), 223–229. doi: 10.1006/mcpr.2002.0415

Nuñez Cerda, P. D., Muster, C., Lisperguer, M. J., Vargas, E., and Bustos, S. (2021). Complete genome of *Xanthomonas arboricola* pv. *corylina* strain A7 isolated from southern Chile. *Mol. Plant-Microbe Interact.* 35 (1), 94–95. doi: 10.1094/mpmi-12-20-0363-a

Obradović, A., Ivanović, M., and Ćalić, A. (2010). Bacterial diseases of hazelnut. *Biljni Lekar (Plant Doctor)* 38 (3), 192–201.

OEPP/EPPO (1986). *Xanthomonas campestris* pv. *corylina*. *EPPO Bull.* 16 (1), 67–78. doi: 10.1111/j.1365-2338.1986.tb01139.x

OEPP/EPPO (2004). *Xanthomonas arboricol*a pv. *corylina*. *EPPO Bull.* 34 (2), 179–181. doi: 10.1111/j.1365-2338.2004.00716.x

OEPP/EPPO (2010a). PM 7/100 (1) Rep-PCR tests for identification of bacteria. *EPPO Bull.* 40 (3), 365–368. doi: 10.1111/j.1365-2338.2010.02409.x

OEPP/EPPO (2010b). PM 7/101 (1) ELISA tests for plant pathogenic bacteria. *EPPO Bull.* 40 (3), 369–372. doi: 10.1111/j.1365-2338.2010.02420.x

Osdaghi, E. (2022). *Xanthomonas arboricola* pv. corylina (bacterial blight of hazelnut). *PlantwisePlus Knowledge Bank*. (CABI International). doi: 10.1079/pwkb.species.56930

Palacio-Bielsa, A., Cambra, M. A., and López, M. M. (2009). PCR detection and identification of plant-pathogenic bacteria: updated review of protocols, (1989-2007). *J. Plant Pathol.* 91 (2), 249–297.

Palacio-Bielsa, A., Cubero, J., Cambra, M. A., Collados, R., Berruete, I. M., and Lopez, M. M. (2011). Development of an efficient real-time quantitative PCR protocol for detection of *Xanthomonas arboricola* pv. *pruni* in *Prunus* species. *Appl. Environ. Microbiol.* 77 (1), 89–97. doi: 10.1128/aem.01593-10

Parkinson, N., Aritua, V., Heeney, J., Cowie, C., Bew, J., and Stead, D. (2007). Phylogenetic analysis of *Xanthomonas* species by comparison of partial gyrase B gene sequences. *Int. J. Syst. Evol. Microbiol.* 57 (12), 2881–2887. doi: 10.1099/ijs.0.65220-0

Pothier, J. F., Kałużna, M., Prokić, A., Obradovic, A., and Rezzonico, F. (2022). Complete genome and plasmid sequence data of three *Xanthomonas arboricola* pv. *corylina* strains, the bacterium responsible for bacterial blight of hazelnut. *Phytopathology* 12 (4), 956–960. doi: 10.1094/phyto-08-21-0356-a

Pothier, J. F., Pagani, M. C., Pelludat, C., Ritchie, D. F., and Duffy, B. (2011a). A duplex-PCR method for species- and pathovar-level identification and detection of the quarantine plant pathogen *Xanthomonas arboricola* pv. *pruni*. *J. Microbiol. Methods* 86, 16–24. doi: 10.1016/j.mimet.2011.03.019

Pothier, J. F., Smits, T. H. M., Blom, J., Vorhölter, F., Goesmann, A., Pühler, A., et al. (2011b). Complete genome sequence of the stone fruit pathogen *Xanthomonas arboricola* pv. *pruni*. *Phytopathology* 101 (6S), S144–S145.

Pothier, J. F., Vorhölter, F.-J., Blom, J., Goesmann, A., Pühler, A., Smits, T. H. M., et al. (2011c). The ubiquitous plasmid pXap41 in the invasive phytopathogen *Xanthomonas arboricola* pv. *pruni*: complete sequence and comparative genomic analysis. *FEMS Microbiol. Lett.* 323 (1), 52–60. doi: 10.1111/j.1574-6968.2011.02352.x

Prokić, A., Gašić, K., Ivanović, M. M., Kuzmanović, N., Šević, M., Pulawska, J., et al. (2012). Detection and identification methods and new tests as developed and used in the framework of COST873 for bacteria pathogenic to stone fruits and nuts - *Xanthomonas arboricola* pv. *corylina*. *J. Plant Pathol.* 94 (S1), S127–S133. doi: 10.4454/jpp.v94i1sup.020

Puławska, J., Kałużna, M., Kołodziejska, A., and Sobiczewski, P. (2010). Identification and characterization of *Xanthomonas arboricola* pv. *corylina* causing bacterial blight of hazelnut: a new disease in Poland. *J. Plant Pathol.* 92 (3), 803–806.

Ramakers, C., Ruijter, J. M., Deprez, R. H. L., and Moorman, A. F. M. (2003). Assumption-free analysis of quantitative real-time polymerase chain reaction (PCR) data. *Neurosci. Lett.* 339 (1), 62–66. doi: 10.1016/S0304-3940(02)01423-4

Retamales, J., Segovia, C., Alvarado, R., Nuñez, P., and Santander, J. (2017). Draft genome sequence of *Xanthomonas arboricola* pv. *juglandis* J303, isolated from infected walnut trees in Southern Chile. *Genome Announc.* 5 (39), e01085–e01017. doi: 10.1128/genomeA.01085-17

Saddler, G. S., and Bradbury, J. F. (2005). "Xanthomonadales *ord. nov*," in *Bergey's Manual of Systematic Bacteriology., 2nd ed* (Boston, MA: Springer), 63–122.

Sambrook, J., Fritsch, E. F., and Maniatis, T. (1989). *Molecular cloning: a laboratory manual* (New York: Cold Spring Harbour Laboratory).

Schaad, N. W., Jones, J. B., and Chun, W. (2001). *Laboratory guide for identification of plant pathogenic bacteria.* (St. Paul, MN: APS Press).

Schneeberger, P. H. H., Pothier, J. F., Bühlmann, A., Duffy, B., Beuret, C., Utzinger, J., et al. (2017). Development and evaluation of a bioinformatics approach for designing molecular assays for viral detection. *PLoS One* 12 (5), e0178195. doi: 10.1371/journal.pone.0178195

Scortichini, M., Rossi, M. P., and Marchesi, U. (2002). Genetic, phenotypic and pathogenic diversity of *Xanthomonas arboricola* pv. *corylina* strains question the representative nature of the type strain. *Plant Pathol.* 51 (3), 374–381. doi: 10.1046/j.1365-3059.2002.00691.x

Teixeira, M., Fernandes, C., Chaves, C., Pinto, J., Tavares, F., and Fonseca, N. A. (2021). Complete genome sequence obtained by Nanopore and Illumina hybrid assembly of *Xanthomonas arboricola* pv. *juglandis* CPBF 427, isolated from buds of a walnut tree. *Microbiol. Resour. Announc.* 10 (10), e00085–e00021. doi: 10.1128/MRA.00085-21

Tindall, B. J. (2014). The family name *Solimonadaceae* Losey et al. 2013 is illegitimate, proposals to create the names '*Sinobacter soli*' comb. nov. and '*Sinobacter variicoloris*' contravene the Code, the family name *Xanthomonadaceae* Saddler and Bradbury 2005 and the order name *Xanthomonadales* Saddler and Bradbury 2005 are illegitimate and notes on the application of the family names *Solibacteraceae* Zhou et al. 2008, Nevskiaceae Henrici and Johnson 1935 (Approved Lists 1980) and *Lysobacteraceae* Christensen and Cook 1978 (Approved Lists 1980) and order name *Lysobacteriales* Christensen and Cook 1978 (Approved Lists 1980) with respect to the classification of the corresponding type genera *Solibacter* Zhou et al. 2008, Nevskia Famintzin 1892 (Approved Lists 1980) and *Lysobacter* Christensen and Cook 1978 (Approved Lists 1980) and importance of accurately expressing the link between a taxonomic name, its authors and the corresponding description/circumscription/emendation. *Int. J. Syst. Evol. Microbiol.* 64 (Pt_1), 293–297. doi: 10.1099/ijs.0.057158-0

Tuang, F. N., Rademaker, J. L. W., Alocilja, E. C., Louws, F. J., and Bruijn, F. J. (1999). Identification of bacterial rep-PCR genomic fingerprints using a backpropagation neural network. *FEMS Microbiol. Lett.* 177 (2), 249–256. doi: 10.1111/j.1574-6968.1999.tb13740.x

Untergasser, A., Cutcutache, I., Koressaar, T., Ye, J., Faircloth, B. C., Remm, M., et al. (2012). Primer3—new capabilities and interfaces. *Nucleic Acids Res.* 40 (15), e115. doi: 10.1093/nar/gks596

Vauterin, L., Hoste, B., Kersters, K., and Swings, J. (1995). Reclassification of *Xanthomonas*. *Int. J. Syst. Bacteriol.* 45 (3), 472–489. doi: 10.1099/00207713-45-3-472

Webber, J. B., Putnam, M., Serdani, M., Pscheidt, J. W., Wiman, N. G., and Stockwell, V. O. (2020). Characterization of isolates of *Xanthomonas arboricola* pv. *corylina*, the causal agent of bacterial blight, from Oregon hazelnut orchards. *J. Plant Pathol.* 102, 799–812. doi: 10.1007/s42161-020-00505-6

Webber, J. B., Wada, S., Stockwell, V. O., and Wiman, N. G. (2021). Susceptibility of some *Corylus avellana* L. cultivars to *Xanthomonas arboricola* pv. *corylina*. *Front. Plant Sci.* 12. doi: 10.3389/fpls.2021.800339

Young, J. M., Park, D.-C., Shearman, H. M., and Fargier, E. (2008). A multilocus sequence analysis of the genus *Xanthomonas*. *Syst. Appl. Microbiol.* 31 (5), 366–377. doi: 10.1016/j.syapm.2008.06.004

Zarei, S., Taghavi, S. M., Rahimi, T., Mafakheri, H., Potnis, N., Koebnik, R., et al. (2022). Taxonomic refinement of *Xanthomonas arboricola*. *Phytopathology* 112 (8), 1630–1639. doi: 10.1094/phyto-12-21-0519-r

Frontiers in Plant Science

Cultivates the science of plant biology and its applications

The most cited plant science journal, which advances our understanding of plant biology for sustainable food security, functional ecosystems and human health.

Discover the latest Research Topics

See more →

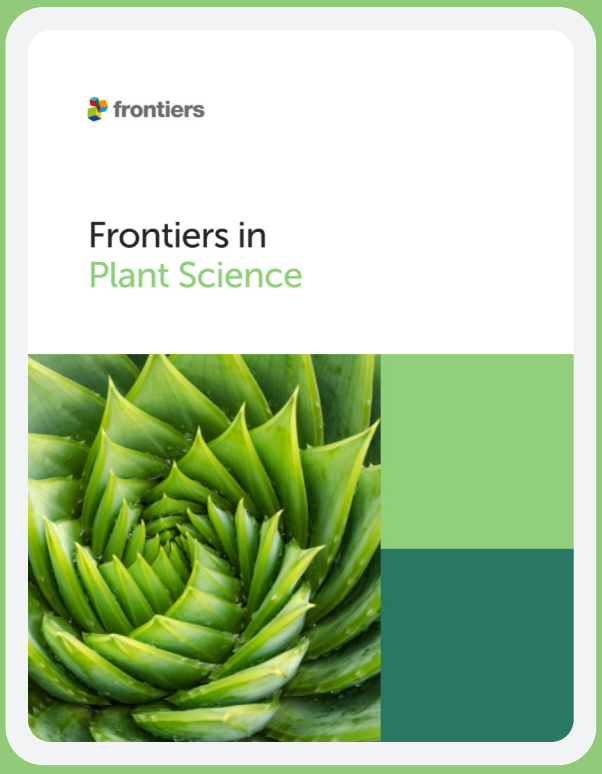

Frontiers

Avenue du Tribunal-Fédéral 34
1005 Lausanne, Switzerland
frontiersin.org

Contact us

+41 (0)21 510 17 00
frontiersin.org/about/contact